

**Block Copolymer Micelles and Vesicles:  
Loading, Release and Cellular Internalization  
with Applications to Drug Delivery**

by

**Patrick Lim Soo**

A thesis submitted to McGill University in partial  
fulfillment of the requirements of the degree of

**Doctor of Philosophy**

Department of Chemistry  
McGill University  
Montreal, Quebec  
Canada, H3A 2K6

© Patrick Lim Soo, 2004

August 2004



Library and  
Archives Canada

Bibliothèque et  
Archives Canada

Published Heritage  
Branch

Direction du  
Patrimoine de l'édition

395 Wellington Street  
Ottawa ON K1A 0N4  
Canada

395, rue Wellington  
Ottawa ON K1A 0N4  
Canada

*Your file* *Votre référence*

*ISBN: 0-494-12884-4*

*Our file* *Notre référence*

*ISBN: 0-494-12884-4*

#### NOTICE:

The author has granted a non-exclusive license allowing Library and Archives Canada to reproduce, publish, archive, preserve, conserve, communicate to the public by telecommunication or on the Internet, loan, distribute and sell theses worldwide, for commercial or non-commercial purposes, in microform, paper, electronic and/or any other formats.

The author retains copyright ownership and moral rights in this thesis. Neither the thesis nor substantial extracts from it may be printed or otherwise reproduced without the author's permission.

#### AVIS:

L'auteur a accordé une licence non exclusive permettant à la Bibliothèque et Archives Canada de reproduire, publier, archiver, sauvegarder, conserver, transmettre au public par télécommunication ou par l'Internet, prêter, distribuer et vendre des thèses partout dans le monde, à des fins commerciales ou autres, sur support microforme, papier, électronique et/ou autres formats.

L'auteur conserve la propriété du droit d'auteur et des droits moraux qui protègent cette thèse. Ni la thèse ni des extraits substantiels de celle-ci ne doivent être imprimés ou autrement reproduits sans son autorisation.

---

In compliance with the Canadian Privacy Act some supporting forms may have been removed from this thesis.

Conformément à la loi canadienne sur la protection de la vie privée, quelques formulaires secondaires ont été enlevés de cette thèse.

While these forms may be included in the document page count, their removal does not represent any loss of content from the thesis.

Bien que ces formulaires aient inclus dans la pagination, il n'y aura aucun contenu manquant.

  
**Canada**

## Abstract

This thesis describes the preparation, physico-chemical characterization and pharmacological studies of block copolymer micelles and vesicles for drug delivery applications. The incorporation and partition coefficients of model hydrophobic compounds (benzo[a]pyrene and Cell Tracker-DiI) are investigated in polycaprolactone-*block*-poly(ethylene oxide) copolymer micelles (PCL-*b*-PEO). The release of the probes is also studied from PCL-*b*-PEO micelles under perfect sink conditions. To investigate the usefulness of PCL-*b*-PEO micelles as a delivery vehicle for hydrophobic drugs, 17 $\beta$ -estradiol (E2) is incorporated and released from the micelles. The biological activity of E2 is retained after micelle preparation and delivery to C57BL female mice. To investigate the cellular internalization of block copolymer micelles, gold labeled poly (4-vinylpyridine)-*block*-poly(ethylene oxide) micelles are internalized into A549 lung cells and HEK 293 kidney cells. The gold labeled P4VP-*b*-PEO micelles are visualized by transmission electron microscopy inside of endosomes and lysosomes of these cells. The incorporation and release of a hydrophilic drug, doxorubicin hydrochloride (DXR), into polystyrene-*block*-poly(acrylic acid) vesicles are investigated. An active pH loading method is used to incorporate DXR into the aqueous center of the vesicle. A plasticizer, dioxane is used to control the loading and release of DXR by tuning the permeability of the vesicle walls.

## Résumé

Cette thèse décrit la préparation, les caractérisations physico-chimiques et les études pharmacologiques de micelles et de vésicules de copolymères blocs pour des applications de relargage de médicaments. L'incorporation et les coefficients de partition de composés hydrophobes typiques (benzo[a]pyrene and Cell Tracker-DiI) sont étudiés dans des micelles de polycaprolactone-*bloc*-poly(ethylene oxide) (PCL-*b*-PEO). La libération de marqueurs est aussi étudiée dans le cas des micelles de PCL-*b*-PEO dans des conditions de dilution parfaites. Pour étudier l'utilité des micelles de PCL-*b*-PEO comme véhicule de médicaments hydrophobes, du 17 $\beta$ -estradiol (E2) est incorporé et relargué par les micelles. L'activité biologique du E2 est maintenue après la préparation des micelles et son relargage à des souris femelles C57BL. Pour étudier l'internalisation cellulaire de micelles de copolymères diblocs, des micelles de poly (4-vinylpyridine)-*bloc*-poly(ethylene oxide) étiquetées avec de l'or sont internalisées dans des cellules de poumon A549 et des cellules de rein HEK 293. Les micelles étiquetées avec de l'or sont observées par microscopie électronique de transmission dans les endosomes et les lysosomes de ces cellules. Enfin, l'incorporation et le largage d'un médicament hydrophile tel que la doxorubicine hydrochloride (DXR), dans des vésicules de polystyrène-*bloc*-poly(acrylic acid) est étudiée. Une méthode de chargement induite par le pH est utilisée pour incorporer la DXR dans le centre aqueux de la vésicule. Un élément plastifiant, le dioxane est utilisé pour contrôler le chargement et la libération de la DXR en réglant la perméabilité de la paroi des vésicules.

## Foreword

In accordance with the specifications of the “Thesis Preparation and Submission Guidelines” (Faculty of Graduate and Postdoctoral Studies), the following text is cited:

“Candidates have the option of including, as part of the thesis, the text of one or more papers submitted, or to be submitted, for publication, or the clearly-duplicated text of one or more published papers. These texts must conform to the "Guidelines for Thesis Preparation" and must be bound together as an integral part of the thesis.”

“The thesis must be more than a collection of manuscripts. All components must be integrated into a cohesive unit with a logical progression from one chapter to the next. In order to ensure that the thesis has continuity, connecting texts that provide logical bridges preceding and following each manuscript are mandatory.”

“The thesis must conform to all other requirements of the "Guidelines for Thesis Preparation" in addition to the manuscripts. The thesis must include the following: a table of contents; a brief abstract in both English and French; an introduction which clearly states the rationale and objectives of the research; a comprehensive review of the literature a final conclusion and summary, and a thorough bibliography.”

“As manuscripts for publication are frequently very concise documents, where appropriate, additional material must be provided (e.g., in appendices) in sufficient detail to allow a clear and precise judgment to be made of the importance and originality of the research reported in the thesis.”

“In general, when co-authored papers are included in a thesis, the candidate is required to make an explicit statement in the thesis as to who contributed to such work and to what extent. The supervisor must attest to the accuracy of this statement at the doctoral oral defense. Since the task of the examiners is made more difficult in these cases, it is in the candidate's interest to clearly specify the responsibilities of all the authors of the co-authored papers.”

## Foreword

This dissertation is written in the form of five original papers, each of which comprises one chapter, with general conclusions contained in the final chapter. Also two additional original papers in published journal format, of work pertaining to the thesis in which I was a co-author, will be included at the end of the thesis (Appendix). Following normal procedures, the papers and review article have either been published or will be submitted shortly for publication in scientific journals. A list of the papers and the review article contained within each chapter is given below:

Chapter 2: *J. Poly. Sci. B: Polymer Physics* **2004**, 42, 923-938

Chapter 3: *Langmuir* **2002**, 18, 9996-10004.

Chapter 4: to be submitted to *Langmuir*

Chapter 5: to be submitted to *PNAS*

Chapter 6: Submitted to *Journal of Controlled Release*

Appendix: *BBA* **2001**, 1539, 205-217 and *Langmuir* **2004**, 20, 3543-3550.

### Contributions of Authors

All of the papers were co-authored by the research director Dr. Adi Eisenberg. Also, several of the papers were co-authored by Dr. Dusica Maysinger as she supervised and directed all of the pharmacological studies. Dr. Laibin Luo is a co-author of Chapter 3, as he synthesized the polycaprolactone-*block*-poly(ethylene oxide) copolymer. In Chapter 4, Ms. Patricia Davidson, an undergraduate student who worked under the direct supervision of the author, is a co-author. Also in Chapter 4, Ms. Jasmina Lovric is a co-author, because she performed the *in vivo* experiments to determine the effectiveness of the estradiol-incorporated polycaprolactone-*block*-poly(ethylene oxide) micelles. For Chapter 5, Dr. Stanislav N. Sidorov is a co-author, because he prepared and characterized some of the gold labeled poly(4-vinylpyridine)-*block*-poly(ethylene oxide) micelles. Also in Chapter 5, Dr. Lyudmila M. Bronstein is a co-author, as she provided useful suggestions and comments to the chapter. In addition, in Chapter 5, Dr. Hojatollah Vali is a co-author, because he performed some of the transmission electron microscopy experiments with the author. Also in Chapter 5, Ms. Jeannie Mui is a co-author, because she prepared some of the samples for transmission electron microscopy. Dr. Amira Choucair is a co-author in Chapter 6, as she performed the loading experiments of doxorubicin into the polystyrene-*block*-poly(acrylic acid) vesicles. Other than the aforementioned contributions to the chapters, the author performed all of the work presented in this dissertation.

## Acknowledgements

Dr. Adi Eisenberg, thank you for your supervision, guidance, advice and enthusiasm throughout my thesis! I also appreciate the uncompromising confidence you had in my abilities when even I had my doubts. I am a better scientist and researcher because of your teachings. I will always be grateful for the opportunity that you have given me by allowing me to join your group, and I hope that I have performed admirably.

Dr. Dusica Maysinger, thank you for your support and guidance on many of the projects in the thesis. I appreciate the opportunity to learn the field of pharmacology from you. I enjoyed all of our meetings and discussions together and I have learned a tremendous amount from you.

Dr. Hojatollah Vali, thank you for all of your teachings on the TEM, I have learned so much during our sessions together. I appreciate your honesty and our scientific discussions together.

Dr. Lyudmila M. Bronstein, thank you for the opportunity to collaborate with you on two of the projects together. I was constantly amazed at how quickly and efficiently you answered my inquiries and provided input into the drafts of our papers. I appreciate all of your efforts and it was a pleasure.

Dr. Stanislav N. Sidorov (Stas), my comrade, it was a pleasure working with you and I enjoyed our TEM sessions and discussions about Russia. I hope your beer mug is never empty and I will try and wear hats in the winter when it is below  $-20^{\circ}\text{C}$ .

Dr. Christine Allen, my mentor and friend, I will always be grateful for all of your help and support from the very beginning of my career. I will always appreciate our discussions together. Thank you for your kindness and all of your help and advice!

Dr. Owen Terreau, for his friendship, thanks for all of the discussions about chemistry and life in general. You have been a very good friend to me and I appreciate all of the computer help that you have provided me.

Dr. Amira Choucair, for her friendship, thanks for all of your help and for all of our discussions about chemistry and life in general. I am so glad that I was able to find someone to laugh at my jokes and stories. Also thank you for proofreading Chapter 6 of my thesis.

Dr. Nicolas Duxin, for his friendship. I enjoyed our conversations together in the lab. Thank you for translating my Abstract into French. J'apprecie votre aide. Merci!

Dr. Carl Bartels, thanks for all of your help and teachings. Also thanks for drawing the perfect sink apparatus for me in Chapter 3.

Dr. Laibin Luo and Dr. Yisong Yu, thank you both for the synthesis of the block copolymers that I used for my thesis work.

Dr. Derek Grey and Dr. Hanadi Sleiman, thank you both for allowing me to use your respective fluorescence instruments and allowing me to take responsibility for these instruments.

Ms. Jeannie Mui, thanks for all of your help in preparing the TEM samples. You were always very kind and helpful.

Jasmina Lovric, Patricia Davidson and Yue Wang, thanks for your hard work on various aspects of the work in Chapter 4.

Dr. Linda Cooper, thank you for your wonderful Scientific Writing Course in which I learned how to write and present effectively. I am very grateful for having taken this course!

Dr. Andrew Rodenheiser and Dr. Peter McGarry, thank you both for help early on with the fluorescence instrument in Pulp and Paper.

I would also like to thank the various group members that I have had the pleasure of meeting and working with, in the Eisenberg group: Amira, Owen, Nicolas, Susan, Carl, Futian, Laibin, Sachiko, Yisong, Christine, Matthew, Luc, Lifeng, Hongwei, Ga-er, Stas,

Izabel, Michael and Marc. Also to the current group members, I pass the torch for you to hold high and may it continue to burn brightly: Tony, Xiaoya, Xingfu, Jun, Renata and Qinghua.

I would like to also thank my friends at McGill in the Chemistry department: Julie, Catherine, Sandra, John, Petr, Andrew, Mike, Debbie, Rajiv, Kim, Susan, Ozzy, Rashida, Emily, Nicolas, Maria, Vicki, Shane, Kazim, Francois, Sophie, Mohua, Hassan and Victor.

Also thanks to my colleagues up the hill in pharmacology: Joseph and Radoslav.

Also thanks to all the people that I have had the pleasure to work with as a general chemistry TA, Dr. Anne Noronha, Badawai, Michel and Jean-Marc!

Thanks to the various staff in Otto Maass who have helped me: Chantal, Paulette, Sandra, Carol, Fay, Renee, Rick and Fred.

Thank you to McGill University for the Alma Travel Student Grants and thank you to the McGill Chemistry Department for the Robert Zamboni Prizes; both prizes have allowed me to attend conferences all over Canada and the US.

Finally, I am eternally grateful to the love and support that I have received from my dearest Mom and Dad, my caring sister, Sandra and my strong and confident brother, Derek. You have always been there for me and I cannot thank you enough. Thanks to my family: aunts and uncles, godmother, cousins (Dean, Caroline, Allen, Lucinda, Lenny) for your support and encouragement. Thanks to all of my good friends: Eric Mahannah, David Roy, Patrick Tea, Mark Eley, Joyce Hung, Marilyn Leung, Corine Lin and Numidia Tam, you provided balance to my life and dragged me out of the lab, my "second home".

Last thank you to any of those people that I might have inadvertently missed, you know who you are, thank you!

# Table of Contents

<b>Abstract</b> .....	ii
<b>Résumé</b> .....	iii
<b>Foreword</b> .....	iv
<b>Acknowledgements</b> .....	xx
<b>Table of Contents</b> .....	xxiii
<b>List of Tables</b> .....	xxviii
<b>List of Figures</b> .....	xxix
<b>Abbreviations</b> .....	xxxiii
<b>Chapter 1. General Introduction</b> .....	1
1.1. Introduction.....	1
1.2. Drug Delivery .....	2
1.2.1. Drug Targeting.....	3
1.2.2. Routes of Elimination from the Body.....	4
1.2.3. Different Types of Drug Delivery Vehicles.....	5
1.3. Polymers .....	7
1.3.1. Synthesis of Block Copolymers.....	9
1.4. Amphiphilic Block Copolymer Micelles in Drug Delivery.....	9
1.4.1. Hydrophobic Core.....	10
1.4.1.1. Polycaprolactone.....	11
1.4.2. Hydrophilic Corona.....	12
1.4.2.1. Poly(ethylene oxide).....	13
1.4.2.2. Poly(acrylic acid).....	14
1.4.3. Preparation and Drug Loading of Block Copolymer Micelles .....	14
1.4.4. Properties of Block Copolymer Micelles.....	16
1.4.4.1. Micellar Size and Distribution.....	17
1.4.4.2. Micelle Stability.....	18
1.4.4.3. Partition Coefficient.....	19
1.4.4.4. Drug Loading in Block Copolymer Micelles.....	20
1.4.4.5. Release from Block Copolymer Micelles .....	22

1.4.4.6. Cellular Internalization .....	22
1.5. Characterization of Block Copolymer Aggregates .....	22
1.5.1. Fluorescence Spectroscopy .....	23
1.5.2. Transmission Electron Microscopy .....	24
1.5.3. Energy Dispersive Spectroscopy .....	26
1.5.4. Dynamic Light Scattering .....	27
1.6. Scope of the Thesis .....	28
1.7. References.....	30
<b>Chapter 2. Preparation of Block Copolymer Vesicles in Solution .....</b>	<b>37</b>
2.1. Abstract .....	37
2.2. Introduction.....	38
2.3. Copolymer Composition and Concentration.....	41
2.4. Water Content and Nature of Common Solvent .....	44
2.5. Temperature .....	47
2.6. Additives (Ions, Surfactants, and Homopolymer) .....	47
2.7. Polydispersity.....	50
2.8. Thermodynamics of Curvature Stabilization in Vesicles .....	51
2.9. Kinetics of Vesicle Size Changes .....	55
2.10. Other Bilayer Morphologies .....	56
2.11. Copolymer Systems Producing Vesicles .....	58
2.12. Other Vesicle Forming Self-Assembled Amphiphilic Systems.....	64
2.13. Hollow Spheres.....	66
2.14. Conclusions.....	67
2.15. Acknowledgement .....	69
2.16. References.....	69
<b>Chapter 3. Incorporation and Release of Hydrophobic Probes in Biocompatible Polycaprolactone-<i>block</i>-poly(ethylene oxide) Micelles: Implications for Drug Delivery .....</b>	<b>76</b>
3.1. Abstract .....	76
3.2. Introduction.....	77

3.3. Experimental Section .....	84
3.3.1. Materials .....	84
3.3.2. Sample Preparation for Loading and Release Kinetics.....	84
3.3.3. Sample Preparation for Partition Coefficient Determination between PCL <sub>23</sub> - <i>b</i> -PEO <sub>45</sub> Micelles and a DMF/H <sub>2</sub> O Solvent Mixture .....	85
3.3.4. Fluorescence Measurements for Loading and Release Kinetics....	85
3.3.5. Release of Fluorescent Probes from PCL <sub>23</sub> - <i>b</i> -PEO <sub>45</sub> Micelles.....	86
3.4. Results and Discussion .....	88
3.4.1. Loading .....	88
3.4.2. Partition Coefficients .....	93
3.4.3. Release Kinetics.....	99
3.5. Conclusions.....	106
3.6. Acknowledgement .....	108
3.7. References.....	108
3.8. Appendix.....	113

#### **Chapter 4. Polycaprolactone-*block*-poly(ethylene oxide) Micelles: A Nano-delivery**

<b>System for 17<math>\beta</math>-estradiol.....</b>	<b>119</b>
4.1. Abstract .....	119
4.2. Introduction.....	120
4.3. Experimental Section .....	122
4.3.1. Materials .....	122
4.3.2. Preparation of PCL- <i>b</i> -PEO micelles with E2 for Loading and Release Studies. ....	123
4.3.3. Fluorescence Measurements for Loading and Release Experiments .....	124
4.3.4. Release of E2 from PCL- <i>b</i> -PEO Micelles .....	124
4.3.5. Transmission Electron Microscopy (TEM) .....	125
4.3.6. Dynamic Light Scattering (DLS).....	126
4.3.7. Assessment of Effectiveness of PCL <sub>23</sub> - <i>b</i> -PEO <sub>45</sub> Micelles Containing the E2 <i>In Vivo</i> .....	126
4.4. Results and Discussion .....	127

4.4.1. Loading Properties of E2 in PCL- <i>b</i> -PEO Micelles.....	127
4.4.2. PCL- <i>b</i> -PEO Morphology and Size .....	134
4.4.3. Release Kinetics of E2 from PCL- <i>b</i> -PEO Micelles.....	136
4.4.4. Biological Effectiveness of PCL <sub>23</sub> - <i>b</i> -PEO <sub>45</sub> Micelles Containing E2 .....	143
4.5. Conclusions.....	143
4.6. Acknowledgement .....	145
4.7. References.....	145
4.8. Appendix.....	150

<b>Chapter 5. Internalization of Gold Labeled Poly (4-vinylpyridine)-<i>block</i>- poly(ethylene oxide) Copolymers into Cell Lines.....</b>	<b>153</b>
5.1. Abstract.....	153
5.2. Introduction.....	154
5.3. Experimental Section .....	157
5.3.1. Synthesis of P4VP <sub>21</sub> - <i>b</i> -PEO <sub>45</sub> Copolymer .....	157
5.3.2. Preparation of Gold Labeled P4VP <sub>21</sub> - <i>b</i> -PEO <sub>45</sub> Micelles.....	158
5.3.3. Characterization of the Gold Labeled Micelles .....	159
5.3.3.1. UV-Vis.....	159
5.3.3.2. Dynamic Light Scattering (DLS).....	159
5.3.3.3. Transmission Electron Microscopy (TEM) .....	159
5.3.4. Treatment of Cells with Gold Labeled Micelles.....	160
5.3.4.1. Cell Types .....	160
5.3.4.2. MTT Assay .....	160
5.3.4.3. Transmission Electron Microscopy .....	160
5.3.4.4. Energy Dispersive Spectrometry (EDS) .....	161
5.4. Results and Discussion .....	161
5.4.1. Gold Labeled Micelles.....	161
5.4.2. MTT Assay .....	165
5.4.3. Internalization of Gold Labeled Micelles into A549 Cells.....	167
5.4.4. Internalization of Gold Labeled Micelles into HEK 293 cells.....	169
5.4.5. Aggregation of Gold Labeled Micelles.....	172

5.5. Conclusions.....	173
5.6. Acknowledgement .....	174
5.7. References.....	175
5.8. Appendix.....	179

## **Chapter 6. Active Loading and Tunable Release of Doxorubicin from Block**

<b>Copolymer Vesicles.....</b>	<b>184</b>
6.1. Abstract.....	185
6.2. Introduction.....	185
6.3. Experimental Section.....	188
6.3.1. Materials .....	188
6.3.2. Preparation of PS <sub>310</sub> - <i>b</i> -PAA <sub>36</sub> Vesicles .....	188
6.3.3. Active Loading of Doxorubicin Hydrochloride into Vesicles.....	189
6.3.4. Determining the Ethylbenzene-Water Partition Coefficient.....	190
6.3.5. Determining the Interaction of DXR with Poly(acrylic acid).....	191
6.3.6. Transmission Electron Microscopy .....	191
6.3.7. Release of DXR from the Vesicles under Sink Conditions.....	191
6.4. Results and Discussion .....	192
6.4.1. Loading of DXR as a Function of Dioxane Content.....	192
6.4.2. Determining the Internal Concentration of Doxorubicin.....	196
6.4.3. Estimating the Interactions of DXR with PS and with PAA .....	199
6.4.4. Release of DXR from the Vesicles .....	200
6.5. Conclusions.....	205
6.6. Acknowledgement .....	206
6.7. References.....	206
6.8. Appendix.....	210

## **Chapter 7. Conclusions, Contributions to Original Knowledge and Suggestions for**

<b>Future Work.....</b>	<b>224</b>
7.1. Conclusions and Contributions to Original Knowledge .....	224
7.2. Suggestions for Future Work.....	227
7.3. References.....	231

## List of Tables

<b>Table 1.1.</b> Different types of drug delivery vehicles.....	5
<b>Table 1.2.</b> Examples of different types of hydrophobic polymers used as the core of the micelle.....	11
<b>Table 1.3.</b> Critical micelle concentrations of biocompatible block copolymers micellar systems.....	19
<b>Table 1.4.</b> Illustrative examples of block copolymer micelle systems and incorporated drugs. ....	21
<b>Table 2.1.</b> Formation of block copolymer vesicles in the presence of different additives.....	48
<b>Table 2.2.</b> Bilayer morphologies structurally related to vesicles obtainable from the block copolymer systems. ....	57
<b>Table 4.1.</b> Loading properties of E2 in PCL <sub>23</sub> - <i>b</i> -PEO <sub>45</sub> micelles. ....	130
<b>Table 4.2.</b> Loading properties of E2 in different PCL <sub><i>x</i></sub> - <i>b</i> -PEO <sub>44</sub> micelles.....	132
<b>Table 4.3.</b> Determination of uterine weight in mice after 1 week treatment.....	143
<b>Table 6.1.</b> Concentrations of DXR in the vesicle samples and controls.....	197

## List of Figures

<b>Figure 1.1.</b> Controlled release profile of a drug after administration.....	2
<b>Figure 1.2.</b> Different types of polymers.....	8
<b>Figure 1.3.</b> Functions of the components of block copolymer micelles in drug delivery. ....	16
<b>Figure 1.4.</b> Jablonski diagram showing fluorescence. ....	23
<b>Figure 1.5.</b> Schematic diagram of a transmission electron microscope (TEM).....	25
<b>Figure 2.1.</b> Representative micrographs of various types of vesicles: (A) small uniform vesicles (PS <sub>410</sub> - <i>b</i> -PAA <sub>13</sub> ), (B) large polydisperse vesicles (PS <sub>100</sub> - <i>b</i> -PEO <sub>30</sub> ), (C) entrapped vesicles (PS <sub>200</sub> - <i>b</i> -PAA <sub>20</sub> ), (D) hollow concentric vesicles (PS <sub>132</sub> - <i>b</i> -PAA <sub>20</sub> ), (E) onions (PS <sub>260</sub> - <i>b</i> -P4VPDecI <sub>70</sub> ), and (F) vesicles with tubes in the wall (PS <sub>100</sub> - <i>b</i> -PEO <sub>30</sub> ). ....	41
<b>Figure 2.2.</b> Segregation in PS <sub>300</sub> - <i>b</i> -PAA <sub>44</sub> copolymer vesicles. The fraction of the pyrene (Py) molecules that are quenched ( $\phi$ ) increases with the length of the PAA segments of the labeled PS-Py- <i>b</i> -PAA copolymer. ....	52
<b>Figure 2.3.</b> Reversibility of vesicle sizes in response to increasing or decreasing water contents for PS <sub>300</sub> - <i>b</i> -PAA <sub>44</sub> vesicles in a THF/dioxane (44.4/55.6) solvent mixture. ....	53
<b>Figure 2.4.</b> Possible mechanisms of (A) the fusion of vesicles and (B) the fission of a vesicle. ....	54
<b>Figure 2.5.</b> Examples of kinetic measurements for increases in the vesicle size in solutions of 0.5 wt % PS <sub>310</sub> - <i>b</i> -PAA <sub>36</sub> after successive 5% increases in the water content.....	55
<b>Figure 2.6.</b> Other examples of amphiphilic systems that produce vesicle structures. ....	65
<b>Figure 3.1.</b> Diagram of the experimental setup used for the release profile experiments under “perfect sink” conditions. ....	87
<b>Figure 3.2.</b> Amount of Dil and benzo[a]pyrene loaded into PCL <sub>21</sub> - <i>b</i> -PEO <sub>44</sub> micelles as a function of the amount of probe per polymer added.....	88

<b>Figure 3.3.</b> Loading efficiencies of DiI and benzo[a]pyrene incorporated into PCL <sub>21</sub> - <i>b</i> -PEO <sub>44</sub> micelles. Horizontal dotted lines represent slopes of lines from Figure 3.2. ....	90
<b>Figure 3.4.</b> Influence of block copolymer concentration (logarithmic scale) on fluorescence intensity (I) of (a) benzo[a]pyrene at 80% H <sub>2</sub> O/20% DMF and (b) DiI at 60% H <sub>2</sub> O/40% DMF. I <sub>0</sub> is the fluorescence in the absence of polymer, I <sub>max</sub> is the fluorescence at saturating conditions of polymer. The line of best fit is meant as only as a guide for the eye. ....	95
<b>Figure 3.5.</b> Partition coefficient determination of (a) benzo[a]pyrene at 80% H <sub>2</sub> O/20% DMF and (b) DiI at 60% H <sub>2</sub> O/40% DMF. ....	97
<b>Figure 3.6.</b> Partition coefficient determination of DiI and benzo[a]pyrene extrapolated to 100% water. For DiI, the plot extrapolates to a value of 5800 on the left y-axis. For benzo[a]pyrene, the plot extrapolates to a value of 690 on the left y-axis. ....	98
<b>Figure 3.7.</b> Diffusional release of benzo[a]pyrene: 14 μM (▲) and 89 μM (●) from PCL <sub>23</sub> - <i>b</i> -PEO <sub>45</sub> micelles (0.6% (w/w) polymer solution). Line of best fit suggests diffusional release, not including the initial burst release and the behavior near 100% release. ....	100
<b>Figure 3.8.</b> Diffusional release of DiI: 12 μM (▲) and 54 μM (●) from PCL <sub>23</sub> - <i>b</i> -PEO <sub>45</sub> micelles (0.6% (w/w) polymer solution). Line of best fit is through the diffusional release, not including the initial burst release and the release near 100% completion. The dotted lines for 12 μM (▲) represent the line of best fit through two sections of possibly diffusional release with two different coefficients. ....	101
<b>Figure 4.1.</b> Loading efficiency (a) and drug content (b) of E2 in PCL <sub>23</sub> - <i>b</i> -PEO <sub>45</sub> micelles. Straight line only meant to serve as a guide for the eye. ....	129
<b>Figure 4.2.</b> Dependence of loading efficiency of E2 on the block length of polycaprolactone in PCL <sub>x</sub> - <i>b</i> -PEO <sub>44</sub> micelles. ....	132
<b>Figure 4.3.</b> (a) Transmission electron microscopy of E2 (conc. 2 mM) in PCL <sub>23</sub> - <i>b</i> -PEO <sub>45</sub> micelles. Size range is 30 ± 7 nm. (b) Dynamic light scattering of E2 (conc. 3 mM) in PCL <sub>23</sub> - <i>b</i> -PEO <sub>45</sub> micelles. Average diameter is 33 nm. ....	135

<b>Figure 4.4.</b> Release of E2 (3 mM (●) and 35 mM (▲)) from PCL <sub>23</sub> - <i>b</i> -PEO <sub>45</sub> micelles under “perfect sink” water conditions. ....	137
<b>Figure 4.5.</b> The fit of the release data to the Higuchi model using two different estradiol concentrations: 3 mM (●) and 35 mM (▲) under “perfect sink” water conditions. The linearity of the line of best fit is indicative of a diffusional release mechanism. The assumption is that the average diameter of the micelle is 25 nm. ....	138
<b>Figure 4.6.</b> Release of E2 (35 mM) from PCL- <i>b</i> -PEO micelles with different PCL lengths: PCL <sub>151</sub> (●) and PCL <sub>23</sub> (▲) under “perfect sink” water conditions. The linearity of the line of best fit is indicative of a diffusional release mechanism. The assumption is that the average diameter of the micelle is 25 nm.....	140
<b>Figure 5.1.</b> UV-Vis spectra of the P4VP <sub>21</sub> - <i>b</i> -PEO <sub>45</sub> copolymer micelles (____) and gold labeled P4VP <sub>21</sub> - <i>b</i> -PEO <sub>45</sub> micelles (____). ....	162
<b>Figure 5.2.</b> Transmission electron microscopy images of gold labeled micelles with an original magnification of (a) 170,000x and (b) 210,000x, both stained with uranyl acetate. ....	163
<b>Figure 5.3.</b> Histogram of the gold particle in each micelle from TEM.....	164
<b>Figure 5.4.</b> Dynamic light scattering data of gold labeled micelles analyzed using Contin analysis by number.....	165
<b>Figure 5.5.</b> MTT assay: Incubation of gold labeled micelles of 0.73 μg/mL in HEK 293 cells and lung A549 cells after 24 hours.....	166
<b>Figure 5.6.</b> Composite TEM images of gold labeled micelles (0.73 μg/mL) internalized into different organelles of the lung A549 cells for 24 hours: (a) original magnification 21,000x, (b) original magnification 21,000x, (c) original magnification 100,000x, and (d) original magnification 250,000x. Symbols are represented as follows: cellular membrane (CM), endosome (E), golgi apparatus (G), entry point (I), lysosome (L), mitochondria (M) and invagination (V). ....	168
<b>Figure 5.7.</b> TEM images of gold labeled micelles (0.32 μg/mL) internalized into different organelles of the HEK 293 cells after 24 hours incubation with original magnification (a) 50,000x and (b) 100,000x.....	170

<b>Figure 5.8.</b> Energy dispersive spectrometry of gold labeled micelles (0.32 $\mu\text{g/mL}$ ) (inset) located inside of the HEK 293 cell after 24 hours incubation (original magnification 100,000x) showing an Au band. ....	172
<b>Figure 6.1.</b> Extent of incorporation of doxorubicin hydrochloride (DXR) in $\text{PS}_{310}\text{-}b\text{-PAA}_{36}$ vesicles as a function of the dioxane content in solution. ....	194
<b>Figure 6.2.</b> TEM image of $\text{PS}_{310}\text{-}b\text{-PAA}_{36}$ vesicles loaded with DXR using a pH gradient at 22% dioxane/78% water content. Initial polymer concentration is 0.5 % (w/w). Internal concentration of the drug is approximately 0.19 M. ....	198
<b>Figure 6.3.</b> Release profile of DXR (240 $\mu\text{M}$ ) from $\text{PS}_{310}\text{-}b\text{-PAA}_{36}$ vesicles (0.08% (w/w)) present in 0%/100% dioxane/water (●), 25%/75% dioxane/water (▲) and 50%/50% dioxane/water (■) mixtures. ....	201
<b>Figure 6.4.</b> The fit of the release data to the Higuchi model in different dioxane/water mixtures. The linearity of the line of best fit is indicative of a diffusional release mechanism. ....	203

## List of Abbreviations

A549	Human lung carcinoma
ATR-IR	Attenuated total reflectance-infrared
BSA	Bovine serum albumin
CMC	Critical micelle concentration
CM-DiI	Cell Tracker DiI
CWC	Critical water concentration
DDV	Drug delivery vehicle
DiI	Cell-Tracker CM-DiI
DHT	Dihydrotestosterone
DLS	Dynamic light scattering
DMEM	Dulbecco's modification of Eagle's minimal essential medium
DMF	Dimethylformamide
DMSO	Dimethyl sulfoxide
DSC	Differential scanning calorimetry
DXR	Doxorubicin hydrochloride
E2	17 $\beta$ -estradiol or estradiol
EDS	Energy dispersive spectroscopy
ELISA	Enzyme linked immunosorbent assay
FDA	Food and Drug Administration
FQRNT	Fonds Québécois de la recherche sur la nature et les technologies
FTIR	Fourier transform infrared
HEK 293	Human embryonic kidney
HPLC	High performance liquid chromatography
IV	Intravenous
K <sub>v</sub>	Partition coefficient
LCM	Large compound micelle
LCV	Large compound vesicle
MF	Melamine formaldehyde
MRI	Magnetic resonance imaging
MSR	Molar solubilization ratio
MTT	3-[4,5-dimethylthiazol-2yl]-2,5-diphenyltetrazolium bromide)
MWCO	Molecular weight cut off
N <sub>agg</sub>	Aggregation number
NMR	Nuclear magnetic resonance
NSERC	Natural Sciences and Engineering Research Council of Canada
oMMA	oligo(methyl methacrylate)
P2VP	Poly(2-vinylpyridine)
P4AMS	Poly[4-(aminomethyl)-styrene]
P4VP	Poly(4-vinylpyridine)
P4VP- <i>b</i> -PEO	Poly(4-vinylpyridine)- <i>b</i> -poly(ethylene oxide)

PAA	Poly(acrylic acid)
PAH	Poly(allylamine hydrochloride)
PBA	Poly( <i>tert</i> -butyl acrylate)
PBLA	Poly( $\beta$ -benzyl-L-aspartate)
PBLG	Poly( $\beta$ -benzyl-L-glutamate)
PBMA	Poly(butyl methacrylate)
PB	Poly(1,2-butadiene)
PBO	Poly(butylene oxide)
PBS	Phosphate-buffered saline
PC	Phosphatidylcholine
PC12	Rat adrenal pheochromocytoma
PCEMA	Poly(2-cinnamoyl ethyl methacrylate)
PCL	Polycaprolactone
PCL- <i>b</i> -PEO	Polycaprolactone- <i>b</i> -poly(ethylene oxide)
PDI	Polydispersity index
PDMS	Poly(dimethylsiloxane)
PEE	Poly(ethyl ethylene)
PEG	Poly(ethylene glycol)
PEO	Poly(ethylene oxide)
PEO- <i>b</i> -PPO- <i>b</i> -PEO	Pluronic (Poly (ethylene oxide)- <i>b</i> -poly(propylene oxide)- <i>b</i> -poly(ethylene oxide))
PEtOz	Poly(2-ethyl-2-oxazoline)
PGA	Poly(L-glutamic acid)
PI	Polyisoprene
PIAA	Poly(isocyano-L-alanine-L-alanine)
PIPAAm	Poly(N-isopropylacrylamide)
PLA	Poly(D,L-lactide)
PLGA	Poly(lactic- <i>co</i> -glycolide)
PMA	Poly(methacrylic acid)
PM4VPI	Poly(1-methyl-4-vinylpyridinium iodide)
PMOXA	Poly(2-methyloxazoline)
PPO	Poly(propylene oxide)
PPO- <i>b</i> -PEO	Poly(propylene oxide)- <i>b</i> -poly(ethylene oxide)
PPQ	Poly(phenylquinoline)
PS	Polystyrene
PSS	Poly(styrene sulfonate sodium)
PS- <i>b</i> -P4VP	Polystyrene- <i>b</i> -poly(4-vinylpyridine)
PS- <i>b</i> -PAA	Polystyrene- <i>b</i> -poly(acrylic acid)
PS- <i>b</i> -PEO	Polystyrene- <i>b</i> -poly(ethylene oxide)
PTMC	Poly(1,3-trimethylene carbonate)
PVP	Poly( <i>N</i> -vinyl-2-pyrrolidone)
RES	Reticuloendothelial system
RPMI	Roswell Park Memorial Institute

SDS	Sodium dodecyl sulfate
TEM	Transmission electron microscope
$T_g$	Glass transition temperature
THF	Tetrahydrofuran
$T_m$	Melting temperature

*Dedicated to my loving and understanding parents,  
Henry and Marie-Claude Lim Soo  
for all of their tremendous support,  
encouragement and teachings.*

*"The most exciting phrase to hear in science, the one that heralds new discoveries, is not "Eureka!" (I've found it!), but "That's funny..."*

*Isaac Asimov*

*"When you come to the edge of all the light you know and are about to step into the darkness of the unknown, faith is knowing that one of two things will happen: There will be solid ground to stand on or you will be taught to fly."*

*Barbara J. Winter*

*"The woods are lovely, dark and deep.  
But I have promises to keep,  
and miles to go before I sleep.*

*Robert Frost*

# Chapter 1

---

---

## General Introduction

---

---

### 1.1. Introduction

This thesis describes the investigation of the physico-chemical characteristics of block copolymer systems developed for various drug delivery applications. Three different amphiphilic copolymer drug delivery systems are examined: one is based on a biodegradable and biocompatible carrier, and two on model systems. The biodegradable drug delivery carrier is a polycaprolactone-*block*-poly(ethylene oxide) copolymer that self assembles to form spherical aggregates, which can incorporate hydrophobic drugs. The two model systems consist of the polystyrene-*block*-poly(acrylic acid) and poly(4-vinylpyridine)-*block*-poly(ethylene oxide) copolymers. The former self assembles to form vesicular aggregates that can incorporate both hydrophobic and hydrophilic drugs. The latter self assembles to form spherical aggregates, which can be labeled with gold if one wishes to investigate the cellular internalization of the aggregates in different cell types.

This introductory chapter is divided into six sections and provides preliminary background to the work presented in this thesis. In section 1.2, an introduction to drug delivery and the different types of drug delivery vehicles is given. An overview of polymers and block copolymers is presented in section 1.3. The properties of block copolymer micelles relevant to drug delivery and a review of the use of block copolymer micelles in drug delivery are the subject of section 1.4. In section 1.5, a discussion of

some of the techniques used to characterize the block copolymer aggregates is provided. Finally the scope of the thesis is given in section 1.6.

## 1.2. Drug Delivery

The term drug delivery vehicle (DDV) implies that a carrier or a vehicle is used to deliver a drug to the designated target region. Using conventional delivery methods (i.e., pills, injection etc.), each time a drug is administered, there is an increase in the drug concentration until it peaks and then eventually declines.<sup>1</sup> Also the amount of drug present in the blood can be too high, resulting in toxicity, or too low, resulting in an ineffective dose. Ideally, the drug concentration should be constant (solid line) and between the toxic level and the minimum therapeutic level as seen in Figure 1.1.

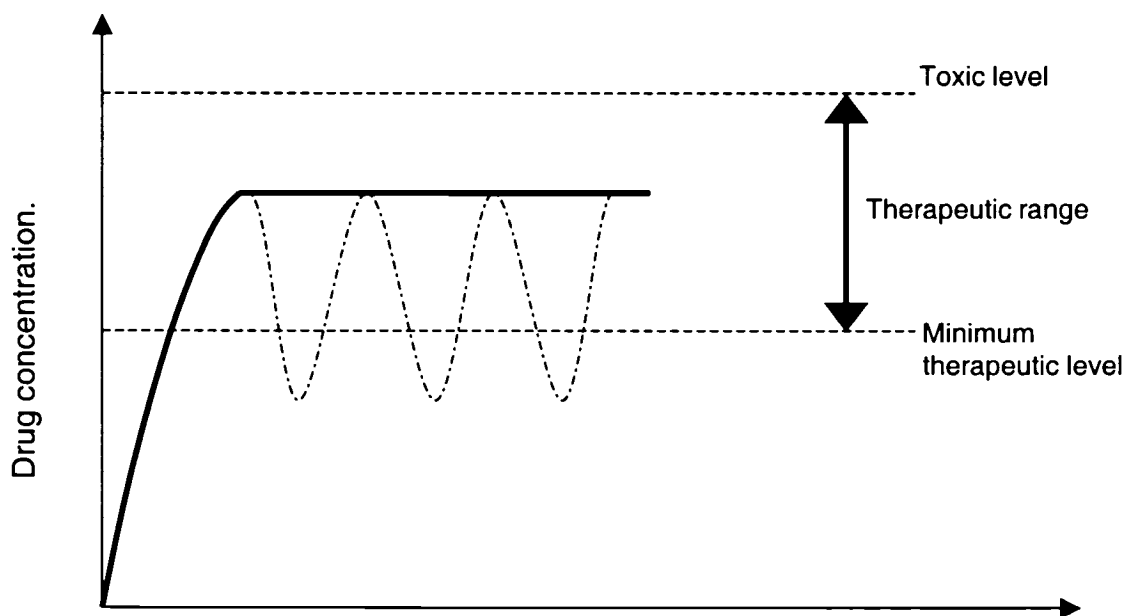


**Figure 1.1.** Controlled release profile of a drug after administration.

A typical pattern resulting from the repeated administration of the drug (dot-dash line) is also shown in Figure 1.1. Ideally, the number of doses should be minimized to improve patient comfort.

Traditional ways of administering a drug such as oral (e.g., tablets, pills and capsules), transdermal (e.g., ointments, creams) and intravenous, intramuscular or subcutaneous (e.g., needles) delivery have been used for many years. However with the development of new types of drugs (e.g., proteins and peptides) and the anticipated complications associated with them, there is a greater need for drug delivery vehicles. There are a number of advantages to using a drug delivery vehicle: 1) Such a carrier can reduce the toxicity and harmful side-effects of some drugs to non-targeted locations in the body. 2) A DDV can protect drugs from degradation prior to reaching its intended target. 3) Targeting moieties can be attached to the carrier in order to help deliver the drug to the intended target. 4) A DDV would help to maintain the drug level in a therapeutically desired range by providing controlled and sustained release. 5) A reduction in the number of doses leading to improved patient compliance is possible with a carrier.<sup>2</sup> 6) From a business perspective, since drug patents held by pharmaceutical companies have a limited lifetime, improvements resulting from the development of new DDVs allow for extension of the patent coverage on these drugs.<sup>3</sup>

### 1.2.1. Drug Targeting

As mentioned in the previous section, one of the potential advantages in drug delivery is the ability to target the desired region. The idea of drug targeting originated approximately 100 years ago from Paul Ehrlich who postulated that there was a need for a “magic bullet” to improve the drug delivery in the body.<sup>4</sup> Drugs can be targeted to

specific sites in the body by two general methods: active and passive targeting. Active targeting utilizes specific biological interactions (e.g., antibody-antigen or ligand-receptor binding) or locally applied external physical signals (e.g., sonication, heating or a magnetic field) to increase delivery of drug to target.<sup>5</sup> Passive targeting aims to increase the targeted to non-targeted ratio of delivered drugs in order to minimize the non-specific interactions with non-target cells, tissues and organs.<sup>6</sup> The delivery vehicles in passive targeting tend to use physical factors such as size and molecular weight, or chemical interactions such as hydrophobic and electrostatic effects.<sup>5</sup> Foreign bodies usually end up in the liver and spleen after they have been cleared by the reticuloendothelial system (RES). This actually represents a form of passive targeting, and is especially useful if the liver and spleen are the intended targets, since these organs usually serve as a natural route of elimination of foreign materials from the body.<sup>7</sup>

### 1.2.2. Routes of Elimination from the Body

There are two major routes of elimination from the body for foreign particles: renal excretion and uptake by the RES. Evasion of renal excretion is not a major concern for DDVs if they are larger than a certain size. Renal excretion of a drug can be avoided by conjugating the drug to a polymeric carrier or incorporation of the drug into either liposomes or microspheres.<sup>5</sup> A more detailed discussion pertaining for block copolymer micelles is given in section 1.4.4.1. After intravenous (IV) administration, the RES represents the major obstacle for drug delivery systems and serves as a defense mechanism against foreign entities. The RES is primarily composed of Kupffer cells in the liver and fixed macrophages in the spleen which serve to remove the drug carriers from circulation. The RES clearance is regulated by two types of blood components:

opsonins, which promote phagocytosis and dysopsonins, which retard the process. After IV administration, the drug carriers will first encounter the blood components, such as opsonins, which will attempt to interact with the surface of the DDV. When opsonins adhere to the drug carrier, the serum proteins that are involved are fibronectin, immunoglobulin G and complement C3b.<sup>8</sup> These will attract macrophages and phagocytic cells, since they are known to possess receptors for these proteins; thus the drug carriers will be recognized and removed from circulation. The rate and extent of uptake by RES depends on the size of the drug delivery vehicle: the larger the DDV, the faster the uptake.<sup>9</sup> Also RES uptake depends on the surface of the DDV: if it is charged or hydrophobic, proteins will adsorb to the foreign material after a few minutes of exposure in the blood.<sup>7</sup> Once adsorbed to the surface, the protein can damage the DDV, leading to its destruction or leakage of the drug.<sup>10</sup>

### 1.2.3. Different Types of Drug Delivery Vehicles

Currently, there are many different types of DDVs and included references to consult for additional information; some of these are listed in Table 1.1.

**Table 1.1.** Different types of drug delivery vehicles.

<b>Drug delivery vehicle</b>	<b>References</b>
Liposomes	11-13
Hydrogels	14-16
Dendrimers	17-19
Polymer-drug conjugates	20-22
Nanoparticles	23-25
Microparticles	26-28
Surfactant Micelles	29-31
Block Copolymer Aggregates	32-34

## *Chapter 1. General Introduction*

Briefly, liposomes are phospholipid bilayer vesicles that encapsulate an aqueous compartment and are surrounded by an aqueous medium. They are advantageous as drug carriers, because they are highly efficient in encapsulating a variety of molecules; also, their particle size, surface and membrane properties can be tailored.<sup>35</sup> However, because they are composed of phospholipids, they suffer from poor stability, so either the drug is incorporated too strongly or the drug is released too rapidly. In addition, they are taken up by macrophages of the RES even when coated with poly(ethylene glycol), and they are also prone to extravasate into undesired tissues. Hydrogels are made from materials that exhibit the ability to swell in water and retain a large fraction of water or biological fluid due to the presence of hydrophilic groups.<sup>1</sup> They are advantageous as drug carriers, because they resemble biological tissues and have high water contents. However, they are prone to stability problems due to poor mechanical strength. Dendrimers are highly branched and well defined molecules. They are relatively stable because the hydrophilic and hydrophobic segments are covalently attached, which makes them advantageous as drug carriers; also, they have a potential for high drug capacity. However, they suffer from rapid clearance in the RES. Polymer-drug conjugates are advantageous because when designing the carrier, the choice of the type of polymer used and the linkage that attaches the drug to the polymer can be selected. However, the drug loading capacity tends to be lower, and the polymer-drug conjugates can be difficult to characterize.<sup>22</sup>

Nanoparticles are drug carriers that typically range in size from 10-1000 nm. They can be made from different polymer systems and have the capacity to load a variety of drugs with high efficiency. However, their larger size makes them susceptible for uptake by RES. Similarly, microparticles are drug carriers that range in size from 1-2000

$\mu\text{m}$  and have similar advantages and disadvantages as nanoparticles. Surfactants are amphiphilic molecules composed of both a hydrophobic and hydrophilic component that self assemble to form micelles in water. They are easy to prepare and can increase the solubility of hydrophobic compounds; however, they have lower drug loading capacities and relatively poor stability.

The previous section presented a brief comparison of the advantages and disadvantages of the different drug delivery systems. As mentioned previously, the thesis focuses exclusively on the use of block copolymer aggregates (micelles and vesicles) as drug delivery systems. Block copolymer micelles are frequently compared with nanoparticles, surfactant micelles and polymer drug conjugates that can also form micelles, whereas block copolymer vesicles are often compared to liposomes. In the following sections, in addition to a review of the use of block copolymer micelles in drug delivery, comparisons will be made with some of the drug delivery systems listed in Table 1.1.

### **1.3. Polymers**

A monomer is the basic unit or building block of a polymer, which is composed of a number of these monomer (or repeat) units that are covalently attached. When all the repeat units in the polymers are exactly the same, the resulting chain is called a homopolymer. If more than one type of repeat unit is involved, then a copolymer is formed. There are many different types of copolymers, as can be seen in Figure 1.2.

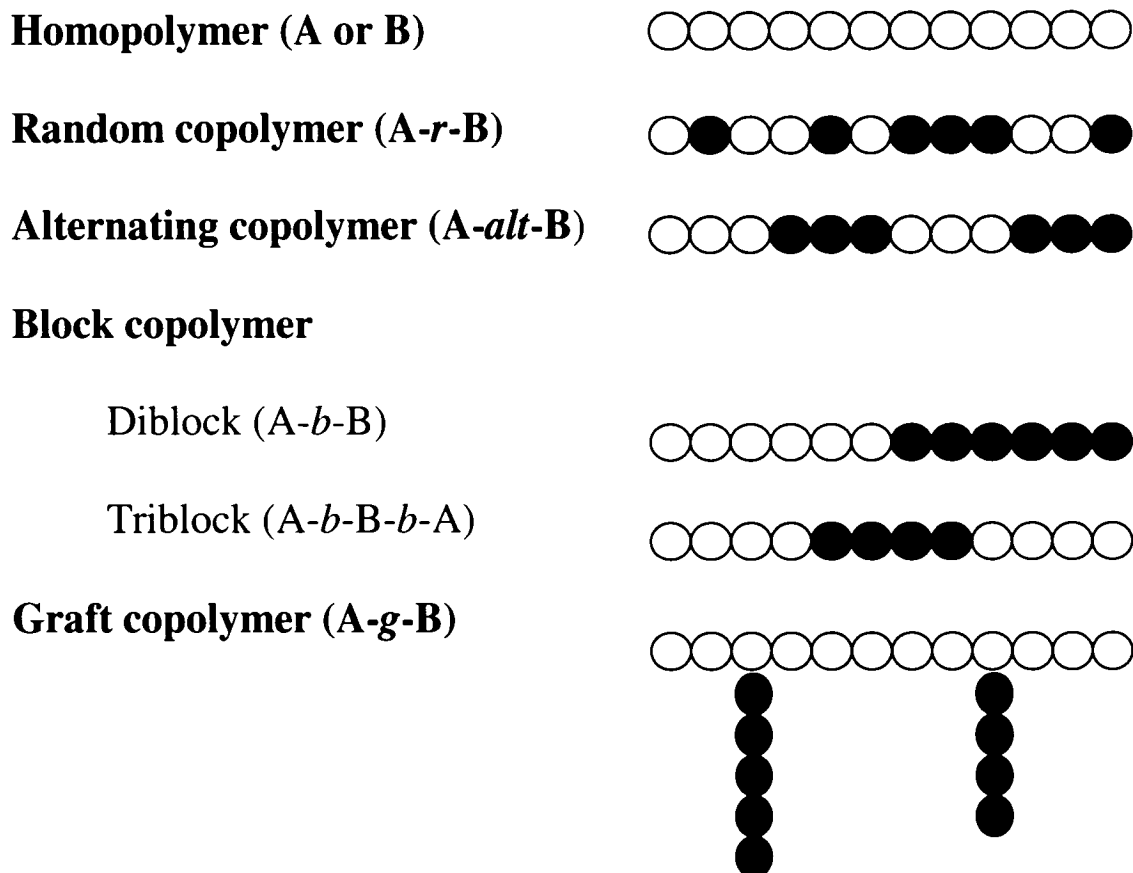


**Figure 1.2.** Different types of polymers.

A random copolymer is one in which the different repeat units are attached in a statistical sequence. This is in contrast to the alternating copolymer, which consists of different units connected in an alternating order. Similarly, a block copolymer consists of units which are attached in a sequence followed by a sequence of different units. If yet another sequence of different units is added, then a triblock copolymer (A-B-A or A-B-C) can be formed. Finally a graft copolymer is composed of a series of units connected as side chains to the backbone of another polymer.

### 1.3.1. Synthesis of Block Copolymers

Block copolymers are frequently synthesized by anionic polymerization, which is a type of addition polymerization. The addition polymerization reaction occurs in three distinct steps: initiation, propagation and termination.<sup>36</sup> The initiation step consists of the creation of an active center. This leads to the propagation step, in which a monomer unit is repeatedly added to a growing chain. Finally this reaction is stopped in the termination step, when the active center is inactivated by either transfer of the active center or neutralization by impurities such as carbon dioxide, methanol, oxygen or water.<sup>36</sup> For anionic polymerization, if the reaction excludes impurities, then the propagation step continues until the monomer is consumed. The system is considered to be “living”, as coined by Szwarc, because if more monomer was introduced, then the polymerization reaction would continue indefinitely until a termination step is introduced.<sup>36</sup>

Many of the block copolymers used in this thesis are synthesized by living anionic polymerization such as polycaprolactone-*block*-poly(ethylene oxide) which are the subjects of Chapters 3 and 4, poly(4-vinylpyridine)-*block*-poly(ethylene oxide) in Chapter 5, and polystyrene-*block*-poly(acrylic acid) discussed in Chapter 6. Synthetic techniques have greatly expanded the types of block copolymers available.

## **1.4. Amphiphilic Block Copolymer Micelles in Drug Delivery**

Drug delivery is one of the many applications of block copolymer aggregates, which include the applications such as catalysis, pollution control and cosmetics. In the early 1980's, Ringsdorf's group was the first to propose the use of block copolymers as drug delivery vehicles.<sup>37</sup> The term “amphiphilic” refers to a molecule which consists of both a hydrophobic and a hydrophilic segment. Amphiphilic block copolymers, which

contain both hydrophobic and hydrophilic sequences, can self assemble to form micelles, which in aqueous solution are composed of a hydrophobic core and a hydrophilic corona or shell. When the corona block is longer than the core block, then star-like micelles will be formed. These structures are thermodynamically stable due to the very long corona blocks. Crew-cut micelles are formed when the corona block is smaller than the core forming block. Due to their smaller corona blocks, these copolymers can undergo a variety of thermodynamically induced morphological changes under different conditions. A review of the types of morphologies with emphasis on block copolymer vesicles, is given in Chapter 2.

#### 1.4.1. Hydrophobic Core

In drug delivery applications, the hydrophobic core can serve as the reservoir for lipophilic molecules while the corona acts as the interface between the core and the exterior environment. Biodegradable and biocompatible species are chosen for both the hydrophobic and hydrophilic blocks, as discussed in the previous section. Biodegradable polymers are often selected for the design of a drug delivery vehicle, because these polymers degrade into nontoxic oligomers or monomers, which are eventually absorbed into the body and eliminated. The polymers can be degraded either chemically or enzymatically, and the rate of degradation will depend upon the stability of hydrolysable linkages, such as amide esters or urethane groups.<sup>38</sup> A number of hydrophobic polymers used as the core block have been investigated; some examples are shown in Table 1.2.

**Table 1.2.** Examples of different types of hydrophobic polymers used as the core of the micelle.

Hydrophobic polymer	Biodegradable	Biocompatible	References
oligo(methyl methacrylate)	No	Yes	39
Poly(aspartic acid)	Yes	Yes	40
Poly( $\beta$ -benzyl-l aspartate)	Yes	Yes	41
Poly( $\gamma$ -benzyl-l glutamate)	Yes	Yes	42
Polycaprolactone	Yes	Yes	10
Poly(l-histidine)	Yes	Yes	43
Poly(d,l-lactide)	Yes	Yes	44
Poly(propylene oxide)	No	Yes	45
Polystyrene	No	No	46
Poly(1,3-trimethylene carbonate)	No	No	47
Poly(4-vinylpyridine)	No	No	48

#### 1.4.1.1. Polycaprolactone

Polycaprolactone (PCL) is a hydrophobic polymer which is used as the core block in the micellar drug delivery system described in this thesis. It is biodegradable, biocompatible and nontoxic; as a result, it has been used in many biomedical applications such as delivery of contraceptives, controlled release devices, operating sutures, implants, orthopaedic casts and splints. Some of the physical properties of polycaprolactone which make it useful in such applications are the following: it is soluble in organic solvents such as chloroform, benzene, toluene, tetrahydrofuran (THF), dimethylformamide (DMF) and dimethyl sulfoxide (DMSO). PCL is semicrystalline and highly permeable to lipophilic drugs.<sup>1</sup> It has a low glass transition temperature ( $T_g$ ) ( $-60^\circ\text{C}$ ) and a melting temperature ( $T_m$ ) of approximately  $60^\circ\text{C}$ .<sup>49</sup> The  $T_g$  and  $T_m$  are important factors affecting the biodegradability of a polymer. When the temperature is below the  $T_g$  then the polymer is glassy; when the temperature is above the  $T_g$  then the polymer is rubberlike and above its

melting temperature (if it is crystalline), the polymer can become a viscous liquid.<sup>36</sup> The  $T_g$  and  $T_m$  of a polymer are also dependent on its molecular weight, so that both the nature and length of the polymer chain will affect the rate of biodegradation.<sup>50</sup>

PCL has a slow degradation rate compared to other biodegradable polyesters, which would make it more suitable for long term release.<sup>51</sup> However, PCL is compatible with a variety of other polymers, so that it is possible to prepare PCL blends with a variety of properties which shorten the release times.<sup>52</sup> The general mechanism of the degradation of PCL is as follows:<sup>53</sup> simple hydrolysis causes disruption of the primary and secondary structure due to hydrogen bonding and van der Waals forces (chain scission). PCL hydrolyzes to form 6-hydroxyhexanoic acid. There is a loss of mechanical strength caused by the rupture of the covalent bonds which form the polymer backbone. This is followed by a material loss resulting in accelerated water absorption, eventually leading to polymer dissolution.

#### 1.4.2. Hydrophilic Corona

The micellar corona is important for stabilizing the micelle in its aqueous environment, as stated earlier. Many of the hydrophilic polymers that are used in micellar delivery systems are biocompatible. These biocompatible polymers do not interfere with the normal biological functions in the body. Some examples of biocompatible polymers that are used include: poly(ethylene oxide), polyacrylamide, polyhydroxyethylmethacrylate, poly(N-vinyl-2-pyrrolidone) and poly(vinyl alcohol).<sup>54</sup> These polymers are all uncharged and water soluble. Poly(ethylene oxide) tends to be the most attractive hydrophilic block for copolymer systems in biomedical applications; the reasons for this popularity will be discussed in the following section.

1.4.2.1. Poly(ethylene oxide)

Poly(ethylene oxide) (PEO) is chosen as the hydrophilic block due to its unique physical properties; and also because of its ability to improve the stability and extend the circulation lifetime of liposomes and proteins.<sup>55,56</sup> PEO is also a nontoxic polymer that has been approved by the Food and Drug Administration (FDA) for various devices destined for internal use. It has been used as an additive in foods, cosmetics, personal care products and pharmaceuticals. The use of PEO has been extended to the field of micellar drug delivery. Typically, the molecular weights of PEO that are used in block copolymers range from 1000 to less than 12 000 g/mol,<sup>32</sup> and the chain length tends to be equal or greater than that of the core block.<sup>10</sup> PEO is sometimes referred to as poly(ethylene glycol) (PEG). In the literature, PEG refers to molecules with terminal hydroxyl groups on each end and below a molecular weight of 20 000 g/mol while PEO refers to polymers with molecular weights above this value, so that the effects of the end groups can be neglected.<sup>56,57</sup>

PEO is a neutral, crystalline polymer that is highly soluble in water and many organic solvents (e.g., acetone, ethanol, methylene chloride and toluene).<sup>56</sup> Judging from the Flory-Huggins interaction parameter( $\chi$ ), water is a moderately good solvent for PEO.<sup>58</sup> PEO has an interaction parameter with water of  $\sim 0.4-0.5$ , depending on solution conditions. In a good solvent,  $\chi < 0.5$  so that the polymer coil swells due to favourable interaction with the solvent, while in a poor solvent  $\chi > 0.5$ , the polymer solvent interactions are poor and the polymer is collapsed. At the theta point,  $\chi$  is 0.5 and the polymer exists as a Gaussian coil and behaves ideally (no second virial coefficient), hence there is no polymer-solvent interaction.<sup>59</sup>

PEO has the ability to exclude sterically other polymers and proteins (steric stabilization) from the surface of the micelles. PEO prevents the adsorption of plasma proteins, and improves the residence time of the micelles in the blood since the carriers are not removed from circulation by the phagocytic cells of the RES. Also, PEO is a highly hydrated polymer with a large exclusion volume.<sup>58</sup> The PEO chains move rapidly in aqueous solution because they are highly flexible and mobile and this leads to a form of “sweeping” which prevents the approach of other molecules. In addition, PEO is poorly immunogenic, i.e., it does not elicit an immune response.<sup>20</sup> Although it is not biodegradable, it is readily excretable after administration.

#### 1.4.2.2. Poly(acrylic acid)

Poly(acrylic acid) (PAA) is another hydrophilic, biocompatible polymer that is used in copolymer systems. It is a member of the carboxylic acid family and soluble in water, DMF, dioxane, ethanol and methanol.<sup>60</sup> It has bioadhesive properties making it suitable for oral and topical delivery applications, specifically delivery of drugs to eye, nose, mouth, throat or skin where PAA would adhere and then slowly release the drug.<sup>39</sup> PAA has a  $pK_a = 4.75$  in the unneutralised state and a  $pK_a = 5.20$  at 50% neutralization.<sup>61</sup> It is also negatively charged at physiological pH. Surfaces covered with anions, in general, would tend to adsorb less protein than cationic surfaces, because most proteins bear a net negative charge.<sup>54</sup> A neutral or slightly negatively charged surface, e.g., one covered by PAA chains, may prove to be useful as the corona block of the micelle.

#### 1.4.3. Preparation and Drug Loading of Block Copolymer Micelles

Micelles can be prepared by different methods: two of the more popular are the direct dissolution method and the dialysis method.<sup>10</sup> The choice of method is based on

the solubility of the block copolymer in the final solvent, usually water. For amphiphilic block copolymers that are easily soluble in water, the direct dissolution method is used, while the dialysis method is used for block copolymers which are not directly soluble in water. In the direct dissolution method, the copolymer is mixed directly into water or an aqueous solution such as phosphate-buffered saline (PBS). To load a drug using this method, one would simply add the drug directly to the micelle solution. Conversely, an aliquot of drug in a volatile solvent (i.e., acetone) could be added to an empty vial and then the solvent would be allowed to evaporate. The micelle solution could be added to the solid drug in the vial. In the dialysis method, the polymer is first dissolved in a common solvent that is miscible with water, such as DMF or THF. The copolymer solvent mixture is then dialyzed against MilliQ water to form the micelles. During this process, water diffuses into the dialysis bag as the organic solvent diffuses out, and the water content increases inside the bag, results in self-assembly. Drug can be incorporated by dissolving both the drug and the copolymer initially and then dialyzing against MilliQ water. This method tends to increase the drug loading as compared to the direct dissolution method.<sup>62</sup>

In this thesis, the majority of the micelle solutions are prepared using the dialysis method. The drug and the copolymer are dissolved in a suitable solvent and stirred for a period of time. In order to form micelles, water is slowly added to decrease the quality of the mixed solvent for the hydrophobic block. Self-assembly occurs at some critical water concentration (CWC) which is very system specific. Finally, the solution is dialyzed against MilliQ water to remove any remaining organic solvent and excess drug. This results in the formation of an aqueous solution of micelles containing the drug.

The formation of aqueous solutions of block copolymer vesicles containing drug is also discussed in this thesis. Vesicles are hollow spherical structures that contain an aqueous cavity in the interior. An extensive review of the preparation of block copolymer vesicles can be found in Chapter 2 and the incorporation and release of a hydrophilic drug, doxorubicin hydrochloride into polystyrene-*block*-poly(acrylic acid) are discussed in Chapter 6.

#### 1.4.4. Properties of Block Copolymer Micelles

A number of properties of block copolymer micelles are important in connection with their use in drug delivery: size, size distribution, stability, loading and release. These parameters will be discussed in the following section, along with some of the factors that influence and/or control these properties. An overview of the advantages of block copolymer micellar systems is given in Figure 1.3.

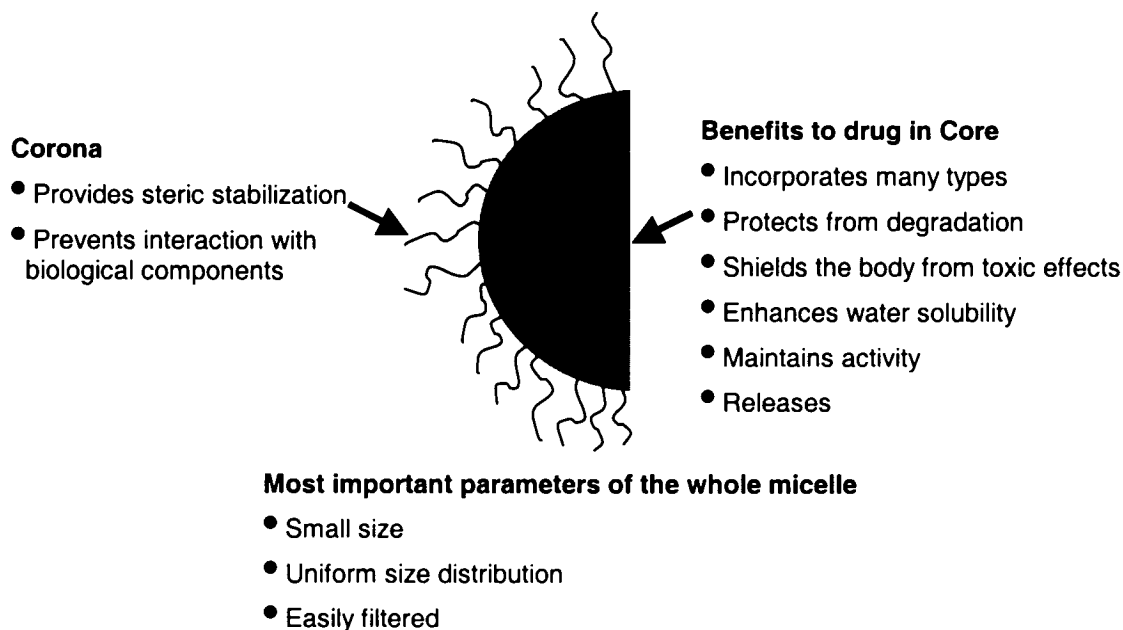


**Figure 1.3.** Functions of the components of block copolymer micelles in drug delivery.

*1.4.4.1. Micellar Size and Distribution*

Block copolymer micelles typically range in size from 10-100 nm. Such small sizes are not easily obtainable by other delivery systems; the micelles thus are generally smaller than liposomes, microspheres and most nanospheres. They resemble viruses (size range: 20-100 nm) or lipoproteins (size range: 10-100 nm), which are both naturally occurring delivery vehicles.<sup>40</sup> In addition to avoiding non-specific capture in the RES (threshold approximately 200 nm), the micelles are ideal to penetrate the sinusoidal and fenestrated capillaries that have pores of approximately 100 nm.<sup>63</sup> Also they are of an ideal size to enter endocytic vesicles (100 nm or less) which enter target cells via endocytosis.<sup>64</sup> Block copolymer micelles are too large to pass through the pores of the renal filtration system. After delivery, the micelles can break down to their individual polymer chains, which are eliminated from the body via renal excretion, at which point, they are small enough to pass through the pores, thus avoiding any possible toxicity associated with the long term accumulation of the polymer.<sup>65</sup> A renal threshold limit of 45,000 to 60,000 g/mol has been reported for polymeric carriers,<sup>66,67</sup> so it is important to design a micellar system in which the individual polymer chains have a molecular weight lower than the threshold value to facilitate elimination via renal filtration. Finally, the small size of the micelles makes them ideal for sterilization by filtration, which separates them from bacteria which are too large to pass through the pores.

Extrusion or filtration is used to narrow the size distribution for carriers such as liposomes, which tend to have wide size distribution upon initial preparation.<sup>5</sup> Micelles tend to have a relatively narrow size distribution naturally. However some micelles do suffer from secondary aggregation, which can be caused by an insufficient coverage of

the core by the hydrophilic block. The insufficient coverage leads to the interaction of the hydrophobic core with other similar cores, causing aggregation. This is the case with PCL-*b*-PEO micelles. However, dilution has been shown to break down the aggregates, leading to smaller average sizes.<sup>68</sup> Also in some cases, even the aggregates formed are smaller than 100 nm.<sup>5</sup>

#### 1.4.4.2. Micelle Stability

The stability of the micelle is important; its decomposition into individual chains is reflected in its critical micelle concentration (CMC), which is the minimum copolymer concentration of individual chains required to form a micelle by self-assembly. Below this concentration, the polymer is in the form of single polymer chains or unimers. The CMC is a very important parameter as it determines the thermodynamic stability of the micelles during dilution.<sup>69</sup> Small molecule surfactants form micelles that tend to have high CMC values, which make them susceptible to dilution and eventual dissociation, even at relatively high concentrations *in vivo*.<sup>29</sup> Block copolymers have significantly lower CMC values than low molecular weight surfactants.<sup>70</sup> Also, for block copolymer micelles, even below the CMC, the micellar system can remain kinetically stable, depending on its glass transition temperature and its crystallinity if the  $T_g$  is high or the system is partly crystalline. Cross linking of the micelle, which can take place in the core or the corona, also stabilizes the micelle against dilution.<sup>62,71</sup>

Some of the essential factors that influence the CMC are the nature and length of the hydrophobic block, the length of the hydrophilic block and the total molecular weight of the copolymer. A series of copolymer systems and the CMC values determined for the block copolymer micelles are shown in Table 1.3.

**Table 1.3.** Critical micelle concentrations of biocompatible block copolymers micellar systems.

Copolymer system	Specific Copolymer Micelle	CMC (mg/L)
oligo(methyl methacrylate)- <i>b</i> -poly(acrylic acid) <sup>39</sup>	oMMA- <i>b</i> -PAA	>10
Poly( $\beta$ -benzyl-l aspartate)- <i>b</i> -poly(ethylene oxide) <sup>41</sup>	PBLA <sub>9</sub> - <i>b</i> -PEO <sub>110</sub>	10
	PBLA <sub>19</sub> - <i>b</i> -PEO <sub>110</sub>	5
	PBLA <sub>20</sub> - <i>b</i> -PEO <sub>270</sub>	10
Polycaprolactone- <i>b</i> -poly(ethylene oxide) <sup>72</sup>	PCL <sub>5</sub> - <i>b</i> -PEO <sub>44</sub>	47
	PCL <sub>12</sub> - <i>b</i> -PEO <sub>44</sub>	2.9
	PCL <sub>21</sub> - <i>b</i> -PEO <sub>44</sub>	1.2
Poly(d,l-lactide)- <i>b</i> -poly(ethylene glycol) <sup>73</sup>	PLA- <i>b</i> -PEG	35
Poly(d,l-lactide)- <i>b</i> -poly( <i>N</i> -vinyl-2-pyrrolidone) <sup>74</sup>	PLA- <i>b</i> -PVP	2-10
Poly(ethylene oxide)- <i>b</i> -poly(propylene oxide)- <i>b</i> -poly(ethylene oxide) <sup>69</sup>	PEO- <i>b</i> -PPO- <i>b</i> -PEO	10-1000
Poly(1,3-trimethylene carbonate)- <i>b</i> -poly(2-ethyl-2-oxazoline) <sup>47</sup>	PTMC- <i>b</i> -PEtOz	3-25

The CMC of a copolymer was found to decrease with increasing hydrophobic block length. An example of this was shown by Astafieva et al. who found that as the length of the polystyrene block increased, the CMC of polystyrene-*block*-sodium acrylate micelles decreased.<sup>75,76</sup> By contrast, when the hydrophilic block length increases and the core length is kept constant, the CMC increases, as has been shown for the Pluronic copolymers.<sup>77</sup> To a lesser extent, this trend was also observed for polystyrene-*block*-sodium acrylate micelles.<sup>75</sup>

#### 1.4.4.3. Partition Coefficient

The partition coefficient is another important thermodynamic parameter that characterizes the drug distribution between the micelles and the aqueous phase.<sup>64</sup> It can be expressed by the following equation:

$$\text{Partition coefficient } (K_v) = \frac{[\text{Drug}]_{\text{mic}}}{[\text{Drug}]_{\text{aq}}} \quad (1.1)$$

where the  $[\text{Drug}]_{\text{mic}}$  is the drug concentration in the micelle and  $[\text{Drug}]_{\text{aq}}$  is the drug concentration in the aqueous phase. The partition coefficient is influenced by the nature and block length of the hydrophobic polymer and the nature of the drug. A discussion of the influence of the partition coefficient on the loading and the release involving different block copolymer systems can be found in Chapter 3.

#### *1.4.4.4. Drug Loading in Block Copolymer Micelles*

A drug can be incorporated into the hydrophobic core, the interface between the hydrophobic core and the corona, or the corona of the micelle. Ideally the drug should be incorporated into the core to provide protection of the drug from the aqueous solution and also enzymes that may degrade the drug. The hydrophobic environment also slows down the rate of release, because the drug needs to diffuse through the hydrophobic core in order to be released. The release of various drugs from block copolymer micelles will be discussed in section 1.4.4.5.

It is highly unlikely that a single block copolymer micellar system will be found that will effectively deliver all types of drugs. Therefore selecting a core block for a particular drug of interest is crucial for enhancing the loading of the drug. Illustrative examples of the different types of micellar block copolymer systems and the types of drugs incorporated into them are listed in Table 1.4.

**Table 1.4.** Illustrative examples of block copolymer micelle systems and incorporated drugs.<sup>a</sup>

Block copolymer	Drug	Micelle size(nm)
Poly( $\beta$ -benzyl-l aspartate)- <i>b</i> -poly(ethylene oxide)	Doxorubicin hydrochloride <sup>78</sup>	20-40
	Indomethacin <sup>79</sup>	NA
	Amphotericin B <sup>80</sup>	26
	KRN 5500 <sup>81</sup>	71
Poly( $\beta$ -benzyl-l aspartate)- <i>b</i> -poly( $\alpha$ -hydroxy ethylene oxide)	Doxorubicin hydrochloride <sup>82</sup>	30
Poly( $\gamma$ -benzyl-l glutamate)- <i>b</i> -poly(ethylene oxide)- <i>b</i> -poly( $\gamma$ -benzyl-l glutamate)	Clonazepam <sup>83</sup>	20-60
	Norfloracin <sup>42</sup>	40-110
Polycaprolactone- <i>b</i> -poly(ethylene oxide)	FK506 <sup>68</sup>	50
	L685,818 <sup>68</sup>	50
	Dihydrotestosterone <sup>84</sup>	50
	Ellipticine <sup>85</sup>	20-24
Poly[ <i>N</i> -(6-hexyl stearate)-l-aspartamide]- <i>b</i> -poly(ethylene oxide)	Amphotericin B <sup>86</sup>	NA
Poly(d,l-lactide)- <i>b</i> -methoxypolyethylene glycol	Paclitaxel <sup>87</sup>	NA
	Taxol <sup>88</sup>	45-47
Polylactide- <i>b</i> -poly(ethylene glycol)	Testosterone <sup>73</sup>	18-24
	Papaverine hydrochloride <sup>89</sup>	30-40
Poly (d,l-lactide)- <i>b</i> -poly( <i>N</i> -vinyl-2-pyrrolidone)	Indomethacin <sup>74</sup>	40-100
Poly(lactone)- <i>b</i> -poly(ethylene oxide)- <i>b</i> -polylactone, where polylactone is polycaprolactone, poly(l-lactide) or polyvalerolactone	Indomethacin <sup>90</sup>	~100
Poly(ethylene oxide)- <i>b</i> -poly(propylene oxide)- <i>b</i> -poly(ethylene oxide)	Haloperidol <sup>91</sup>	NA
Poly(ethylene oxide)- <i>b</i> -poly(propylene oxide)- <i>b</i> -poly(ethylene oxide)- <i>g</i> -poly(acrylic acid)	Estradiol <sup>92</sup>	NA

<sup>a</sup> NA= Not available

The factors that can affect drug loading include the length and nature of the hydrophobic and hydrophilic blocks, the copolymer concentration and the concentration of the drug.<sup>10</sup>

A discussion of some of the factors that influence the loading capacity and loading efficiency are given in Chapters 3 and 4 of the thesis.

*1.4.4.5. Release from Block Copolymer Micelles*

The interaction between the hydrophobic core and the drug is also an important factor in the release of the drug from the micellar core. A balance must be achieved between the loading and the release. If the interaction between the polymer and drug is too strong, incorporation will be enhanced, but release will be hindered. Other factors that can influence the release rate include the location of the drug within the micelle, the physical state of the drug in the micelle, the length of the hydrophobic block and the drug molecule size.<sup>10</sup> More detailed discussions of some of the factors that influence the release from block copolymer micelles are given in Chapters 3 and 4 of the thesis.

*1.4.4.6. Cellular Internalization*

After a drug has been released, the cellular fate of the block copolymers is a topic of great interest. In general, polymers can be internalized into the cell by a process called endocytosis.<sup>4</sup> Endocytosis occurs when the polymer is enclosed by a part of the membrane to form an intracellular vesicle. The vesicles containing the polymers are first transferred to endosomes then eventually to lysosomes. In the lysosomes, the pH of 5 will degrade the polymers with lysosomal enzymes.<sup>93</sup> A more detailed discussion of the cellular internalization of block copolymers is given in Chapter 6.

**1.5. Characterization of Block Copolymer Aggregates**

A number of different techniques were used to characterize the block copolymer aggregates described in this thesis, namely fluorescence spectroscopy, transmission electron microscopy, energy dispersive spectroscopy and dynamic light scattering, among others. A brief description of each of these techniques is given in the following sections.

1.5.1. Fluorescence Spectroscopy

In fluorescence spectroscopy, a fluorophore is excited by a photon of appropriate energy supplied from an external source, such as a lamp or a laser. The photon is absorbed and an electron goes from the ground state ( $S_0$ ) to an excited singlet state ( $S_1$ ), which lasts for a finite time ( $10^{-8}$  to  $10^{-9}$  seconds); the process is illustrated in Figure 1.4.<sup>94</sup>

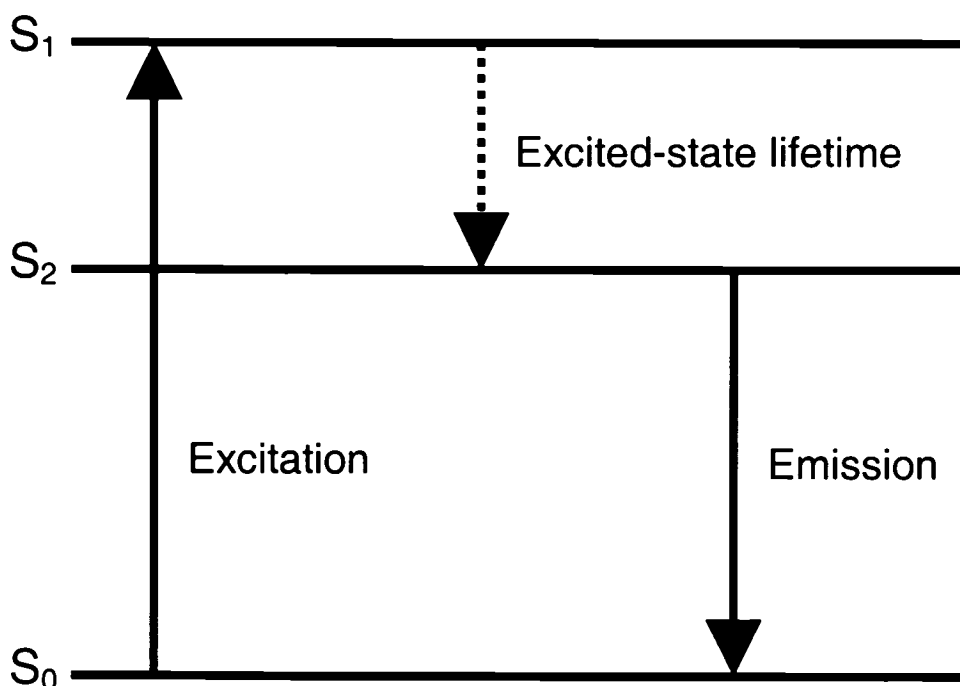


**Figure 1.4.** Jablonski diagram showing fluorescence.

The excited molecule undergoes changes in which energy can be partially dissipated (i.e., vibration relaxation) to a relaxed excited state ( $S_2$ ). The emission from the excited singlet state to the ground state is referred to as fluorescence.<sup>95</sup> Since energy was lost during the excited lifetime of the fluorophore, the wavelength will always be longer for the emission (i.e., red shifted) than for the excitation. The difference in the energy or wavelength is

known as the Stokes shift.<sup>94</sup> When there is no relaxation during the excited lifetime of the fluorophore, the excited molecule returns to the ground state by emitting photons of the same wavelength as the excitation radiation; this process is known as resonance fluorescence.<sup>96</sup>

Fluorescence spectroscopy was used extensively for this thesis work, because it is 100-1000 times more sensitive than other spectrophotometric techniques and allows rapid analysis of the samples.<sup>97</sup> As a result, this technique was used to quantitatively determine the amount of probe or drug present in the block copolymer aggregates for the incorporation, partition coefficient and release studies reported in the thesis.

#### 1.5.2. Transmission Electron Microscopy

Transmission electron microscopy is a powerful technique that was used to visualize the block copolymer aggregates to determine both their morphology and size. The technique relies on the transmission of electrons through a sample. Therefore typically, only very thin samples ( $< 10 \mu\text{m}$ ) can be visualized in any detail.<sup>98</sup> The basic components that make up a transmission electron microscope (TEM) are a source of illumination, condenser lenses, objective lenses, intermediate lenses, projector lenses and a fluorescent screen, as seen in Figure 1.4.

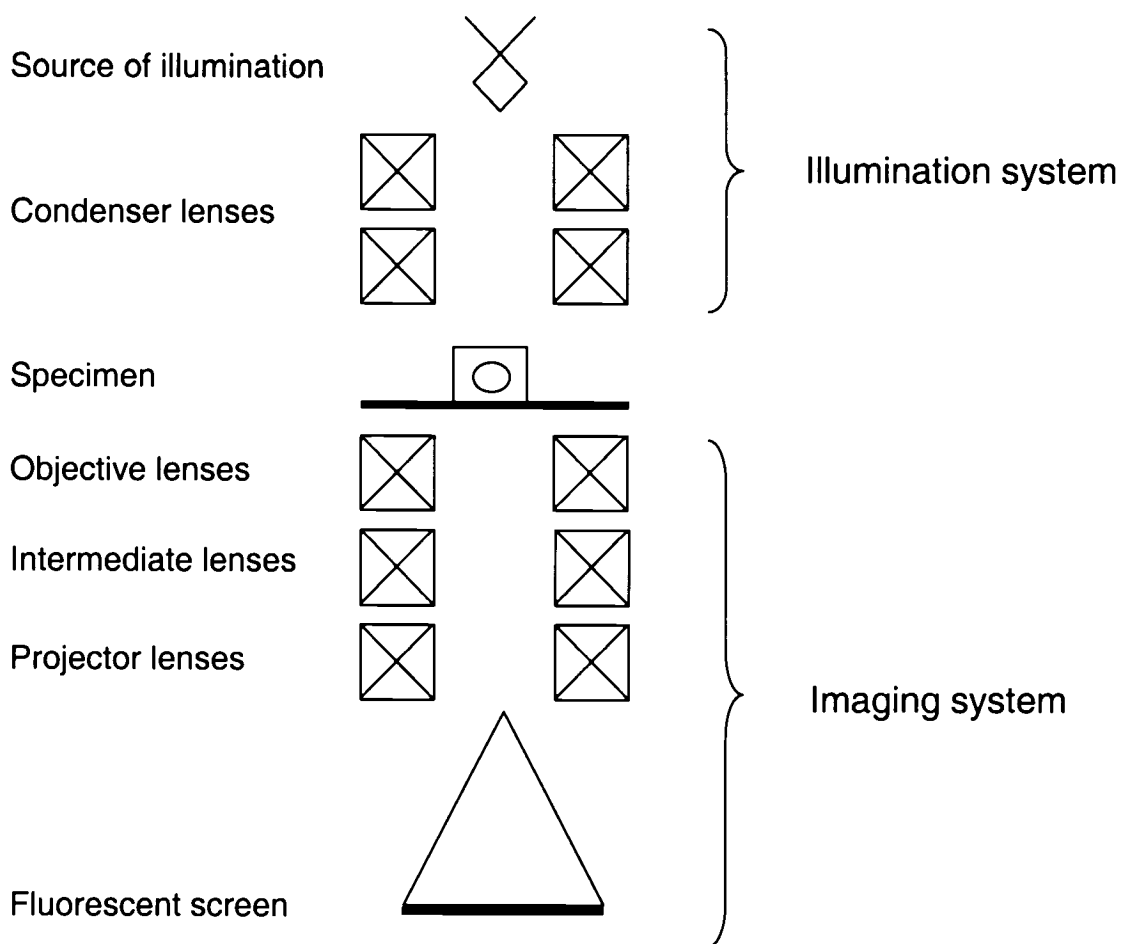


**Figure 1.5.** Schematic diagram of a transmission electron microscope.

The illuminating system of the electron microscope is composed of the source of illumination and the condenser lenses.<sup>99</sup> The illumination is provided by electrons that are produced from a heated tungsten hairpin filament or a pointed lanthanum hexaboride (LaB<sub>6</sub>) rod; the electrons are then accelerated into a narrow beam by an electron gun under high vacuum ( $> 10^{-5}$  torr).<sup>100</sup> The resolution of the TEM depends on the wavelength, which is a function of the accelerating voltage.<sup>98</sup> The accelerating voltage for a TEM can range from 100-10,000 kV; and the higher the voltage, the greater the resolution.<sup>99</sup> The electron beam passes through a series of condenser lenses, which serve

to gather the electrons, control the intensity of the beam onto the specimen and determine the illuminated specimen area.<sup>101</sup> The beam will then strike the specimen and some of the electrons are absorbed or scattered.<sup>98</sup> The attenuated beam is then passed through a series of lenses. All of the lenses in the TEM, with the exception of the electrostatic lens in the electron gun are rotationally symmetrical magnetic lenses made from a series of electromagnetic coils, which serve to focus and direct the electron beam.<sup>102</sup>

The imaging system consists of the objective lenses, the intermediate lenses, the projector lenses and the fluorescent screen.<sup>100</sup> The objective lenses create and magnify the image of the specimen. The intermediate lenses also magnify the image, which is then further magnified by the projector lenses.<sup>102</sup> The final image is viewed on a fluorescent screen, with a maximum emission of around 550 nm, corresponding to the green colour region, which is the region that the sensitivity of the human eye is maximum.<sup>100</sup> Finally the image can be recorded using either photographic film or a charge-coupled device camera.

### 1.5.3. Energy Dispersive Spectroscopy

Energy dispersive spectroscopy (EDS) was used to confirm the presence of the gold labeled micelles in different cell types in Chapter 5. It is a technique that is used in conjunction with the transmission electron microscope. This technique is also known as energy dispersive analysis of x-rays. An electron from the TEM will interact with the inner shell electron of a specimen atom causing it to eject the inner electron from the shell; leaving the atom as an ion in an excited state.<sup>103</sup> In order for the atom to relax to its ground state, outer shell electrons will fill the space of the inner shell electrons through allowed transitions. When this occurs, x-rays of energies and wavelengths specific to the

atomic number of the atoms are emitted.<sup>98</sup> The x-rays can be used to rapidly identify the specific atoms present in a sample.<sup>103</sup>

A semiconductor detector, usually a lithium-drifted silicon (Si(Li)) crystal, collects the x-rays produced. It is mounted above the specimen holder and does not interfere with the normal function of the TEM.<sup>104</sup> The detector converts the energy of the incident x-ray photons into pulses of current.<sup>101</sup> The pulses are then analysed by a computer and the whole spectrum is displayed. Despite its simple use and rapid results, the EDS suffers from poor spectral resolution, which can cause peak overlaps and difficulty in analysis.<sup>98</sup> Also, the EDS can be limited to elements with an atomic number greater than 11 (i.e., Na), depending on the detector.

#### 1.5.4. Dynamic Light Scattering

In the research reported in this thesis, dynamic light scattering (DLS) was used to determine the size and size distribution of the block copolymer aggregates in solution. DLS provides information about the dimensions of the macromolecules. The technique is also known as photon correlation spectroscopy or quasi-elastic light scattering.<sup>105</sup> The light scattered from a polymer in solution is measured at a single scattering angle.<sup>106</sup> The light scattering intensity is measured in the microsecond time domain.<sup>107</sup> Since the intensity of light scattered is not constant, an autocorrelator is needed in order to distinguish between the random motions and the motions of the polymer in solution. The autocorrelator calculates the average of the product of two scattering intensities  $I(t)$  and  $I(t + \tau)$ , where  $\tau$  is the delay time.<sup>106</sup> From this autocorrelation function, the translational diffusion coefficient can be calculated by fitting the function to an exponential decay. The hydrodynamic radius ( $R_h$ ) can be measured using the Stokes-Einstein equation:<sup>108</sup>

$$D = \frac{k_b T}{6\pi\eta R_h} \quad (1.2)$$

where  $k_b$  is the Boltzmann's equation,  $T$  is the absolute temperature,  $\eta$  is the solvent viscosity and  $D$  is the diffusion coefficient. In order to characterize the size distribution obtained, the CONTIN method (inverse-Laplace transform) was used.<sup>109</sup> The CONTIN method is applicable to size distributions that may be broad or even bimodal. When the size distribution is narrow, then a cumulant expansion can be used.

### 1.6. Scope of the Thesis

The thesis deals with two types of aggregate morphologies, namely block copolymer micelles and block copolymer vesicles. In this Chapter, a brief review of the literature of the use of block copolymer micelles in drug delivery has been provided, as well as a rationale for the selection of each of the components that make up our block copolymers. The properties of block copolymers relevant to drug delivery are given. Also a brief introduction to a few of the instruments used to characterize the block copolymer aggregates is also presented.

Chapter 2 is a review of the different amphiphilic polymer systems that can form vesicles. This article was originally written for Journal of Polymer Science: Part B Polymer Physics.<sup>110</sup> The review article was included in the thesis, because the article deals with an amphiphilic copolymer system that is used in the thesis, namely, polystyrene-*block*-poly(acrylic acid). In addition, polystyrene-*block*-poly(ethylene oxide) copolymers and a number of other types of copolymer systems are discussed. In addition, many of the factors that influence and exert control over the preparation of block copolymer vesicles and micelles are also given.

Chapter 3 describes the investigation of the incorporation and release of fluorescent and hydrophobic probes (Cell Tracker CM-DiI and benzo[a]pyrene) from biodegradable and biocompatible polycaprolactone-*block*-poly(ethylene oxide) (PCL-*b*-PEO) micelles. These probes are not drugs, but rather model molecules designed to provide more information about the loading and release capabilities of PCL-*b*-PEO. Also, an investigation of the affinity of the probe molecules for the PCL-*b*-PEO micelles compared to the external environment is reflected in the partition coefficient for each probe is described.

Chapter 4 deals with the incorporation and release of a female steroid hormone drug, 17 $\beta$ -Estradiol (E2) in different PCL-*b*-PEO micelles. The aim is to investigate the usefulness of PCL-*b*-PEO micelles as a drug delivery vehicle. The loading and release properties of E2 are studied as a function of the PCL block length. Also, the biological activity of E2 is evaluated in young female mice.

Chapter 5 reports on the preparation and characterization of gold labeled poly(4-vinylpyridine)-*block*-poly(ethylene oxide) (P4VP-*b*-PEO) micelles. These gold labeled micelles are internalized into two different cell lines: A549 lung cells and HEK 293 kidney cells to determine their subcellular localization by transmission electron microscopy.

In Chapter 6, the incorporation and release of an anticancer drug, doxorubicin hydrochloride (DXR) in polystyrene-*block*-poly(acrylic acid) (PS-*b*-PAA) vesicles is described. The PS-*b*-PAA does not represent a biodegradable and biocompatible copolymer system, however, it is an excellent model system. This study investigates the incorporation and release of a drug from this model system in order to provide information for future medically acceptable polymeric vesicular systems.

Finally Chapter 7 includes a discussion of the conclusions, contributions to original knowledge and suggestions for future work.

### 1.7. References

- (1) Kost, J. In *Polymeric Materials Encyclopedia*, 1st ed.; Salamone, J. C., Ed.; CRC Press: New York, 1996; Vol. 2 (C).
- (2) Langer, R. *Nature* **1998**, 392, 5-10.
- (3) Langer, R. *Science* **1990**, 249, 1527-1533.
- (4) Kataoka, K. *Controlled Drug Delivery* **1997**, 49-71.
- (5) Yokoyama, M. In *Biorelated Polymers and Gels: Controlled Release and Applications in Biomedical Engineering*; Okano, T., Ed., 1998; pp 193-229.
- (6) Yokoyama, M.; Okano, T. *Advanced Drug Delivery Reviews* **1996**, 21, 77-80.
- (7) Muller, R. H. *Colloidal Carriers for Controlled Drug Delivery and Targeting: Modification, Characterization and In Vivo Distribution*; CRC Press, Inc.: Boca Raton, Florida, 1991.
- (8) Scholes, P. D.; Coombes, A. G. A.; Davies, M. C.; Illum, L.; Davis, S. S. *Controlled Drug Delivery* **1997**, 73-106.
- (9) Malmsten, M. In *Amphiphilic Block Copolymers: Self Assembly and Applications*; Lindman, B., Ed.; Elsevier Science B.V.: Amsterdam, The Netherlands, 2000; pp 319-346.
- (10) Allen, C.; Maysinger, D.; Eisenberg, A. *Colloids and Surfaces B: Biointerfaces* **1999**, 16, 3-27.
- (11) Mayhew, E.; Papahadjopoulos, D. In *Liposomes*; Ostro, M. J., Ed.; Marcel Dekker, Inc.: New York, 1983; pp 289-341.
- (12) Gabizon, A.; Papahadjopoulos, D. *Proceedings of the National Academy of Sciences of the United States of America* **1988**, 85, 6949-6953.
- (13) Allen, T. M.; Hansen, C. B.; de Menezes, D. E. L. *Advanced Drug Delivery Reviews* **1995**, 16, 267-284.
- (14) Jeong, B.; Bae, Y. H.; Lee, D. S.; Kim, S. W. *Nature* **1997**, 388, 860-862.

Chapter 1. General Introduction

- (15) Qiu, Y.; Park, K. *Advanced Drug Delivery Reviews* **2001**, 53, 321-339.
- (16) Kim, B.; Peppas, N. A. *International Journal of Pharmaceutics* **2003**, 266, 29-37.
- (17) Liu, M.; Kono, K.; Frechet, J. M. J. *Journal of Controlled Release* **2000**, 65, 121-131.
- (18) Patri, A. K.; Majoros, I. J.; Baker, J. R. *Current Opinion in Chemical Biology* **2002**, 6, 466-471.
- (19) Kakkar, A. K. *Macromolecular Symposia* **2003**, 196, 145-154.
- (20) Zalipsky, S. *Advanced Drug Delivery Reviews* **1995**, 16, 157-182.
- (21) Yokoyama, M.; Okano, T.; Sakurai, Y.; Suwa, S.; Kataoka, K. *Journal of Controlled Release* **1996**, 39, 351-356.
- (22) Duncan, R. *Nature Reviews Drug Discovery* **2003**, 2, 347-360.
- (23) Gref, R.; Minamitake, Y.; Peracchia, M. T.; Trubetskoy, V.; Torchilin, V.; Langer, R. *Science* **1994**, 263, 1600-1603.
- (24) Leroux, J.-C.; Allemann, E.; De Jaeghere, F.; Doelker, E.; Gurny, R. *Journal of Controlled Release* **1996**, 39, 339-350.
- (25) Jeong, Y.-I.; Cheon, J.-B.; Kim, S.-H.; Na, J.-W.; Lee, Y.-M.; Sung, Y.-K.; Akaike, T.; Cho, C.-S. *Journal of Controlled Release* **1998**, 51, 169-178.
- (26) Jalil, R.; Nixon, J. R. *Journal of Microencapsulation* **1990**, 7, 297-325.
- (27) Atkins, T. W.; Peacock, S. J.; Yates, D. J. *Journal of Microencapsulation* **1998**, 15, 31-44.
- (28) Kulbaba, K.; Cheng, A.; Bartole, A.; Greenberg, S.; Resendes, R.; Coombs, N.; Safa-Sefat, A.; Greedan, J. E.; Stoeber, H. D. H.; Ozin, G. A.; Manners, I. *Journal of the American Chemical Society* **2002**, 124, 12522-12534.
- (29) Lawrence, M. J. *Chemical Society Reviews* **1994**, 23, 417-424.
- (30) Bronich, T. K.; Nehls, A.; Eisenberg, A.; Kabanov, V. A.; Kabanov, A. V. *Colloids and Surfaces, B: Biointerfaces* **1999**, 16, 243-251.
- (31) Malmsten, M. *Surfactants and Polymers in Drug Delivery*; Marcel Dekker, Inc.: New York, 2002.
- (32) Kwon, G. S. *Critical Reviews in Therapeutic Drug Carrier Systems* **1998**, 15, 481-512.

## Chapter 1. General Introduction

- (33) Alexandridis, P.; Lindman, B., Editors. *Amphiphilic Block Copolymers: Self-Assembly and Applications*; Elsevier Science B.V.: Amsterdam, 2000.
- (34) Torchilin, V. P. *Journal of Controlled Release* **2001**, *73*, 137-172.
- (35) Allen, T. M. *Drugs* **1997**, *54 Supplement 4*, 8-14.
- (36) Cowie, J. M. G. *Polymers: Chemistry & Physics of Modern Materials*, 2nd ed.; Blackie Academic & Professional: London, 1996.
- (37) Bader, H.; Ringsdorf, H.; Schmidt, B. *Angewandte Makromolekulare Chemie* **1984**, *123/124*, 457-485.
- (38) Kelen, T. In *Polymer Degradation*, 1st ed.; Van Nostrand Reinhold Co. Inc.: USA, 1983.
- (39) Inoue, T.; Chen, G.; Nakamae, K.; Hoffman, A. S. *Journal of Controlled Release* **1998**, *51*, 221-229.
- (40) Kataoka, K.; Kwon, G. S.; Yokoyama, M.; Okano, T.; Sakurai, Y. *Journal of Controlled Release* **1993**, *24*, 119-132.
- (41) Kwon, G.; Naito, M.; Yokoyama, M.; Okano, T.; Sakurai, Y.; Kataoka, K. *Langmuir* **1993**, *9*, 945-949.
- (42) Nah, J.-W.; Jeong, Y., II; Cho, C.-S. *Bulletin of the Korean Chemical Society* **1998**, *19*, 962-967.
- (43) Lee, E. S.; Na, K.; Bae, Y. H. *Journal of Controlled Release* **2003**, *91*, 103-113.
- (44) Riley, T.; Govender, T.; Stolnik, S.; Xiong, C. D.; Garnett, M. C.; Illum, L.; Davis, S. S. *Colloids and Surfaces B: Biointerfaces* **1999**, *16*, 147-159.
- (45) Alexandridis, P. *Current Opinion in Colloid Interface Science* **1997**, *2*, 478-489.
- (46) Zhang, L.; Eisenberg, A. *Polymers for Advanced Technologies* **1998**, *9*, 677-699.
- (47) Kim, C.; Lee, S. C.; Shin, J. H.; Yoon, J.-S.; Kwon, I. C.; Jeong, S. Y. *Macromolecules* **2000**, *33*, 7448-7452.
- (48) Bronstein, L.; Antonietti, M.; Valetsky, P. *Nanoparticles and Nanostructured Films* **1998**, 145-171.
- (49) Koleske, J. V. In *Polymeric Materials Encyclopedia*, 1st ed.; Salamone, J. C., Ed.; CRC Press: New York, 1996; Vol. 8 (P).
- (50) Allen, C.; Eisenberg, A.; Maysinger, D. *S.T.P. Pharma Sciences* **1999**, *9*, 139-151.

## Chapter 1. General Introduction

- (51) Perrin, D. E.; English, J. P. In *Handbook of Biodegradable Polymers*, 1st ed.; Wiseman, D. M., Ed.: The Netherlands, 1997.
- (52) Brode, G. L.; Koleske, J. V. *Journal of Macromolecular Science, Chemistry* **1972**, *6*, 1109-1144.
- (53) Lin, W. J.; Flanagan, D. R.; Linhardt, R. J. *Pharmaceutical Research* **1994**, *11*, 1030-1034.
- (54) Elbert, D. L.; Hubbell, J. A. *Annual Review of Materials Science* **1996**, *26*, 365-394.
- (55) Torchilin, V. P. *Journal of Liposome Research* **1996**, *6*, 99-116.
- (56) Harris, J. M. In *Poly(Ethylene Glycol) Chemistry: Biotechnical and Biomedical Applications*; Harris, J. M., Ed.; Plenum Press: New York, 1992; pp 1-14.
- (57) Saltzman, W. M. *Drug Delivery: Engineering Principles for Drug Therapy*; Oxford University Press, Inc.: New York, USA, 2001.
- (58) Allen, C.; Dos Santos, N.; Gallagher, R.; Chiu, G. N. C.; Shu, Y.; Li, W. M.; Johnstone, S. A.; Janoff, A. S.; Mayer, L. D.; Webb, M. S.; Bally, M. B. *Bioscience Reports* **2002**, *22*, 225-250.
- (59) Lee, J. H.; Lee, H. B.; Andrade, J. D. *Progress in Polymer Science* **1995**, *20*, 1043-1079.
- (60) Nemeo, J. W.; Bauer Jr., W. In *Encyclopedia of Polymer Science and Engineering*, 2nd ed.; John Wiley and Sons, Inc.: New York, 1985; Vol. 1 (A to Amorphous Polymers).
- (61) Tamburic, S.; Craig, D. Q. M. *Journal of Controlled Release* **1995**, *37*, 59-68.
- (62) Yang, L.; Alexandridis, P. *Current Opinion in Colloid and Interface Science* **2000**, *5*, 132-143.
- (63) Yokoyama, M.; Miyauchi, M.; Yamada, N.; Okano, T.; Kataoka, K.; Inoue, S. *Journal of Controlled Release* **1990**, *11*, 269-278.
- (64) Kabanov, A. V.; Alakhov, V. Y. In *Amphiphilic Block Copolymers: Self Assembly and Applications*; Lindman, B., Ed.; Elsevier Science B.V.: Amsterdam, The Netherlands, 2000; pp 347-376.
- (65) Yokoyama, M.; Kwon, G. S.; Okano, T.; Sakurai, Y.; Kataoka, K. *ACS Symposium Series* **1994**, *545*, 126-134.
- (66) Seymour, L. W.; Duncan, R.; Strohmalm, J.; Kopecek, J. *Journal of Biomedical Materials Research* **1987**, *21*, 1341-1358.

## Chapter 1. General Introduction

- (67) Kishida, A. *Trends in Pharmacological Sciences* **2003**, *24*, 611-613.
- (68) Allen, C.; Yu, Y.; Maysinger, D.; Eisenberg, A. *Bioconjugate Chemistry* **1998**, *9*, 564-572.
- (69) Kabanov, A. V.; Nazarova, I. R.; Astafieva, I. V.; Batrakova, E. V.; Alakhov, V. Y.; Yaroslavov, A. A.; Kabanov, V. A. *Macromolecules* **1995**, *28*, 2303-2314.
- (70) Wilhelm, M.; Zhao, C. L.; Wang, Y.; Xu, R.; Winnik, M. A.; Mura, J. L.; Riess, G.; Croucher, M. D. *Macromolecules* **1991**, *24*, 1033-1040.
- (71) Rosler, A.; Vandermeulen, G. W. M.; Klok, H.-A. *Advanced Drug Delivery Reviews* **2001**, *53*, 95-108.
- (72) Allen, C. J. In *Ph.D. Thesis (Chemistry)*; McGill University: Montreal, Quebec, Canada, 2000; p 251.
- (73) Hagan, S. A.; Coombes, A. G. A.; Garnett, M. C.; Dunn, S. E.; Davies, M. C.; Illum, L.; Davis, S. S.; Harding, S. E.; Purkiss, S.; Gellert, P. R. *Langmuir* **1996**, *12*, 2153-2161.
- (74) Benahmed, A.; Ranger, M.; Leroux, J.-C. *Pharmaceutical Research* **2001**, *18*, 323-328.
- (75) Astafieva, I.; Zhong, X. F.; Eisenberg, A. *Macromolecules* **1993**, *26*, 7339-7352.
- (76) Astafieva, I.; Khougaz, K.; Eisenberg, A. *Macromolecules* **1995**, *28*, 7127-7134.
- (77) Alexandridis, P.; Holzwarth, J. F.; Hatton, T. A. *Macromolecules* **1994**, *27*, 2414-2425.
- (78) Kwon, G. S.; Natio, M.; Yokoyama, M.; Okano, T.; Sakurai, Y.; Kataoka, K. *Pharmaceutical Research* **1995**, *12*, 192-195.
- (79) La, S. B.; Okano, T.; Kataoka, K. *Journal of Pharmaceutical Sciences* **1996**, *85*, 85-90.
- (80) Yu, B. G.; Okano, T.; Kataoka, K.; Kwon, G. *Journal of Controlled Release* **1998**, *53*, 131-136.
- (81) Yokoyama, M.; Satoh, A.; Sakurai, Y.; Okano, T.; Matsumura, Y.; Kakizoe, T.; Kataoka, K. *Journal of Controlled Release* **1998**, *55*, 219-229.
- (82) Cammas, S.; Matsumoto, T.; Okano, T.; Sakurai, Y.; Kataoka, K. *Materials Science & Engineering, C: Biomimetic Materials, Sensors and Systems* **1997**, *C4*, 241-247.
- (83) Nah, J.-W.; Jeong, Y.-I.; Cho, C.-S.; Kim, S.-I. *Journal of Applied Polymer Science* **2000**, *75*, 1115-1126.

## Chapter 1. General Introduction

- (84) Allen, C.; Han, J.; Yu, Y.; Maysinger, D.; Eisenberg, A. *Journal of Controlled Release* **2000**, *63*, 275-286.
- (85) Liu, J.; Xiao, Y.; Allen, C. *Journal of Pharmaceutical Sciences* **2004**, *93*, 132-143.
- (86) Lavasanifar, A.; Samuel, J.; Kwon, G. S. *Journal of Controlled Release* **2002**, *79*, 165-172.
- (87) Liggins, R. T.; Burt, H. M. *Advanced Drug Delivery Reviews* **2002**, *54*, 191-202.
- (88) Kim, J.-H.; Emoto, K.; Iijima, M.; Nagasaki, Y.; Aoyagi, T.; Okano, T.; Sakurai, Y.; Kataoka, K. *Polymers for Advanced Technologies* **1999**, *10*, 647-654.
- (89) Lee, J.; Cho, E. C.; Cho, K. *Journal of Controlled Release* **2004**, *94*, 323-335.
- (90) Lin, W.-J.; Juang, L.-W.; Lin, C.-C. *Pharmaceutical Research* **2003**, *20*, 668-673.
- (91) Kabanov, A. V.; Chekhonin, V. P.; Alakhov, V. Y.; Batrakova, E. V.; Lebedev, A. S.; Melik-Nubarov, N. S.; Arzhakov, S. A.; Levashov, A. V.; Morozov, G. V.; et al. *FEBS Letters* **1989**, *258*, 343-345.
- (92) Bromberg, L.; Magner, E. *Langmuir* **1999**, *15*, 6792-6798.
- (93) Villee, C. A.; Solomon, E. P.; Martin, C. E.; Martin, D. W.; Berg, L. R.; Davis, P. W. *Biology*, 2nd ed.; Saunders College Publishing: Orlando, Florida, 1989.
- (94) Johnson, I. D. In *Handbook of Fluorescent Probes and Research Chemicals*, 6th ed.; Haughland, R. P., Ed.; Molecular Probes Inc.: Eugene, OR, 1996.
- (95) Straughan, B. P.; Walker, S., Eds. *Spectroscopy*; Chapman and Hall Ltd.: London, 1976; Vol. 3.
- (96) Sun, S. F. *Physical Chemistry of Macromolecules: Basic Principles and Issues*, 2nd ed.; John Wiley & Sons, Inc.: Hoboken, New Jersey, 2004.
- (97) Strasburg, G. M.; Ludescher, R. D. *Trends in Food Science & Technology* **1995**, *6*, 69-75.
- (98) Evans, R. J. In *Encyclopedia of Physical Science and Technology*, 1st ed.; Meyers, R. A., Ed.; Academic Press Inc., 1987; Vol. 8.
- (99) Thomas, E. L. In *Encyclopedia of Polymer Science and Engineering*, 2nd ed., 1985; Vol. 5.
- (100) Reimer, L. *Transmission Electron Microscopy: Physics of Image Formation and Microanalysis*, 4th ed.; Springer-Verlag: Berlin, 1997.

## Chapter 1. General Introduction

- (101) Watt, I. M. *The Principles and Practice of Electron Microscopy*; Cambridge University Press: Cambridge, 1985.
- (102) Kirkland, E. J. *Advanced Computing in Electron Microscopy*; Plenum Press: New York, 1998.
- (103) Goldstein, J. I.; Newbury, D. E.; Echlin, P.; Joy, D. C.; Lyman, C. E.; Lifshin, E.; Sawyer, L.; Michael, J. R., Eds. *Scanning Electron Microscopy and X-Ray Microanalysis*, 3rd ed.; Kluwer Academic/Plenum Publishers: New York, 2003.
- (104) Bender, S. L.; Duff, R. H. In *Energy Dispersion X-ray Analysis: X-Ray and Electron Probe Analysis*; Russ, J. C., Ed., 1971; pp 180-196.
- (105) Finsy, R. *Advances in Colloid and Interface Science* **1994**, *52*, 79-143.
- (106) Teroka, I., Ed. *Polymer Solutions: An Introduction to Physical Properties*; John Wiley & Sons, Inc.: New York, 2002.
- (107) Santos, N. C.; Castanho, M. A. R. B. *Biophysical Journal* **1996**, *71*, 1641-1650.
- (108) Cussler, E. L.; Editor. *Diffusion: Mass Transfer in Fluid Systems*, 2nd ed., 1996.
- (109) Provencher, S. W. *Makromolekulare Chemie* **1979**, *180*, 201-209.
- (110) Lim Soo, P.; Eisenberg, A. *Journal of Polymer Science: Part B: Polymer Physics* **2004**, *42*, 923-938.

# Chapter 2

---

## Preparation of Block Copolymer Vesicles in Solution\*

---

### 2.1. Abstract

Block copolymer vesicles can be prepared in solution from a variety of different amphiphilic systems. Polystyrene-*block*-poly(acrylic acid), polystyrene-*block*-poly(ethylene oxide), and many other block copolymer systems can produce vesicles of a wide range of sizes; those in the range of 100-1000 nm have been explored extensively. Different factors, such as the absolute and relative block lengths, the presence of additives (ions, homopolymers and surfactants), the water content in the solvent mixture, the nature and composition of the solvent, the temperature, and the polydispersity of the hydrophilic block, provide control over the types of vesicles produced. Their high stability, resistance to many external stimuli, and ability to package both hydrophilic and hydrophobic compounds make them excellent candidates for use in the medical, pharmaceutical, and environmental fields.

## 2.2. Introduction

Over the past decade, a large number of publications have appeared on the topic of block copolymer morphologies in solution.<sup>1-23</sup> These structures are of intrinsic interest, but they are also receiving attention because of their potential use in cosmetics, drug delivery, electronics, pollution control and separations, among others areas. Of particular interest are the block copolymer vesicles,<sup>1-3,5,6,8,10-12,14,15,24</sup> which can be used, for example, in biomedicine as artificial cells or in drug delivery. Because of this high level of activity, it is useful to review the formation of vesicles, with special emphasis on the factors that control their size, the nature of the interface, and their stability. This review also includes a description of the different block copolymer systems that can form vesicles, as well as a brief comparison with other materials that can form vesicles, that is, surfactants and still other amphiphiles. Structures that resemble vesicles, (e.g. hollow spheres prepared from materials other than block copolymers) are also discussed briefly.

Different aggregate morphologies have been seen in various small-molecule amphiphiles. These morphologies include, among others, spheres, rods, lamellae, and vesicles. The control of these different morphologies is based on the ability to manipulate factors such as the nature of the polar head group, the number and length of the hydrophobic tails, the type and concentration of ions, and the temperature. It is primarily the value of the critical packing parameter  $\nu/a_0l_c$  that determines the morphology of the aggregates, where  $\nu$  is the volume of the hydrocarbon chains,  $a_0$  is the optimal area of the hydrophilic group and  $l_c$  is the critical chain length of the hydrophobic group.<sup>25</sup> When the packing parameter is less than 1/3, spherical micelles are formed; when  $\nu/a_0l_c$  is between 1/3 and 1/2, the morphologies formed are cylinders; and when the

parameter is between 1/2 and 1, flexible bilayers or vesicles are observed. If  $\nu/a_0l_c$  is approximately equal to 1, then planar bilayers are formed. Finally, when the parameter is greater than 1, inverted structures are observed. Illustrative examples of aggregate morphologies formed from small-molecule surfactants are given in several books and the included references.<sup>26-28</sup>

Various morphologies are also seen in block copolymers in the bulk. The formation of these morphologies is due to the inherent incompatibility of most polymers above a certain molecular weight threshold, which, because of the chemical attachment of the segments, leads to microphase separation.<sup>29</sup> The equilibrium morphologies that have been seen in the diblocks in the bulk include spheres, hexagonally packed cylinders, gyroids, other bicontinuous structures, and lamellae.<sup>30</sup> The field has been reviewed extensively in recent books and the given references.<sup>31,32</sup> The phase behavior of the block copolymers in the bulk is controlled by three different factors: the overall degree of polymerization, the Flory-Huggins interaction parameter and the volume fraction of the components.<sup>30</sup>

Block copolymer aggregates of various morphologies can also be produced in solution. Our group has synthesized asymmetric amphiphilic diblocks from a range of block copolymers, with most of the work focused on polystyrene-*b*-poly(acrylic acid) (PS-*b*-PAA) and polystyrene-*b*-poly(ethylene oxide) (PS-*b*-PEO); in most of these, the length of the hydrophobic block was much longer than that of the hydrophilic segment.<sup>2,33</sup> Because in most of the systems that we have investigated the corona block is much shorter than the core block, the aggregates are called *crew-cut*.<sup>34</sup> Usually, the cores of the micelles and rods and the walls of the vesicles are hydrophobic. The aggregates

are prepared first by the dissolution of the copolymer in a suitable solvent that is favorable for both the core and corona blocks. Then, water is added as a precipitant for the hydrophobic block, and self-assembly takes place at some critical water content, which depends on the relative and absolute block lengths and the nature of the polymer. The addition of water is continued until a predetermined point in the phase diagram has been reached, depending on whether the desired aggregates are micelles, rods or vesicles. The system is then quenched by the addition of a large excess of water to freeze the morphologies, and the colloidal solution is dialyzed against MilliQ water for the removal of the organic solvent. The various copolymer aggregates that can be formed from these asymmetric diblocks include spheres, rods, lamellae, vesicles, large compound micelles (LCMs), large compound vesicles (LCVs), and many others.<sup>7,35-38</sup>

In solution, the formation of block copolymer aggregates of various morphologies is controlled by a force balance between three different factors: the degree of stretching of the core-forming blocks, interfacial tension between the micelle core and the solvent outside the core, and the repulsive interaction among corona-forming chains.<sup>7</sup> The morphologies can be controlled through variations in the copolymer composition, the initial copolymer concentration, the nature of the common solvent, the amount of water present in the solvent mixture, the temperature, the presence of additives such as ions, homopolymers or surfactants, and the polydispersity of the corona chain. In the following sections, we discuss the factors that can influence the self-assembly of the various block copolymers to yield aggregates of various morphologies through the interplay of the three main forces that govern their formation, with particular emphasis on

the formation of vesicles. A wide range of vesicles can be prepared, as illustrated in Figure 2.1; however this review focuses primarily on the unilamellar bilayer vesicles.

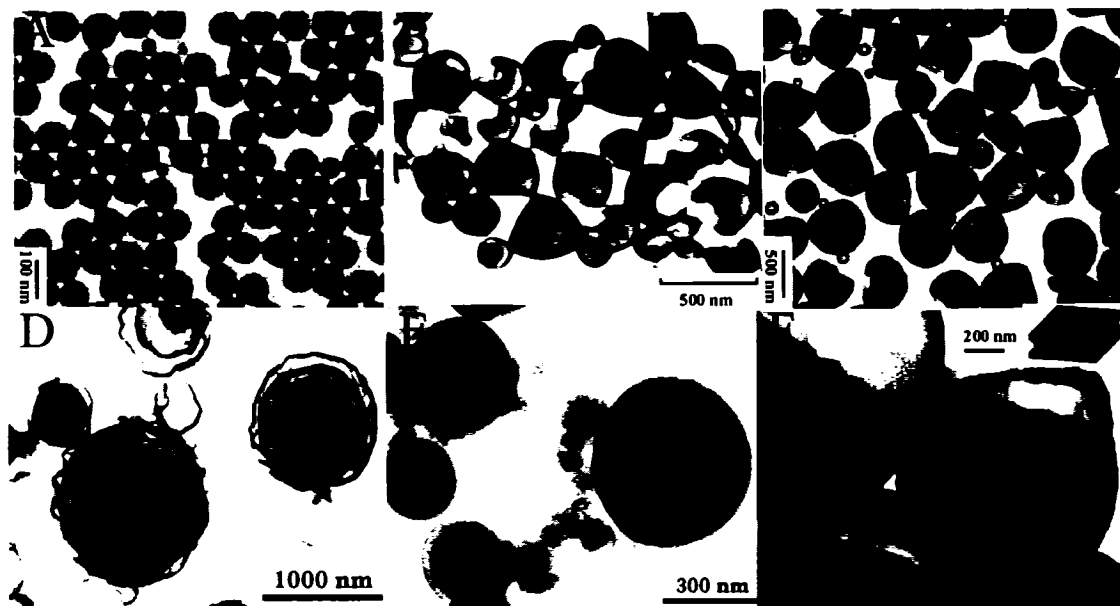


**Figure 2.1.** Representative micrographs of various types of vesicles: (A) small uniform vesicles ( $PS_{410}\text{-}b\text{-}PAA_{13}$ ), (B) large polydisperse vesicles ( $PS_{100}\text{-}b\text{-}PEO_{30}$ ), (C) entrapped vesicles ( $PS_{200}\text{-}b\text{-}PAA_{20}$ ), (D) hollow concentric vesicles ( $PS_{132}\text{-}b\text{-}PAA_{20}$ ), (E) onions ( $PS_{260}\text{-}b\text{-}P4VPDecI_{70}$ ), and (F) vesicles with tubes in the wall ( $PS_{100}\text{-}b\text{-}PEO_{30}$ ). (From S. Burke et al., *Macromol Symp* 2001, 175, 273.)

### 2.3. Copolymer Composition and Concentration

In the  $PS\text{-}b\text{-}PAA$  micelles prepared as previously described, the degree of polystyrene (PS) stretching ( $S_c$ ) is dependent on the copolymer composition, as shown in the following equation:<sup>39</sup>  $S_c \approx N_{PS}^{-0.1} N_{PAA}^{-0.15}$ , where the degrees of polymerization of PS and PAA are  $N_{PS}$  and  $N_{PAA}$  respectively. The equation shows that an increase in the core or corona block length results in a decrease in the degree of stretching of the core-forming block. This equation applies only to spherical micelles in aqueous solution

without any organic solvents present in their cores. However, before dialysis, the cores are swollen with an organic solvent, and so the value of  $S_c$  will actually be larger than the value obtained after dialysis.<sup>39</sup> It should be recalled, however, that during the dialysis process, the solvent content of the core drops progressively and that at some point, PS goes through its glass transition temperature. Below the glass transition temperature, thermodynamic considerations are no longer meaningful because the morphology is frozen. Although the aggregate is still in thermodynamic equilibrium, the degree of stretching is different when polymers form aggregates of different morphologies.<sup>40</sup> For example, Zhang and Eisenberg<sup>2</sup> showed that spheres, rods, and vesicles were formed, from PS<sub>200</sub>-*b*-PAA<sub>21</sub>, PS<sub>200</sub>-*b*-PAA<sub>15</sub> and PS<sub>200</sub>-*b*-PAA<sub>8</sub> copolymers, respectively, in dimethylformamide (DMF)/water solutions. The degree of PS stretching in these three types of aggregates was 1.41, 1.26, and 0.99, respectively.<sup>35</sup> This example illustrates the reduction of the degree of stretching as the morphology changes from spheres to rods to vesicles. At the degree of PS stretching of 0.99, the wall thickness of the vesicles was approximately 18 nm for the PS<sub>200</sub>-*b*-PAA<sub>8</sub> copolymer. Shen and Eisenberg<sup>41</sup> showed that PS-*b*-PAA copolymers with a range of 250-300 PS units and a fixed poly(acrylic acid) (PAA) length of 50 formed aggregates of vesicles under appropriate conditions. The lower the block length ratio was of PAA to PS, the greater the tendency was to form vesicles. Yu et al.<sup>42</sup> showed that with 2 wt % PS-*b*-PAA copolymer in dioxane, when the block length ratio of PAA to PS was 0.178 (equivalent to 15.1 mol % PAA in the PS<sub>490</sub>-*b*-PAA<sub>87</sub> diblock), cylinders were obtained. However, when the ratio dropped to 0.116 (10.4 mol % PAA of PS<sub>500</sub>-*b*-PAA<sub>58</sub>), small vesicles were formed, and as the ratio decreased further to 0.105 (9.5 mol % PAA of PS<sub>390</sub>-*b*-PAA<sub>41</sub>), the vesicle sizes increased

from 100-150 nm to 150-500 nm. Still larger vesicles were formed when the block length ratio of PAA to PS decreased further to 0.06 (equivalent to 5.8 mol % PAA in the PS<sub>420</sub>-*b*-PAA<sub>26</sub> diblock).

The area per corona chain on the core surface ( $A_c$ ) is also related to the copolymer composition, as shown in the following equation:<sup>39</sup>  $A_c \approx N_{PS}^{0.6} N_{PAA}^{0.15}$ . The equation shows that an increase in the core or corona block length results in an increase in  $A_c$ . Because the intra-corona interactions are inversely proportional to  $A_c$ , an increase in the core or corona block length will result in a decrease in the intracore chain repulsions. This may seem counterintuitive; however, it may be recalled that as the length of the PS block increases, the size of the core increases, and for equal PAA block lengths, this results in a decrease in repulsion. However, an increase in the PAA block length results in a decrease in the aggregation number ( $N_{agg}$ ), which reduces the radius of curvature, increases the solid angle per acrylic acid chain, and thus decreases the repulsion. This consideration applies only to spheres. The value of  $A_c$  also depends on the morphology; there is a decrease in  $A_c$  from spheres to rods to vesicles. For example, Zhang and Eisenberg<sup>7</sup> showed that for PS<sub>200</sub>-*b*-PAA<sub>21</sub> copolymers in a DMF/water (75/25 w/w) solvent mixture, spheres were produced (i.e.,  $A_c = 8 \text{ nm}^2$ ). However as the PAA block length decreased to 15 units (i.e.,  $A_c = 5.8 \text{ nm}^2$ ), rods were produced, and when it was reduced further to 8 units (i.e.,  $A_c = 4.2 \text{ nm}^2$ ), vesicles were formed.

The morphology of the block copolymer aggregates depends also on the initial copolymer concentration.<sup>35</sup> Zhang and Eisenberg<sup>35</sup> prepared three different concentrations of PS<sub>410</sub>-*b*-PAA<sub>25</sub> solutions in DMF. For the 2 wt % solution, the aggregates were spherical, at 2.6 wt %, rodlike micelles were formed; and at 4 wt %, the

aggregates were vesicular with some rods present. At 4 wt %, the vesicle sizes ranged from 50 to 500 nm. An increase in the copolymer concentration results in an increase in the aggregation number of the micelles. The PS chains must stretch more, but this is entropically unfavorable. Therefore, at some point, the aggregates change to a more thermodynamically favorable morphology (i.e., from spheres to rods or from rods to vesicles). The dependence of morphology on concentration can be seen very clearly in the phase diagram (discussed later).<sup>43</sup> Shen and Eisenberg<sup>41</sup> showed that in the phase diagrams for different PS-*b*-PAA copolymer systems, when the water content is at a fixed value, the initial copolymer concentration is important in determining if vesicles can be formed. For example, at a fixed water content of 25 wt %, vesicles only form at concentrations greater than approximately 0.6 wt % PS<sub>310</sub>-*b*-PAA<sub>52</sub> copolymer. They also showed that as the polymer concentration increased from 0.6 wt % to 5.0 wt %, the mean diameter of the vesicles increased from 90 to 124 nm.<sup>43</sup> Generally, with increasing copolymer concentration, the aggregate morphology tends to change similarly to that observed with increasing water content.<sup>43</sup>

#### 2.4. Water Content and Nature of Common Solvent

The water content influences both the size and shape of the block copolymer aggregates. As mentioned earlier, water acts as a precipitant for the hydrophobic block in the common solvent. At the critical water concentration (CWC), the single polymer chains present in solution start aggregating into spherical micelles. The CWC depends on the molecular weight, the polymer concentration and the nature of the common solvent.<sup>7</sup> As more water is added to the polymer solution, the morphologies are transformed from spheres to rods and then eventually to vesicles. The morphological transitions induced by

water can again be explained by the force balance between the three factors (described earlier) that govern the formation of the aggregates of morphologies. For example, as more water is added to the spherical aggregates, the solvent becomes poorer for the hydrophobic block, and the interfacial energy between the core and the corona increases.<sup>43</sup> To reduce the total interfacial area in response to the increasing interfacial energy, there is an increase in the micelle diameter (i.e., an increase in the aggregation number), accompanied by a decrease in the number of micelles. However, this is thermodynamically unfavorable for some of the components of the free energy, as both the core-chain stretching and the corona-chain repulsion increase. If the corona chains are long with respect to the core chains, the morphology freezes (with continuing water addition) in the spherical form, and starlike micelles are formed. When the corona chains are shorter, the micelle can continue to increase in size until the driving force to reduce the interfacial energy is exceeded by the thermodynamic penalty incurred by core-chain stretching and corona repulsion. At this point, to reduce the total free energy of the system, the spherical aggregates transform to rodlike aggregates of a smaller diameter, thus reducing the core-chain stretching and corona-chain repulsion. As more water is added, the tendency to reduce the free energy of the system continues, and the rods, in turn, are transformed into vesicles.<sup>41,43</sup> The effect of water content on vesicle sizes is discussed in another section dealing with the thermodynamics of curvature stabilization in vesicles.

The common solvent also influences the morphology of the aggregates.<sup>42,44</sup> A common solvent is needed to dissolve both the hydrophobic and hydrophilic blocks to form a copolymer solution before the precipitant is added to induce self-assembly.

Different common solvents change the relative coil dimensions of both the core and corona chains. The different solvents also influence the rate of change of coil dimensions with the water content and the onset of self assembly upon addition of water. The relative coil dimensions can influence the morphology in the same way that the packing factor influences the morphologies of small-molecule amphiphile aggregates. Yu and Eisenberg<sup>44</sup> showed that spherical aggregates were obtained from PS<sub>500</sub>-*b*-PAA<sub>58</sub> in DMF, but vesicles were obtained when the initial solvent was tetrahydrofuran (THF) or dioxane. At the onset of micellization, the core of the aggregates was larger in THF and in dioxane than in DMF. The closeness of the solubility parameters of THF and dioxane to that of homopolystyrene resulted in a higher degree of swelling of both the homopolymer and the cores of the PS-*b*-PAA aggregates.<sup>7</sup> Yu et al.<sup>42</sup> showed that the wall thickness of the PS<sub>500</sub>-*b*-PAA<sub>58</sub> and PS<sub>390</sub>-*b*-PAA<sub>41</sub> copolymers was greater when the common solvent used was THF instead of dioxane. The control of the block copolymer aggregates can be achieved not only with single solvents but also with mixed solvents. Using the polystyrene-*b*-poly(4-vinyl pyridine methyl iodide) (PS<sub>195</sub>-*b*-P4VPMeI<sub>18</sub>) copolymer, Yu and Eisenberg<sup>44</sup> obtained spheres in pure THF and LCMs in pure dioxane, but using a mixture of 60/40 (w/w) THF/dioxane, they obtained rods, and from a mixture of 50/50 (w/w) THF/dioxane, they obtained vesicles. Similarly, for the PS<sub>200</sub>-*b*-PAA<sub>18</sub> copolymer, they obtained spheres and LCMs from pure DMF and pure THF, respectively; using a mixed solvent system of DMF and THF resulted in the formation of either rods (95/5 w/w DMF/THF) or vesicles (75/25 w/w DMF/THF), depending on the solvent composition.<sup>42</sup>

## 2.5. Temperature

In the preparation of the block copolymer aggregates, the addition of water serves to modify the polymer-solvent  $\chi$  parameter to induce self-assembly and morphological change. The same can be accomplished in a single solvent through changes in the temperature. In the work of Desbaumes and Eisenberg,<sup>45</sup> alcohols were used to prepare aggregates of various morphologies from the PS<sub>386</sub>-*b*-PAA<sub>79</sub> copolymer. Low alkanols (i.e., methanol, ethanol, 2-propanol and *n*-butanol) were heated to temperatures greater than 140 °C (at elevated pressures) to enhance the solubility of the hydrophobic block. Well-defined aggregates formed at those temperatures, and the morphologies froze in as the solution temperature decreased. In this case, the polymer-solvent  $\chi$  parameters changed with the temperature. Different temperatures yielded aggregates of different morphologies. For example, in propanol at 140 °C, only vesicles and LCVs were formed, but when the temperature was raised to 160 °C, connected strings of vesicles were seen.<sup>45</sup> Similarly, in butanol, only solid spheres were seen at 160 °C, but a combination of solid spheres and vesicles were present at 115 °C. To our knowledge, no clear correlation has emerged yet between the temperature and the sizes of block copolymer vesicles.

## 2.6. Additives (Ions, Surfactants, and Homopolymer)

The addition of ions (acid, base or salt) in micromolar amounts [CaCl<sub>2</sub>, Ca(Ac)<sub>2</sub>, HCl and NaOH] or millimolar amounts (NaCl) can be used to control the morphologies of block copolymer aggregates.<sup>46,47</sup> For example, when CaCl<sub>2</sub>, HCl or NaCl is added to a PS<sub>410</sub>-*b*-PAA<sub>25</sub> copolymer/DMF solution, at zero ion content, solid spheres can be observed. As more ions are added, spheres are converted to rods and rods are converted

to vesicles, with LCVs forming at progressively higher ion concentrations.<sup>47</sup> Table 2.1 gives a summary of some conditions under which vesicles are formed with different additives; the size ranges of the vesicles are also given.

**Table 2.1.** Formation of block copolymer vesicles in the presence of different additives.<sup>a</sup>

System	Additive	Concentration	Dominant Morphology	Size Ranges (nm)	References
PS <sub>410</sub> - <i>b</i> -PAA <sub>13</sub>	HCl	155 $\mu$ M	Vesicles	30-60	47
PS <sub>410</sub> - <i>b</i> -PAA <sub>25</sub>	HCl	240-420 $\mu$ M	Vesicles	30-200	46,47
PS <sub>660</sub> - <i>b</i> -PAA <sub>24</sub>	HCl	570-850 $\mu$ M	Vesicles	NA	47
PS <sub>410</sub> - <i>b</i> -PAA <sub>13</sub>	NaOH	28 $\mu$ M	Spheres and occasional vesicles	30-110	47
PS <sub>410</sub> - <i>b</i> -PAA <sub>25</sub>	NaCl	5.3-16 mM	Vesicles	50-400	46,47
PS <sub>410</sub> - <i>b</i> -PAA <sub>13</sub>	CaCl <sub>2</sub>	9-11 $\mu$ M	Vesicles	50-300	47
PS <sub>410</sub> - <i>b</i> -PAA <sub>25</sub>	CaCl <sub>2</sub>	140-200 $\mu$ M	Vesicles	NA	46,47
PS <sub>240</sub> - <i>b</i> -PEO <sub>80</sub>	LiCl	1.3 mM	Lamellae and vesicles	100-300	46
PS <sub>310</sub> - <i>b</i> -PAA <sub>52</sub>	SDS	12.1 mM	Vesicles	50-150	48
PS <sub>310</sub> - <i>b</i> -PAA <sub>52</sub>	Tridecanoic acid	115 mM	Vesicles	NA	48

<sup>a</sup> NA = not applicable.

The addition of HCl favors the formation of vesicles from spheres or rods because it results in a decrease in the repulsion between the PAA chains on account of the protonation of the small number of ionized sites on PAA. This leads to an increase in the aggregate size and an increase in the degree of stretching of the core chain. The addition of Na<sup>+</sup> results in the screening of the electrostatic field along the partially ionized PAA chains. In both cases, the corona repulsion is reduced. Divalent ions such as Ca<sup>2+</sup> have a greater effect than univalent ions such as Na<sup>+</sup> in inducing a morphological change. For example, it requires at least a 4 mM solution of NaCl, as opposed to a 85  $\mu$ M solution of

CaCl<sub>2</sub> to produce the first appearance of vesicles in a PS<sub>410</sub>-*b*-PAA<sub>25</sub> copolymer/DMF solution.<sup>47</sup> The addition of NaOH, as might be expected, has an effect opposite to that observed with HCl. The PAA chains are neutralized, and this results in an increase in the degree of ionization, and therefore, an increased repulsion between corona chains. For example, in a 2 wt % PS<sub>410</sub>-*b*-PAA<sub>25</sub> copolymer/DMF solution and in the absence of additives, the aggregates are vesicles. When NaOH is added to the copolymer solution, the morphology progressively changes from vesicles to spheres and then to smaller spheres at higher NaOH contents.<sup>47</sup>

The effect of a surfactant [sodium dodecyl sulfate (SDS)] on PS-*b*-PAA aggregates was investigated by Burke and Eisenberg.<sup>48</sup> The addition of SDS lowered the water content needed to induce a morphological change in PS<sub>310</sub>-*b*-PAA<sub>53</sub> aggregates. For example, in dioxane containing 1.0 wt % polymer, at a water concentration of 12.5 wt %, as the amount of added SDS progressively increased from 7.1 to 14.3 mM, the morphologies changed from a mixture of spheres and rods, to rods alone, to a mixture of rods and vesicles, and finally to vesicles alone. They also showed that at certain solvent compositions, SDS induced changes in the morphologies that NaCl could not induce. For example, at a 10 wt % water concentration, a range of 3.2-12.1 mM SDS was added to induce the morphological transitions from spheres to rods to vesicles, whereas NaCl was ineffective at these concentrations. SDS was more soluble than NaCl in the solvent mixture, and the hydrophobic tail was assumed to partition into the aggregate core. The corona chains were then spaced further apart, and there was an increase in the core diameter and a consequent increase in the degree of stretching of the PS block.

The addition of homopolystyrene causes spherical aggregates to change their size. Zhang and Eisenberg<sup>39</sup> showed that, with the addition of homopolystyrene to the PS<sub>500</sub>-*b*-PAA<sub>58</sub> copolymer, the spheres increased in size from 30 nm to 37 nm as the weight ratio of the block copolymer to the homopolystyrene changed by 30% (i.e., 100 to 70). The addition of homopolymer did not induce a change in PS in the spherical morphology because the preferential accumulation of homopolymer styrene in the center of the hydrophobic core reduced the degree of stretching of the PS segments in the block. Because morphological changes from spheres to rods were induced, among others, by an increase in stretching, it was clear that a decrease in the degree of stretching was not able to induce rod formation in a sphere or vesicle formation in a rod. By contrast, adding homopolymer PS to non-spherical aggregates (rods and vesicles) could change their morphology. For example, the addition of the homopolymer (10 wt % PS) caused vesicles made from PS<sub>410</sub>-*b*-PAA<sub>16</sub> to convert into spheres, and similarly at 5 wt % PS, rods made from PS<sub>180</sub>-*b*-PAA<sub>14</sub> converted into spheres. This was caused by an accumulation of the homopolymer in the micellar core, and as a result, there was reduced stretching of the core chains.

## 2.7. Polydispersity

Recently, the effect of the PAA block polydispersity on the aggregate morphology was investigated with a series of PS-*b*-PAA copolymers.<sup>49</sup> The PAA block length was artificially broadened through the mixing of different copolymers with the same PS block (the number-average molecular weight of the PAA block was kept constant at PS<sub>310</sub>-*b*-PAA<sub>28</sub>, but its weight-average molecular weight was varied). Terreau et al.<sup>49</sup> showed that the vesicle sizes generally decreased as the PAA polydispersity index (PDI) increased.

For example, at a low PAA PDI of 1.10, the average vesicle size was 270 nm, but when the PDI was increased to 2.13, the vesicle size decreased to 85 nm. The decrease was ascribed to segregation of the long chains preferentially to the outside and the short chains segregated to the inside of the vesicle, as suggested by Luo and Eisenberg<sup>50</sup> (discussed later). They also showed that there was no segregation into different aggregates but rather segregation within the same aggregate.

## 2.8. Thermodynamics of Curvature Stabilization in Vesicles

Shen and Eisenberg<sup>43</sup> developed a phase diagram for the PS<sub>310</sub>-*b*-PAA<sub>52</sub> copolymer in a dioxane/water mixture that showed the region of stability of vesicles. They showed that increasing the water content in the solvent mixture resulted in an increase in the vesicle diameter. They were also able to demonstrate the reversibility of the vesicle size as a function of water content. The work by Shen and Eisenberg highlighted the fact that vesicles were potentially equilibrium structures. This was proven recently when Luo and Eisenberg<sup>50</sup> showed a mechanism for thermodynamic curvature stabilization in block copolymer vesicles. They were able to show that in PS-*b*-PAA vesicles, the long PAA chains were preferentially segregated to the outside and the shorter PAA chains to the inside. The repulsions of the PAA chains on the outside were stronger than those on the inside, and so the curvature was stabilized and the vesicles remained in thermodynamic equilibrium. Luo and Eisenberg used fluorescent quenching techniques to prove the segregation hypothesis. They attached pyrene molecules at the junction points of the various diblock copolymers. Using a fluorescently labeled diblock with a short PAA chain, they found that only a small fraction of the pyrene could be quenched by Tl<sup>+</sup>. Similarly labeled polymers with long PAA segments were almost

completely quenched because they were located on the outside and were thus accessible to the quencher (Figure 2.2).

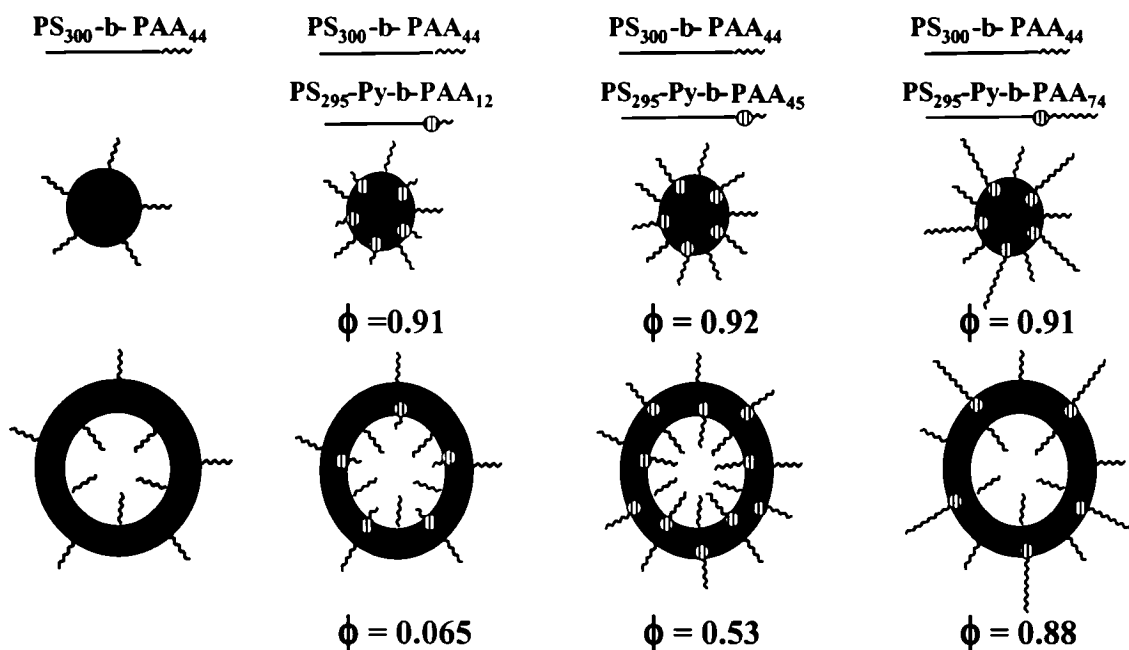


**Figure 2.2.** Segregation in  $PS_{300}\text{-}b\text{-}PAA_{44}$  copolymer vesicles. The fraction of the pyrene (Py) molecules that are quenched ( $\phi$ ) increases with the length of the PAA segments of the labeled PS-Py-*b*-PAA copolymer.<sup>51</sup> (From L. Luo and A. Eisenberg, *Langmuir* 2002, 17, 6804.)

Luo and Eisenberg<sup>52</sup> took this one step further by preparing block copolymer vesicles with segregated acidic and basic coronas. They used  $PS_{310}\text{-}b\text{-}P4VP_{33}$  [where P4VP is poly(4-vinylpyridine)] and  $PS_{300}\text{-}b\text{-}PAA_{11}$  copolymers and found that, under the appropriate conditions, the longer P4VP chains segregated to the outside, whereas the shorter PAA chains segregated into the inside. To prove that the P4VP chains were on the outside, they showed that the pH dependence of the  $\zeta$  potential of the vesicles was identical to that of the vesicles prepared from PS-*b*-P4VP alone, and to prove that the

PAA segments were on the inside, they added fluorescently labeled PS-*b*-PAA chains of an identical PAA length and showed that the fluorescence could not be quenched.

Additional studies by Luo and Eisenberg suggested that the sizes of PS-*b*-PAA block copolymer vesicles were also under thermodynamic control.<sup>51</sup> By changing the solvent content and specifically increasing the water content, they reduced the solvent quality for the PS core. This resulted in an increase in the interfacial energy between the core and the solvent outside the core. In response to the increase in the interfacial energy, there was an increase in the vesicle sizes to minimize the total interfacial area. Figure 2.3 illustrates the size changes resulting from changes in the water content.

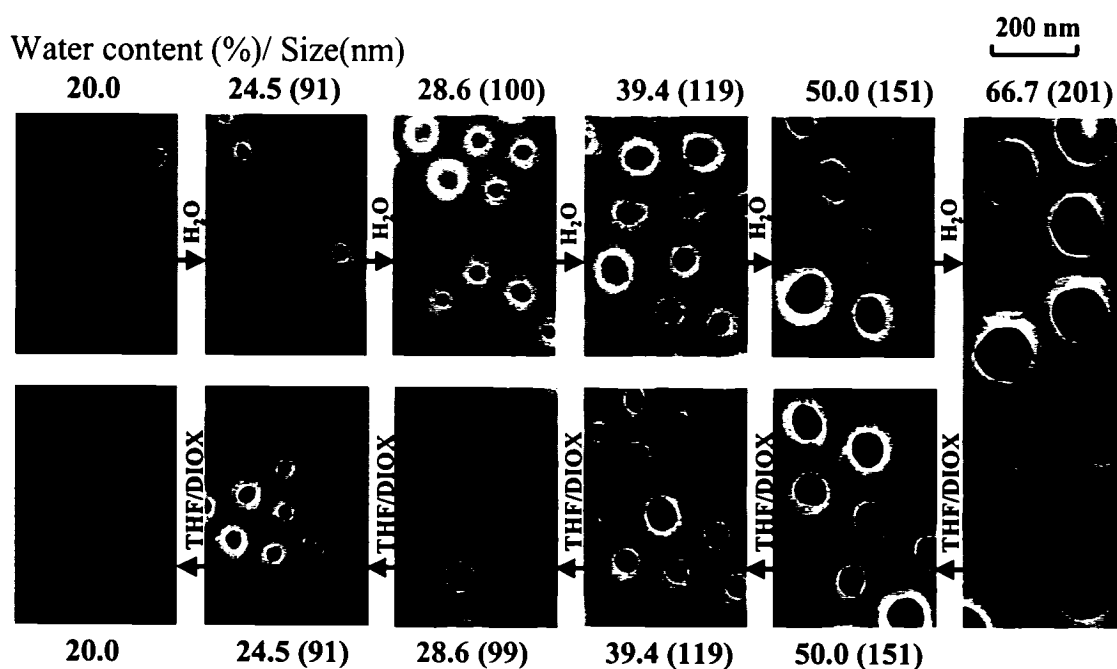


**Figure 2.3.** Reversibility of vesicle sizes in response to increasing or decreasing water contents for PS<sub>300</sub>-*b*-PAA<sub>44</sub> vesicles in a THF/dioxane (44.4/55.6) solvent mixture. (From L. Luo and A. Eisenberg, *Langmuir* 2002, 18, 1952.)

Fluorescence quenching techniques proved again to be useful in showing that the preferential segregation of the longer PAA chains on the outside and the shorter PAA chains on the inside was size dependent (i.e., the larger the vesicles, the lower the degree of segregation) and reversible in response to changes in size. Fusion and fission mechanisms are involved in the increase and decrease of vesicle sizes.<sup>51</sup> The proposed mechanisms are shown in Figure 2.4.

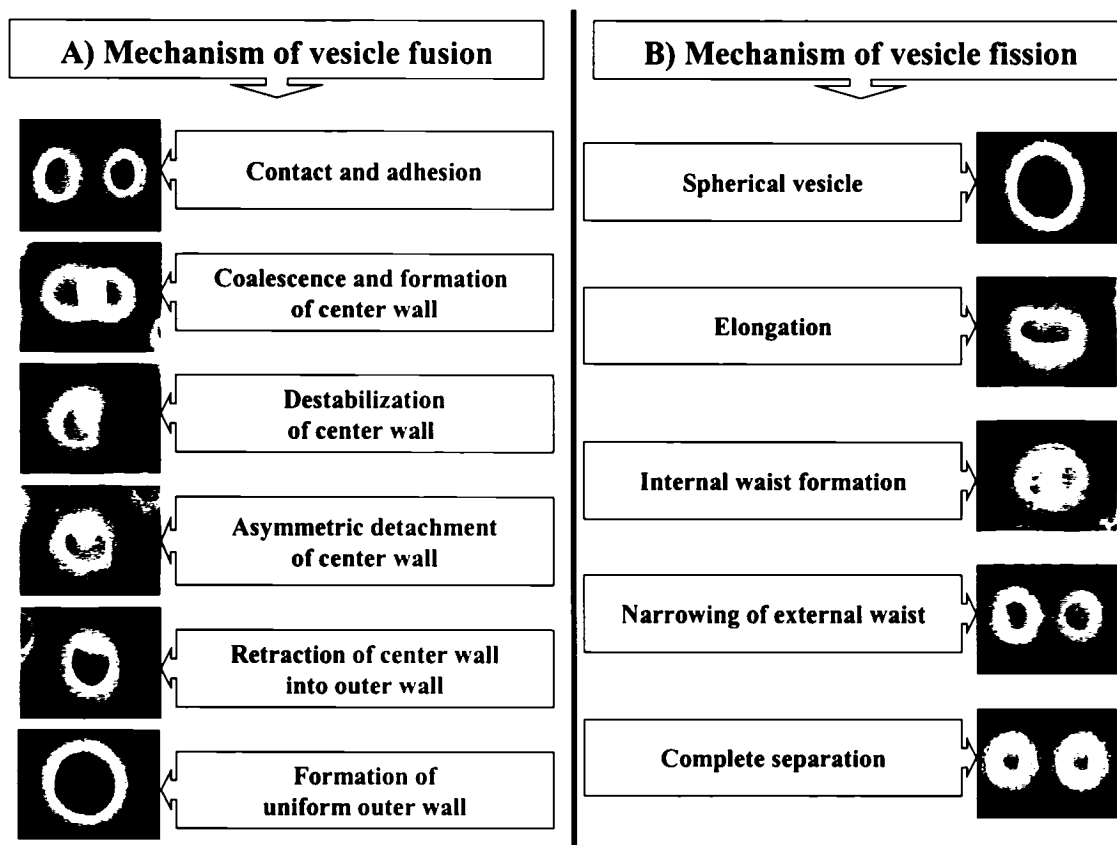


**Figure 2.4.** Possible mechanisms of (A) the fusion of vesicles and (B) the fission of a vesicle. (From L. Luo and A. Eisenberg, *Langmuir* 2002, 17, 6804.)

The first fusion step involves the contact and adhesion of two vesicles. This is followed by coalescence and the formation of a center wall between the two vesicles. The wall is

then destabilized and retracted into the outer wall. Finally, there is a smoothing of the outer wall to form uniform vesicles. The fission process involves the elongation of the vesicle, followed by the formation of an internal waist, and the narrowing of the external waist. At this point, a connection between the two compartments can still be seen; eventually, complete separation is achieved.

## 2.9. Kinetics of Vesicle Size Change

Recently, Choucair et al.<sup>53</sup> investigated the kinetics of increases in the vesicle size of PS-*b*-PAA copolymers in solution as a function of water content. They showed that as the water content increased, the rate of increase in the vesicle size decreased (as reflected by an increase in the relaxation time; see Figure 2.5).

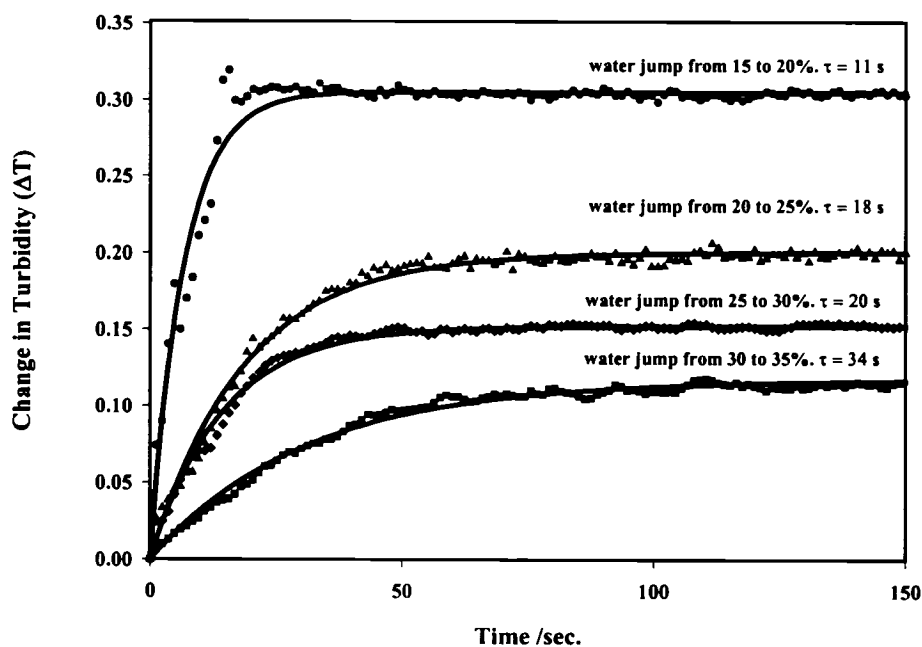


**Figure 2.5.** Examples of kinetic measurements for increases in the vesicle size in solutions of 0.5 wt % PS<sub>310</sub>-*b*-PAA<sub>36</sub> after successive 5% increases in the water content. (From A.A. Choucair et al., Langmuir 2003, 19, 1001.)

At higher water contents, the rate of vesicle fusion decreased because of a decrease in the frequency of vesicle collisions and a decrease in the chain mobility. The effect of the magnitude of the water content perturbation was also investigated; it was found that the larger the perturbation was, the faster the kinetics were (or the lower the relaxation times were). Choucair et al also investigated the effect of the acrylic acid block length and initial polymer concentration and found that increasing either factor resulted in an increase in the rate of vesicle fusion. The calculated average relaxation times were between 10 and 700 seconds and were highly dependent on the experimental conditions (i.e., water content, magnitude of the water jump, PAA block length, and polymer concentration).<sup>53</sup>

## **2.10. Other Bilayer Morphologies**

The focus of this review is block copolymer vesicles; it should be noted, however, that there are many different types of bilayer morphologies structurally related to vesicles. These include tubules, hollow doughnuts with one or more holes, lamellae with protruding rods, concentric vesicles with uniform spacing (onions with spacing), multi-lamellar onions with no spacing between the walls (solid onions), entrapped vesicles, and vesicles with hollow rods in the walls. More information about these nonclassical vesicle structures can be found in a review by Burke et al.<sup>54</sup> and a brief summary (including vesicle sizes) and additional references are given in Table 2.2.

**Table 2.2.** Bilayer morphologies structurally related to vesicles obtainable from the block copolymer systems.

Morphology	Polymer	Conditions	Size ranges	Reference
Tubules	PS <sub>200</sub> - <i>b</i> -PAA <sub>18</sub>	25/25/50 (w/w/w) (THF/dioxane/water) mixture	100's of micrometers (length)	42
Tubules Linear Branched Tubules with a hole in a branch Plumber's nightmare	PS <sub>240</sub> - <i>b</i> -PEO <sub>15</sub>	DMF/water mixture (1.5-2 wt %)	10's of nanometers to 100's of micrometers (length)	55,56
Hollow doughnuts with one or more holes	PS <sub>240</sub> - <i>b</i> -PEO <sub>15</sub>	DMF/water mixture (1.5-2 wt %)	100's of nanometers	55
Lamallae with protruding rods	PS <sub>240</sub> - <i>b</i> -PEO <sub>45</sub>	DMF/water mixture (1.5 wt %)	100's of nanometers	33,55,56
Onions with spacing	PS <sub>132</sub> - <i>b</i> -PAA <sub>20</sub>	60/40 (w/w) (dioxane/water) (10 wt %)	500-1200 nm	57
Solid onions	PS <sub>260</sub> - <i>b</i> - P4VPDecI <sub>70</sub>	DMF/water mixture (1 wt %)	100-500 nm	57
Entrapped vesicles	PS <sub>200</sub> - <i>b</i> -PAA <sub>18</sub>	25/25/50 (w/w/w) DMF/THF/water mixture	200-300 nm	42
Entrapped vesicles	PS <sub>240</sub> - <i>b</i> -PEO <sub>15</sub>	50/50 (w/w) DMF/water	300-600 nm	56
Vesicles with hollow tubes in the wall	PS <sub>100</sub> - <i>b</i> -PEO <sub>30</sub> PS <sub>125</sub> - <i>b</i> -PEO <sub>30</sub> PS <sub>215</sub> - <i>b</i> -PEO <sub>37</sub>	THF/water mixture (1 wt %)	200-400 nm 200-400 nm 200-400 nm	58
Bowl-shaped morphology	PAI <sub>11</sub> -PS <sub>228</sub> - <i>b</i> - PAI <sub>11</sub>	THF/water or dioxane/water mixture (1 wt %)	70-600 nm	59

Recently, Riegel et al.<sup>59</sup> observed a bowl-shaped morphology from triblock copolymers, [5-(*N,N*-diethylamino)isoprene-*b*-polystyrene-5-(*N,N*-diethylamino)isoprene] (PAI<sub>11</sub>-PS<sub>228</sub>-*b*-PAI<sub>11</sub>) in THF/water or dioxane/water mixtures. They showed that these

structures, which had some similarity to vesicles although they are not unilamellar structures, were only kinetically stable and not under equilibrium control.

### 2.11. Copolymer Systems Producing Vesicles

The work on block copolymer vesicles that has already been discussed has come almost exclusively from our group. There are many other groups involved in this ever-expanding field, and we highlight some of their most significant contributions next. Several reviews have been written recently.<sup>11,15,54,57</sup> Many amphiphilic block copolymer systems have been synthesized that produce vesicles. Among the most common core blocks are PS, polyisoprene, polysiloxane, poly(propylene oxide), poly(ethyl ethylene) and polybutadiene, but others have also received attention.

Blocks containing PS as one of the components are described in a great number of publications on block copolymer vesicles. Meijer's group examined amphiphilic molecules, which were similar to surfactants in shape and to block copolymers in size, to produce vesicular structures. They synthesized PS with poly(propylene imine) dendrimers, specifically PS-dendr-(NH<sub>2</sub>)<sub>8</sub>, which produced vesicle structures of approximately 50-100 nm.<sup>1</sup> They were also able to form 20-200 nm vesicles in acidic solutions from amphiphilic dendrimers attached to palmitoyl- and azobenzene-containing alkyl chains.<sup>60</sup> Evidence for the existence of the vesicle structures was given by cryo-transmission electron microscopy through direct visualization in solution and by osmotic experiments that showed the existence of an inner aqueous compartment.<sup>60</sup> Cornelissen et al.<sup>6</sup> made an amphiphilic block copolymer with a head group composed of amino acids, that is, polystyrene-*block*-poly(isocyano-l-alanine-l-alanine) (PS<sub>40</sub>-*b*-PIAA<sub>10</sub>). They produced collapsed vesicles ranging in size from tens to hundreds of nanometers

with a bilayer thickness of 16 nm in a sodium acetate buffer solution.<sup>6</sup> Jenekhe and Chen<sup>5</sup> synthesized a rod-coil block copolymer [poly(phenylquinoline)-*b*-polystyrene (PPQ-*b*-PS)]. The vesicles produced from PPQ<sub>50</sub>-*b*-PS<sub>300</sub> ranged in size from 500 to 1000 nm with a wall thickness of 200 nm in a mixed solvent of dichloromethane and trifluoroacetic acid. Recently, Yuan et al.<sup>61</sup> synthesized polystyrene-*b*-poly(ethylene oxide)-*b*-polystyrene triblock copolymers for the purpose of creating crew-cut aggregates in aqueous solutions. They formed vesicles ranging in size from 200 to 1000 nm from 1 wt % copolymer in THF and dioxane alone and 2 wt % copolymer in THF/water and dioxane/water solvent mixtures. Gravano et al.<sup>62</sup> made poly[4-(aminomethyl)-styrene]-*block*-polystyrene (P4AMS-*b*-PS) with a small number of units of poly[4-(aminomethyl)-styrene] (< 10) and various number of units of PS (46-130) to form unilamellar vesicles of less than 300 nm in DMF and THF/dioxane solvents. Very large vesicles, up to 10 μm in diameter, were produced with P4AMS<sub>8</sub>-*b*-PS<sub>130</sub> in THF because of the large bending moduli of the P4AMS-*b*-PS bilayers. In addition, Rotello's group<sup>63</sup> synthesized random copolymers of functionalized PSs, and the self-assembly of the complementary polymer chains through specific hydrogen bonding resulted in the formation of giant vesicles that were approximately 3 μm in diameter. Many of the vesicles were unilamellar, but fused vesicles and vesicles within other vesicles were also observed. Similarly, Rotello's group<sup>64</sup> also produced giant vesicles ranging in size from 3 to 4 μm in diameter from polynorborene-based random copolymers with complementary side chains. Giant vesicles have been extensively described in a large number of publications<sup>65,66</sup> and the given references and are not covered in this review.

Poly(2-cinnamoyl ethyl methacrylate) has been used as the wall material by Liu's group,<sup>67</sup> who formed vesicles from polyisoprene-*block*-poly(2-cinnamoyl ethyl methacrylate) (PI-*b*-PCEMA). The stability of these vesicles in aqueous media was made possible by the hydroxylation of the polyisoprene chains to form hydroxylated polyisoprene. Ding and Liu<sup>67</sup> loaded rhodamine B, a fluorescent probe, into PI-*b*-PCEMA vesicles in methanol and released the contents into aqueous media. Ding and Liu<sup>68</sup> also formed PI-*b*-PCEMA vesicles in a THF/hexanes solvent mixture. Further treatment by photo cross-linking followed by ozonolysis produced hairy, semi-shaved and fully shaved hollow vesicles at the different stages of modification.<sup>68</sup>

Polysiloxane-based block copolymers have resulted in the formation of block copolymer vesicles. Meier's group<sup>12</sup> synthesized the triblock copolymer poly(2-methyloxazoline)-*block*-poly(dimethylsiloxane)-*block*-poly(2-methyloxazoline) (PMOXA-*b*-PDMS-*b*-PMOXA). The polymerized vesicles that they formed ranged in size from 50 to 500 nm, and crosslinking did not change the shape of the vesicles. Meier's group<sup>69</sup> also was able to form giant vesicles ranging in size from 1 to 2  $\mu\text{m}$  from the PMOXA-*b*-PDMS-*b*-PMOXA copolymer, and these were used to control the calcium concentration during the precipitation of calcium phosphate. Recently, they synthesized poly(ethylene oxide)-*block*-poly(dimethylsiloxane)-*block*-poly(2-methyloxazoline) (PEO-*b*-PDMS-*b*-PMOXA) and produced vesicles ranging in size from 60 to 300 nm.<sup>70</sup> Using the ideas and methodology from Luo and Eisenberg,<sup>51</sup> they were able to show that the vesicles formed from the triblock in which the poly(2-methyloxazoline) (PMOXA) chains were longer than the poly(ethylene oxide) (PEO) chains and the PMOXA chains were located on the outside; similarly, for the triblock in

which the PMOXA chains were shorter, these chains were located on the inside of the vesicles. Kickelbick et al.<sup>71</sup> formed poly(dimethylsiloxane)-*b*-poly(ethylene oxide) vesicles ranging in size from 20 nm up to several hundred nanometers in water. Similarly, vesicles ranging from 100 to 180 nm were produced from poly(methylphenylsilane)-*block*-poly(ethylene oxide) in THF/water mixtures.<sup>72</sup>

The Pluronics series [poly(ethylene oxide)-*block*-poly(propylene oxide)-*block*-poly(ethylene oxide)] has also been used to form different block copolymer vesicles. Schillen et al.<sup>73</sup> created unilamellar vesicles from the triblock system PEO<sub>5</sub>-*b*-PPO<sub>68</sub>-*b*-PEO<sub>5</sub> with an extrusion method. Cryo-transmission electron microscopy images showed that the apparent wall thickness was 3-5 nm. Multilamellar vesicles (onions) were created by shear at low concentrations of the Pluronic P123 (PEO<sub>20</sub>-*b*-PPO<sub>70</sub>-*b*-PEO<sub>20</sub>) and F127 (PEO<sub>100</sub>-*b*-PPO<sub>70</sub>-*b*-PEO<sub>100</sub>) copolymers in butanol/water systems.<sup>74,75</sup> Valentini et al.<sup>76</sup> formed 15-250 nm sized vesicles from poly(propylene sulfide)-*block*-poly(ethylene glycol). They were able to determine the border between the hydrophobic and hydrophilic junctions in the polymeric vesicles using various NMR techniques, this being important for pinpointing water penetration.

Harris et al.<sup>77</sup> synthesized a series of poly(butylene oxide)-*block*-poly(ethylene oxide) copolymers (PBO-*b*-PEO) ranging in length from 10 to 12 units for butylene oxide and from 5 to 18 units for ethylene oxide. They obtained multilamellar vesicles at copolymer concentrations as low as 0.05 wt % and as high as 20 wt %. The vesicles were also found to be resistant to sonication and moderate shear.<sup>77</sup> Recently, they formed 120-175 nm vesicles from sulfonated butylene oxide oligomers ranging in length of 4 to 17

units for butylene oxide.<sup>78</sup> The vesicles were stable for at least five months at room temperature and were stable for nine days at 100 °C.<sup>78</sup>

Discher et al.<sup>10</sup> synthesized poly(ethyl ethylene)-*block*-poly(ethylene oxide) (PEE<sub>37</sub>-*b*-PEO<sub>40</sub>) and formed small vesicles (< 200 nm) or large vesicles (20-50 μm) which they called “polymersomes”. They showed that the walls of their PEE<sub>37</sub>-*b*-PEO<sub>40</sub> vesicles were an order of magnitude more robust than phospholipid bilayers and less permeable to water by several orders of magnitude. The thickness of the hydrophobic wall (~d = 8 nm) was greater than that of typical phospholipid bilayers (d = 3-4 nm).<sup>11</sup> Santore et al.<sup>79</sup> demonstrated that the addition of a surfactant (Pluronic L31) to the PEE<sub>37</sub>-*b*-PEO<sub>40</sub> copolymer weakened the polymeric membrane. This would allow the drug to diffuse through the polymer walls more readily. Also, the triblock copolymer PEO-*b*-PEE-*b*-PEO formed vesicles along with cylinders and spheres in solution.<sup>80</sup> Recently, Photos et al.<sup>81</sup> injected various vesicles formed from PEO-*b*-PEE and poly(ethylene oxide)-*block*-polybutadiene copolymers into rats and showed that their *in vivo* circulation times were approximately two times longer than Stealth liposomes [coated with poly(ethylene glycol) (PEG)].

Polybutadiene based systems have also been used for the formation of vesicles. Antonietti's group<sup>82</sup> used polybutadiene-*block*-poly(2-vinylpyridine) (PB-*b*-P2VP) copolymers as templates for the synthesis of mesoporous silica. They found that, at a 50 wt % concentration of PB<sub>210</sub>-*b*-P2VP<sub>99</sub> copolymer in an aqueous solution, the 100-150 nm pores were filled with multilamellar vesicles. Maskos and Harris<sup>83</sup> obtained double-shell vesicles and strings of vesicles from crosslinking poly(1,2-butadiene)-*block*-poly(ethylene oxide) copolymers (PB<sub>27</sub>-*b*-PEO<sub>28</sub>). Schrage et al.<sup>84</sup> combined two

different ionomers, poly(1,2-butadiene)-*block*-poly(cesium methacrylate) (PB<sub>216</sub>-*b*-PCM<sub>29</sub>) and polystyrene-*block*-poly(1-methyl-4-vinylpyridinium iodide) (PS<sub>211</sub>-*b*-PM4VPI<sub>33</sub>), in THF and produced vesicles with the poly(1,2-butadiene) chains segregated in the inside and the PS chains segregated on the outside. Transmission electron microscopy results showed the vesicles to be approximately 100-200 nm in size. Discher's group<sup>85</sup> produced a range of vesicle sizes, small (~100 nm) to large (up to several micrometers), from poly(butadiene)-*block*-poly(ethylene oxide) (PB<sub>46</sub>-*b*-PEO<sub>26</sub>) copolymers. Crosslinking the PB-*b*-PEO vesicles in solution imparted an even greater stability, and this allowed the drying, storage, and rehydration of the vesicles to their original size and shape.<sup>86</sup> Bermudez et al.<sup>87</sup> showed that as the molecular weight of PB-*b*-PEO increased, the hydrophobic wall thickness increased up to approximately 20 nm. Recently, Bates' group<sup>22</sup> demonstrated that PB-*b*-PEO copolymer produced vesicle structures as well as y-junctions and three-dimensional networks. Biodegradable vesicles coexisting with tubules were created from polylactide-*block*-poly(ethylene glycol) copolymers ranging in size from 70 nm to 50  $\mu$ m in chloroform/water systems.<sup>88</sup> Meng et al.<sup>88</sup> also formed poly(trimethylene carbonate)-*block*-poly(ethylene glycol) and polycaprolactone-*block*-poly(ethylene glycol) vesicles.

Vesicles including a peptide group have also been prepared; these are called "peptosomes". A peptide vesicle was formed by Kimura et al.<sup>89</sup> with the fabrication of approximately 85 nm vesicular aggregates from a peptide antibiotic (Gramicidin A) conjugated with PEG. They showed that their peptide-PEG vesicles were resistant to high concentrations of Triton X-100 that normally destroyed dimyristoylphosphatidylcholine liposomes.<sup>89</sup> Kukula et al.<sup>14</sup> synthesized different

polybutadiene-*block*-poly(l-glutamic acid) (PB-*b*-PGA) copolymers ranging in length from 27 to 119 units for polybutadiene and 24 to 64 units for poly(l-glutamic acid). They were able to form vesicles ranging in size from 110 to 190 nm in pure water. Chécot et al.<sup>90</sup> formed approximately 120 nm vesicles from PB<sub>40</sub>-*b*-PGA<sub>100</sub> in a water/glycerol solvent mixture. The presence of the peptide group potentially allowed for the regulation of the system via pH or ionic strength changes.

The use of surfactants in conjunction with polymer systems has also resulted in the formation of many different vesicle systems. Kabanov et al.<sup>8</sup> formed vesicles from a complex of a block ionomer, poly(sodium methacrylate)-*block*-poly(ethylene oxide), and different single-tail cationic surfactants. The vesicles that were produced ranged in size from 85 to 120 nm. Similarly, Bronich et al.<sup>91</sup> used poly(sodium methacrylate)-*block*-poly(ethylene oxide) with a single-tail cationic surfactant, isothiuroniummethylhexadecyldimethylammonium bromide, to form small vesicles ranging in size from 80 to 100 nm. These vesicles were stable at high ionic strengths, and the vesicle sizes remained the same within a pH range of 3-9 and a temperature range of 23-60 °C. The first vesicles seen for an inorganic-surfactant system were reported by Pevzner et al.<sup>92</sup> The lamellar thickness was approximately 7 nm, and vesicle formation was thought to be driven by the presence of silicate oligomers in the system.<sup>92</sup>

## 2.12. Other Vesicle Forming Self-Assembled Amphiphilic Systems

Amphiphilic macrocyclic systems, including those containing cyclodextrins, cryptands, and calixarenes, have produced vesicles. The first bilayer vesicles composed of hydroxyethylated  $\beta$ -cyclodextrins ranged in size from 50 to 300 nm in water.<sup>93</sup> The vesicles were composed of bilayers of cyclodextrins that enclosed an aqueous interior.

Recently, Ravoo's group<sup>94</sup> showed that a disulfide reducing agent, dithiothreitol, could break down the vesicles in water. This could potentially be used to trigger release from the vesicles. Approximately 550-650 nm vesicles were formed from cryptand-based bola amphiphiles.<sup>95</sup> The structure was two macrobicyclic cryptands joined by three hydrophobic chains. Polyhydroxy macrocyclic calix[4]resorcarene and calix[4]pyrogallolarene systems produced 50-200 nm vesicles in a mixed THF/buffer system.<sup>96</sup> The calixarene vesicles retained their stability despite drying under a high vacuum and subsequent rehydration by the addition of water (see Figure 3.6 for schematics of the discussed structures).

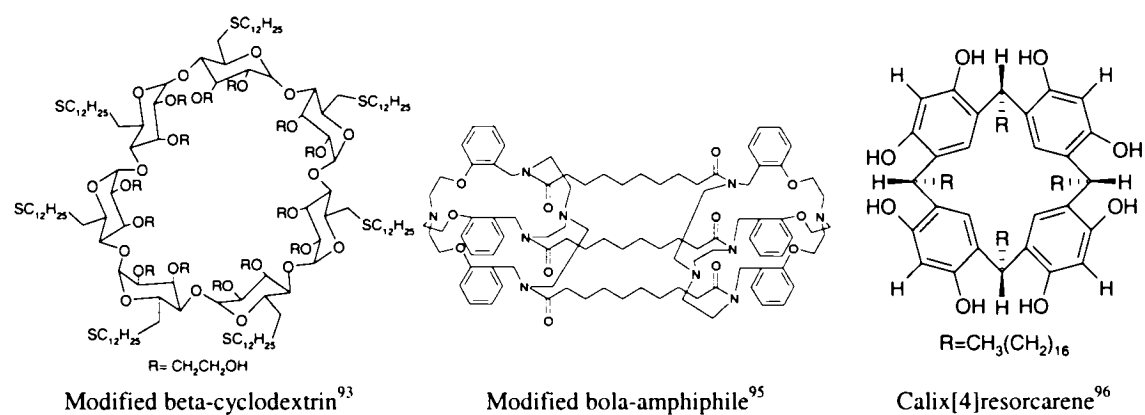


**Figure 3.6.** Other examples of amphiphilic systems that produce vesicle structures.

In addition, a synthetic amphiphilic biopolymer, meso-tetrakis[(bixinylamino)-o-phenyl]porphyrin, formed vesicles ranging in size from 30 to 120 nm with a wall thickness of about 5 nm.<sup>97</sup> The vesicles were quite stable, as they were resistant to NaCl addition and adsorption to solid surfaces, and they remained intact in 95% ethanol. Fullerenes can be made to be more hydrophilic by the replacement of hydrogens with phenyl groups, thus rendering them amphiphilic. The potassium salt of pentaphenyl

fullerene was shown to create spherical bilayer vesicles.<sup>98</sup> These vesicles were quite stable because of the rigidity of the geometrically constrained hydrophobic C<sub>60</sub> units.

### 2.13. Hollow Spheres

Hollow spheres are not vesicles in the strict sense of the word but are structurally similar in that they can potentially incorporate a variety of guest molecules, including hydrophilic agents, within their interior. Their versatility has generated much interest in this field,<sup>23,99-108</sup> and only a few representative examples can be given here. Donath et al.<sup>109</sup> constructed hollow spheres by depositing layer by layer of polyelectrolytes [poly(styrene sulfonate sodium) (PSS) and poly (allylamine hydrochloride) (PAH)] on melamine formaldehyde (MF) colloidal particles. The hollow spheres were typically 2  $\mu\text{m}$  in diameter after the removal of the MF core by HCl. Similarly, Dai et al.<sup>110</sup> formed hollow capsules with layers of PSS and PAH with interlayers of silica nanoparticles on either MF or PS particles. The addition of HCl created hollow capsules, and the further addition of HF removed the silica nanoparticles and led to hollow capsules with shells. Recently, biocompatible polyelectrolytes in layer-by-layer assembly were used in the formation of hollow capsules. Chitosan and sodium alginate were used to create hollow capsules with biocompatible, biodegradable poly (d,l-lactic acid) and poly (d,l-lactic-co-glycolic acid) microparticles as templates.<sup>111</sup> The polyelectrolytes were applied to the surface of the particles by layer-by-layer sequential adsorption and produced stable, hollow capsules ranging in size from approximately 1 to 11  $\mu\text{m}$ . Hollow polymer spheres ranging in size from several tens of nanometers up to hundreds of micrometers can be created by the crosslinking polymerization of hydrophobic monomers inside dimethyldioctadecylammonium chloride vesicles, followed by removal of the surfactant

matrix.<sup>100</sup> Similarly, McKelvey et al.<sup>104</sup> created styrene and divinyl benzene hollow polymer spheres from cationic vesicles produced from a mixture of anionic and cationic surfactants. The approximately 60 nm vesicles, with a wall thickness of 3-9 nm, retained their original structure even after vacuum drying and resuspension in water. As a result of the mixing of two homopolymers, that is, a rodlike polyimide and a coil-like P4VP in chloroform, Duan et al.<sup>112</sup> created hollow spheres ranging in size from 400 to 600 nm. That group<sup>113</sup> also investigated the mixing of hydroxyl-containing PS in chloroform and P4VP in nitromethane, followed by crosslinking and core removal by DMF, to produce hollow spheres that were resistant to vacuum drying. Li et al.<sup>106</sup> used *tert*-butyl hydroperoxide to treat amine-substituted biopolymers (e.g., bovine serum albumin (BSA) and gelatin) and synthetic polymers in water in the presence of methyl methacrylate to create graft copolymers that were then used to form 60-160 nm hollow spheres. Kramer et al.<sup>108</sup> constructed core-shell structures from dendritic polymers, polyglycerol and poly(ethylene imine) by selective and reversible functionalization. They were able to incorporate various polar or ionic organic dyes (e.g. Congo red and fluorescein), and depending on the different conditions (i.e., pH and temperature), they were able to achieve release that lasted from several hours to a few days.

#### 2.14. Conclusions

Many different types of vesicles and vesicle-like structures can now be prepared. In the case of block copolymers vesicles, each of the blocks can be tailored synthetically to modify its length and polydispersity, which, in turn, affect the vesicle size. In terms of the preparation of the block copolymer vesicles, the composition, concentration, common solvent and water contents, and temperature can affect the types of vesicles produced.

After the vesicles are created, additives such as ions, homopolymers, and surfactants can be added to alter their properties. The three fundamental parameters that affect the block copolymer vesicle morphology are core stretching, interfacial energy between the core and the outside solvent, and the corona-corona repulsion; these factors represent the key to the formation and modification of the block copolymer vesicles under equilibrium conditions.

We believe that there is also great potential for the use of vesicles in fields such as drug delivery, cosmetics and pollution control. The study of these structures in both academia and industry makes this a rapidly growing field.

After reviewing the preparation of different type of vesicles from mainly polymeric systems, the focus of the following chapter will switch to the formation of block copolymer micelles, namely polycaprolactone-*block*-poly(ethylene oxide) (PCL-*b*-PEO). In order to evaluate and better understand the loading and release properties of PCL-*b*-PEO micelles for drug delivery applications, two model hydrophobic probes, benzo[a]pyrene and Cell Tracker CM-DiI, were chosen. Benzo[a]pyrene is a member of the polycyclic aromatic hydrocarbon family, which are environmental pollutants formed by the incomplete combustion of inorganic material. It is highly carcinogenic, fluorescent and available in a radiolabelled form. CM-DiI is a fluorescent probe that is used to stain cellular membranes.<sup>114</sup> Structurally, benzo[a]pyrene and CM-DiI are very different, and their molecular weights differ by up to four times, which provides an interesting comparison. Partition coefficients of the fluorescent probes in the PCL<sub>23</sub>-*b*-PEO<sub>45</sub> micelles are also determined to ascertain the affinity of the molecules for the micelles as opposed to the aqueous solution. The partition coefficient is important in

providing information about the loading and release properties of the probes. The release of the probes is also studied using a perfect sink apparatus. Many release studies in the literature do not use a perfect sink device and hence their results may not be indicative of the actual release experiment. We use a continuous flow of water in order to wash away the probe molecules as they are released from the micelles, so they are eliminated from the reservoir, thus providing true sink conditions.

### 2.15. Acknowledgement

The authors thank the Natural Sciences and Engineering Research Council of Canada (NSERC) and Fonds Québécois de la recherche sur la nature et les technologies (FQRNT) for their continued support, and they acknowledge Rhodia for its financial support. The authors also thank A. Choucair and O. Terreau for useful suggestions in the preparation of this article.

### 2.16. References

- (1) van Hest, J. C. M.; Delnoye, D. A. P.; Baars, M. W. P. L.; van Genderen, M. H. P.; Meijer, E. W. *Science* **1995**, *268*, 1592-1595.
- (2) Zhang, L.; Eisenberg, A. *Science* **1995**, *268*, 1728-1731.
- (3) Correa, N. M.; Schelly, Z. A. *Langmuir* **1998**, *14*, 5802-5805.
- (4) Percec, V.; Ahn, C. H.; Ungar, G.; Yeardley, D. J. P.; Moller, M.; Sheiko, S. S. *Nature* **1998**, *391*, 161-164.
- (5) Jenekhe, S. A.; Chen, X. L. *Science* **1998**, *279*, 1903-1907.
- (6) Cornelissen, J. J. L. M.; Fischer, M.; Sommerdijk, N. A. J. M.; Nolte, R. J. M. *Science* **1998**, *280*, 1427-1430.
- (7) Zhang, L.; Eisenberg, A. *Polymers for Advanced Technologies* **1998**, *9*, 677-699.

- (8) Kabanov, A. V.; Bronich, T. K.; Kabanov, V. A.; Yu, K.; Eisenberg, A. *Journal of the American Chemical Society* **1998**, *120*, 9941-9942.
- (9) Harada, A.; Kataoka, K. *Science* **1999**, *283*, 65-67.
- (10) Discher, B. M.; Won, Y.-Y.; Ege, D. S.; Lee, J. C. M.; Bates, F. S.; Discher, D. E.; Hammer, D. A. *Science* **1999**, *284*, 1143-1146.
- (11) Discher, B. M.; Hammer, D. A.; Bates, F. S.; Discher, D. E. *Current Opinion in Colloid & Interface Science* **2000**, *5*, 125-131.
- (12) Nardin, C.; Hirt, T.; Leukel, J.; Meier, W. *Langmuir* **2000**, *16*, 1035-1041.
- (13) Alexandridis, P.; Lindman, B., Editors. *Amphiphilic Block Copolymers: Self-Assembly and Applications*; Elsevier Science B.V.: Amsterdam, 2000.
- (14) Kukula, H.; Schlaad, H.; Antonietti, M.; Foerster, S. *Journal of the American Chemical Society* **2002**, *124*, 1658-1663.
- (15) Discher, D. E.; Eisenberg, A. *Science* **2002**, *297*, 967-973.
- (16) Raez, J.; Manners, I.; Winnik, M. A. *Journal of the American Chemical Society* **2002**, *124*, 10381-10395.
- (17) Ma, Q.; Remsen, E. E.; Clark, C. G., Jr.; Kowalewski, T.; Wooley, K. L. *Proceedings of the National Academy of Sciences of the United States of America* **2002**, *99*, 5058-5063.
- (18) Stephan, T.; Muth, S.; Schmidt, M. *Macromolecules* **2002**, *35*, 9857-9860.
- (19) You, L.-C.; Lu, F.-Z.; Li, Z.-C.; Zhang, W.; Li, F.-M. *Macromolecules* **2003**, *36*, 1-4.
- (20) Hoppenbrouwers, E.; Li, Z.; Liu, G. *Macromolecules* **2003**, *36*, 876-881.
- (21) Erhardt, R.; Zhang, M.; Boeker, A.; Zettl, H.; Abetz, C.; Frederik, P.; Krausch, G.; Abetz, V.; Mueller, A. H. E. *Journal of the American Chemical Society* **2003**, *125*, 3260-3267.
- (22) Jain, S.; Bates, F. S. *Science* **2003**, *300*, 460-464.
- (23) Dou, H.; Jiang, M.; Peng, H.; Chen, D.; Hong, Y. *Angewandte Chemie, International Edition* **2003**, *42*, 1516-1519.
- (24) Rosoff, M.; Editor. *Vesicles*; Marcel Dekker, Inc.: New York, 1996; Vol. 62.
- (25) Israelachvili, J. N. *Intermolecular and Surface Forces*, 2nd ed.; Academic Press Limited: San Diego, CA, 1992.

- (26) Robb, I. D.; Editor. *Specialist Surfactants*; Blackie Academic & Professional: London, 1997.
- (27) Evans, D. F.; Wennerstrom, H. *The Colloidal Domain: Where Physics, Chemistry, Biology, and Technology Meet*, 2nd ed.; Wiley-VCH: New York, 1998.
- (28) Holmberg, K.; Jonsson, B.; Kronberg, B.; Lindman, B. *Surfactants and Polymers in Aqueous Solution*; John Wiley & Sons Ltd.: West Sussex, 2003.
- (29) Helfand, E.; Wasserman, Z. R. *Microdomain Structure and the Interface in Block Copolymers*; Applied Science Publishers Ltd.: Essex, 1982.
- (30) Bates, F. S.; Fredrickson, G. H. *Annual Review of Physical Chemistry* **1990**, *41*, 525-557.
- (31) Hamley, I. *The Physics of Block Copolymers*; Oxford University Press Inc.: New York, 1998.
- (32) Hadjichristidis, N.; Pispas, S.; Floudas, G. A. *Block Copolymers Synthetic Strategies, Physical Properties, and Applications*; John Wiley & Sons, Inc.: Hoboken, NJ, USA, 2003.
- (33) Yu, K.; Eisenberg, A. *Macromolecules* **1996**, *29*, 6359-6361.
- (34) Halperin, A.; Tirrell, M.; Lodge, T. P. *Advances in Polymer Science* **1992**, *100*, 31-71.
- (35) Zhang, L.; Eisenberg, A. *Macromolecular Symposia* **1997**, *113*, 221-232.
- (36) Cameron, N. S.; Corbierre, M. K.; Eisenberg, A. *Canadian Journal of Chemistry* **1999**, *77*, 1311-1326.
- (37) Burke, S.; Eisenberg, A. *High Performance Polymers* **2000**, *12*, 535-542.
- (38) Choucair, A.; Eisenberg, A. *The European Physical Journal E* **2003**, *10*, 37-44.
- (39) Zhang, L.; Eisenberg, A. *Journal of the American Chemical Society* **1996**, *118*, 3168-3181.
- (40) Allen, C.; Maysinger, D.; Eisenberg, A. *Colloids and Surfaces B: Biointerfaces* **1999**, *16*, 3-27.
- (41) Shen, H.; Eisenberg, A. *Macromolecules* **2000**, *33*, 2561-2572.
- (42) Yu, Y.; Zhang, L.; Eisenberg, A. *Macromolecules* **1998**, *31*, 1144-1154.
- (43) Shen, H.; Eisenberg, A. *Journal of Physical Chemistry B* **1999**, *103*, 9473-9487.

- (44) Yu, Y.; Eisenberg, A. *Journal of the American Chemical Society* **1997**, *119*, 8383-8384.
- (45) Desbaumes, L.; Eisenberg, A. *Langmuir* **1999**, *15*, 36-38.
- (46) Zhang, L.; Yu, K.; Eisenberg, A. *Science* **1996**, *272*, 1777-1779.
- (47) Zhang, L.; Eisenberg, A. *Macromolecules* **1996**, *29*, 8805-8815.
- (48) Burke, S. E.; Eisenberg, A. *Langmuir* **2001**, *17*, 8341-8347.
- (49) Terreau, O.; Luo, L.; Eisenberg, A. *Langmuir* **2003**, *19*, 5601-5607.
- (50) Luo, L.; Eisenberg, A. *Journal of the American Chemical Society* **2001**, *123*, 1012-1013.
- (51) Luo, L.; Eisenberg, A. *Langmuir* **2001**, *17*, 6804-6811.
- (52) Luo, L.; Eisenberg, A. *Angewandte Chemie, International Edition* **2002**, *41*, 1001-1004.
- (53) Choucair, A. A.; Kycia, A. H.; Eisenberg, A. *Langmuir* **2003**, *19*, 1001-1008.
- (54) Burke, S.; Shen, H.; Eisenberg, A. *Macromolecular Symposia* **2001**, *175*, 273-283.
- (55) Yu, K.; Zhang, L.; Eisenberg, A. *Langmuir* **1996**, *12*, 5980-5984.
- (56) Yu, K.; Eisenberg, A. *Macromolecules* **1998**, *31*, 3509-3518.
- (57) Shen, H.; Eisenberg, A. *Angewandte Chemie, International Edition* **2000**, *39*, 3310-3312.
- (58) Yu, K.; Bartels, C.; Eisenberg, A. *Langmuir* **1999**, *15*, 7157-7167.
- (59) Riegel, I. C.; Eisenberg, A.; Petzhoid, C. L.; Samios, D. *Langmuir* **2002**, *18*, 3358-3363.
- (60) Schenning, A. P. H. J.; Elissen-Roman, C.; Weener, J.-W.; Baars, M. W. P. L.; Van der Gaast, S. J.; Meijer, E. W. *Journal of the American Chemical Society* **1998**, *120*, 8199-8208.
- (61) Yuan, J.; Li, Y.; Li, X.; Cheng, S.; Jiang, L.; Feng, L.; Fan, Z. *European Polymer Journal* **2003**, *39*, 767-776.
- (62) Gravano, S. M.; Borden, M.; von Werne, T.; Doerffler, E. M.; Salazar, G.; Chen, A.; Kisak, E.; Zasadzinski, J. A.; Patten, T. E.; Longo, M. L. *Langmuir* **2002**, *18*, 1938-1941.

- (63) Ilhan, F.; Galow, T. H.; Gray, M.; Clavier, G.; Rotello, V. M. *Journal of the American Chemical Society* **2000**, *122*, 5895-5896.
- (64) Drechsler, U.; Thibault, R. J.; Rotello, V. M. *Macromolecules* **2002**, *35*, 9621-9623.
- (65) Menger, F. M.; Keiper, J. S. *Current Opinion in Chemical Biology* **1998**, *2*, 726-732.
- (66) Dobereiner, H.-G. *Current Opinion in Colloid & Interface Science* **2000**, *5*, 256-263.
- (67) Ding, J.; Liu, G. *Journal of Physical Chemistry B* **1998**, *102*, 6107-6113.
- (68) Ding, J.; Liu, G. *Chemistry of Materials* **1998**, *10*, 537-542.
- (69) Sauer, M.; Haefele, T.; Graff, A.; Nardin, C.; Meier, W. *Chemical Communications* **2001**, 2452-2453.
- (70) Stoenescu, R.; Meier, W. *Chemical Communications* **2002**, 3016-3017.
- (71) Kickelbick, G.; Bauer, J.; Huesing, N.; Andersson, M.; Palmqvist, A. *Langmuir* **2003**, *19*, 3198-3201.
- (72) Holder, S. J.; Sommerdijk, N. A. J. M.; Williams, S. J.; Nolte, R. J. M.; Hiorns, R. C.; Jones, R. G. *Chemical Communications* **1998**, 1445-1446.
- (73) Schillen, K.; Bryskhe, K.; Mel'nikova, Y. S. *Macromolecules* **1999**, *32*, 6885-6888.
- (74) Zipfel, J.; Lindner, P.; Tsianou, M.; Alexandridis, P.; Richtering, W. *Langmuir* **1999**, *15*, 2599-2602.
- (75) Zipfel, J.; Berghausen, J.; Schmidt, G.; Lindner, P.; Alexandridis, P.; Tsianou, M.; Richtering, W. *Physical Chemistry Chemical Physics* **1999**, *1*, 3905-3910.
- (76) Valentini, M.; Napoli, A.; Tirelli, N.; Hubbell, J. A. *Langmuir* **2003**, *19*, 4852-4855.
- (77) Harris, J. K.; Rose, G. D.; Bruening, M. L. *Langmuir* **2002**, *18*, 5337-5342.
- (78) Harris, J. K.; Rose, G. D.; Bruening, M. L. *Langmuir* **2003**, *19*, 5550-5552.
- (79) Santore, M. M.; Discher, D. E.; Won, Y.-Y.; Bates, F. S.; Hammer, D. A. *Langmuir* **2002**, *18*, 7299-7308.
- (80) Won, Y.-Y.; Brannan, A. K.; Davis, H. T.; Bates, F. S. *Journal of Physical Chemistry B* **2002**, *106*, 3354-3364.

- (81) Photos, P. J.; Bacakova, L.; Discher, B.; Bates, F. S.; Discher, D. E. *Journal of Controlled Release* **2003**, *90*, 323-334.
- (82) Kraemer, E.; Foerster, S.; Goeltner, C.; Antonietti, M. *Langmuir* **1998**, *14*, 2027-2031.
- (83) Maskos, M.; Harris, J. R. *Macromolecular Rapid Communications* **2001**, *22*, 271-273.
- (84) Schrage, S.; Sigel, R.; Schlaad, H. *Macromolecules* **2003**, *36*, 1417-1420.
- (85) Lee, J. C. M.; Bermudez, H.; Discher, B. M.; Sheehan, M. A.; Won, Y.-Y.; Bates, F. S.; Discher, D. E. *Biotechnology and Bioengineering* **2001**, *73*, 135-145.
- (86) Discher, B. M.; Bermudez, H.; Hammer, D. A.; Discher, D. E.; Won, Y.-Y.; Bates, F. S. *Journal of Physical Chemistry B* **2002**, *106*, 2848-2854.
- (87) Bermudez, H.; Brannan, A. K.; Hammer, D. A.; Bates, F. S.; Discher, D. E. *Macromolecules* **2002**, *35*, 8203-8208.
- (88) Meng, F.; Hiemstra, C.; Engbers, G. H. M.; Feijen, J. *Macromolecules* **2003**, *36*, 3004-3006.
- (89) Kimura, S.; Kim, D.-H.; Sugiyama, J.; Imanishi, Y. *Langmuir* **1999**, *15*, 4461-4463.
- (90) Checot, F.; Lecommandoux, S.; Gnanou, Y.; Klok, H.-A. *Angewandte Chemie, International Edition* **2002**, *41*, 1339-1343.
- (91) Bronich, T. K.; Ouyang, M.; Kabanov, V. A.; Eisenberg, A.; Szoka, F. C., Jr.; Kabanov, A. V. *Journal of the American Chemical Society* **2002**, *124*, 11872-11873.
- (92) Pevzner, S.; Regev, O.; Lind, A.; Linden, M. *Journal of the American Chemical Society* **2003**, *125*, 652-653.
- (93) Ravoo, B. J.; Darcy, R. *Angewandte Chemie, International Edition* **2000**, *39*, 4324-4326.
- (94) Nolan, D.; Darcy, R.; Ravoo, B. J. *Langmuir* **2003**, *19*, 4469-4472.
- (95) Bandyopadhyay, P.; Bharadwaj, P. K. *Langmuir* **1998**, *14*, 7537-7538.
- (96) Tanaka, Y.; Mayachi, M.; Kobuke, Y. *Angewandte Chemie, International Edition* **1999**, *38*, 504-506.
- (97) Komatsu, T.; Tsuchida, E.; Boettcher, C.; Donner, D.; Messerschmidt, C.; Siggel, U.; Stocker, W.; Rabe, J. P.; Fuhrhop, J.-H. *Journal of the American Chemical Society* **1997**, *119*, 11660-11665.

- (98) Zhou, S.; Burger, C.; Chu, B.; Sawamura, M.; Nagahama, N.; Toganoh, M.; Hackler, U. E.; Isobe, H.; Nakamura, E. *Science* **2001**, *291*, 1944-1947.
- (99) Caruso, F.; Caruso, R. A.; Mohnwald, H. *Science* **1998**, *282*, 1111-1114.
- (100) Hotz, J.; Meier, W. *Langmuir* **1998**, *14*, 1031-1036.
- (101) Buetuen, V.; Billingham, N. C.; Armes, S. P. *Journal of the American Chemical Society* **1998**, *120*, 12135-12136.
- (102) Stewart, S.; Liu, G. *Chemistry of Materials* **1999**, *11*, 1048-1054.
- (103) Zhang, Q.; Remsen, E. E.; Wooley, K. L. *Journal of the American Chemical Society* **2000**, *122*, 3642-3651.
- (104) McKelvey, C. A.; Kaler, E. W.; Zasadzinski, J. A.; Coldren, B.; Jung, H. T. *Langmuir* **2000**, *16*, 8285-8290.
- (105) Sanji, T.; Nakatsuka, Y.; Ohnishi, S.; Sakurai, H. *Macromolecules* **2000**, *33*, 8524-8526.
- (106) Li, P.; Zhu, J.; Sunintaboon, P.; Harris, F. W. *Langmuir* **2002**, *18*, 8641-8646.
- (107) Smith, R.; Reven, L.; Barrett, C. *Polymer Preprints (American Chemical Society, Division of Polymer Chemistry)* **2002**, *43*, 1213-1214.
- (108) Kramer, M.; Stumbe, J.-F.; Turk, H.; Krause, S.; Komp, A.; Delineau, L.; Prokhorova, S.; Kautz, H.; Haag, R. *Angewandte Chemie, International Edition* **2002**, *41*, 4252-4256.
- (109) Donath, E.; Sukhorukov, G. B.; Caruso, F.; Davis, S. A.; Mohnwald, H. *Angewandte Chemie, International Edition* **1998**, *37*, 2202-2205.
- (110) Dai, Z.; Mohnwald, H.; Tiersch, B.; Daehne, L. *Langmuir* **2002**, *18*, 9533-9538.
- (111) Shenoy, D. B.; Antipov, A. A.; Sukhorukov, G. B.; Mohnwald, H. *Biomacromolecules* **2003**, *4*, 265-272.
- (112) Duan, H.; Chen, D.; Jiang, M.; Gan, W.; Li, S.; Wang, M.; Gong, J. *Journal of the American Chemical Society* **2001**, *123*, 12097-12098.
- (113) Wang, M.; Jiang, M.; Ning, F.; Chen, D.; Liu, S.; Duan, H. *Macromolecules* **2002**, *35*, 5980-5989.
- (114) Maysinger, D.; Berezovska, O.; Savic, R.; Lim Soo, P.; Eisenberg, A. *Biochimica Biophysica Acta* **2001**, *1539*, 205-217.

## Chapter 3

---

---

### Incorporation and Release of Hydrophobic Probes in Biocompatible Polycaprolactone-*block*-poly(ethylene oxide) Micelles: Implications for drug delivery\*

---

---

#### 3.1. Abstract

Block copolymer micelles have shown high potential as hydrophobic drug carriers. The loading efficiency, partition coefficient, and release profile all play critical roles in micellar drug delivery. As part of a series of studies on these polycaprolactone-*block*-poly(ethylene oxide) (PCL-*b*-PEO) micelles in drug delivery, we investigated the solubilization and release of the hydrophobic probes, benzo[a]pyrene and Cell-Tracker CM-DiI (DiI) from these micelles using fluorescence spectroscopy. The same method was also used to determine the partition coefficients of each probe between the core and the exterior solution, which were calculated at different solvent compositions and extrapolated to 100% water. The maximum loading efficiencies of DiI and benzo[a]pyrene were 87% and 32%, respectively. The large difference in the loading efficiency is related to the values of the partition coefficients, which were calculated to be 5800 for DiI and 700 for benzo[a]pyrene. DiI is more highly miscible with the polycaprolactone core compared to benzo[a]pyrene. The release of the hydrophobic probes from the micelles showed a biphasic profile under “perfect sink” conditions; there is an initial burst release, followed by a slow and prolonged release until, eventually, complete release is achieved. The release of the probes from the micelles is under diffusion control as shown by the linearity of the release as a function of the square root of time. Approximate diffusion coefficients of the order of  $10^{-15}$  cm<sup>2</sup>/s for DiI and benzo[a]pyrene were obtained. We demonstrate that the type and the concentration of the incorporated agent influence the loading and the release from PCL-*b*-PEO micelles. In addition to providing new information on the incorporation and release of benzo[a]pyrene and DiI from these micelles, this study also demonstrates the importance of probe-micelle compatibility in the evaluation of a micellar drug delivery system.

### 3.2. Introduction

In recent years, the exploration of block copolymer micelles as drug delivery vehicles has resulted in many publications, which illustrate the current status of the field.<sup>1-14</sup> The properties that make block copolymer micelles advantageous for drug delivery applications include the fact that they can be made of polymers that are biocompatible and/or biodegradable; and they have a small size and ability to incorporate and release poorly water soluble, hydrophobic, and/or highly toxic compounds.

Amphiphilic block copolymer micelles are defined by their core-shell architecture. In a polar environment, the hydrophilic shell or corona stabilizes the core in its external environment. Many of the block copolymer systems being explored at this time for drug delivery applications have a corona-forming block consisting of biocompatible poly(ethylene oxide).<sup>15-18</sup> The PEO coating has been shown to prevent opsonization and subsequent recognition by the macrophages of the reticuloendothelial system (RES).<sup>19</sup> The hydrophobic core serves as the reservoir for the incorporation of various lipophilic drugs and diagnostic agents.<sup>18</sup> It is imperative that the drug delivery carrier be formed from a biocompatible polymer; hence, the selection of core-forming blocks tends to be limited to a few polymers such as poly(propylene oxide),<sup>4,6,20,21</sup> poly( $\beta$ -benzyl l-aspartate),<sup>22</sup> poly( $\gamma$ -benzyl-l-glutamate),<sup>23</sup> polycaprolactone,<sup>24,25</sup> and poly(D,L-lactide).<sup>26-28</sup>

The length of the core-forming block is an important factor that determines the size of the micelle and the loading efficiency of the carrier system. Spherical block copolymer aggregates generally range in size from 10 to 100 nm.<sup>11</sup> The small size improves circulation times and decreases the likelihood of uptake by the RES.<sup>11</sup> The loading efficiency of the micellar carrier is important for drug delivery, because it is an

indication of the amount of drug per micelle that can be incorporated. Other factors that influence drug loading are the total molecular weight and concentration of the copolymer, the nature and concentration of the solute (drug or probe), the length and nature of the corona forming block, and the method of preparation of the delivery system.<sup>4</sup> However, the most important factor is the compatibility between the drug and the core-forming block.<sup>4</sup> The Flory-Huggins interaction parameter  $\chi_{sp}$  characterizes the compatibility between the solubilize and the polymer.  $\chi_{sp}$  can be determined from the Hildebrand-Scatchard equation:

$$\chi_{sp} = (\delta_s - \delta_p)^2 \frac{v_s}{kT} \quad (3.1)$$

where  $\delta_s$  and  $\delta_p$  are the solubility parameters for the solubilize and the core-forming polymer block respectively,  $v_s$  is the molar volume of the solubilize,  $k$  is the Boltzmann's constant, and  $T$  is the temperature in degrees kelvin.<sup>29</sup> In addition, the molar solubilization ratio (MSR) can be used to correlate the measured solubilization capacity with the Flory-Huggins interaction parameter.

$$\text{MSR} = a\chi_{sp}^{-b} = a \left[ (\delta_s - \delta_p)^2 \frac{v_s}{kT} \right]^{-b} \quad (3.2)$$

Here  $a$  and  $b$  are defined as the positive constants dependent on the block copolymer molecule.<sup>30</sup> Nagarajan et al. studied the solubilization of aromatic and aliphatic molecules in poly(propylene oxide)-*block*-poly(ethylene oxide) (PPO-*b*-PEO) and polystyrene-*block*-poly(*N*-vinyl-pyrrolidone) systems.<sup>29</sup> They found that the

aromatic solubilizates had very low  $\chi_{sp}$  values, which indicated a very good compatibility between the aromatics and either the poly(propylene oxide) and polystyrene cores, and also produced very large MSR values.<sup>29,30</sup> In addition, the aromatic molecules were solubilized to a greater extent than were the aliphatic molecules, because of their lower interfacial tension against water.<sup>29</sup> Ideally, to achieve very high loading into the micelles, the solubility parameters of the solubilizate and the core-forming polymer block should be the same (i.e.,  $\delta_s = \delta_p$ ).<sup>14</sup> Since each probe or drug is unique, this would suggest that there is no universal core-forming block. It is important to match the probe or drug with the core-forming polymer block in order to achieve maximal loading into the micelles.

The hydrophilic block length influences the micelle loading. An increase in the corona block will result in the increase in the critical micelle concentration (CMC) and a decrease in the aggregation number ( $N_{agg}$ ). Gabelle et al. showed that increasing the PEO block length resulted in an increase in the CMC, a decrease in the  $N_{agg}$ , and ultimately a decrease in the solubilization of hydroprobes.<sup>31</sup> Similarly, Nagarajan et al.<sup>32</sup> and Hurter et al.<sup>33</sup> found that increasing the PEO content decreased the solubilization capacity of the PPO-*b*-PEO and Pluronic [poly(ethylene oxide)-*block*-poly(propylene oxide)-*block*-poly(ethylene oxide) (PEO-*b*-PPO-*b*-PEO)] micelles, respectively. Xing et al. showed that a small corona chain has little or no effect on the solubilization of the probe into a micelle made from a triblock copolymer, because the short corona blocks do not contribute significantly to the micellar core size.<sup>34</sup> However, a significant increase in the corona block length is associated with an increased solubilization in the triblock system, if the copolymer symmetry is modified.<sup>34</sup>

Several groups have achieved different maximal loadings with various lipophilic drugs into a range of block copolymer micelles. Burt et al., have solubilized paclitaxel, a poorly water soluble anticancer drug for ovarian and breast cancer, into its block copolymers composed of either poly(d,l-lactide), poly(d,l-lactide-*co*-caprolactone) or poly(glycolide-*co*-caprolactone) and methoxypoly(ethylene glycol).<sup>28</sup> They achieved a 5-10% (w/w), 15-25% (w/w), and 15-20% (w/w) loading of paclitaxel into their micellar carriers, respectively. Indomethacin, a potent nonsteroidal antiinflammatory drug used in the treatment of rheumatoid arthritis, was incorporated into poly ( $\beta$ -benzyl l-aspartate)-*block*-poly(ethylene oxide) (PBLA-*b*-PEO) copolymer micelles by La et al.<sup>22</sup> Using two different methods of preparation; i.e., dialysis and the oil-water emulsion methods, they achieved an entrapment efficiency of 20 and 22% (w/w), respectively. Doxorubicin (or adriamycin), an anticancer drug, has been incorporated into many different block copolymer micelles. Yoo et al. loaded 0.5% (w/w) doxorubicin into 60 nm poly(d,l-lactic-*co*-glycolic acid)-*b*-poly(ethylene glycol) micelles.<sup>35</sup> Kwon et al. loaded doxorubicin into PBLA-*b*-PEO block copolymer micelles of approximately 37 nm and achieved loading of 5-12% (w/w).<sup>36</sup> Using the same copolymer, Kataoka et al. obtained 15-20% (w/w) loading of doxorubicin into micelles that were 50-70 nm in diameter.<sup>37</sup> In comparison, Jeong et al. achieved 12-19% (w/w) drug loading content of adriamycin into poly( $\gamma$ -benzyl l-glutamate)-*b*-poly(ethylene oxide) (PBLG-*b*-PEO) micelles.<sup>23</sup> Allen et al., observed an unusually high amount of loading of dihydrotestosterone, 240% (w/w), in PCL-*b*-PEO micelles.<sup>17</sup> This wide range of degrees of incorporation (0.5 to 240% w/w) reflects the different affinities of the pharmaceutical agents for the micelle or its aqueous environment (i.e., partition coefficient).

The partition coefficient of the probe between the micelle core and the exterior solution is another important factor in the determination of its loading and release profiles. It is also a value that characterizes the thermodynamics of the drug in the micelle. The partition coefficient ( $K_v$ ) is defined as:

$$K_v = \frac{[\text{PROBE}]_m}{[\text{PROBE}]_a} \quad (3.3)$$

where  $[\text{PROBE}]_m$  is the probe concentration in the micellar phase and  $[\text{PROBE}]_a$  is the probe concentration in the aqueous phase.<sup>20</sup> The length of the hydrophobic block influences both the critical micelle concentration and the partition coefficient.<sup>33</sup> The influence of the hydrophobic block length can be seen in the paper by Kim et al.,<sup>38</sup> who determined that the partition coefficients of pyrene increased when the molecular weight of hydrophobic poly(2-ethyl-2-oxazoline) block increased from  $9 \times 10^4$  to  $2 \times 10^5$ . Also, Kozlov et al. observed a strong dependence of the partition coefficient of pyrene on the length of the hydrophobic PPO block.<sup>16</sup> Allen et al. showed that the partition coefficient of pyrene molecules between PCL-*b*-PEO micelles and the external solution increased from 240 to 1450 as the block length of the polycaprolactone block increased from 14 to 40 units.<sup>39</sup> Similarly, Xing et al. showed that an increase in the hydrophobic block led to an increase in the partition coefficient of the probe.<sup>34</sup> The partition coefficient influences the loading efficiency of the probe, because, as the partition coefficient increases, the probe favors the hydrophobic core versus the external solution, and more probe molecules are incorporated.

Each probe or drug is distinct, and its interaction with the core-forming block will be unique. Therefore, the partition coefficient of the same probe or drug in different

block copolymers will be distinct. For example, the partition coefficients of pyrene were  $1.6-3.3 \times 10^3$  in PEO-*b*-PPO-*b*-PEO,<sup>20</sup>  $7.5 \times 10^4$  in Pluronic-*block*-poly(acrylic acid) (PEO-*b*-PPO-*b*-PEO-*b*-PAA),<sup>40</sup>  $10^4$  in PBLA-*b*-PEO,<sup>41</sup>  $2.2 \times 10^5$  in poly(methacrylic acid)-*block*-polystyrene-poly(methacrylic acid) (PMA-*b*-PS-PMA),<sup>42</sup> and  $1.3 \times 10^5$  and  $3 \times 10^5$  in polystyrene-*block*-poly(ethylene oxide) (PS-*b*-PEO).<sup>43,44</sup> From these accumulated data, it appears that the more polar the core, the less pyrene it can incorporate.<sup>14</sup> In a separate study, Teng et al. determined that the partition coefficients of pyrene and phenanthrene increased from  $4 \times 10^4$  to  $3 \times 10^5$  when the cores were changed from relatively polar poly(*tert*-butyl acrylate) and poly(2-vinylpyridine) to polystyrene.<sup>45</sup> Therefore, the selection of the core-forming block is crucial to maximize the loading capacity. In addition, Case et al. investigated the partitioning of molecules in Pluronic gels in order to determine into which phase (PPO, PEO or entrapped water phases) the molecule partitions.<sup>46</sup> They found that, in certain cases, the partitioning of the molecule depended on the favorable interactions between the molecule and either the PPO or PEO blocks. If the probe preferentially partitions into the corona, then a burst release is likely to occur.

The factors that need to be considered in the release of drugs from block copolymer micelles are their rate of diffusion from the micelles, rate of copolymer biodegradation, and stability of the micelle. Assuming that the rate of biodegradation is slow and the micelle is stable, then under sink conditions, drug release is influenced by interactions between the core block and the drug, the physical state and the length of the core-forming block, the amount of drug incorporated, the molecular volume of the drug and the localization of the drug in the micelle.<sup>14</sup> On the other hand, if the interaction

between the drug and polymer is strong and the rate of biodegradation is fast, then this governs the rate of release. The localization of the drug in the micelle, i.e., in the core, at the interface of the core and the corona, or in the corona itself, will also affect the release kinetics.

Our group has examined block copolymer micelles formed from hydrophobic polycaprolactone and hydrophilic poly(ethylene oxide).<sup>15,17,47</sup> Polycaprolactone is a semicrystalline polymer that is both nontoxic and biodegradable.<sup>48</sup> As a result of its favorable properties, PCL has been used for medical applications such as delivery of contraceptives, implants, prosthetics and operating sutures.<sup>49</sup> Poly(ethylene oxide) is a crystalline, water soluble polymer known to be nontoxic and nonimmunogenic.<sup>22</sup> PEO has been shown to prevent protein adsorption and cellular adhesion, factors that are crucial for avoiding RES uptake.<sup>19</sup> Recently, polycaprolactone-*b*-poly(ethylene oxide) block copolymer micelles have been explored as a delivery vehicle for neurotrophic agents FK506<sup>50</sup> and L-685,818<sup>15</sup> and dihydrotestosterone, a lipophilic steroid.<sup>17</sup> However, fundamental aspects of the incorporation of hydrophobic probes into the polycaprolactone core and their release profiles from the PCL-*b*-PEO micelles are not well understood.

To understand better the compatibility of hydrophobic probes with PCL-*b*-PEO micelles, two model probes, benzo[a]pyrene and Cell-Tracker CM-DiI (DiI) were chosen for this study. Benzo[a]pyrene is a polycyclic aromatic hydrocarbon. It is a fluorescent, hydrophobic probe that is also available in a radioactive form. Studies of <sup>3</sup>H-benzo[a]pyrene-incorporated micelles with PC12 cells have been carried out.<sup>51</sup> DiI is a fluorescent, hydrophobic probe that has been used to label cells and tissues.<sup>52</sup> The aim of

this study was to examine the loading and release kinetics of these probes. In addition, the partition coefficients between water and the micelles were determined for both benzo[a]pyrene and DiI in order to determine the affinity of the probe for the micelles. Fluorescence spectroscopy was used to investigate the loading and release process, as well as to determine the partition coefficients for each fluorophore.

### 3.3. Experimental Section

#### 3.3.1. Materials

The block copolymers used were polycaprolactone-*b*-poly(ethylene oxide) (PCL<sub>21</sub>-*b*-PEO<sub>44</sub>) and (PCL<sub>23</sub>-*b*-PEO<sub>45</sub>). The subscripted refers to the number of repeat units in each block. The first block copolymer was synthesized by anionic polymerization by Yu et al.,<sup>53</sup> and the second block copolymer was synthesized by Luo et al.<sup>54</sup> The polymers differ only in the presence of the end group at the end of the PEO block; in the case of the PCL<sub>23</sub>-*b*-PEO<sub>45</sub>, the end group is a methoxy compared to that of diphenyl methyl on PCL<sub>21</sub>-*b*-PEO<sub>44</sub>. Benzo[a]pyrene was purchased from Sigma-Aldrich (Canada). DiI was purchased from Molecular Probes Co. The structures and some physical properties of the probes are included in Tables A1 and A2 in the Appendix.

#### 3.3.2. Sample Preparation for Loading and Release Kinetics

Sample solutions were prepared by first dissolving the fluorescent probe in a suitable solvent (DMF for benzo[a]pyrene and acetone for DiI). An aliquot of the probe in the solvent was added to an empty vial in quantities such that the concentration of benzo[a]pyrene in the final solution ranged from 0.5 to 600  $\mu$ M and that of DiI ranged from 0.5 to 230  $\mu$ M. The block copolymer (5 mg) was then added to each vial followed

by varying amounts of DMF (in the case of DiI, the acetone was allowed to evaporate prior to DMF addition). The solution was then allowed to stir for 4 hours. Micellization was achieved by slow addition of water at a rate of approximately 2.5%/minute until the desired water content was attained. The total mass of this solution was ca. 0.5 g, which yielded a 1% polymer solution by weight. The solution was stirred overnight and dialyzed against MilliQ water in the dark. During the dialysis, the water was changed six times during the first 8 hours and then left overnight.<sup>55</sup>

### 3.3.3. Sample Preparation for Partition Coefficient Determination between PCL<sub>23</sub>-*b*-PEO<sub>45</sub> Micelles and a DMF/H<sub>2</sub>O Solvent Mixture

DiI or benzo[a]pyrene were dissolved in acetone, and an aliquot of the probe in acetone was added to empty vials to obtain concentrations in the final solution of 0.1  $\mu\text{M}$  (DiI) and 0.01  $\mu\text{M}$  (benzo[a]pyrene). The acetone was allowed to evaporate, and different amounts of PCL<sub>23</sub>-*b*-PEO<sub>45</sub> copolymer in DMF were then added to each vial. Micellization was induced by the slow addition of water (2.5%/min), the amount depending on the desired final water concentration. The solution was allowed to stir overnight in the dark before fluorescence measurements were taken.

### 3.3.4. Fluorescence Measurements for Loading and Release Kinetics

The loading efficiencies of benzo[a]pyrene and DiI incorporated into the polycaprolactone-*b*-poly(ethylene oxide) micelles were determined by fluorescence. A calibration curve of benzo[a]pyrene and DiI in DMF, respectively, was created to determine the linear range of fluorescence vs concentration of each probe. A small aliquot of micelles containing the probe was dissolved in DMF (good solvent for

copolymer). Thus, the probe was surrounded by DMF and this solution was analyzed by fluorescence. The PCL-*b*-PEO copolymer and the solvent did not contribute significantly to the fluorescence signal, and the background value obtained was subtracted. Steady-state fluorescent spectra were measured using a SPEX Fluorolog-2 spectrometer in the right-angle geometry (90° emission collection). A 3.0 mL quantity of solution was placed into a 10 mm square quartz cell. For the release kinetics experiment, a microcuvette was used and only 500  $\mu$ L of solution was required. All spectra were run on air-equilibrated solutions. For fluorescence emission spectra,  $\lambda_{\text{ex}}$  was 381 nm for benzo[a]pyrene and 553 nm for DiI. Spectra were accumulated with an integration time of 1 s/1 nm.

#### 3.3.5. Release of Fluorescent Probes from PCL<sub>23</sub>-*b*-PEO<sub>45</sub> Micelles

A dialysis bag (MWCO: 50,000) containing 2 mL of the probe-loaded micelle suspension was placed into a 250 mL beaker filled with tap water (temperature: 24 °C). The beaker was then put into a crystallization dish (160 × 100) equipped with a side neck for outflowing water, which rested on top of a stirring plate as illustrated in Figure 3.1.

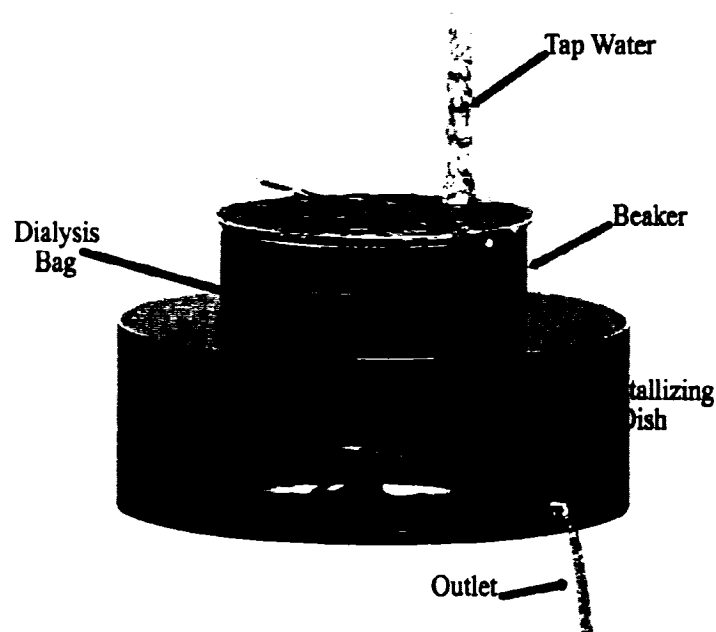


**Figure 3.1.** Diagram of the experimental setup used for the release profile experiments under “perfect sink” conditions.

Tap water was allowed to run (at a rate of ca. 430 mL/min) through a piece of Tygon tubing that led directly to the bottom of the beaker. The tap water overflowed from the beaker and into the crystallization dish, and excess water was removed through a tube attached to the side neck at the bottom of the dish. This enabled the release experiment to have constant stirring while observing near “perfect sink” conditions. At specific time intervals, 0.5 mL of the micelle solution in the dialysis bag was sampled and subsequently analyzed by fluorescence spectroscopy to determine the amount of probe release from the dialysis bag. The aliquot was then replaced into the dialysis bag without any dilution of the micelle solution.

### 3.4. Results and Discussion

#### 3.4.1. Loading

The loading efficiency and the probe content of a micelle are influenced by the properties of the probe and the copolymer. The molecular weight of the core, the corona block length, the initial solvent chosen for the probe and polymer, and the partition coefficient are factors that influence the loading. To determine the amount of probe incorporated into the micelles, the probe content, as defined by Riley et al.,<sup>56</sup> was utilized:

$$\text{Probe content (\% w/w)} = \frac{\text{mass of probe in micelles (g)}}{\text{mass of micelles (g)}} \times 100 \quad (3.4)$$

The probe contents of DiI and benzo[a]pyrene are plotted versus the weight ratio of probe to polymer in the original solution is shown in Figure 3.2.

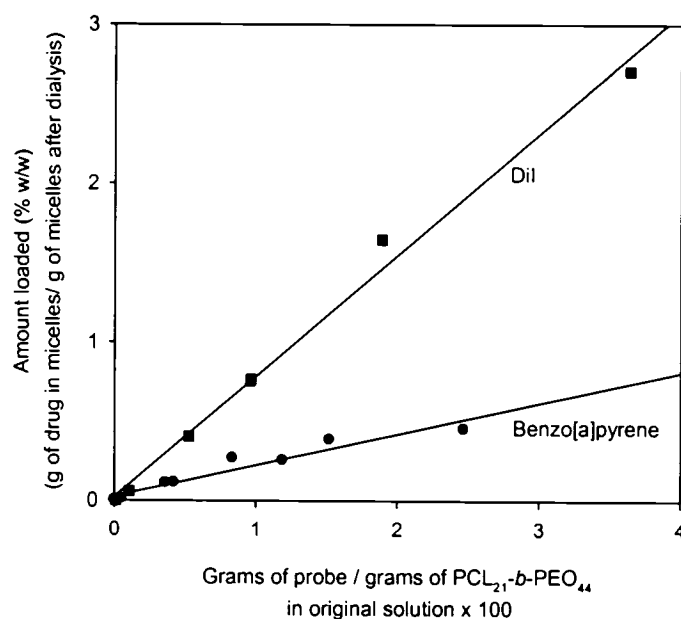


**Figure 3.2.** Amount of DiI and benzo[a]pyrene loaded into PCL<sub>21</sub>-b-PEO<sub>44</sub> micelles as a function of the amount of probe per polymer added.

The probe content for both probes increases linearly as more probe molecules are added, because there are more molecules available for entrapment. The slope of the line for DiI is steeper than that for benzo[a]pyrene, so for a given weight ratio of probe to polymer, the probe content of DiI will be higher. By comparison, at a 20% weight ratio of probe per polymer, Riley et al. have achieved a 3.1% (w/w) of procaine hydrochloride incorporated into poly(d,l-lactide)-*block*-poly(ethylene glycol) micelles.<sup>56</sup> At such a high weight ratio, the probe content of DiI in PCL<sub>21</sub>-*b*-PEO<sub>44</sub> micelles, calculated from the slope of the line ( $y = 76x + 0.02$ ), would be ca. 15% (w/w). In the case of benzo[a]pyrene, the extrapolated probe content would be ca. 4% (w/w) calculated from the slope of the line ( $y = 20x + 0.03$ ). Again, it is seen that the polycaprolactone core has a strong affinity for the DiI molecules and a lower affinity for benzo[a]pyrene.

Another means of expressing the loading of probe molecules into the micelle is through the loading efficiency. The definition of the loading efficiency was taken from Riley et al.,<sup>56</sup> who called it drug entrapment, and expressed it as

$$\text{Loading efficiency (\%)} = \frac{\text{mass of probe in micelles (g)}}{\text{total mass of probe used (g)}} \times 100 \quad (3.5)$$

The loading efficiency parameter is important in that it is an indication of the percentage of probe trapped into the micelle for a given amount of probe used. The loading efficiency (%) versus the weight ratio of probe to polymer in the original solution for DiI and benzo[a]pyrene in PCL<sub>21</sub>-*b*-PEO<sub>44</sub> micelles is shown in Figure 3.3.

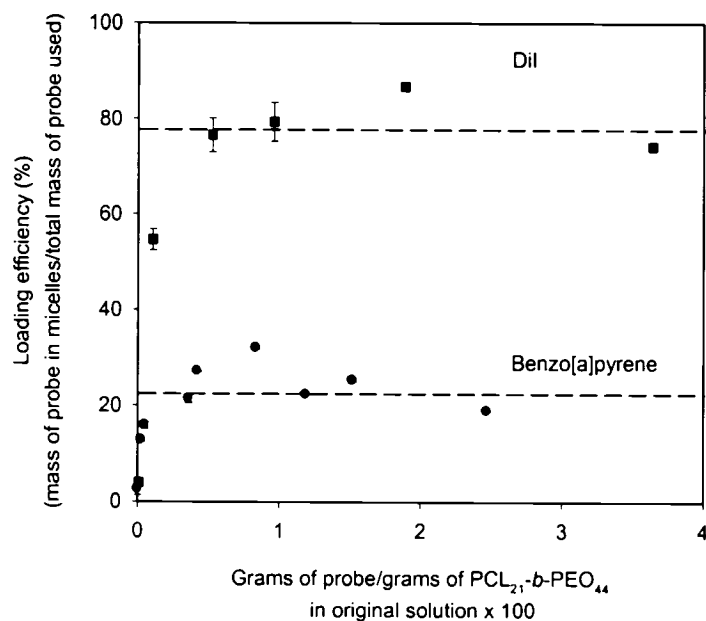


**Figure 3.3.** Loading efficiencies of DiI and benzo[a]pyrene incorporated into PCL<sub>21</sub>-b-PEO<sub>44</sub> micelles. Horizontal dotted lines represent slopes of lines from Figure 3.2.

There is an increase in the loading efficiency as the ratio of probe to polymer increases, but eventually a maximum loading efficiency is reached. The maximum for DiI was seen at 87%, while for benzo[a]pyrene it was seen at 32%. At any given weight ratio of probe per polymer, DiI has a greater loading efficiency than benzo[a]pyrene. Also, the horizontal dotted straight lines in Figure 3.3 represent the lines of slopes 76 and 22 (from top to bottom) in Figure 3.2. Both plots are related in that the value of the amount loaded over the amount of probe per polymer initially loaded (Figure 3.2) gives the loading efficiency (Figure 3.3). As the concentration of the probe molecules increases, there is an initial increase in the loading efficiency, followed by a decrease in the loading efficiency. This trend has been seen by studies previously published by our group,<sup>17</sup> by other groups,<sup>7,36</sup> and from our current results. We speculate that as probe

molecules become incorporated, the core becomes more similar to the probe<sup>57</sup> and, as a result, there is an increase in the loading efficiency. As more probe is incorporated, the core diameter increases, and without an increase in the aggregation number, the number of corona chains remains unchanged. Therefore the number of contacts between the core and the water will increase, which will lead to a decrease in the loading efficiency.

The hydrophobic core is one of the many factors that influence the loading content of the probe or drug in the micelle. A related factor is the molecular weight of the core, because it is important in determining the particle size. Increasing the length of the hydrophobic block decreases the CMC and increases the core size of the micelles, which, in turn, increases the loading capacity of the probe or drug per micelle.<sup>31</sup> This has been confirmed by the work of several groups. Kabanov's group found that increasing the block length of PPO increases the  $N_{agg}$  and the core size of the micelle, and also the solubilization of hydrophobic substances.<sup>16</sup> Hurter et al. also observed an increase in the uptake of naphthalene in the Pluronic polymers when the block length of PPO was increased.<sup>58</sup> Similarly, Nah et al. showed that increasing the sizes of hydrophobic PBLG decreased the CMC of PBLG-*b*-PEO micelles and increased the sizes of the particles, which facilitated the incorporation of greater amounts of clonazepam.<sup>59</sup> Also, Wang et al. showed that an increase in the molecular weight of poly-l-lysine, increased the size of their particles and allowed them to incorporate more fluorescein isothiocyanate-dextran probe.<sup>60</sup> Yoo et al. achieved loading efficiencies of 26 to 47% (w/w) with a model drug, enalapril maleate, into their PCL-*b*-PEO micelles when the PCL block length increased from 22 to 66 units.<sup>61</sup> Similarly, Allen et al.<sup>39</sup> showed that the loading efficiency of DiI increased from 25% to 81% as the number of polycaprolactone units in the block

increased from 3 to 76. In a recent study, our group showed that the loading efficiency of  $17\beta$ -estradiol increases from 10 to 90% when the PCL block length increases from 12 to 151 units.<sup>55</sup>

Selecting an appropriate solvent is also important in maximizing drug loading into the hydrophobic core. The initial solvent has to be chosen for its ability to solubilize both the corona and core blocks of the polymer as well as the probe or drug of interest. In the present case, acetone, a volatile solvent, is chosen to transfer both the benzo[a]pyrene and DiI, and DMF is the solvent used to dissolve both the probe and the PCL-b-PEO copolymer. The chosen solvent also influences the partition coefficient of the probe or drug between the polymer and the solvent precipitant mixture. Nah et al. showed that depending on the initial solvent used, they achieved different drug loadings in their PBLG-b-PEO micelles.<sup>59</sup> They obtained 19% (w/w) and 24% (w/w) drug loading of clonazepam using THF and 1,4-dioxane, respectively, compared to only 10% (w/w) drug loading using DMF or DMSO.

As seen above, the loading efficiency and the probe content of block copolymer micelles are influenced by several different factors. However, to achieve maximal loading, the most important factor is the compatibility of the probe and the core polymer. Our results would seem to suggest that PCL is a suitable core for DiI, but not a good choice for benzo[a]pyrene. The values of the partition coefficients determined support this information since the partition coefficients and the loading efficiencies are related.

### 3.4.2. Partition Coefficients

The determination of the partition coefficients of both benzo[a]pyrene and DiI between the micelles and pure water is made difficult, because they are highly hydrophobic. The total concentration of the hydrophobic probe in water is low, and this limits the accuracy of the calculation of the partition coefficient. There are several different methods for calculating the partition coefficient, as shown by Wilhelm et al.,<sup>43</sup> Kabanov et al.,<sup>20</sup> and Allen et al.<sup>44</sup> The method employed by Wilhelm et al. to determine the partition coefficient of hydrophobic pyrene in PS-*b*-PEO polymers involved the monitoring of the well-defined I<sub>3</sub> to I<sub>1</sub> ratio.<sup>43</sup> Kabanov et al. monitored the emission peak at 395 nm in their method to determine the partition coefficient of pyrene in PPO-*b*-PEO-*b*-PPO polymers.<sup>20</sup> Allen et al. used a modified combination of methods developed by Wilhelm et al. and Kabanov et al. to determine the partition coefficient of pyrene in polystyrene-*block*-poly(acrylic acid) copolymers.<sup>44</sup> The difficulty in using solely the method of Wilhelm et al. for DiI is that pyrene possesses very characteristic peaks, the relative heights of which are solvent dependent, while DiI does not. As a result, the method developed by Kabanov et al. was used in the present study to determine the partition coefficients of both benzo[a]pyrene and DiI.<sup>20</sup>

Initially, the fluorescence of each probe is measured in the absence of block copolymer (represented by the symbol: I<sub>0</sub>). The probe concentration is fixed at a given concentration ( $1 \times 10^{-7}$  M for DiI and  $1 \times 10^{-8}$  M for benzo[a]pyrene) at different water contents in the solvent (ranging from 60 to 90 wt% water). At each different water content, a series of solutions is prepared with different PCL<sub>23</sub>-*b*-PEO<sub>45</sub> concentrations, ranging from 0.001 to 5 wt %. The fluorescence of each of these solutions (represented

by the symbol  $I$ ) is determined to ascertain the intensity of fluorescence at saturation in the copolymer (represented by the symbol  $I_{\max}$ ). The fluorescence beyond the saturation point for each probe does not change with increasing polymer concentration. From the plot of  $I-I_0$  for benzo[a]pyrene vs the concentration of the block copolymer, as illustrated in Figure 3.4a, we observe an increase in the fluorescence as the concentration of copolymer is increased, until  $I_{\max}$  is reached, beyond which it levels off. Similarly, the results for DiI are shown in Figure 3.4b.

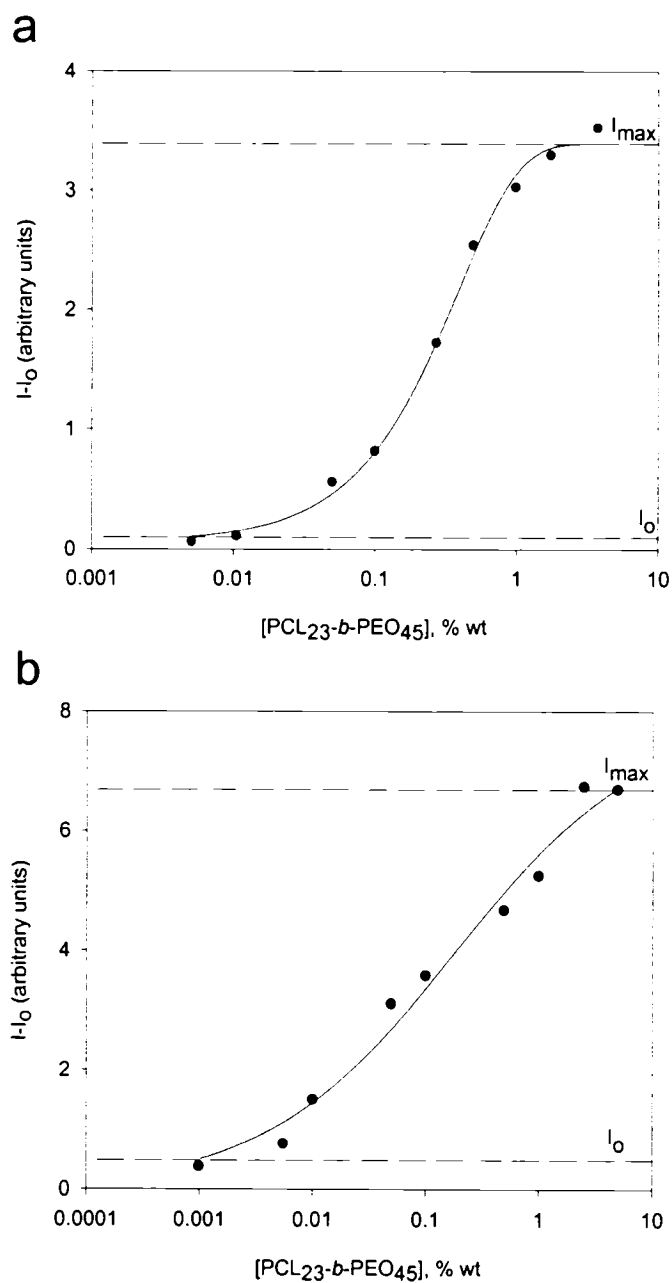


**Figure 3.4.** Influence of block copolymer concentration (logarithmic scale) on fluorescence intensity ( $I$ ) of (a) benzo[a]pyrene at 80% H<sub>2</sub>O/20% DMF and (b) DiI at 60% H<sub>2</sub>O/40% DMF.  $I_0$  is the fluorescence in the absence of polymer,  $I_{max}$  is the fluorescence at saturating conditions of polymer. The line of best fit is meant as only as a guide for the eye.

From the derivation as given by Kabanov et al.,<sup>16,20</sup> we obtain an equation for an expression ( $\alpha$ ) which is used in the calculation of the partition coefficient for each of the probes incorporated into the micelles.

$$\alpha = \frac{(I - I_o)}{I_{\max} - I_o} \quad (3.6)$$

$\alpha$  can also be expressed as

$$\alpha = \frac{\theta K_v}{1 + (K_v - 1)\theta} \quad (3.7)$$

where  $\theta$  is the volume fraction of the micelle phase in solution ( $0.01 \nu - [\text{polymer}] - \text{CMC}$ ),  $K_v$  is the partition coefficient,  $\nu$  is the partial specific volume ( $\text{cm}^3/\text{g}$ ), and CMC is the critical micelle concentration. A value of  $1 \text{ cm}^3/\text{g}$  was used for  $\nu$  and a value obtained for the CMC for PCL<sub>21</sub>-b-PEO<sub>44</sub> was determined to be  $2.8 \times 10^{-7} \text{ M}$  by Allen et al.<sup>14</sup> Since the CMC value is so small, it is negligible relative to the polymer concentration, which in the most dilute solution is  $1 \times 10^{-3} \text{ M}$ . Combining equations 3.6 and 3.7, we obtain the following equation:

$$\frac{(I_{\max} - I_o)}{(I - I_o)} - 1 = \frac{1}{(K_v \theta)} - \frac{1}{K_v} \quad (3.8)$$

Details of the derivation of equation 3.8 can be found in the Appendix. The points in Figures 3.4a and 3.4b are then recalculated and replotted as  $\frac{(I_{\max} - I)}{(I - I_o)}$  versus  $1/\theta$ . The plots are shown in Figures 3.5a and 3.5b, for benzo[a]pyrene and DiI, respectively.

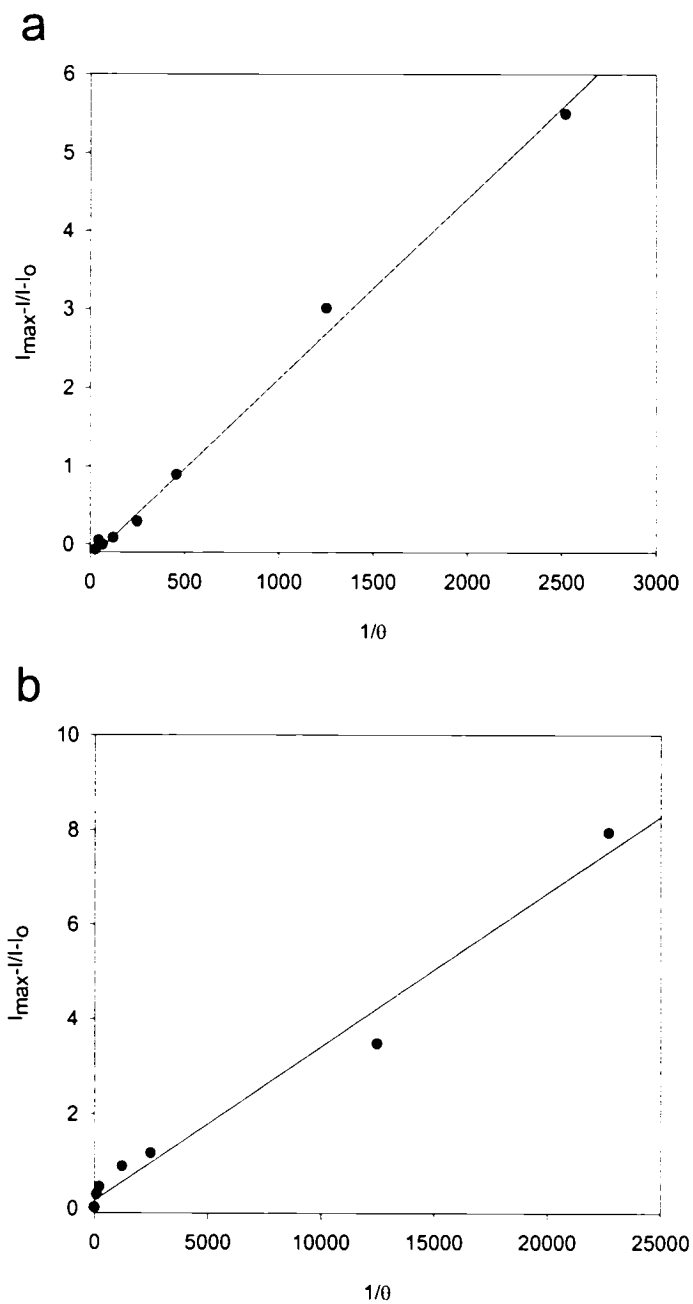


**Figure 3.5.** Partition coefficient determination of (a) benzo[a]pyrene at 80% H<sub>2</sub>O/20%DMF and (b) DiI at 60% H<sub>2</sub>O/40% DMF.

A straight line with a slope equal to  $1/K_v$  is obtained from the plots, as can be seen in equation 3.7. In Figure 3.5a, the slope of the line is  $2.3 \times 10^{-3}$ , from which we calculate a partition coefficient of 435 for benzo[a]pyrene at a solvent ratio of 80% H<sub>2</sub>O/20% DMF. In Figure 3.5b, the slope of the line is  $3.2 \times 10^{-4}$ , and the calculated partition coefficient is 3080 for DiI at a solvent ratio of 60% H<sub>2</sub>O/40% DMF.

The partition coefficients of each probe determined at different water contents are plotted against the water content (in %), in Figure 3.6.

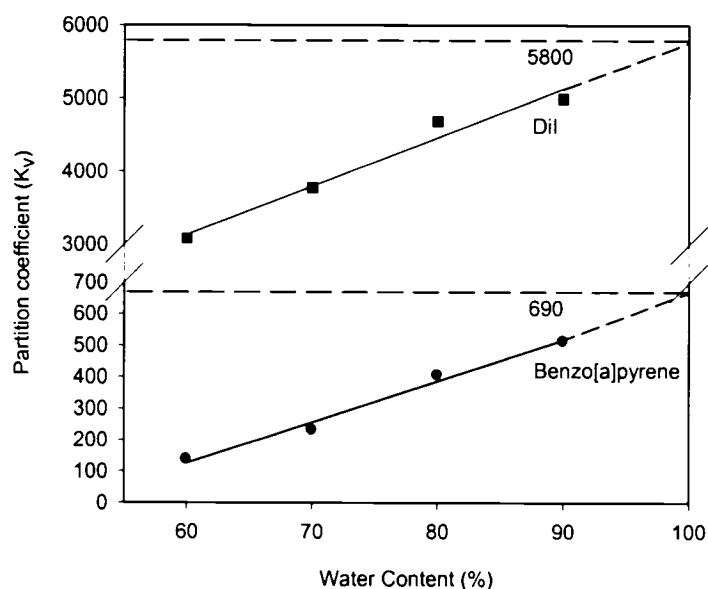


**Figure 3.6.** Partition coefficient determination of DiI and benzo[a]pyrene extrapolated to 100% water. For DiI, the plot extrapolates to a value of 5800 on the left y-axis. For benzo[a]pyrene, the plot extrapolates to a value of 690 on the left y-axis.

Extrapolation of each plot to 100% water yields a partition coefficient of 690 for benzo[a]pyrene and 5800 for DiI. The large difference in the partition coefficients between the two probes, DiI and benzo[a]pyrene, can be explained in part as due to their

different chemical structures (Appendix). Structurally, polycaprolactone is more similar to DiI, because of its aliphatic groups, than to benzo[a]pyrene, which has only aromatic groups. Thus, the interaction parameter of DiI and polycaprolactone would be lower than that between benzo[a]pyrene and PCL. As a result, the compatibility between DiI and polycaprolactone is higher, which would result in a higher partition coefficient. No partition coefficient has been determined for DiI in small molecule surfactants or micelles; however, a value has been reported by Encinas et al. for benzo[a]pyrene in sodium dodecyl sulfate (SDS) micelles; the partition coefficient is 1500.<sup>62</sup> The higher partition coefficient of DiI correlates with the higher loading efficiency and high probe content in the PCL-*b*-PEO micelles.

#### 3.4.3. Release Kinetics

The release of benzo[a]pyrene and DiI from PCL<sub>23</sub>-*b*-PEO<sub>45</sub> micelles was examined under sink conditions. Figure 3.7 shows the plot of the percent released from PCL<sub>23</sub>-*b*-PEO<sub>45</sub> micelles vs the square root of time for two different concentrations of benzo[a]pyrene.

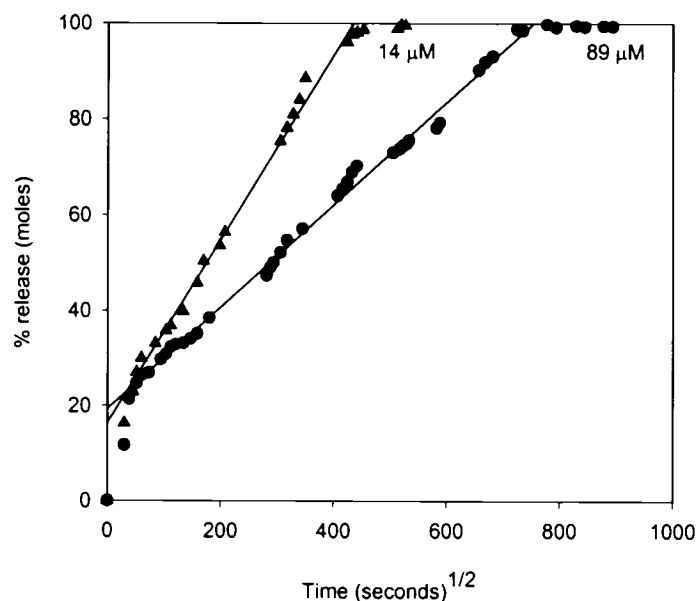


**Figure 3.7.** Diffusional release of benzo[a]pyrene: 14  $\mu\text{M}$  ( $\blacktriangle$ ) and 89  $\mu\text{M}$  ( $\bullet$ ) from  $\text{PCL}_{23}\text{-}b\text{-PEO}_{45}$  micelles (0.6% (w/w) polymer solution). Line of best fit suggests diffusional release, not including the initial burst release and the behavior near 100% release.

The more concentrated sample (89  $\mu\text{M}$ ) showed slower release, both in relative and absolute terms, than the less concentrated sample (14  $\mu\text{M}$ ). Similarly, as illustrated in Figure 3.8, the more concentrated DiI sample (54  $\mu\text{M}$ ) showed slower release compared to the less concentrated sample (12  $\mu\text{M}$ ).

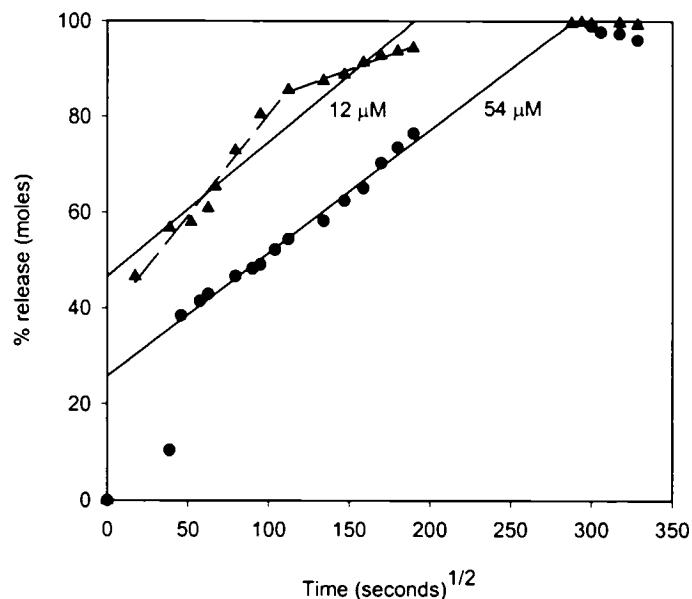


**Figure 3.8.** Diffusional release of DiI: 12  $\mu\text{M}$  ( $\blacktriangle$ ) and 54  $\mu\text{M}$  ( $\bullet$ ) from  $\text{PCL}_{23}\text{-}b\text{-PEO}_{45}$  micelles (0.6% (w/w) polymer solution). Line of best fit is through the diffusional release, not including the initial burst release and the release near 100% completion. The dotted lines for 12  $\mu\text{M}$  ( $\blacktriangle$ ) represent the line of best fit through two sections of possibly diffusional release with two different coefficients.

Figures 3.7 and 3.8 are plotted vs the square root of time to show the diffusive nature of the release probes as will be discussed below. The original plots of the percent release vs time can be found in the Appendix (Figures A1 and A2).

During the experiment, the probe molecules were continually released from the micelles in the dialysis bag, since the water was constantly being replenished outside of the dialysis bag, ensuring that there was no saturation of the probe in the external solution. It should be recalled that both the probes move through the dialysis bag very rapidly. Complete release of the probe molecules from the micelles was taken to have been achieved when the fluorescence reading was close to or equal to the fluorescence

background (i.e., empty micelles). The 14  $\mu\text{M}$  sample of benzo[a]pyrene reached complete release after 77 hours as opposed to the 89  $\mu\text{M}$  sample of benzo[a]pyrene, which took 175 hours. The release of DiI followed a similar pattern.

The release of both benzo[a]pyrene and DiI from PCL-b-PEO micelles was found to be slow and prolonged. This finding agrees with that of many other groups for release from micelles: Kim et al. showed that less than 30% of indomethacin was released from Pluronic/PCL micelles (diameter: 116-196 nm) over a period of ca. 100 hours.<sup>63</sup> Slow release of doxorubicin (20% released over 100 hours) from PBLA-b-PEO micelles was observed by Kwon et al.<sup>36</sup> Also, Jeong et al. found that the release of clonazepam from PBLG-b-PEO micelles was very slow, in that 40 wt% was released over 70 days.<sup>64</sup> It is interesting to note that none of the previous studies involved true sink conditions, in which the probe molecules are constantly being washed away from the exterior solution. Either a large reservoir was used or the water was changed periodically rather than continuously. The large reservoir has the potential disadvantage of allowing the probe molecules to accumulate, which would lead to the establishment of an equilibrium between the probe molecules in the reservoir with the probe molecules in the dialysis bag. Periodically changing the water may cause a “jump” in the release each time the water is replenished.

A burst release is observed in the release of both benzo[a]pyrene and DiI immediately upon exposure to water, as shown in Figures 3.7 and 3.8. After 1 hour, ca. 30% of benzo[a]pyrene molecules were released quickly from both samples. In the case of DiI, after 1 hour, the 12  $\mu\text{M}$  sample showed ca. 57% burst release compared to the 54  $\mu\text{M}$  sample, which showed ca. 40% burst release. A burst effect can occur when a

significant amount of the drug resides at the core-corona interface or in the corona. The release from core-corona interface region and also the outer corona region is rapid, because the probe does not have to traverse large segments of the core to exit the micelle. In the present case, it is likely that an equilibrium was reestablished between the probe in the core and in the corona since the samples were left in the refrigerator for 2-3 days prior to use for the release experiment. The burst release would have resulted from the probe molecules located in the corona, and their release was rapid because of the shorter diffusion path, i.e., the probe molecules do not have to diffuse through the core.<sup>14</sup> The percentage of the burst release of DiI is larger than that of benzo[a]pyrene from the micelles, because of the higher partition coefficient of DiI compared to that of benzo[a]pyrene. A greater number of DiI molecules will partition to the core-corona interface and/or corona than benzo[a]pyrene molecules and, as a result, will have a greater chance to be released quickly. The partition coefficient has an influence not only on the local concentration of the probe or drug but also on the release profile of the solute molecule from the block copolymer micelle, as was pointed out before.<sup>65</sup>

Many groups have observed a burst release with their respective micellar systems. Bromberg et al. observed a fast initial rate of release of both pyrene and 17 $\beta$ -estradiol from the corona of their Pluronic-*b*-poly(acrylic acid) micelles.<sup>4</sup> Teng et al. observed the rapid release of two hydrophobic probes (pyrene and phenanthrene) from two different block copolymers: polystyrene-*b*-poly(methacrylic acid) and poly(*tert*-butyl acrylate)-*b*-poly(2-vinylpyridine) due to the localization of some of the probe in the hydrophilic corona.<sup>45</sup> Chung et al. observed a small initial burst release from their dialyzed adriamycin incorporated poly(butyl methacrylate)-*b*-poly(*N*-isopropylacrylamide)

micelles due to the distribution of adriamycin in the poly(*N*-isopropylacrylamide) corona.<sup>66</sup> In some cases, a burst release can be advantageous if the amount of drug released is quantified since it provides an initial dose followed by a controlled release.<sup>67</sup>

The location of the probe is an important factor not only in terms of the burst release but also in terms of the release profile in general. If the probe is located predominantly in the corona, then the length of the core-forming block, the size of the particle, and the molecular volume of the drug are less important in determining the rate of release. An illustration of this was shown by Gorshova et al., where a faster release of daunomycin was observed with a smaller number of PEO units (300 vs 1000) attached to a copolymer of maleic anhydride and divinyl ether.<sup>68</sup> The authors argue that the shorter PEO units introduced into the copolymer-daunomycin conjugates lead to some macromolecular expansion, resulting in the reduction of hydrophobic daunomycin interaction.

The number of probe molecules incorporated in the micelle core influences their rate of release. Many groups have reported that the higher the concentration of drug or probe, the slower the release. Jeong et al. have shown that the release of both adriamycin<sup>23</sup> and clonazepam<sup>64</sup> from PBLG-*b*-PEO micelles is slower for higher concentrations of the respective drugs. At low loadings, Gref et al. also observed that lidocaine was molecularly dispersed in the hydrophobic cores of the poly(lactic-*co*-glycolic acid)-*block*-poly(ethylene oxide) micelles, resulting in a faster release.<sup>3</sup> At high loadings, Gref et al. showed that the release of lidocaine was slower, because of possible drug crystallinity. Similarly, at high loadings of lidocaine, Gorner et al. observed crystallinity of the drug in poly(d,l-lactide) nanospheres.<sup>69</sup> Crystallinity of the drug

slows the release, because release from the particles is possible only after the crystallized drug has dissolved and diffused to the outer solution. In the present case, DSC studies of a 14  $\mu\text{M}$  sample of benzo[a]pyrene suggest that there are no benzo[a]pyrene crystals present in the PCL<sub>23</sub>-*b*-PEO<sub>45</sub> micelles (results not shown). Similarly, DSC studies of 54 $\mu\text{M}$  sample of DiI indicate no crystallized DiI. It is possible that the concentrations of benzo[a]pyrene and DiI were too low to be able to detect any crystallinity in the micelles.

To determine the nature of the release of benzo[a]pyrene and DiI from the PCL<sub>23</sub>-*b*-PEO<sub>45</sub> micelles, the release profiles from Figures 3.7 and 3.8 were fit to those predicted by the Higuchi model.<sup>70</sup> According to the model, the percentage of probe released should be plotted against the square root of time, for benzo[a]pyrene and DiI, respectively. The fits for the release of the hydrophobic probes do not include the burst stage. The plots for benzo[a]pyrene show very good correlation coefficients (0.996 and 0.994) with the Higuchi model, indicating a diffusional release from the PCL<sub>23</sub>-*b*-PEO<sub>45</sub> micelles. The more concentrated DiI sample also showed a very good correlation coefficient (0.990) with the Higuchi model. However, the least concentrated sample showed an initial good correlation with the Higuchi model with a single constant, but then changed slope to give another line, which also showed a good correlation with the Higuchi model. An attempt to fit all of the points to the Higuchi model with a single time constant gave a poor correlation coefficient (0.936). A possible explanation is based on the possibility of a relatively quick release of the least concentrated DiI sample from the micelle. There seem to be two different mechanisms for the least concentrated DiI probe, but, generally, the release from PCL<sub>23</sub>-*b*-PEO<sub>45</sub> micelles is diffusional.

We have calculated approximate diffusion coefficients from Higuchi's equation:

$$Q = 2C_0 \left( \frac{Dt}{\pi} \right)^{1/2} \quad (3.9)$$

where  $Q$  is the amount of probe released per unit area,  $C_0$  is the initial concentration of the probe in the drug delivery vehicle,  $t$  is the time in seconds, and  $D$  is the apparent diffusion coefficient.<sup>71</sup> The approximate diffusion coefficients were calculated with the following conditions: PCL-*b*-PEO micelles are 25 nm in diameter, the burst release is not included, and the amount released is less than 30% of the total probe in the micelle.<sup>72</sup> For the more concentrated sample of DiI (54  $\mu\text{M}$ ),  $D = 4.0 \times 10^{-15} \text{ cm}^2/\text{s}$ , while for the least concentrated sample (12  $\mu\text{M}$ ),  $D = 6.2 \times 10^{-15} \text{ cm}^2/\text{s}$ . For the most (89  $\mu\text{M}$ ) and the least (14  $\mu\text{M}$ ) concentrated benzo[a]pyrene samples, the apparent diffusion coefficients were  $3.4 \times 10^{-15} \text{ cm}^2/\text{s}$  and  $2.7 \times 10^{-15} \text{ cm}^2/\text{s}$ , respectively. An increase of the diameter to 50 nm would have resulted in a 16-fold decrease in the diffusion coefficient. The calculated diffusion coefficients for DiI are higher than those for benzo[a]pyrene, which indicates that the more soluble DiI diffuses faster from the polycaprolactone core compared to benzo[a]pyrene.

### 3.5. Conclusions

The extent of solubilization, the partition coefficients and the release profiles of two model fluorescent compounds (benzo[a]pyrene and DiI) in polycaprolactone-*block*-poly(ethylene oxide) micelles have been investigated. These parameters are of importance in evaluating PCL-*b*-PEO as a suitable drug delivery system. The solubility of hydrophobic benzo[a]pyrene and DiI in PCL-*b*-PEO micelles is higher than in water. The maximum loading efficiency of PCL-*b*-PEO for DiI (87%) was higher than that for

benzo[a]pyrene (32%). Structurally, polycaprolactone is more compatible with DiI, because it has a greater number of aliphatic groups compared to that of benzo[a]pyrene, which explains the higher partition coefficient of DiI. These results are consistent with the higher loading efficiency results obtained for DiI. To investigate the release of the probes from the micelles, a new “perfect sink” method was used, which ensured that all of the probe molecules that were released from the micelles were washed away. The release of both probes was fitted to the Higuchi model and generally was found to be diffusional. We obtained approximate diffusion coefficients of the order of  $10^{-15}$  cm<sup>2</sup>/s for both DiI and benzo[a]pyrene. The information obtained from this study provides evidence for the usefulness of PCL-*b*-PEO micelles as a delivery vehicle for hydrophobic materials.

After investigating the incorporation and release of model hydrophobic probes in polycaprolactone-*block*-poly(ethylene oxide) micelles, it is clear that the compatibility between the micelle core and the molecule selected is important in evaluating its loading and release properties. In order to assess a pharmacologically relevant drug, we chose 17 $\beta$ -estradiol (E2), the principal female hormone. Among the advantages of choosing E2 as a model drug for our PCL-*b*-PEO micelles are that it is highly hydrophobic and easily detectable because it is fluorescent, and also available in a radiolabeled form. In addition, previous work in the group by Allen et al. investigated dihydrotestosterone (a hormone which mediates many of the biological actions of testosterone, the principal male hormone) inside of PCL<sub>21</sub>-*b*-PEO<sub>44</sub> micelles.<sup>17</sup> The selection of E2 also allows for another evaluation of the compatibility of the polycaprolactone-*block*-poly(ethylene oxide) micelles for the drug chosen. In the next chapter, the investigation of the

incorporation and release of E2 in different polycaprolactone-*block*-poly(ethylene oxide) micelles is reported.

### 3.6. Acknowledgement

The work was supported by the Natural Sciences and Engineering Research Council of Canada. The authors thank Dr. Christine Allen for many useful discussions, Carl Bartels for designing the release experiment diagram, Dr. Andrew Rodenheiser for assistance with the fluorescence instrument, and Dr. Derek Gray for generous use of the fluorometer. P.L.S. acknowledges the benefit of a scientific writing course given by Professor Linda Cooper.

### 3.7. References

- (1) Kataoka, K.; Harada, A.; Nagasaki, Y. *Advanced Drug Delivery Reviews* **2001**, *47*, 113-131.
- (2) Lemieux, P.; Vinogradov, S. V.; Gebhart, C. L.; Guerin, N.; Paradis, G.; Nguyen, H. K.; Ochiatti, B.; Suzdaltseva, Y. G.; Bartakova, E. V.; Bronich, T. K.; St-Pierre, Y.; Alakhov, V. Y.; Kabanov, A. V. *Journal of Drug Targeting* **2000**, *8*, 91-105.
- (3) Gref, R.; Minamitake, Y.; Peracchia, M. T.; Trubetskoy, V.; Torchilin, V.; Langer, R. *Science* **1994**, *263*, 1600-1603.
- (4) Bromberg, L.; Magner, E. *Langmuir* **1999**, *15*, 6792-6798.
- (5) Torchilin, V. P. *Journal of Controlled Release* **2001**, *73*, 137-172.
- (6) Rapoport, N.; Marin, A.; Luo, Y.; Prestwich, G. D.; Muniruzzaman, M. *Journal of Pharmaceutical Sciences* **2002**, *91*, 157-170.
- (7) Hagan, S. A.; Coombes, A. G. A.; Garnett, M. C.; Dunn, S. E.; Davies, M. C.; Illum, L.; Davis, S. S.; Harding, S. E.; Purkiss, S.; Gellert, P. R. *Langmuir* **1996**, *12*, 2153-2161.
- (8) Alexandridis, P.; Lindman, B.; Editors. *Amphiphilic Block Copolymers: Self-Assembly and Applications*; Elsevier Science B.V., 2000.

- (9) Discher, B. M.; Won, Y.-Y.; Ege, D. S.; Lee, J. C. M.; Bates, F. S.; Discher, D. E.; Hammer, D. A. *Science* **1999**, *284*, 1143-1146.
- (10) Ding, J.; Liu, G. *Journal of Physical Chemistry B* **1998**, *102*, 6107-6113.
- (11) Kwon, G. S.; Okano, T. *Advanced Drug Delivery Reviews* **1996**, *21*, 107-116.
- (12) Inoue, T.; Chen, G.; Nakamae, K.; Hoffman, A. S. *Journal of Controlled Release* **1998**, *51*, 221-229.
- (13) Jones, M. C.; Leroux, J. C. *European Journal of Pharmaceutics and Biopharmaceutics* **1999**, *48*, 101-111.
- (14) Allen, C.; Maysinger, D.; Eisenberg, A. *Colloids and Surfaces B: Biointerfaces* **1999**, *16*, 3-27.
- (15) Allen, C.; Yu, Y.; Maysinger, D.; Eisenberg, A. *Bioconjugate Chemistry* **1998**, *9*, 564-572.
- (16) Kozlov, M. Y.; Melik-Nubarov, N. S.; Batrakova, E. V.; Kabanov, A. V. *Macromolecules* **2000**, *33*, 3305-3313.
- (17) Allen, C.; Han, J.; Yu, Y.; Maysinger, D.; Eisenberg, A. *Journal of Controlled Release* **2000**, *63*, 275-286.
- (18) Torchilin, V.; Babich, J.; Weissig, V. *Journal of Liposome Research* **2000**, *10*, 483-499.
- (19) Lee, J. H.; Lee, H. B.; Andrade, J. D. *Progress in Polymer Science* **1995**, *20*, 1043-1079.
- (20) Kabanov, A. V.; Nazarova, I. R.; Astafieva, I. V.; Batrakova, E. V.; Alakhov, V. Y.; Yaroslavov, A. A.; Kabanov, V. A. *Macromolecules* **1995**, *28*, 2303-2314.
- (21) Alexandridis, P. *Current Opinion in Colloid Interface Science* **1997**, *2*, 478-489.
- (22) La, S. B.; Okano, T.; Kataoka, K. *Journal of Pharmaceutical Sciences* **1996**, *85*, 85-90.
- (23) Jeong, Y. I.; Nah, J. W.; Lee, H. C.; Kim, S. H.; Cho, C. S. *International Journal of Pharmaceutics* **1999**, *188*, 49-58.
- (24) Gan, Z.; Jim, T. F.; Li, M.; Yuer, Z.; Wang, S.; Wu, C. *Macromolecules* **1999**, *32*, 590-594.
- (25) Zhang, L.; Eisenberg, A. *Polymers for Advanced Technologies* **1998**, *9*, 677-699.

- (26) Riley, T.; Stolnik, S.; Heald, C. R.; Xiong, C. D.; Garnett, M. C.; Illum, L.; Davis, S. S.; Purkiss, S. C.; Barlow, R. J.; Gellert, P. R. *Langmuir* **2001**, *17*, 3168-3174.
- (27) Yasugi, K.; Nagasaki, Y.; Kato, M.; Kataoka, K. *Journal of Controlled Release* **1999**, *62*, 89-100.
- (28) Burt, H. M.; Zhang, X.; Toleikis, P.; Embree, L.; Hunter, W. L. *Colloids and Surfaces B: Biointerfaces* **1999**, *16*, 161-171.
- (29) Nagarajan, R.; Barry, M.; Ruckenstein, E. *Langmuir* **1986**, *2*, 210-215.
- (30) Nagarajan, R. *Polymers for Advanced Technologies* **2001**, *12*, 23-43.
- (31) Gadelle, F.; Koros, W. J.; Schechter, R. S. *Macromolecules* **1995**, *28*, 4883-4892.
- (32) Nagarajan, R.; Ganesh, K. *Macromolecules* **1989**, *22*, 4312-4325.
- (33) Hurter, P. N.; Scheutjens, J. M. H. M.; Hatton, T. A. *Macromolecules* **1993**, *26*, 5592-5601.
- (34) Xing, L.; Mattice, W. L. *Macromolecules* **1997**, *30*, 1711-1717.
- (35) Yoo, H. S.; Park, T. G. *Journal of Controlled Release* **2001**, *70*, 63-70.
- (36) Kwon, G.; Naito, M.; Yokoyama, M.; Okano, T.; Sakurai, Y.; Kataoka, K. *Journal of Controlled Release* **1997**, *48*, 195-201.
- (37) Kataoka, K.; Matsumoto, T.; Yokoyama, M.; Okano, T.; Sakurai, Y.; Fukushima, S.; Okamoto, K.; Kwon, G. S. *Journal of Controlled Release* **2000**, *64*, 143-153.
- (38) Kim, C.; Lee, S. C.; Shin, J. H.; Yoon, J.-S.; Kwon, I. C.; Jeong, S. Y. *Macromolecules* **2000**, *33*, 7448-7452.
- (39) Allen, C. J. In *Ph.D. Thesis (Chemistry)*; McGill University: Montreal, Quebec, Canada, 2000; p 251.
- (40) Bromberg, L.; Temchenko, M. *Langmuir* **1999**, *15*, 8627-8632.
- (41) Kwon, G. S.; Naito, M.; Kataoka, K.; Yokoyama, M.; Sakurai, Y.; Okano, T. *Colloids and Surfaces B: Biointerfaces* **1994**, *2*, 429-434.
- (42) Cao, T.; Munk, P.; Ramireddy, C.; Tuzar, Z.; Webber, S. E. *Macromolecules* **1991**, *24*, 6300-6305.
- (43) Wilhelm, M.; Zhao, C. L.; Wang, Y.; Xu, R.; Winnik, M. A.; Mura, J. L.; Riess, G.; Croucher, M. D. *Macromolecules* **1991**, *24*, 1033-1040.

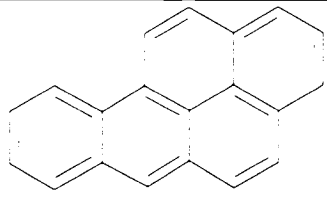
- (44) Zhao, J.; Allen, C.; Eisenberg, A. *Macromolecules* **1997**, *30*, 7143-7150.
- (45) Teng, Y.; Morrison, M. E.; Munk, P.; Webber, S. E.; Prochazka, K. *Macromolecules* **1998**, *31*, 3578-3587.
- (46) Case, F. H. *Abstracts of Papers - American Chemical Society* **2000**, *220th*, PHYS-576.
- (47) Allen, C.; Yu, Y.; Eisenberg, A.; Maysinger, D. *Biochimica Biophysica Acta* **1999**, *1421*, 32-38.
- (48) Engelberg, I.; Kohn, J. *Biomaterials* **1991**, *12*, 292-304.
- (49) van der Giessen, W. J.; Lincoff, A. M.; Schwartz, R. S.; van Beusekom, H. M.; Serruys, P. W.; Holmes, D. R., Jr.; Ellis, S. G.; Topol, E. J. *Circulation* **1996**, *94*, 1690-1697.
- (50) Allen, C.; Eisenberg, A.; Mrcsic, J.; Maysinger, D. *Drug Delivery* **2000**, *7*, 139-145.
- (51) Savic, R.; Lim Soo, P.; Eisenberg, A.; Maysinger, D. *Unpublished results*.
- (52) Haughland, R. P., 6th ed.; Molecular Probes Inc.: Eugene, OR, 1996.
- (53) Yu, Y.; Eisenberg, A. *Polymeric Materials: Science & Engineering* **1998**, *79*, 288-289.
- (54) Luo, L.; Tam, J.; Maysinger, D.; Eisenberg, A. *Bioconjugate Chemistry* **2002**, *13*, 1259-1265.
- (55) Lim Soo, P.; Lovric, J.; Davidson, P.; Maysinger, D.; Eisenberg, A. *To be submitted to Langmuir*.
- (56) Riley, T.; Govender, T.; Stolnik, S.; Xiong, C. D.; Garnett, M. C.; Illum, L.; Davis, S. S. *Colloids and Surfaces B: Biointerfaces* **1999**, *16*, 147-159.
- (57) Yokoyama, M.; Fukushima, S.; Uehara, R.; Okamoto, K.; Kataoka, K.; Sakurai, Y.; Okano, T. *Journal of Controlled Release* **1998**, *50*, 79-92.
- (58) Hurter, P. N.; Hatton, T. A. *Langmuir* **1992**, *8*, 1291-1299.
- (59) Nah, J.-W.; Jeong, Y.-I.; Cho, C.-S.; Kim, S.-I. *Journal of Applied Polymer Science* **2000**, *75*, 1115-1126.
- (60) Wang, W.; Tetley, L.; Uchegbu, I. F. *Langmuir* **2000**, *16*, 7859-7866.
- (61) Yoo, Y.; Kim, D.-C.; Kim, T.-Y. *Journal of Applied Polymer Science* **1999**, *74*, 2856-2867.

- (62) Encinas, M. V.; Lissi, E. A. *Chemical Physics Letters* **1982**, *91*, 55-57.
- (63) Kim, S. Y.; Ha, J. C.; Lee, Y. M. *Journal of Controlled Release* **2000**, *65*, 345-358.
- (64) Jeong, Y.-I.; Cheon, J.-B.; Kim, S.-H.; Na, J.-W.; Lee, Y.-M.; Sung, Y.-K.; Akaike, T.; Cho, C.-S. *Journal of Controlled Release* **1998**, *51*, 169-178.
- (65) Yang, L.; Alexandridis, P. *ACS Symposium Series* **2000**, *752*, 364-374.
- (66) Chung, J. E.; Yokoyama, M.; Okano, T. *Journal of Controlled Release* **2000**, *65*, 93-103.
- (67) Parikh, B. V.; Upadrashta, S. M.; Neau, S. H.; Nuessle, N. O. *Journal of Microencapsulation* **1993**, *10*, 141-153.
- (68) Gorshkova, M. Y.; Stotskaya, L. L. *Polymers for Advanced Technologies* **1998**, *9*, 362-367.
- (69) Gomer, T.; Gref, R.; Michenot, D.; Sommer, F.; Tran, M. N.; Dellacherie, E. *Journal of Controlled Release* **1999**, *57*, 259-268.
- (70) Higuchi, T. *Journal of Pharmaceutical Sciences* **1961**, *50*, 874-875.
- (71) Higuchi, T. *Journal of Pharmaceutical Sciences* **1963**, *52*, 1145-1149.
- (72) Solinis, M. A.; de la Cruz, Y.; Hernandez, R. M.; Gascon, A. R.; Calvo, B.; Pedraz, J. L. *International Journal of Pharmaceutics* **2002**, *239*, 61-68.

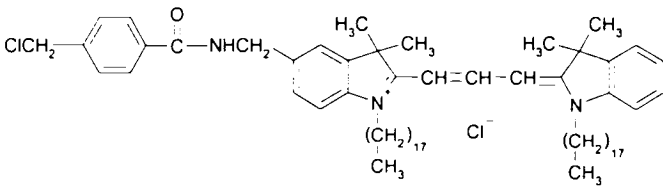
## Appendix

### 1. Hydrophobic fluorescent probes

**Table A1.** Physical Properties of Benzo[a]pyrene

Structure	
Molecular formula	$C_{20}H_{12}$
Molecular weight (g/mol)	252.3
Melting point ( $^{\circ}C$ )	177-180
Solubility in water (mol/L)	$1.5 \times 10^{-8}$
<u>Fluorescence properties</u> <sup>1</sup>	
Excitation:	381 nm
Emission (Main peak):	402 nm

**Table A2.** Physical Properties of CM-DiI

Structure	
Molecular formula	$C_{68}H_{105}Cl_2N_3O$
Molecular weight (g/mol)	1051.5
<u>Fluorescence properties</u> <sup>2</sup>	
Excitation:	553 nm
Emission (Main peak):	570 nm
Molar extinction coefficient ( $cm^{-1}M^{-1}$ ):	134000

**2. Determination of the partition coefficients of DiI and benzo[a]pyrene using the method developed by Kabanov et al.<sup>3</sup>**

Given

$$K_v = \frac{[\text{probe}]_m}{[\text{probe}]_w} \quad (\text{A3.1})$$

where  $[\text{probe}]_m$  is the probe concentration in the micelles and  $[\text{probe}]_w$  is the probe concentration in the aqueous solution.

Using the material balance equation, the bulk concentrations of the probe in the micelles ( $C_m$ ) and in the aqueous solution ( $C_w$ ) can be expressed as:

$$C_m = \frac{\theta K_v C_o}{[1 + (K_v - 1)\theta]} \quad (\text{A3.2})$$

and

$$C_w = \frac{(1 - \theta)C_o}{[1 + (K_v - 1)\theta]} \quad (\text{A3.3})$$

where  $C_o$  is the total probe concentration ( $C_m + C_w$ ) and  $\theta$  is the volume portion of the micellar phase, which can also be expressed as follows:

$$\theta = 0.01v - ([\text{polymer}] - \text{CMC}) \quad (\text{A3.4})$$

where  $v$  is the partial specific volume,  $[\text{polymer}]$  is the polymer concentration and CMC is the critical micelle concentration.

The portion of the probe in the micelles ( $\alpha$ ) can be obtained by dividing equation A3.2 by the total probe concentration ( $C_o$ ).

$$\alpha = \frac{C_m}{C_o} = \frac{\frac{\theta K_v C_o}{[1 + (K_v - 1)\theta]}}{\frac{\theta K_v C_o}{[1 + (K_v - 1)\theta]} + \frac{(1 - \theta)C_o}{[1 + (K_v - 1)\theta]}} \quad (\text{A3.5})$$

$$\alpha = \frac{\theta K_v C_o}{[1 + (K_v - 1)\theta]} \times \frac{[1 + (K_v - 1)\theta]}{\theta K_v C_o + (1 - \theta)C_o}$$

$$\alpha = \frac{\theta K_v C_o}{(\theta K_v + (1 - \theta))C_o}$$

$$\alpha = \frac{\theta K_v}{[1 + (K_v - 1)\theta]} \quad (\text{A3.6})$$

According to equation A3.6, an increase in the polymer concentration results in an increase in the probe in the micelles. This leads to an increase in the fluorescence emission intensity of the probe. Under saturating conditions of the polymer, all of the probe molecules are incorporated into the micelles and the emission reaches a maximum value and does not change ( $I_{\max}$ ). As a result, 2 assumptions are made: 1) The value for  $I_{\max}$  increases linearly with the probe concentration. 2) There is a linear relationship between the fluorescence intensity and the probe concentration in the aqueous solution in the absence of polymer ( $I_o$ ).

Therefore, the following equations are obtained:

$$I_o = f_w c_o \quad (\text{A3.7})$$

and

$$I_{\max} = f_m c_o \quad (\text{A3.8})$$

where  $f_m$  is the molar coefficient of emission in the micelles and  $f_w$  is the molar coefficient of emission in the aqueous solution.

The emission in the polymer solutions as a 1<sup>st</sup> approximation consists of emission of the probe in the micelles and aqueous solution.

$$I = [(1 - \alpha)f_w + \alpha f_m]C_o \quad (\text{A3.9})$$

As a result, the portion of the probe in the micelles can be expressed as follows:

$$\alpha = \frac{I - I_o}{I_{\max} - I_o} \quad (\text{A3.10})$$

Combining equations A3.6 and A3.10, we obtain the following:

$$\alpha = \frac{I - I_o}{I_{\max} - I_o} = \frac{\theta K_v}{[1 + (K_v - 1)\theta]}$$

$$\frac{I_{\max} - I_o}{I - I_o} - 1 = \frac{[1 + (K_v - 1)\theta]}{\theta K_v} - 1$$

$$\frac{I_{\max} - I_o}{I - I_o} - 1 = \frac{1 + \theta K_v - \theta - \theta K_v}{\theta K_v}$$

$$\frac{I_{\max} - I_o}{I - I_o} - 1 = \frac{1}{K_v \theta} - \frac{1}{K_v} \quad (\text{A3.11})$$

By plotting  $\frac{I_{\max} - I}{I - I_o}$  vs.  $\frac{1}{\theta}$ , we can determine the partition coefficient from the slope.

## 3. Release Kinetics

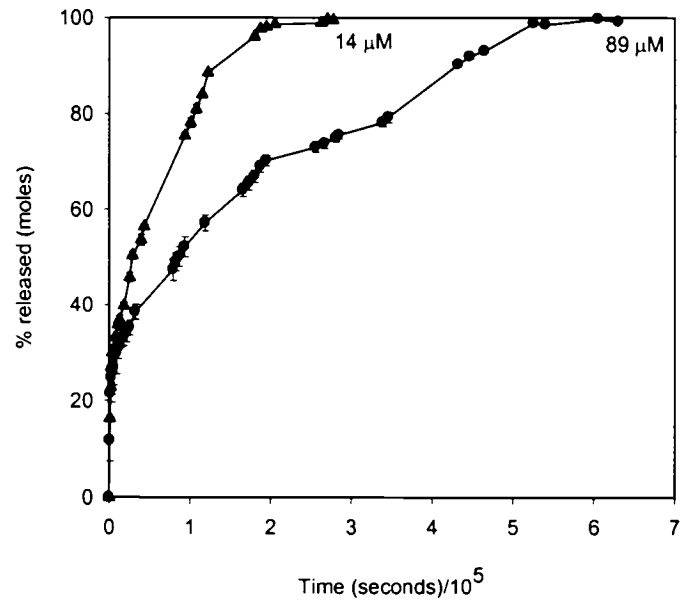


**Figure A1.** Release profile of benzo[a]pyrene: 14  $\mu\text{M}$  (▲) and 89  $\mu\text{M}$  (●) from PCL<sub>23</sub>-*b*-PEO<sub>45</sub> micelles (0.6% (w/w) polymer solution).

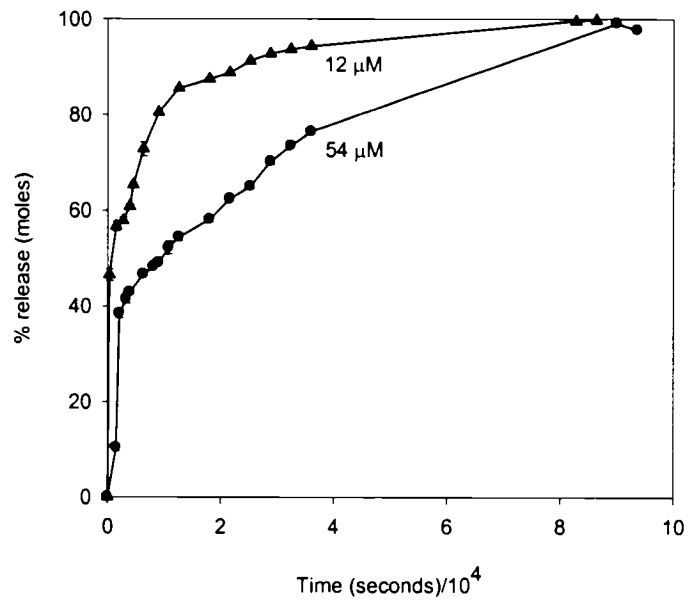


**Figure A2.** Release profile of DiI: 12  $\mu\text{M}$  (▲) and 54  $\mu\text{M}$  (●) from PCL<sub>23</sub>-*b*-PEO<sub>45</sub> micelles (0.6% (w/w) polymer solution).

## References

- (1) Ibbetson, A. L.; Freedman, R. B. *Biochemical Society Transactions* **1974**, *2*, 343-345.
- (2) Haughland, R. P., 6th ed.; Molecular Probes Inc.: Eugene, OR, 1996.
- (3) Kabanov, A. V.; Nazarova, I. R.; Astafieva, I. V.; Batrakova, E. V.; Alakhov, V. Y.; Yaroslavov, A. A.; Kabanov, V. A. *Macromolecules* **1995**, *28*, 2303-2314.

## Chapter 4

---

---

### Polycaprolactone-*block*-poly(ethylene oxide) Micelles: A Nano-delivery System for 17 $\beta$ -estradiol

---

---

#### 4.1. Abstract

Various hormone replacement regimens and delivery systems have been developed; however, there is still a need for additional, easily controllable and biocompatible systems. We have developed and characterized biocompatible polycaprolactone-*block*-poly(ethylene oxide) (PCL-*b*-PEO) micelles for the delivery of 17 $\beta$ -estradiol (E2) and investigated their loading and release properties using fluorescence spectroscopy. The micelles are spherical aggregates that range in size from 20-40 nm, as determined by both transmission electron microscopy and dynamic light scattering. A high loading efficiency for E2 of up to 96%, as well as a high drug loading capacity of up to 4000 molecules of E2 per micelle (equivalent to 190% (w/w)) is obtainable. In addition, the E2 loading and release can be controlled by modifying the block length of the polycaprolactone core and the initial estradiol concentration. The release of E2 from the micelles showed a biphasic profile under “perfect sink” conditions: there is an initial burst release, followed by a slow and prolonged release for up to 5 days, until complete release is achieved. The release of E2 from the micelles was shown to be diffusional, as shown by the linearity of the release as a function of the square root of time. Approximate diffusion coefficients of the order of  $10^{-17}$  cm<sup>2</sup>/s were obtained. *In vivo* experiments confirmed that the biological activity of E2 was retained after preparation of the micelles. This micelle carrier could serve as a versatile and efficient nano-delivery system for steroids and other poorly water soluble drugs that require solubilizing agents for delivery.

## 4.2. Introduction

Estrogen replacement therapy has been used over the past 60 years by millions of postmenopausal women.<sup>1,2</sup> Estradiol (E2) has several beneficial effects: it prevents osteoporosis<sup>3</sup>, reduces the risk of colorectal cancer<sup>4</sup> and decreases the risk of hip and other fractures.<sup>5</sup> However, hormone replacement therapies have also been the subject of controversy; for example, a study by the Women's Health Initiative of more than 16,000 women revealed that taking estradiol and a progesterone derivative increased the risk of heart disease, breast cancer and stroke.<sup>4</sup> Estrogen replacement therapy was originally proposed as a solution for estrogen deficiency, however oral delivery requires high concentrations, and is subject to metabolism and degradation in the liver and intestine.<sup>6</sup> Also, the use of estrogen therapy risks endometrial hyperplasia (a precancerous lesion) for postmenopausal women with an intact uterus.<sup>7</sup>

A variety of drug delivery systems for estradiol and contraceptives have been developed. Transdermal delivery systems including Estraderm®<sup>7</sup>, FemPatch®<sup>8</sup> and other FDA approved systems are reviewed in Ramachandran et al.<sup>9</sup> Liposomes containing phosphatidylcholine and surfactants, that serve to disturb the lipid bilayer, have also been used as a transdermal delivery vehicle for E2.<sup>10</sup> Both proniosomes (liposomes that are formed from non-ionic surfactants) and niosomes (proniosomes that have been hydrated in water) have also been used to increase the permeation of estradiol across the skin.<sup>11,12</sup> Among the advantages of the transdermal delivery system are avoidance of the hepatic first pass elimination, improved patient compliance, and reduction of some side effects.<sup>7</sup> However, variation in a patient's skin permeability results in insufficient or excess mean serum concentrations in the blood. In addition, adverse effects such as depression, breast

tenderness, headaches and nausea are associated with both oral and transdermal E2 formulations.<sup>9</sup>

Biocompatible polymers have also been used to deliver 17 $\beta$ -estradiol. Poly(lactide-*co*-glycolide) (PLGA) microspheres have been used to load and release E2.<sup>13,14</sup> A range of concentrations (0.15-15% (w/w)) can be loaded into the microspheres and controlled release is achievable. However the large sizes of microspheres are not ideal for avoiding the body's defense mechanisms, i.e., the reticuloendothelial system (RES), and there is a large burst release lasting up to 24 hours due to the presence of E2 on the surface of the particles.<sup>14,15</sup> Block copolymers made from polycaprolactone and polylactide have been used to create microspheres.<sup>16</sup> Also, disc and cylinder-type laminate systems have been employed for the controlled release of E2.<sup>17</sup>

Block copolymers have also been used in the preparation of micellar drug delivery systems.<sup>18-25</sup> Amphiphilic self-assembled systems are attractive drug delivery vehicles, mostly due to their size, stability, versatility and biocompatibility. Very few micellar systems exist for estradiol aside from Pluronic-*b*-poly(acrylic acid)<sup>26</sup> and various Carbopol (poly(acrylic acid))/surfactant systems.<sup>27</sup> However, a new biocompatible micelle system for the delivery of estradiol might prove advantageous. In our group, polycaprolactone-*block*-poly(ethylene oxide) (PCL-*b*-PEO) copolymer micelles have been explored as a drug delivery system.<sup>28-30</sup> PCL, the hydrophobic or core block is a well known biodegradable and biocompatible polymer that has been used in various biomedical applications because of its excellent biocompatibility and degradability. Poly(ethylene oxide) (PEO) serves as the hydrophilic block in the corona of the micelle. It is one of few water soluble polymers that has been widely used to improve the

biocompatibilities of blood-contacting biomaterials, because it helps prevent uptake by the RES by prolonging the circulation time of the carrier in the blood.<sup>31</sup> It has been shown that PCL-*b*-PEO micelles are an effective carrier for hydrophobic probes,<sup>32</sup> and lipophilic drugs such as FK506,<sup>33</sup> L-685,818,<sup>34</sup> and dihydrotestosterone (DHT).<sup>35</sup>

To investigate and assess polycaprolactone-*block*-poly (ethylene oxide) micelles as a delivery system for E2, we examined its loading and release parameters. E2 is fluorescent and its presence can be quantified using fluorescence spectroscopy. The influence of the initial concentration of E2 and of the polycaprolactone block length on the loading and release parameters are also examined. The release of E2 from the micelles is studied using a “perfect sink” apparatus in order to obtain information about the profile of drug release, and diffusion coefficients are calculated. *In vivo* experiments involving C57BL female mice are also examined to investigate the biological activity of E2 after the preparation of the micelles. The results from these studies provide evidence for the possibility of controlling these relevant properties of the micelle self-assembly drug delivery system, and for its versatility in incorporating other sex hormones.

### 4.3. Experimental Section

#### 4.3.1. Materials

The block copolymer that was used in this study was polycaprolactone-*block*-poly(ethylene oxide). A description of the complete synthesis of PCL<sub>23</sub>-*b*-PEO<sub>45</sub> block copolymers can be found in a previous publication by Luo et al. in connection with another project.<sup>34</sup> A series of block copolymers with the same number of units of ethylene oxide but different polycaprolactone units (PCL<sub>12</sub>-*b*-PEO<sub>44</sub> to PCL<sub>151</sub>-*b*-PEO<sub>44</sub>) were synthesized by anionic polymerization by Yu et al. in connection with another

project.<sup>36</sup> The subscripts after PCL or PEO refer to the number of repeat units in each block. 17 $\beta$ -estradiol was purchased from Sigma Aldrich (Oakville ON, Canada) and used as received. E2 has a molecular weight of 272.4 g/mol and a melting point of 173-179 °C (refer to Table A3 in the Appendix for the structure of E2 and its physical properties). Mini dialysis chambers (Slide-A-Lyzer® Mini Dialysis Unit) used for the release experiments were purchased from MJS BioLynx Inc. (Brockville ON, Canada) and had a molecular weight cutoff (MWCO) of 3500 g/mol.

#### 4.3.2. Preparation of PCL-*b*-PEO micelles with E2 for Loading and Release Studies

An aliquot of E2 solution in acetone was placed into an empty vial in quantities such that, in the final solution, the concentration of the drug ranged from 10 to 72 mM. The acetone was allowed to evaporate. The block copolymer (5-10 mg) was then added to the vial and 15 mg of dimethylformamide (DMF) was added to dissolve both the drug and the copolymer. The solution was allowed to stir for 4 hours. To induce micellization, MilliQ water was added slowly at a rate of approximately 2.5%/minute until 35 mg of MilliQ water had been added. The total mass of this solution was ca. 500 mg, which yielded a 1-2% (w/w) polymer solution. The micelle solution was stirred overnight and dialyzed against MilliQ water in the dark to remove the DMF solvent and any excess E2 molecules. For the first 4 hours, the water was changed twice every 2 hours, then once every hour for the next 4 hours, and then left overnight. After dialysis, the micelle solution was diluted to 0.4-1.0% (w/w) of polymer.

### 4.3.3. Fluorescence Measurements for Loading and Release Experiments

The loading efficiency of 17 $\beta$ -estradiol into the micelles was determined by fluorescence spectroscopy. A calibration curve of E2 in dimethyl sulfoxide (DMSO) was created to determine the linear range of fluorescence as a function of concentration of the drug. A small aliquot of micelles containing drug (i.e., 10  $\mu$ L) was dissolved in 490  $\mu$ L of DMSO and placed into a quartz microcuvette. This was performed for determinations of the concentration of E2 in both loading and release experiments. The micelles are completely dissolved in DMSO, releasing all of the E2, and the solution is then analyzed by fluorescence. The copolymer and the solvent do not contribute significantly to the fluorescence, and the background value obtained was subtracted. The fluorescence was measured using a SPEX FluoroMax 2 in the right-angle geometry (90<sup>0</sup> emission collection). The emission fluorescence spectra were obtained at an excitation wavelength ( $\lambda_{ex}$  = 281 nm). The loading efficiency and the drug content were calculated using the experimental values from fluorescence spectroscopy and from the following equations:<sup>37</sup>

$$\text{Loading efficiency (\%)} = \frac{\text{mass of drug in micelles (g)}}{\text{total mass of drug used (g)}} \times 100 \quad (4.1)$$

$$\text{Drug content (\% w/w)} = \frac{\text{mass of drug in micelles (g)}}{\text{mass of micelles (g)}} \times 100 \quad (4.2)$$

### 4.3.4. Release of E2 from PCL-*b*-PEO Micelles

The solution of the micelles with the incorporated E2 used for the release experiment had a polymer concentration of 0.4-1.0% (w/w) and an initial concentration of 3 to 35 mM. 10-20  $\mu$ L samples of micelles containing the E2 were placed into dialysis

chambers (MWCO: 3500 g/mol). 380-390  $\mu\text{L}$  of MilliQ water was then added to each dialysis chamber. The experiment was performed under “perfect sink” conditions; after being released from the micelles, all of the drug molecules were immediately washed away into the exterior solution, hence there was no drug that accumulates in the reservoir and steady state conditions were not reached. Briefly, a number of dialysis chambers (up to 20) were placed into a dialysis float device, which was placed into a large beaker filled with tap water. This beaker was placed into a crystallization dish ( $160 \times 100$ ) equipped with a side neck. Tap water was allowed to run into the beaker so that when the water overflowed from the beaker, the excess water would go into the crystallization dish and out the side neck attached with a tube. This allowed for constant stirring and also for “perfect sink” conditions to be observed. At specific time intervals, a dialysis chamber was removed and an aliquot was sampled, dissolved in DMSO, and analyzed by fluorescence.

#### 4.3.5. Transmission Electron Microscopy (TEM)

The micelles in the solutions were examined using a JEOL JEM-2000FX electron microscope operating at an accelerating voltage of 80 keV. Dilute solutions of the micelles containing the E2 in water (0.05% (w/w)) was deposited on 400 mesh copper grids (EMS Sciences, USA) that were precoated with a thin film of Formvar (poly(vinylformal)) and carbon. The samples were allowed to remain on the grids for a few seconds and then a blotter was applied to remove the excess solution. The grids were then left overnight to air dry. Digital images were taken with a Gatan 792 Bioscan 1k x 1k Wide Angle Multiscan CCD camera (JEM-2000 FX).

#### 4.3.6. Dynamic Light Scattering (DLS)

The sizes and size distributions of the micelles containing the E2 were determined on a Brookhaven Instruments photon correlation spectrophotometer with a BI-9000AT digital correlator. The instrument was equipped with a compass 315M-150 laser (Coherent Technologies, USA) that was used at a wavelength of 532 nm. Micelles containing the E2 were filtered through a 200 nm filter and used at a concentration of 0.05% (w/w). Dust free vials were used for the aqueous micelle solutions and measurements were performed at an angle of 90° at room temperature. The CONTIN algorithm was used to analyze the DLS data.

#### 4.3.7. Assessment of Effectiveness of PCL<sub>23</sub>-*b*-PEO<sub>45</sub> Micelles Containing the E2 *In Vivo*

All animal work was performed according to guidelines approved by the local Animal Research Committee of the Institute and all efforts were made to minimize animal suffering and to reduce the number of animals used. 24 days old female mice (C57BL) were fed *ab libitum* with mouse standard diet and kept in a 12 hour light/dark cycle. Prior to injecting, 20 µL of micelle stock solution (27 mM) was redispersed in saline to make a total volume of 100 µL (retaining the polymer concentration approximately 950 times above the critical micelle concentration (CMC)<sup>28</sup>: 2.8 x 10<sup>-7</sup>M). The Appendix contains details of the calculation. At postnatal day 17, the suspension providing pharmacological plasma concentration (150 µg of E2 in olive oil) was injected into the backs of mice (i.e., subcutaneous). One week later, the animals were sacrificed by decapitation. Positive control animals were treated once a day (0.5 µg of E2) and were also sacrificed one week after treatment. Negative controls were injected with empty

micelles or a vehicle for E2 (i.e., olive oil). There was no significant difference between animals treated with empty micelles or olive oil, so these two groups were merged into the control group. After sacrificing the animals, uteri were collected and stored at -80 °C for subsequent analysis. The wet tissue was weighed and the data analyzed using statistical methods.

#### 4.4. Results and Discussion

##### 4.4.1. Loading Properties of E2 in PCL-*b*-PEO Micelles

The loading of E2 into PCL<sub>23</sub>-*b*-PEO<sub>45</sub> micelles was investigated for a series of samples ranging in initial (prior to loading) drug concentrations from 10 to 72 mM. The loading efficiency is an indication of the percentage of the drug present in solution that can potentially be incorporated into the carrier. The loading efficiency of micelles for E2 can be determined from equation 4.1, and the results are shown in Figure 4.1a. The loading efficiency increases from 36% when the weight ratio of drug to polymer is 0.1 (w/w) to 67%, as this value increases to 0.8 (w/w) and reaches 96% (w/w) when the weight ratio of drug to polymer is 2 (w/w). The increase in the loading efficiency of E2 with initial drug concentration was generally seen for copolymer micelles. For example, Hagan et al.<sup>38</sup> reported this trend for both testosterone and sudan black B in poly(d,l-lactide)-*block*-poly(ethylene glycol) (PLA-*b*-PEG) micelles. Similarly, Govender et al.<sup>39</sup> also observed this trend for procaine hydrochloride in PLA-*b*-PEG micelles. In all of these cases, as the drug concentration in the solution increased, one eventually reaches a point when the loading efficiency decreases because the micelles are unable to take up any more drug molecules.<sup>32</sup> Increases in loading efficiency with initial drug concentration were also seen for microspheres; for example, Birnbaum et al. showed that

an increase in the initial concentration of E2 increased the loading efficiency of the drug.<sup>14</sup> They reported loading efficiencies ranging from 67-100% into PLGA microspheres.

The drug content (i.e., the actual amount of drug incorporated in the micelles), of E2 is determined from equation 4.2 and is shown in Figure 4.1b. There is a nearly linear relation between the drug content and the weight ratio of drug to polymer in the initial solution. A remarkably high amount of E2 can be incorporated into the PCL<sub>23</sub>-*b*-PEO<sub>45</sub> micelles. The drug content of E2 ranges from approximately 5 to 190% (w/w) for a weight ratio of drug to polymer of 0.1 to 2 (w/w). By comparison with microspheres, 0.2-2.3% (w/w) and 5-15% (w/w) were reported in PLGA microspheres ranging in size of 30-150  $\mu\text{m}$ <sup>13</sup> and 60-75  $\mu\text{m}$ <sup>14</sup> respectively. Thus, the PCL<sub>23</sub>-*b*-PEO<sub>45</sub> micelles can incorporate approximately 13 times the maximum drug content achieved in these PLGA microspheres (15% vs. 190% (w/w)). However, from the microspheres studies, it is not clear whether the limits of incorporation had been reached, so it is conceivable that a greater amount of drug could have been incorporated.

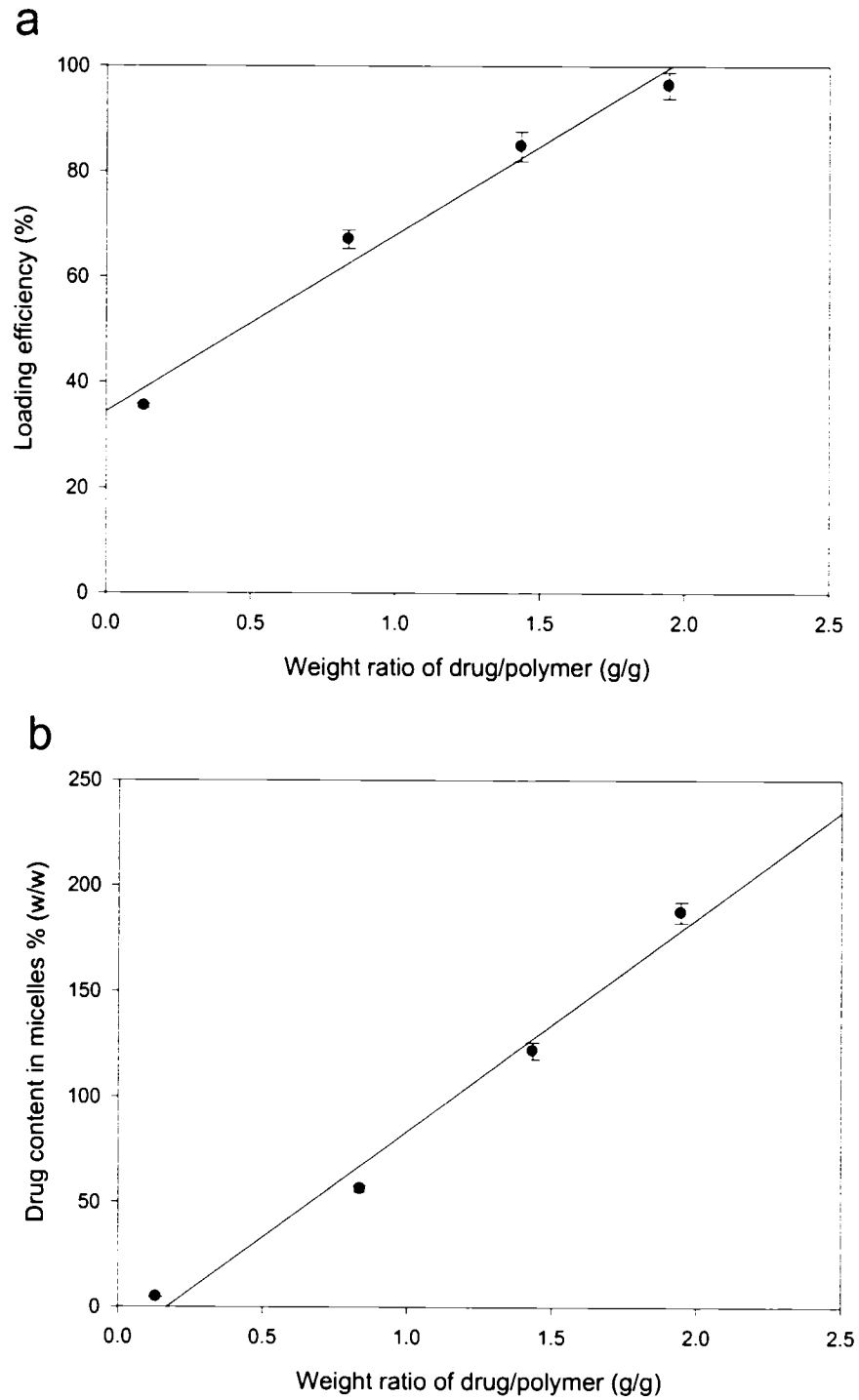


**Figure 4.1.** Loading efficiency (a) and drug content (b) of E2 in PCL<sub>23</sub>-*b*-PEO<sub>45</sub> micelles. Straight line only meant to serve as a guide for the eye.

Additional insight into the loading capacity can be obtained from the data in Table 4.1.

**Table 4.1.** Loading properties of E2 in PCL<sub>23</sub>-*b*-PEO<sub>45</sub> micelles.

Weight ratio of drug/polymer (w/w)	Loading efficiency (%)	Drug content % (w/w)	Molecules of E2/Micelle	Weight of E2/Weight of PCL core % (w/w)
0.1	36	5	$9.9 \times 10^1$	10
0.8	67	55	$1.2 \times 10^3$	100
1.4	85	120	$2.6 \times 10^3$	215
2.0	96	190	$4.0 \times 10^3$	330

The number of molecules per micelle is another indication of the loading properties of the delivery system. The PCL<sub>23</sub>-*b*-PEO<sub>45</sub> micelles can incorporate up to a maximum of ca. 4000 molecules of E2 per micelle, representing a drug content of 190% (w/w). These numbers suggest that these block copolymers micelles can be suitable carriers for steroids and similar hydrophobic drugs, in contrast to what has been stated for small molecule surfactants.<sup>40</sup> In general, the great affinity of PCL for steroid molecules such as E2 is well documented.<sup>41</sup> It is also of interest to compare estradiol with DHT loaded into block copolymer micelles. Allen et al. incorporated DHT into PCL<sub>21</sub>-*b*-PEO<sub>44</sub> micelles (ca. 50 nm) and showed that at a weight ratio of drug to polymer of 2 (w/w), ca. 1300 DHT molecules were incorporated, representing 134% (w/w).<sup>35</sup> Hence, for any given weight ratio of drug to polymer, PCL<sub>23</sub>-*b*-PEO<sub>45</sub> micelles can incorporate approximately two to three times more E2 than DHT molecules.

The weight ratio of the amount of E2 and the PCL core is also an important indication of the loading properties of the micelle, because most of the hydrophobic drug

should be present in the hydrophobic core. The weight ratio of E2 and PCL core ranges from approximately 10 to 330% (w/w) for a weight ratio of drug to polymer of 0.1 to 2 (w/w). In comparison, DHT ranges from approximately 6 to 130 for a weight ratio of drug to polymer of 0.1 to 2 (w/w).<sup>35</sup> For the same drug per polymer ratios in the initial solution, the incorporation of E2 is approximately two to three folds higher than for DHT in the PCL cores. This comparison is more meaningful, because we compare the amount of drug incorporated in the PCL core. Exact comparisons between micelle systems are not trivial, due to the differences in the total molecular weight, the size of the micelles, the size of the core, and the size of the corona chains; hence this was the reason why we compared the loading data using many different units.

In order to investigate the effect of polycaprolactone block length on the loading capacity of E2, a series of copolymers were synthesized with different polycaprolactone blocks (ranging from 12 to 151 units) with the same poly(ethylene oxide) blocks (e.g., 44 units). The influence of the PCL block length on the loading efficiency of E2 is shown in Figure 4.2.

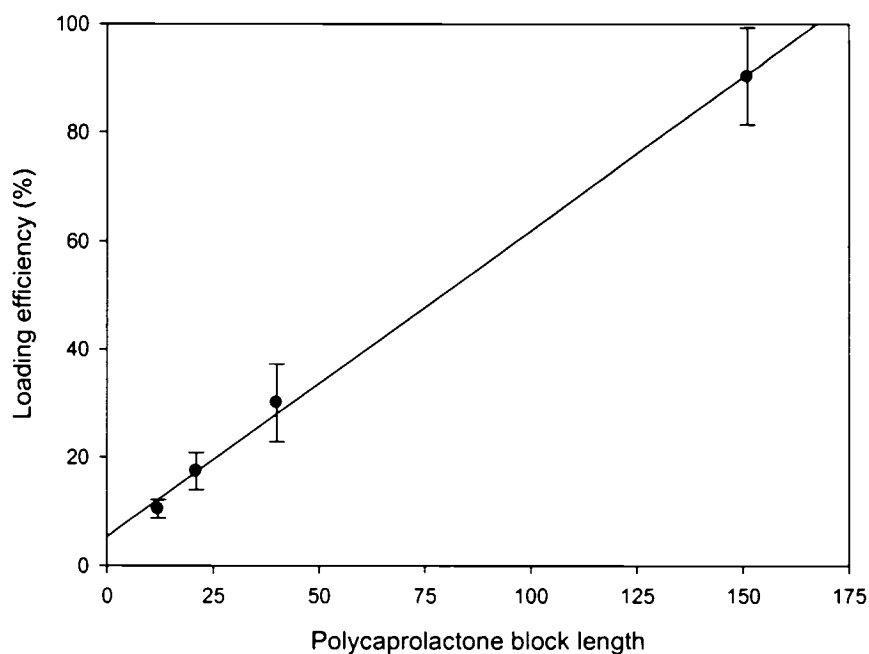


**Figure 4.2.** Dependence of loading efficiency of E2 on the block length of polycaprolactone in PCL<sub>x</sub>-*b*-PEO<sub>44</sub> micelles.

There is a linear increase ( $r^2 = 0.998$ ) in the loading efficiency, from 10 to 90%, as the PCL block length increases. More information about the loading characteristics of the different PCL<sub>x</sub>-*b*-PEO<sub>44</sub> copolymers is given in Table 4.2.

**Table 4.2.** Loading properties of E2 in different PCL<sub>x</sub>-*b*-PEO<sub>44</sub> micelles.

PCL block length	Loading efficiency (%)	Drug content % (w/w)	Molecules of E2/Micelle	Weight of E2/Weight of PCL core % (w/w)
12	10	15	$2.3 \times 10^2$	36
21	17	22	$5.1 \times 10^2$	40
40	30	45	$1.3 \times 10^3$	64
151	90	130	$1.1 \times 10^4$	144

The drug content ranges from 15 to 130% (w/w) as the PCL block length increases. The number of molecules of E2 increases from approximately 230 to 11000, which leads to a weight ratio of drug and PCL core of 36 to 144% (w/w) as the PCL block length increases. The increase in the block length of PCL should result in a larger core diameter and more drug molecules can be incorporated. The reason for this is that as the PCL block length increases, the aggregation number of the micelle increases, resulting in a larger core, which allows for a higher loading efficiency. This has been reported in the literature by Gadelle et al., who showed that as the length of the hydrophobic block increases, the CMC decreases and a resulting increase in the diameter of the core facilitates the loading of more drug molecules into the core.<sup>42</sup> Similarly, Kozlov et al. showed that a decrease in the CMC was the direct result of increasing the length of the core-forming block.<sup>43</sup>

The increase in the PCL block length also influences the partition coefficient, which is a convenient way to express the drug's affinity for the micelle core or for the external environment. The partition coefficient increases with increasing PCL block lengths. Allen et al. showed that the partition coefficient of pyrene increased from 240 to 1450 as the PCL block length increased from 14 to 40.<sup>28</sup> In the previous section, the high estradiol loading into the micelles would suggest that there is a great affinity of the drug molecules for the polycaprolactone core.  $17\beta$ -estradiol is highly lipophilic and prefers to partition into the hydrophobic PCL core of the micelle. In the cell membrane, E2 tends to associate with the hydrophobic domains.<sup>44</sup>

A value for E2 in the PCL-*b*-PEO micelles was not determined, but a comparison of the partition coefficients reported in the literature gives a good indication of the value.

Lundberg et al. determined the log water-octanol partition of E2 and testosterone to be 4.0 and 3.8 respectively.<sup>45</sup> Testosterone is more water soluble than estradiol (e.g., 19.8 mg/L vs. 1.7 mg/L).<sup>45</sup> The log apparent partition coefficient of DHT was determined to range from 2.9 to 4.3 in PCL<sub>20</sub>-*b*-PEO<sub>44</sub> micelles,<sup>35</sup> so since the structures of DHT and testosterone are similar (DHT has a carbonyl group on the six membered ring, instead of a hydroxy group as in the case of E2), we estimate that the partition coefficient for E2 would be larger than that for DHT. E2 molecules are more hydrophobic than testosterone (and similarly DHT) and would partition into the PCL core. Hence the interaction between the E2 molecules and PCL<sub>23</sub>-*b*-PEO<sub>45</sub> micelles is strong and leads to extensive incorporation. In comparison with another system, Ye et al. calculated the log partition coefficient of E2 in block copolymers of varying ratios of caprolactone and lactide and found that increasing amount of caprolactone (from 60 to 90%) lead to an increase of log P from 3.0 to 4.3.<sup>46</sup> Similarly, a high partition coefficient (log P = 3.8) was determined between a model fluorescent hydrophobic probe (CM-DiI) and PCL-*b*-PEO micelles and resulted in a high loading capacity for the probe.<sup>32</sup>

#### 4.4.2. PCL-*b*-PEO Morphology and Size

The size and morphology of the PCL<sub>23</sub>-*b*-PEO<sub>45</sub> micelles were determined previously<sup>34</sup> and the findings are confirmed in the present study. Briefly, the micelle aggregates were spherical in morphology and the sizes by DLS and TEM were both  $25 \pm 2$  nm. A TEM image of micelles containing the E2 (2 mM) can be seen in Figure 4.3a. The micelles are spherical in morphology with a diameter of  $30 \pm 7$  nm. Dynamic light scattering was also used to determine the size of the micelles containing the E2 (3 mM) and the results are shown in Figure 4.3b.

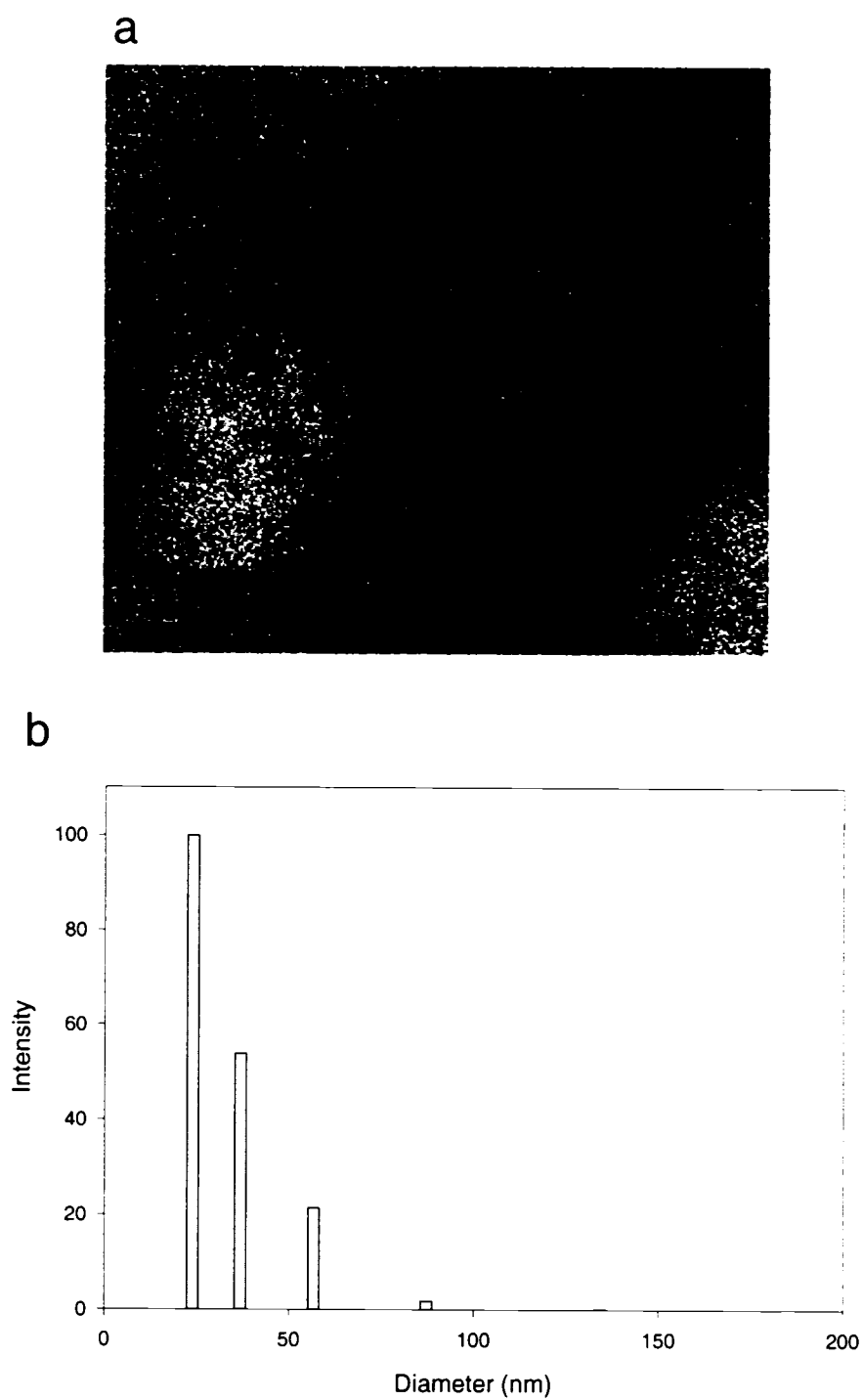


**Figure 4.3.** (a) Transmission electron microscopy of E2 (conc. 2 mM) in PCL<sub>23</sub>-*b*-PEO<sub>45</sub> micelles. Size range is  $30 \pm 7$  nm. (b) Dynamic light scattering of E2 (conc. 3 mM) in PCL<sub>23</sub>-*b*-PEO<sub>45</sub> micelles. Average diameter is 33 nm.

Insufficient sample did not allow for the analysis of the same concentrations by both methods, hence, two different concentrations were needed to be used. There should not be a significant change in the size and size distributions due to small differences in drug loading. The majority of the micelles are less than 50 nm and the average micelle diameter is 33 nm, as determined by Contin analysis using DLS. Although we haven't studied the effect of drug loading of E2 on the micelle size, we speculate that with higher amounts of E2 loaded, there may be a possible increase in the micelle size. Such an increase has been previously observed for the incorporation of estrone into PLA microspheres<sup>47</sup> and antiestrogen (RU 58668) into PLGA, PLA and PCL nanospheres.<sup>48</sup>

#### 4.4.3. Release Kinetics of E2 from PCL-*b*-PEO Micelles

The release of PCL<sub>23</sub>-*b*-PEO<sub>45</sub> micelles with different E2 loading contents was examined under “perfect sink” conditions. The release of two different concentrations of E2 (3 and 35 mM) from the micelles is seen in Figure 4.4.

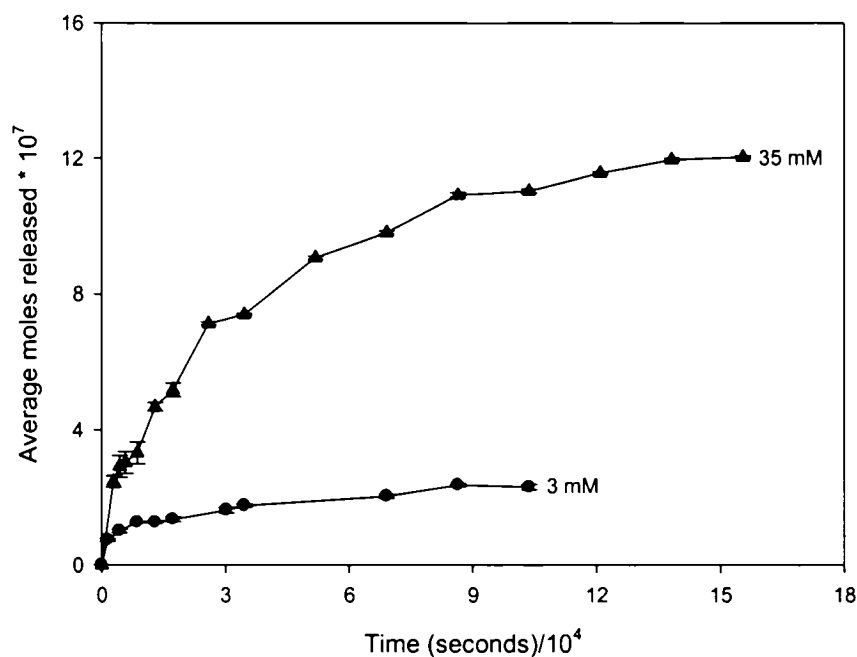


**Figure 4.4.** Release of E2 (3 mM (●) and 35 mM (▲)) from PCL<sub>23</sub>-*b*-PEO<sub>45</sub> micelles under “perfect sink” water conditions.

The more E2 concentrated sample took up to five days for almost complete release (> 90% release) and the least concentrated sample took up to three days.

In order to obtain more useful information on the release of estradiol from the micelles, the release data was plotted against the square root of time; the linearity of the plot is indicative of a diffusional release. We determined the diffusion coefficients,  $D$  (expressed in cm<sup>2</sup>/s) from these release plots using the Higuchi equation:<sup>49</sup>

$$Q = 2C_0 \left( \frac{Dt}{\pi} \right)^{1/2} \quad (4.3)$$

where  $Q$  is the amount of E2 released per unit area of the micelles (expressed in moles/cm<sup>2</sup>),  $C_0$  is the initial concentration of E2 per volume of PCL (expressed in

moles/cm<sup>3</sup>) and  $t$  is the time (expressed in seconds). Previously, we have used this model to fit release data of model hydrophobic probes from these micelles.<sup>32</sup> The release plotted against the square root of time, is shown in Figure 4.5.

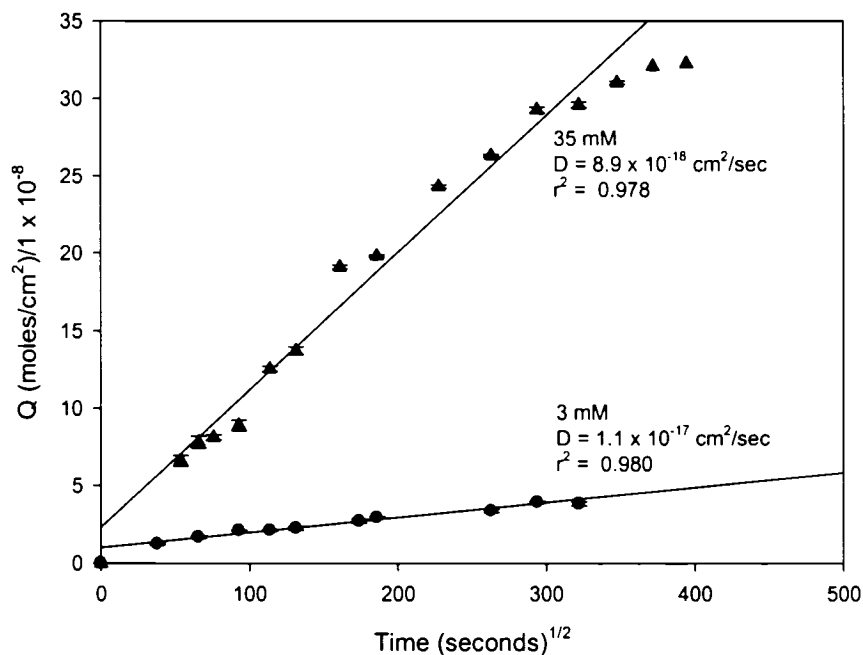


**Figure 4.5.** The fit of the release data to the Higuchi model using two different estradiol concentrations: 3 mM (●) and 35 mM (▲) under “perfect sink” water conditions. The linearity of the line of best fit is indicative of a diffusional release mechanism. The assumption is that the average diameter of the micelle is 25 nm.

The release fits relatively well with the Higuchi model (i.e., correlation coefficients of 0.978 for 35 mM and 0.980 for 3 mM). The linearity confirms that the release of E2 from the micelles is diffusion controlled. Diffusion coefficients were determined assuming a micelle diameter of 25 nm, and omitting the data for the burst release phase.<sup>49</sup> For the more concentrated sample (35 mM), the diffusion coefficient was  $8.9 \times 10^{-18} \text{ cm}^2/\text{s}$ , while for the lower concentration sample (3 mM), the diffusion coefficient was  $1.1 \times 10^{-17}$

cm<sup>2</sup>/s. Refer to Appendix for sample calculations. The release from the more concentrated sample is slower than the less concentrated sample. This has been reported in the literature by many groups for block copolymer micelles. Gref et al. showed that at low loadings of lidocaine, the release of the drug occurred more quickly from PLGA-*b*-PEO micelles than for higher loadings.<sup>18</sup> The release of norfloxacin from poly( $\gamma$ -benzyl-L-glutamate)-*block*-poly(ethylene oxide) (PBLG-*b*-PEO) micelles was observed to be slower at higher drug contents due to increased hydrophobic interaction between the PBLG core and the hydrophobic drug.<sup>50</sup> Similarly, in a recent paper, we showed that the release of higher concentrations of hydrophobic probes (CM-DiI and benzo[a]pyrene) was slower than for lower concentrations.<sup>32</sup> Diffusion controlled release was reported in the literature for E2 from another micelle system. Bromberg et al. observed a slow diffusional release from Pluronic-PAA micelles.<sup>26</sup>

The influence of the PCL block length on the release of estradiol (35 mM) was determined using different PCL-*b*-PEO micelles (PCL<sub>23</sub>-*b*-PEO<sub>45</sub> and PCL<sub>151</sub>-*b*-PEO<sub>44</sub>) as seen in Figure 4.6.

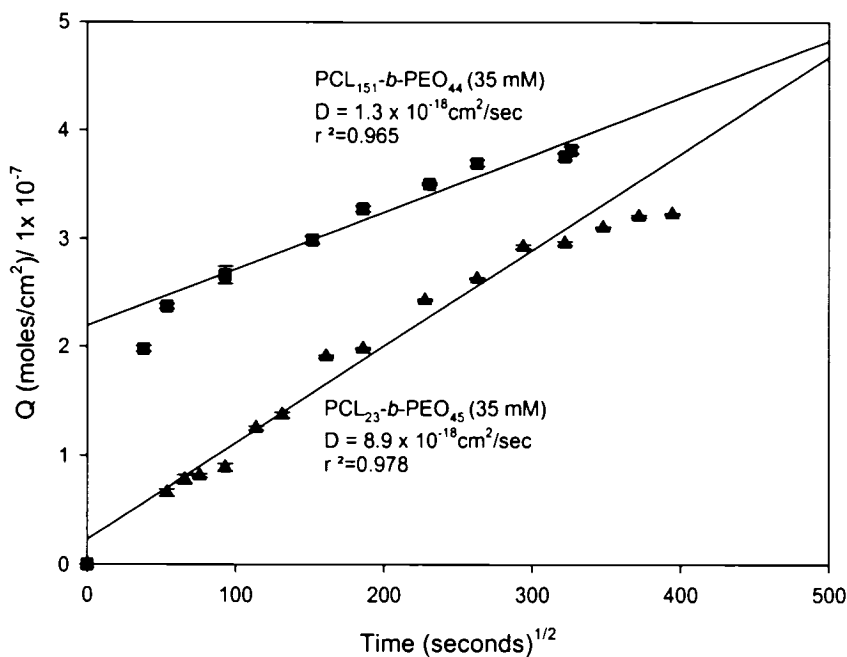


**Figure 4.6.** Release of E2 (35 mM) from PCL-*b*-PEO micelles with different PCL lengths PCL<sub>151</sub> (●) and PCL<sub>23</sub> (▲) under “perfect sink” water conditions. The linearity of the line of best fit is indicative of a diffusional release mechanism. The assumption is that the average diameter of the micelle is 25 nm.

The release of E2 from the PCL<sub>23</sub>-*b*-PEO<sub>45</sub> micelles ( $D = 8.9 \times 10^{-18} \text{ cm}^2/\text{s}$ ) occurred more quickly than the release from PCL<sub>151</sub>-*b*-PEO<sub>44</sub> micelles ( $D = 1.3 \times 10^{-18} \text{ cm}^2/\text{s}$ ). The drug is released more slowly from PCL<sub>151</sub>-*b*-PEO<sub>44</sub> because it presumably has a larger core due to the longer hydrophobic block (151 units of PCL), compared to the shorter hydrophobic block (23 units of PCL). The drug has further to diffuse in a core with a longer hydrophobic block. A longer core block would also have a higher glass transition temperature, so that closer to room temperature, the higher the viscosity of the medium would result in a slower release. Finally, the larger core diameter could result in a higher crystallinity of the core in comparison to a smaller core diameter; the crystallinity would

slow the release of the drug. Similar findings of increased hydrophobic blocks resulting in a slower release have also been reported in the literature for copolymer micelles. Jeong et al. showed that for poly( $\gamma$ -benzyl L-glutamate)-*b*-poly(ethylene oxide) (PBLG-*b*-PEO) micelles with different PBLG contents, but similar loadings of adriamycin, the release was slower for the copolymer with higher PBLG content.<sup>51</sup> The increased hydrophobic interactions between the drug and the micelles with higher PBLG content were responsible for the slower release. Similarly, Nah et al. incorporated norfloxacin and clonazepam into the PBLG-*b*-PEO micelles and observed that release of the drugs were slower for longer PLBG chains.<sup>50,52</sup> Gorshokova et al. found that over a 15 day period, the release rate of daunomycin is reduced from 16% to 4% due to the introduction of hydrophobic blocks (decylamine).<sup>53</sup>

During our release experiments, all the micelle samples showed a small initial burst release (i.e., 20-30% in the first hour) of 17 $\beta$ -estradiol. This is a result of the E2 being released from the micelle interface regions of the micelles. Burst release seems to be common for most micelle systems and, as a result, a biphasic release is usually seen with an initial burst followed by a sustained release. Burst release has also been observed for other micelle systems: e.g., Bromberg et al. observed a 5-11% initial rate of release of E2 from the expanded PAA corona of the Pluronic-PAA micelles.<sup>26</sup> Similarly, Teng et al., showed an initial burst release of pyrene from the inner corona of poly(*tert*-butyl acrylate)-*b*-poly(2-vinylpyridine) and PBA-*b*-P2VP/P2VP-*b*-PEO micelles.<sup>54</sup> Burst release has also been observed in microspheres: Dickinson et al. found that in their PLGA microspheres, there was a burst release of E2 lasting up to 1 day, and the initial burst release of E2 was a result of the frequent changes of the release medium.<sup>15</sup> Studies

showed that incorporating PLGA microparticles within a silicone matrix reduced the initial burst release of E2.<sup>55</sup> Also, Makino et al. controlled the time interval between the initial burst and the subsequent release by mixing different types of PLGA microspheres.<sup>56</sup> A burst release is an undesired effect for a drug delivery system expected to deliver the drug at a constant rate. However, in some cases, the delivery of a high initial amount of drug can be beneficial.<sup>47</sup>

In addition to block copolymer micelles, many groups have investigated the release of E2 from microspheres. Mogi et al. obtained a sustained release ranging in duration of 30 or 100 days for E2 from PLGA microspheres.<sup>13</sup> The rate of release is constant only after the first 5 days; during the initial period, they obtained higher release rates due to the presence of the E2 at the surface of the microspheres. Birnbaum et al. demonstrated that the release of E2 from PLGA microspheres (size range: 30-90  $\mu\text{m}$ ) was initially high (significant burst release of ~65% over 24 hours), but eventually a slow and sustained release (40-50 days) is achieved.<sup>14</sup> They also showed that the solvated E2 released from microparticles provided a more constant release than solid E2 released from microparticles.<sup>14</sup> Dickinson et al. showed a constant release of E2 for up to 30 days from PLGA microspheres.<sup>15</sup> Buntner et al., found that microspheres made from copolymers of polylactide and polycaprolactone released E2 over a period of 40 to 70 days.<sup>16</sup> Ye et al., investigated the release of E2 from disc and cylinder-type (matrix/matrix) laminate systems created from block copolymers of caprolactone and d,l-lactide.<sup>17</sup> Depending on the combination used, they were able to achieve a constant release of E2.

#### 4.4.4. Biological Effectiveness of PCL<sub>23</sub>-*b*-PEO<sub>45</sub> Micelles Containing E2

To test the effectiveness of PCL<sub>23</sub>-*b*-PEO<sub>45</sub> micelles containing E2, we have injected micelles into female C57BL mice (n=5). The uterine weights were determined after one week and the results (Table 4.3) clearly show that there is a significant increase in uterine weight following the treatment both with E2 alone or micelles containing the E2. These results indicate that E2 has not lost its biological activity during the preparation of the micelles.

**Table 4.3.** Determination of uterine weight in mice after 1 week treatment.

Treatment	Uterine weight (mg)
Control	13.7 ± 1.0
Estradiol alone	43.8 ± 2.7
Micelles containing E2	52.2 ± 8.6

#### 4.5. Conclusions

The incorporation and release of 17 $\beta$ -estradiol from polycaprolactone-*block*-poly(ethylene oxide) micelles were investigated as a potential hormone nano-delivery system. PCL-*b*-PEO micelles are suitable carriers for the delivery of E2. A high percentage of E2 (loading efficiency up to 96% (w/w)) and a high drug content (up to 4000 molecules of E2 per micelle (equivalent to 190% (w/w)) can be incorporated. The compatibility between E2 molecules and the polycaprolactone is well documented. Using transmission electron microscopy and dynamic light scattering, the micelles were determined to be spherical and to range in size from 20-40 nm. A “perfect sink” apparatus was used to investigate the release of E2 from the micelles. Application of the Higuchi

model showed that the release followed a diffusional mechanism and diffusion coefficients of the order of  $10^{-17}$  cm<sup>2</sup>/s were obtained. The loading and release of E2 can be controlled by the initial concentration of E2 and by the length of the PCL block. The biological activity of E2 was retained after the preparation of the micelles. This biocompatible, tailorable, self-assembled nano-delivery vehicle is not only suitable for 17 $\beta$ -estradiol, but could also provide a versatile, non-invasive system for other sex hormones individually or in combination.

The PCL-*b*-PEO copolymer micelles were loaded with hydrophobic probes (Chapter 3) and a hydrophobic drug (Chapter 4). The question needs to be answered where are the micelles localized in a cell after internalization upon delivery of the micelles loaded with probe or drug? This is the focus of the following chapter. Previous work done in our group by Allen et al. has shown that PCL<sub>21</sub>-*b*-PEO<sub>44</sub> are internalized into PC12 cells by an endocytic mechanism.<sup>57</sup> Time, temperature and pH dependence experiments were used to confirm the mechanism of transport of the micelles. More recent work done in our group has shown that fluorescently labeled PCL<sub>23</sub>-*b*-PEO<sub>45</sub> micelles are internalized into subcellular compartments such as lysosomes and other subcellular compartments in different cell lines.<sup>30</sup> The time, temperature and pH dependence studies along with the fluorescence experiments provide a very good beginning in terms of determining the fate of the micelles *in vitro*. However, there is a lack of visual evidence of the localization of the micelles inside the subcellular compartments. Detection via confocal microscopy of fluorescently labeled micelles has a resolution of ca. 500 nm and it is difficult to see individual cellular compartments at this resolution. In the following chapter, we describe the preparation and characterization of

gold labeled poly(4-vinylpyridine)-*block*-poly(ethylene oxide) micelles to be used for internalization studies. The gold labeled micelles are incubated for periods up to 24 hours into two different cell types, HEK 293 cells and A549 lung cells. Transmission electron microscopy is used to visualize these gold labeled micelles; this technique has the advantage of a greater than 10 fold improvement in resolution over confocal microscopy. The gold labeled micelles are clearly seen inside of the subcellular compartments such as endosomes and lysosomes.

#### 4.6. Acknowledgment

The work was supported by the Natural Sciences and Engineering Research Council of Canada and the Partnership for Tomorrow Program. The authors thank Professor Christine Allen for many useful discussions, Dr. Laibin Luo and Dr. Yisong Yu for synthesizing the PCL-*b*-PEO copolymers used in this study, Ms. Yue Wang for her work done on a related undergraduate project and Dr. Hanadi Sleiman for generous use of the fluorescence instrument.

#### 4.7. References

- (1) Kousteni, S.; Chen, J. R.; Bellido, T.; Han, L.; Ali, A. A.; O'Brien, C. A.; Plotkin, L.; Fu, Q.; Mancino, A. T.; Wen, Y.; Vertino, A. M.; Powers, C. C.; Stewart, S. A.; Ebert, R.; Parfitt, A. M.; Weinstein, R. S.; Jilka, R. L.; Manolagas, S. C. *Science* **2002**, 298, 843-846.
- (2) Constantine, G. D.; Pickar, J. H. *Current Opinion in Pharmacology* **2003**, 3, 626-634.
- (3) Khosla, S.; Melton, L. J., 3rd; Riggs, B. L. *Lupus* **1999**, 8, 393-396.
- (4) Rossouw, J. E.; Anderson, G. L.; Prentice, R. L.; LaCroix, A. Z.; Kooperberg, C.; Stefanick, M. L.; Jackson, R. D.; Beresford, S. A. A.; Howard, B. V.;

- Johnson, K. C.; Kotchen, J. M.; Ockene, J. *Journal of the American Medical Association* **2002**, *288*, 321-333.
- (5) Anderson, G. L.; Limacher, M.; Assaf, A. R.; Bassford, T.; Beresford, S. A. A.; Black, H.; Bonds, D.; Brunner, R.; Brzyski, R.; Caan, B.; Chlebowski, R.; Curb, D.; Gass, M.; Hays, J.; Heiss, G.; Hendrix, S.; Howard, B. V.; Hsia, J.; Hubbell, A.; Jackson, R.; Johnson, K. C.; Judd, H.; Kotchen, J. M.; Kuller, L.; LaCroix, A. Z.; Lane, D.; Langer, R. D.; Lasser, N.; Lewis, C. E.; Manson, J.; Margolis, K.; Ockene, J.; O'Sullivan, M. J.; Phillips, L.; Prentice, R. L.; Ritenbaugh, C.; Robbins, J.; Rossouw, J. E.; Sarto, G.; Stefanick, M. L.; Van Horn, L.; Wactawski-Wende, J.; Wallace, R.; Wassertheil-Smoller, S. *Journal of the American Medical Association* **2004**, *291*, 1701-1712.
- (6) Buntner, B.; Nowak, M.; Bero, M.; Dobrzynski, P.; Kasperczyk, J. *Journal of Bioactive and Compatible Polymers* **1996**, *11*, 110-121.
- (7) Good, W. R.; Powers, M. S.; Campbell, P.; Schenkel, L. *Journal of Controlled Release* **1985**, *2*, 89-97.
- (8) Boyd, R. A.; Yang, B.-B.; Abel, R. B.; Eldon, M. A.; Sedman, A. J.; Fogue, S. T. *Journal of Clinical Pharmacology* **1996**, *36*, 998-1005.
- (9) Ramachandran, C.; Fleisher, D. *Advanced Drug Delivery Reviews* **2000**, *42*, 197-223.
- (10) El Maghraby, G. M.; Williams, A. C.; Barry, B. W. *International Journal of Pharmaceutics* **2000**, *196*, 63-74.
- (11) Van Hal, D.; Van Rensen, A.; De Vringer, T.; Junginger, H.; Bouwstra, J. *S.T.P. Pharma Sciences* **1996**, *6*, 72-78.
- (12) Fang, J. Y.; Yu, S. Y.; Wu, P. C.; Huang, Y. B.; Tsai, Y. H. *International Journal of Pharmaceutics* **2001**, *215*, 91-99.
- (13) Mogi, T.; Ohtake, N.; Yoshida, M.; Chimura, R.; Kamaga, Y.; Ando, S.; Tsukamoto, T.; Nakajima, T.; Uenodan, H.; Otsuka, M.; Matsuda, Y.; Ohshima, H.; Makino, K. *Colloids and Surfaces B: Biointerfaces* **2000**, *17*, 153-165.
- (14) Birnbaum, D. T.; Kosmala, J. D.; Henthorn, D. B.; Brannon-Peppas, L. *Journal of Controlled Release* **2000**, *65*, 375-387.
- (15) Dickinson, P. A.; Kellaway, I. W.; Taylor, G.; Mohr, D.; Nagels, K.; Wolff, H.-M. *International Journal of Pharmaceutics* **1997**, *148*, 55-61.
- (16) Buntner, B.; Nowak, M.; Kasperczyk, J.; Ryba, M.; Grieb, P.; Walski, M.; Dobrzynski, P.; Bero, M. *Journal of Controlled Release* **1998**, *56*, 159-167.

- (17) Ye, W.-P.; Chien, Y. W. *Journal of Controlled Release* **1996**, *41*, 259-269.
- (18) Gref, R.; Minamitake, Y.; Peracchia, M. T.; Trubetskoy, V.; Torchilin, V.; Langer, R. *Science* **1994**, *263*, 1600-1603.
- (19) Kwon, G.; Naito, M.; Yokoyama, M.; Okano, T.; Sakurai, Y.; Kataoka, K. *Journal of Controlled Release* **1997**, *48*, 195-201.
- (20) Rapoport, N. *Colloids and Surfaces, B: Biointerfaces* **1999**, *16*, 93-111.
- (21) Zhang, Q.; Remsen, E. E.; Wooley, K. L. *Journal of American Chemical Society* **2000**, *122*, 3642-3651.
- (22) Kataoka, K.; Harada, A.; Nagasaki, Y. *Advanced Drug Delivery Reviews* **2001**, *47*, 113-131.
- (23) Benahmed, A.; Ranger, M.; Leroux, J.-C. *Pharmaceutical Research* **2001**, *18*, 323-328.
- (24) Liggins, R. T.; Burt, H. M. *Advanced Drug Delivery Reviews* **2002**, *54*, 191-202.
- (25) Liu, J.; Xiao, Y.; Allen, C. *Journal of Pharmaceutical Sciences* **2004**, *93*, 132-143.
- (26) Bromberg, L.; Magner, E. *Langmuir* **1999**, *15*, 6792-6798.
- (27) Barreiro-Iglesias, R.; Alvarez-Lorenzo, C.; Concheiro, A. *Journal of Controlled Release* **2003**, *93*, 319-330.
- (28) Allen, C.; Maysinger, D.; Eisenberg, A. *Colloids and Surfaces B: Biointerfaces* **1999**, *16*, 3-27.
- (29) Allen, C.; Maysinger, D.; Eisenberg, A. In *Canadian Patent Application*; (McGill University, Canada). Canada, 2000; p 31.
- (30) Savic, R.; Luo, L.; Eisenberg, A.; Maysinger, D. *Science* **2003**, *300*, 615-618.
- (31) Lee, J. H.; Lee, H. B.; Andrade, J. D. *Progress in Polymer Science* **1995**, *20*, 1043-1079.
- (32) Lim Soo, P.; Luo, L.; Maysinger, D.; Eisenberg, A. *Langmuir* **2002**, *18*, 9996-10004.
- (33) Allen, C.; Eisenberg, A.; Masic, J.; Maysinger, D. *Drug Delivery* **2000**, *7*, 139-145.
- (34) Allen, C.; Yu, Y.; Maysinger, D.; Eisenberg, A. *Bioconjugate Chemistry* **1998**, *9*, 564-572.

- (35) Allen, C.; Han, J.; Yu, Y.; Maysinger, D.; Eisenberg, A. *Journal of Controlled Release* **2000**, *63*, 275-286.
- (36) Yu, Y.; Eisenberg, A. *Polymeric Materials: Science & Engineering* **1998**, *79*, 288-289.
- (37) Riley, T.; Govender, T.; Stolnik, S.; Xiong, C. D.; Garnett, M. C.; Illum, L.; Davis, S. S. *Colloids and Surfaces B: Biointerfaces* **1999**, *16*, 147-159.
- (38) Hagan, S. A.; Coombes, A. G. A.; Garnett, M. C.; Dunn, S. E.; Davies, M. C.; Illum, L.; Davis, S. S.; Harding, S. E.; Purkiss, S.; Gellert, P. R. *Langmuir* **1996**, *12*, 2153-2161.
- (39) Govender, T.; Riley, T.; Ehtezazi, T.; Garnett, M. C.; Stolnik, S.; Illum, L.; Davis, S. S. *International Journal of Pharmaceutics* **2000**, *199*, 95-110.
- (40) Scholes, P. D.; Coombes, A. G. A.; Davies, M. C.; Illum, L.; Davis, S. S. *Controlled Drug Delivery* **1997**, 73-106.
- (41) Kost, J. In *Polymeric Materials Encyclopedia*, 1st ed.; Salamone, J. C., Ed.; CRC Press: New York, 1996; Vol. 2 (C).
- (42) Gadelle, F.; Koros, W. J.; Schechter, R. S. *Macromolecules* **1995**, *28*, 4883-4892.
- (43) Kozlov, M. Y.; Melik-Nubarov, N. S.; Batrakova, E. V.; Kabanov, A. V. *Macromolecules* **2000**, *33*, 3305-3313.
- (44) Clarke, R.; Van den Berg, H. W.; Murphy, R. F. *Journal of the National Cancer Institute* **1990**, *82*, 1702-1705.
- (45) Lundberg, B. *Acta Pharmaceutica Suecica* **1979**, *16*, 151-159.
- (46) Ye, W.-P.; Chien, Y. W. *Pharmaceutical Development and Technology* **1996**, *1*, 1-9.
- (47) Parikh, B. V.; Upadrashta, S. M.; Neau, S. H.; Nuessle, N. O. *Journal of Microencapsulation* **1993**, *10*, 141-153.
- (48) Ameller, T.; Marsaud, V.; Legrand, P.; Gref, R.; Renoir, J.-M. *European Journal of Pharmaceutical Sciences* **2004**, *21*, 361-370.
- (49) Higuchi, W. I. *Journal of Pharmaceutical Sciences* **1962**, *51*, 802-804.
- (50) Nah, J.-W.; Jeong, Y., II; Cho, C.-S. *Bulletin of the Korean Chemical Society* **1998**, *19*, 962-967.
- (51) Jeong, Y. I.; Nah, J. W.; Lee, H. C.; Kim, S. H.; Cho, C. S. *International Journal of Pharmaceutics* **1999**, *188*, 49-58.

- (52) Nah, J.-W.; Jeong, Y.-I.; Cho, C.-S.; Kim, S.-I. *Journal of Applied Polymer Science* **2000**, *75*, 1115-1126.
- (53) Gorshkova, M. Y.; Stotskaya, L. L. *Polymers for Advanced Technologies* **1998**, *9*, 362-367.
- (54) Teng, Y.; Morrison, M. E.; Munk, P.; Webber, S. E.; Prochazka, K. *Macromolecules* **1998**, *31*, 3578-3587.
- (55) Brannon-Peppas, L. *Journal of Biomaterials Science - Polymer Edition* **1994**, *5*, 339-351.
- (56) Makino, K.; Mogi, T.; Ohtake, N.; Yoshida, M.; Ando, S.; Nakajima, T.; Ohshima, H. *Colloids and Surfaces B: Biointerfaces* **2000**, *19*, 173-179.
- (57) Allen, C.; Yu, Y.; Eisenberg, A.; Maysinger, D. *Biochimica Biophysica Acta* **1999**, *1421*, 32-38.

---

---

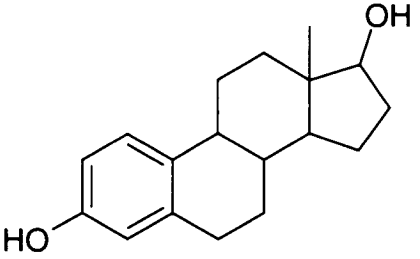
## Appendix

---

---

### 1. Hydrophobic fluorescent drug

**Table A3.** Physical Properties of 17 $\beta$ -Estradiol

Structure	
Molecular formula	C <sub>18</sub> H <sub>24</sub> O <sub>2</sub>
Molecular weight (g/mol)	272.4
Melting point (°C)	173-179
Solubility in water (mol/L) <sup>1</sup>	6.2 x 10 <sup>-6</sup>
Octanol water partition coefficient (ln P) <sup>1</sup>	9.3
<u>Fluorescence properties</u>	
Excitation:	281 nm
Emission (Main peak):	305 nm

### 2. Determining the polymer concentration of the micelle stock injected into the C57BL female mice.

#### A. Preparation of micelles containing E2 (27.1 mM)

##### Given

Grams of PCL<sub>23</sub>-*b*-PEO<sub>45</sub> copolymer in micelle solution: 0.056 g

Volume of micelle solution: 923  $\mu$ L = 0.923 mL

Molecular weight of PCL<sub>23</sub>-*b*-PEO<sub>45</sub> copolymer: 4602 g/mol

$$\begin{aligned}\text{Moles of polymer in micelle solution} &= \text{grams of polymer} / \text{MW of polymer} \\ &= 0.0056 \text{ g} / 4602 \text{ g/mol} \\ &= 1.22 \times 10^{-6} \text{ moles}\end{aligned}$$

Conc. of polymer in micelle solution = moles /volume

$$\begin{aligned}
 &= 1.22 \times 10^{-6} \text{ moles} / 9.23 \times 10^{-4} \text{ liters} \\
 &= 1.32 \times 10^{-3} \text{ M} \\
 &= 1.3 \text{ mM}
 \end{aligned}$$

Injected into the C57BL female mice: 20  $\mu\text{L}$  of  $1.32 \times 10^{-3} \text{ M}$  polymer solution is mixed with 80  $\mu\text{L}$  of saline solution. Hence the total solution is 100  $\mu\text{L}$ .

$$\begin{aligned}
 \text{Concentration of polymer injected into the mice} &= 1.32 \times 10^{-3} \text{ M} \times (20 \mu\text{L} / 100 \mu\text{L}) \\
 &= 2.64 \times 10^{-4} \text{ M}
 \end{aligned}$$

**B. Compare with the critical micelle concentration**

CMC of PCL<sub>21</sub>-*b*-PEO<sub>44</sub> micelles:  $2.8 \times 10^{-7} \text{ M}$

$$\begin{aligned}
 \text{Number of times above CMC} &= 2.64 \times 10^{-4} \text{ M} / 2.8 \times 10^{-7} \text{ M} \\
 &= 943 \approx 950
 \end{aligned}$$

Hence, the polymer concentration of the micelle stock injected into the mice is approximately 950 times above the critical micelle concentration.

**3. Determination of the diffusion coefficients for E2 released from PCL<sub>23</sub>-*b*-PEO<sub>45</sub> micelles.**

Given

Molecular weight of PCL<sub>23</sub>-*b*-PEO<sub>45</sub> copolymer: 4602 g/mol

Molecular weight of PCL: 114 g/mol

Molecular weight of PEO: 44 g/mol

Density of PCL: 1.143 g/mL

Weight of polymer in each chamber:  $5 \times 10^{-6} \text{ g}$

Assume radius of PCL<sub>23</sub>-*b*-PEO<sub>45</sub> micelles is 12.5 nm =  $1.25 \times 10^{-6} \text{ cm}$

$$\begin{aligned}
 \text{Since the micelle is spherical, the surface area of 1 micelle} &= 4 \pi r^2 \\
 &= 4 \pi (1.25 \times 10^{-6})^2 \\
 &= 1.96 \times 10^{-11} \text{ cm}^2
 \end{aligned}$$

Wt. of PCL in each chamber = Wt. of polymer in each chamber  $\times$  % of PCL in micelle

$$\begin{aligned}
 &= 5 \times 10^{-6} \text{ g} \times \frac{(23 \times 114)}{(23 \times 114) + (45 \times 44)} \\
 &= 2.85 \times 10^{-6} \text{ g}
 \end{aligned}$$

$$\begin{aligned} \text{Wt. of micelle assuming core is all PCL} &= 4/3 \pi r^3 \times D \\ &= 4/3 \pi (1.25 \times 10^{-6})^3 \times 1.143 \\ &= 9.35 \times 10^{-18} \text{ g/micelle} \end{aligned}$$

$$\begin{aligned} \text{Number of micelles in the chamber} &= \text{Wt. of PCL in each chamber/Wt. of micelle (PCL)} \\ &= 2.85 \times 10^{-6} \text{ g} / 9.35 \times 10^{-18} \text{ g/micelle} \\ &= 3.08 \times 10^{11} \text{ micelles} \end{aligned}$$

$$\begin{aligned} \text{Total area of micelles} &= \text{Surface area of 1 micelle} \times \text{Number of micelles in chamber} \\ &= 1.96 \times 10^{-11} \text{ cm}^2 \times 3.08 \times 10^{11} \text{ micelles} \\ &= 6.05 \text{ cm}^2 \end{aligned}$$

From equation 4.3 in Chapter 4:  $Q = 2C_o \left( \frac{Dt}{\pi} \right)^{1/2}$ , we plot Q vs.  $t^{1/2}$ . From the slope, we can determine D, the diffusion coefficient in units of  $\text{cm}^2/\text{s}$ .

Given

$$C_o: 2.6 \times 10^{-2} \text{ moles/cm}^3$$

$$\text{Slope: } 9.6 \times 10^{-11}$$

$$\text{Slope} = 2C_o \left( \frac{D}{\pi} \right)^{1/2}$$

$$D = \frac{(\text{Slope})^2 \times \pi}{4C_o^2}$$

$$D = \frac{(9.6 \times 10^{-11})^2 \times \pi}{4(2.6 \times 10^{-2})^2}$$

$$D = 1.1 \times 10^{-17} \text{ cm}^2/\text{s}$$

### References

- (1) Lundberg, B. *Acta Pharmaceutica Suecica* **1979**, *16*, 151-159.

## Chapter 5

---

---

### Internalization of Gold Labeled Poly (4-vinylpyridine)-*block*-poly(ethylene oxide) Copolymers into Cell Lines

---

---

#### 5.1. Abstract

Block copolymer micelles are being explored extensively as drug delivery vehicles. However, little is known about the interactions between the micelles and subcellular structures. To investigate these interactions, we used gold labeled micelles and studied their internalization into subcellular compartments of two different cell lines (human embryonic kidney (HEK 293) cells and human lung carcinoma (A549) cells). Poly(4-vinylpyridine)-*block*-poly(ethylene oxide) (P4VP<sub>21</sub>-*b*-PEO<sub>45</sub>) micelles labeled with gold were prepared. These gold labeled micelles were characterized by UV-Vis, dynamic light scattering, transmission electron microscopy and energy dispersive x-ray spectrometry. The size of the gold particle within the micelle core was 4-8 nm. Time and concentration dependent internalization of the micelles was revealed by transmission electron microscopy. The cells survived greater than 24 hours in the presence of the micelles and up to a micellar concentration of 0.73  $\mu\text{g/mL}$ . In the present paper, we show that the micelles could clearly be seen inside endosomes and lysosomes of both HEK 293 and A549 cell lines. There is also greater than a ten fold improvement in the resolution over fluorescently labeled micelles. Thus, gold labeled micelles can serve as a valuable and useful tool for exploring the interactions between micelles and subcellular compartments of cells for drug delivery applications.

## 5.2. Introduction

Amphiphilic block copolymers are versatile materials being explored for applications in medical, cosmetic, environmental and industrial fields.<sup>1,2</sup> The recent developments of different synthetic techniques, and the availability of numerous types of core and corona blocks with varying properties, have provided a wide range of block copolymers. In typical micellar applications, the core is composed of a hydrophobic block and the corona is formed from a hydrophilic block. Under appropriate conditions, these amphiphilic copolymers can produce different aggregates of a wide range of shapes and sizes (especially spheres, rods and vesicles).<sup>3-12</sup> These aggregates can serve as versatile delivery vehicles for both hydrophobic and hydrophilic agents.<sup>13-24</sup>

Specifically, biocompatible block copolymers have shown great promise for use as drug delivery vehicles. Detection of the block copolymer micelles is crucial in order to be able to determine their subcellular fate and the mechanism of entry into the cell. Typically, fluorescent molecules either incorporated into or attached to the micelles have been used.<sup>25-30</sup> A few examples of studies of the internalization of micelles are given below. Kabanov et al. speculated that Pluronic [poly(ethylene oxide)-*block*-poly(propylene oxide)-*block*-poly(ethylene oxide) (PEO-*b*-PPO-*b*-PEO)] micelles containing fluorescein were internalized into human T-cells and Madin-Darby canine kidney cells likely by endocytosis.<sup>25</sup> Allen et al. suggested that the cellular internalization into rat adrenal pheochromocytoma (PC12) cells of polycaprolactone-*block*-poly(ethylene oxide) micelles (PCL<sub>20</sub>-*b*-PEO<sub>44</sub>) appears to proceed by endocytosis.<sup>31</sup> Kabanov's group also suggested that Pluronic micelles enter both bovine brain microvessel endothelial cells and human colonic adenocarcinoma cells by a receptor-mediated endocytosis mechanism.<sup>26</sup> Kataoka's group studied internalization of micelles prepared from poly(ethylene oxide)-

*block*-poly ( $\beta$ -benzyl-L-aspartate) conjugated with fluorescein isothiocyanate into aortic endothelial cells, which appeared to occur by energy-dependent endocytosis.<sup>27</sup> Recently, Burt's group showed that methoxypoly(ethylene glycol)-*block*-poly (caprolactone) micelles containing rhodamine 123 may be taken up by an endocytotic mechanism in Caco-2 cells.<sup>30</sup> Savic et al. has shown using confocal microscopy that PCL<sub>23</sub>-*b*-PEO<sub>45</sub> micelles labeled with rhodamine were localized in different organelles of PC12 and fibroblasts of disaggregated Swiss mouse embryos cells.<sup>32</sup>

Despite a number of studies reported above, there is no conclusive evidence concerning the subcellular fate of the micelles. In order to prove that micelles are internalized into cells, labeled micelles are required. Fluorescence and confocal microscopy have been used with different fluorescent dyes to observe the co-localization in different organelles, but the micelles cannot be visualized in the individual cellular compartments. Also, as advantageous as fluorescent molecules are in terms of simplicity in use and accessibility, they still suffer from photobleaching, which can lead to both cell damage and background fluorescence from the cells.<sup>33</sup> Heavy metal labeled materials, because of their high electron density and stability, can be used for the visualization of the micelles by transmission electron microscopy (TEM), which would pinpoint their location *in vitro* and *in vivo* with much better resolution than is achievable by optical microscopy. To date, there are no reports of any clear visual evidence of the micelles in subcellular compartments using TEM.

Many groups have investigated the use of heavy metals associated with polymers.<sup>34-39</sup> Block copolymers are particularly useful in this context, for a number of reasons. For example, the block copolymers are effective as colloidal stabilizers, which

allow for the control of the particle size and the size distribution of the metal particles; they can provide an environment which prevents corrosion or leakage of heavy metals, and they can also protect catalytic nanoparticles from deactivation.<sup>4,40,41</sup> A few examples of the use of block copolymers for metal ion incorporation are given below. Antonietti et al. used polystyrene-*block*-poly-4-vinylpyridine (PS-*b*-P4VP) micelles and  $\text{HAuCl}_4$ , followed by hydrazine reduction to stabilize gold nanoparticles of ca. 10 nm in diameter.<sup>4</sup> Spatz et al. used polystyrene-*block*-poly(ethylene oxide) micelles to incorporate  $\text{LiAuCl}_4$  in toluene and reduced the salt with an electron beam to produce gold particles of less than 1.5 nm in diameter.<sup>42</sup> Larger particles with diameters of 2.5, 4, and 6 nm were also obtainable. Moffitt et al. investigated cadmium sulfide nanoparticles incorporated into block copolymer micelles as well as large compound micellar aggregates of polystyrene-*block*-poly (acrylic acid).<sup>43,44</sup> Corbierre et al. incorporated PS-Au nanoparticles covered with covalently bound thiol-capped polystyrene into a PS matrix to form a uniform dispersion of metal nanoparticles.<sup>45</sup> Triblock copolymers were used to form shell crosslinked micelles for the preparation of 1-5 nm gold particles by Liu et al.<sup>46</sup> Also, Jungmann et al. used a liquid-liquid phase transfer procedure followed by subsequent reduction to form 2-5 nm gold, silver and platinum particles incorporated in amphiphilic poly(organosiloxane) nanospheres.<sup>47</sup>

For block copolymers, the selection of the core-forming block is important because a strong interaction between the polymer core and the metal precursor facilitates its incorporation. Thus, gold labeled micelles have been prepared using diblocks of either poly (2-vinylpyridine) (P2VP)<sup>48</sup> or poly (4-vinylpyridine) (P4VP), and poly(ethylene oxide) (PEO) in water.<sup>49</sup> Gold particles formed from  $\text{P2VP}_{135}$ -*b*- $\text{PEO}_{350}$  micelles ranged in size from 1-4 nm, while the gold particles formed from  $\text{P4VP}_{28}$ -*b*- $\text{PEO}_{45}$  ranged in size

from 5-10 nm. The advantage of forming gold labeled micelles with PEO coronas is that it allows for the preparation of the micelles in water, an environmentally friendly option. Also, the ability of the PEO block to reduce absorption of proteins and thus reduce clearance of the micelles by the reticuloendothelial system (RES) in the body is important.<sup>50</sup> We have chosen to use P4VP as the core-forming block, because it coordinates a wide range of metal ions in the micelle core more strongly than P2VP.<sup>4</sup> The interaction between P4VP is less sterically hindered compared to P2VP, thus P4VP would result in a larger degree of gold incorporation and in more stable gold colloids.<sup>51</sup>

In this study, we prepared P4VP<sub>21</sub>-*b*-PEO<sub>45</sub> micelles that contain a gold particle ranging in size from 4-8 nm within each individual micelle. This system was used to explore the internalization of the micelles into and their visualization in two different cell types (human embryonic kidney (HEK 293) cells and human lung carcinoma (A549) cells) at different time periods (5 minutes to 24 hours) and different concentrations (0.15 to 0.73  $\mu\text{g/mL}$ ). In the present paper, we see the presence of gold labeled micelles predominantly in the subcellular compartments, i.e., endosomes and lysosomes, using TEM at a 10 fold improvement in the resolution and demonstrate the usefulness of the micelles as a valuable tool in the studies of subcellular localization.

### 5.3. Experimental Section

#### 5.3.1. Synthesis of P4VP<sub>21</sub>-*b*-PEO<sub>45</sub> Copolymer

The P4VP<sub>21</sub>-*b*-PEO<sub>45</sub> copolymer was synthesized using atom transfer radical polymerization of the 4-vinylpyridine monomer<sup>52</sup> and poly(ethylene oxide) with a 2-chloropropionyl terminated group as a macroinitiator. A full description of the synthesis can be found in our recent publication (see Appendix at the end of the thesis).<sup>49</sup>

### 5.3.2. Preparation of Gold Labeled P4VP<sub>21</sub>-*b*-PEO<sub>45</sub> Micelles

P4VP<sub>21</sub>-*b*-PEO<sub>45</sub> copolymer was dissolved in water to form a solution with a concentration of 4 g/L. Gold (III) chloride (AuCl<sub>3</sub> 99.99+%, Aldrich) was added to the micelle solution in order to obtain a molar ratio of 4-vinylpyridine to gold of 4:1. When AuCl<sub>3</sub> is dissolved in aqueous solution, immediate hydrolysis leads to the formation of an acid H<sub>2</sub>AuCl<sub>4</sub>.<sup>53</sup> The 4VP units are protonated by the acid, thus electrostatic interaction between the AuCl<sub>3</sub>(OH)<sup>-</sup> ions and the protonated pyridine groups is a driving force for incorporation of AuCl<sub>3</sub>(OH)<sup>-</sup> ions into the P4VP core protected by the PEO corona. The resulting micellar solution was allowed to stir for two days. A 5 fold molar excess of hydrazine hydrate (N<sub>2</sub>H<sub>4</sub> × H<sub>2</sub>O, 98+%) was then added to the solution, which turned from yellow to a dark purple. The solution was allowed to stir again for one day. Upon reduction of the gold ions inside the P4VP<sub>21</sub>-*b*-PEO<sub>45</sub> micelles by hydrazine hydrate, a solution of micelles containing gold particles was obtained, which we will refer to as gold labeled micelles.

For the internalization experiments, the micelles were filtered using a 0.2 μm Nalgene filter and then lyophilized to remove the water. To avoid contamination, the micelles were reconstituted in cell culture serum-free media corresponding to the cell type of interest (i.e., Roswell Park Memorial Institute (RPMI) 1640 medium for human embryonic kidney cells (HEK 293) and Dulbecco's modification of Eagle's minimal essential medium (DMEM) for lung carcinoma cells (A549 cells)).

### 5.3.3. Characterization of the Gold Labeled Micelles

#### *5.3.3.1. UV-Vis*

The UV-Vis spectra of the gold labeled micelles were recorded on a Cary 50 Bio UV-Visible Spectrophotometer (Varian, USA), equipped with two silicon diode detectors and a xenon flash lamp.

#### *5.3.3.2. Dynamic Light Scattering (DLS)*

The sizes and size distributions of the gold labeled micelles were determined on a Brookhaven Instruments photon correlation spectrophotometer with a BI-9000AT digital correlator. The instrument was equipped with a compass 315M-150 laser (Coherent Technologies, USA) that was used at a wavelength of 532 nm. Dust free solution vials were used for the aqueous micelle solutions and measurements were performed at an angle of 90° at room temperature. The CONTIN algorithm was used to analyze the DLS data.

#### *5.3.3.3. Transmission Electron Microscopy (TEM)*

The gold labeled micelles were examined under a JEOL JEM-2000FX instrument operating at an accelerating voltage of 80 keV. Dilute solutions of the gold labeled micelles were deposited on 400 mesh copper grids (EMS Sciences, USA) that were precoated with a thin film of Formvar (poly(vinylformal)) and carbon. The samples were allowed to sit on the grids for a few seconds and then a kimwipe was applied to remove the excess solution. The grids were then left overnight to air dry. The samples were stained with uranyl acetate (for PEO corona) for 2 minutes. Digital images were taken with a Gatan 792 Bioscan 1k x 1k Wide Angle Multiscan CCD camera (JEM-2000 FX).

### 5.3.4. Treatment of Cells with Gold Labeled Micelles

#### *5.3.4.1. Cell Types*

The A549 cells have characteristic lamellar bodies (i.e. loose and dense). The cell line was first established from solid tumors (human pulmonary adenocarcinoma).<sup>54</sup> The cells serve as a model for type II alveolar epithelial cells of the lung.<sup>55</sup> Smith et al. reported the doubling time of A549 cells to be 48.3 hrs in DMEM.<sup>56</sup> In the case of the HEK 293 cells, they are also epitheloid in nature.<sup>57</sup> They were first reported to be established by exposing human embryonic kidney cells to sheared fragments of adenovirus type 5 DNA.<sup>58</sup> Specific information on the cell culture of the HEK 293 and A549 cells and the cell culture treatment for the purposes of TEM can be found in the Appendix.

#### *5.3.4.2. MTT Assay*

A MTT (3-[4,5-dimethylthiazol-2yl]-2,5-diphenyltetrazolium bromide) assay was used to assess the metabolic status of the HEK 293 cells and the A549 cells in the presence of the gold labeled micelles.<sup>59,60</sup> More detailed information about the MTT assay can be found in the Appendix.

#### *5.3.4.3. Transmission Electron Microscopy*

For the study of the internalization of the gold labeled P4VP<sub>21</sub>-*b*-PEO<sub>45</sub> micelles into the cells, thin sections (0.1  $\mu\text{m}$ ) were prepared from a monolayer of cells using an Ultracut-E ultramicrotome (Reichert-Jung, Leica Microsystems, Austria). The thin sections were then placed on to 200 mesh copper grids (EMS Sciences, USA) and allowed to dry for 24 hours. The grids were then doubly stained with uranyl acetate

(negative stain for background) and Reynolds lead citrate stain (provides contrast for cellular membranes). The grids were allowed to dry for 24 hours after staining.

#### 5.3.4.4. Energy Dispersive Spectrometry (EDS)

The elements contained on the copper TEM grid were analyzed by energy dispersive spectrometry. The electron beam of the TEM was positioned specifically inside of the cell structures to confirm the location of the gold containing micelles.

### 5.4. Results and Discussion

#### 5.4.1. Gold Labeled Micelles

The poly(4-vinylpyridine)-*block*-poly(ethylene oxide) copolymer (P4VP<sub>21</sub>-*b*-PEO<sub>45</sub>) was dissolved in water and yielded micelles by direct dissolution. The UV-visible spectra of the yellowish colored solution of the copolymer micelles in water show a minimal contribution in the absorbance, in the region of 300-800 nm, as seen in Figure 5.1.

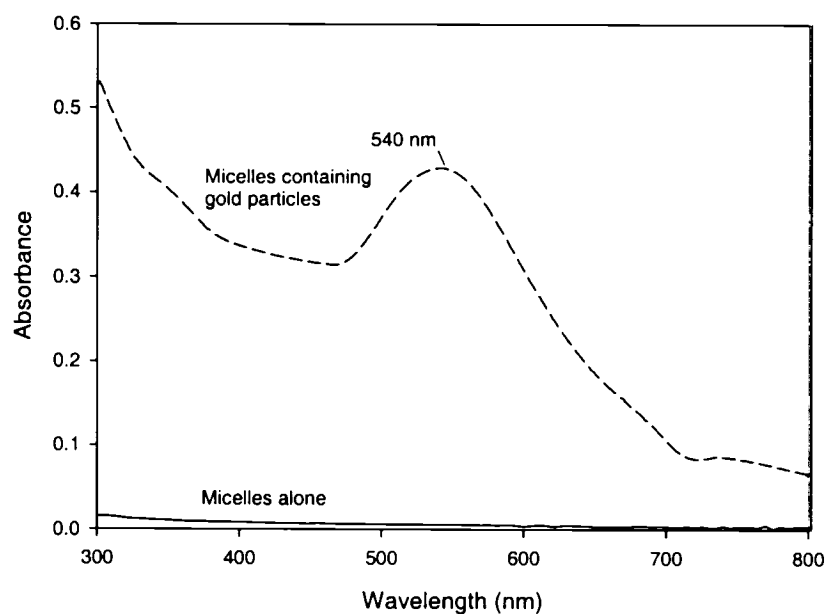


**Figure 5.1.** UV-Vis spectra of the P4VP<sub>21</sub>-*b*-PEO<sub>45</sub> copolymer micelles (—) and gold labeled P4VP<sub>21</sub>-*b*-PEO<sub>45</sub> micelles (---).

The copolymer micelles absorb at around 200 nm. However when gold particles are formed inside of each of the micelles, there is a peak at 540 nm as seen in Figure 5.1, which corresponds to the plasmon band of the purple colored micellar solution, suggesting formation of gold nanoparticles. The block copolymer serves as a stabilizer of the gold nanoparticles and controls their size. TEM was used to study the morphology directly and to identify the presence of the gold particles. The gold particle is seen as a very dark circle under the TEM as shown in Figure 5.2a. The sample was additionally stained with uranyl acetate, which normally stains the PEO corona, so the micelle coronas are seen at a higher magnification (Figure 5.2b) as lighter gray areas surrounding the darker gold nanoparticle. Also, a clear separation is seen between the individual gold

particles (as indicated by the arrows in Figure 5.2a), which could indicate the presence of a polymer in between the gold particles.

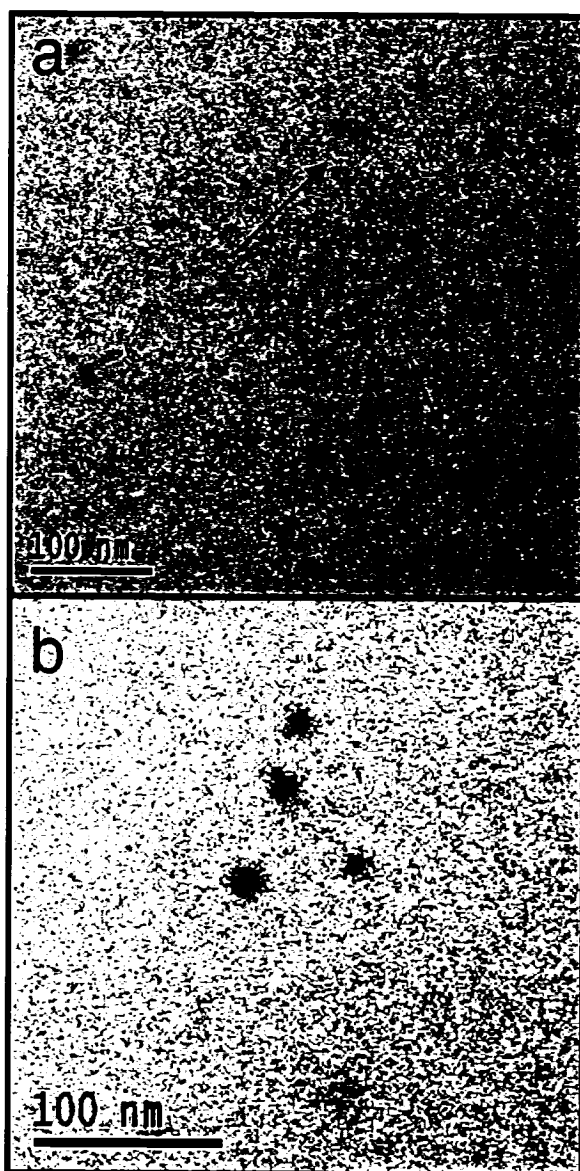


**Figure 5.2.** Transmission electron microscopy images of gold labeled micelles with an original magnification of (a) 170,000x and (b) 210,000x, both stained with uranyl acetate.

We have estimated that there are approximately  $3.2 \times 10^3$  gold atoms per micelle, the details of the calculation is shown in the Appendix. If we assume that the particles are spherical, we obtain a particle radius ca. 2.5 nm, thus the diameter of a gold particle would be approximately 5 nm. This is consistent with the TEM pictures seen in Figure 5.2. A histogram from the TEM data based on a sample size of 200 shows that the sizes of the gold particles also have a typical Gaussian distribution with a diameter of  $6 \pm 2$  nm (average  $\pm$  standard deviation) as seen in Figure 5.3.

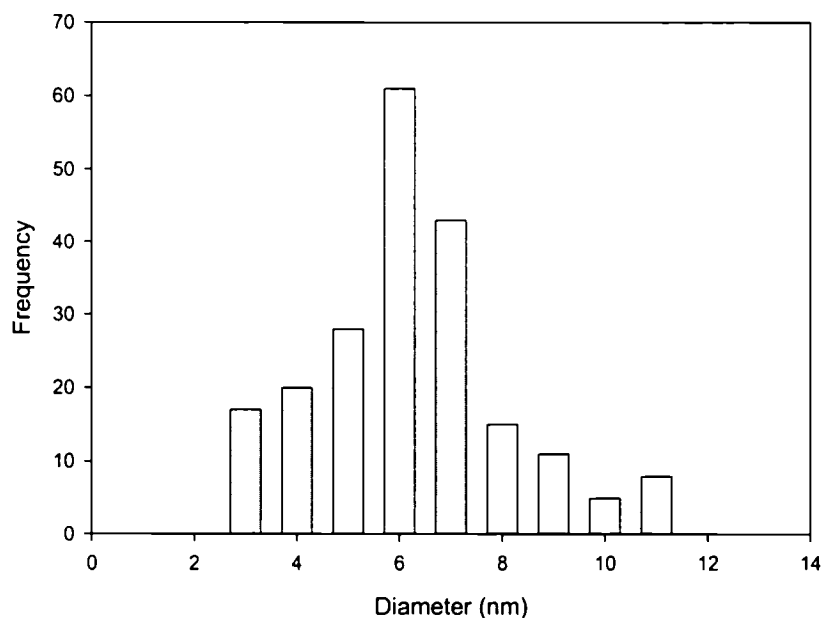


**Figure 5.3.** Histogram of the gold particle in each micelle from TEM .

Dynamic light scattering (DLS) was also used to examine the size and size population distribution of the P4VP<sub>21</sub>-*b*-PEO<sub>45</sub> gold labeled micelles as seen in Figure 5.4.

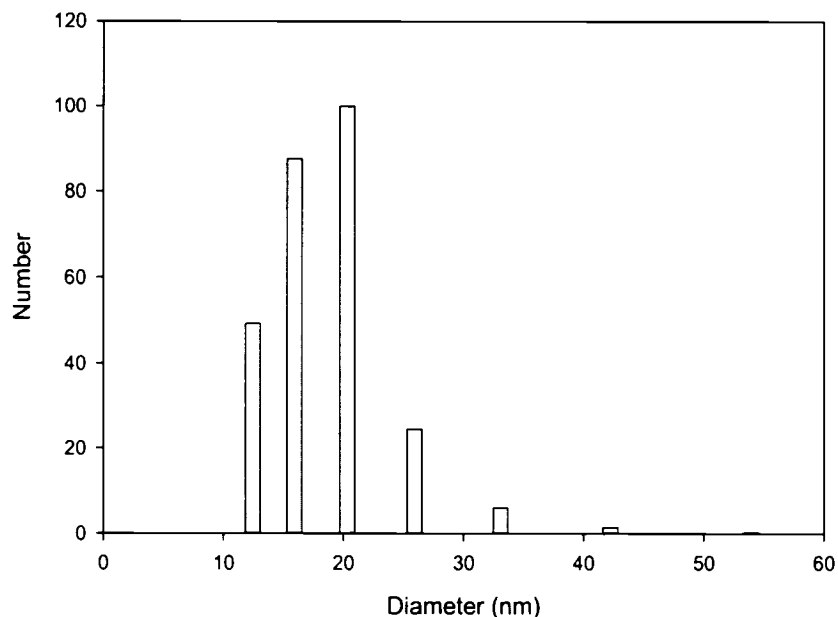


**Figure 5.4.** Dynamic light scattering data of gold labeled micelles analyzed using Contin analysis by number.

The average diameter of the whole micelle was found to be ca. 18 nm, calculated using Contin analysis by number. This is in agreement with the average diameter found by TEM to be  $22 \pm 4$  nm (see Figure A3 in the Appendix).

#### 5.4.2. MTT Assay

The toxicity of the P4VP copolymer was also a point of contention, especially for *in vitro* experiments. Because the P4VP units are well adsorbed on the gold nanoparticle surface,<sup>61</sup> we do not anticipate the rapid detachment of the block copolymer molecules into the cell. Also, we are not using the P4VP-*b*-PEO micelles as a drug delivery system, but rather as a tool to observe the localization into different cell types. Nevertheless, to explore the toxicity aspect further, additional information was needed concerning the

concentration and time dependence of the internalization of the gold labeled micelles into both cell types.

A MTT assay was used to assess the metabolic activity of both HEK 293 and A549 cells in the presence of the gold labeled micelles as a function of time and concentration. The cleavage of the yellow MTT salt by the mitochondrial enzyme succinate-dehydrogenase results in a purple formazan product.<sup>60</sup> The cells were incubated with the MTT solution for 24 hours. As shown in Figure 5.5, there is a greater than  $86 \pm 6\%$  cell survival compared with untreated controls for the HEK 293 cells when exposed to the micelles.

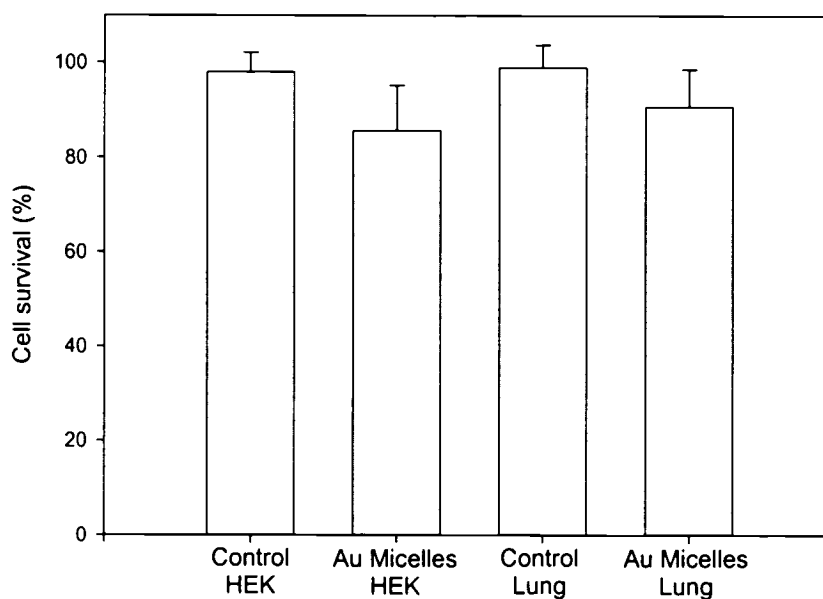


**Figure 5.5.** MTT assay: Incubation of gold labeled micelles of 0.73  $\mu\text{g/mL}$  in HEK 293 cells and lung A549 cells after 24 hours.

Similarly, the MTT results for the lung 549 cells show that more than  $91 \pm 5\%$  of the cells survive compared with untreated controls after exposure to the  $0.73 \mu\text{g/mL}$  of gold labeled micelles for 24 hours. Our studies revealed that cell survival is a function of the concentration of gold labeled micelles. Both cell types survive at low micelle concentrations ( $< 0.73 \mu\text{g/mL}$ ), but kidney cells were more sensitive to higher concentrations than the lung cells. In addition, the cell survival is also time dependent; the cells can survive in the cell medium for up to 24 hours. Therefore the length of time we have chosen for the study was up to 24 hours and for that time period, the micelles were suitable for internalization experiments.

#### 5.4.3. Internalization of Gold Labeled Micelles into A549 Cells

The internalization of the gold labeled micelles ( $0.73 \mu\text{g/mL}$ ) at 24 hours into the A549 cells near the cellular membrane (CM) as well as their localization into the various subcellular organelles, endosomes (E) or lysosomes (L) is shown in Figure 5.6. The subcellular organelles are clearly visible, for example the golgi apparatus (G) and the mitochondria (M) are seen in Figure 5.6b. The amount of gold labeled micelles within the organelles varies, as seen in Figure 5.6. The variation may be due to the varying individual affinities of the micelles for the different lipid compositions of the many subcellular compartments.

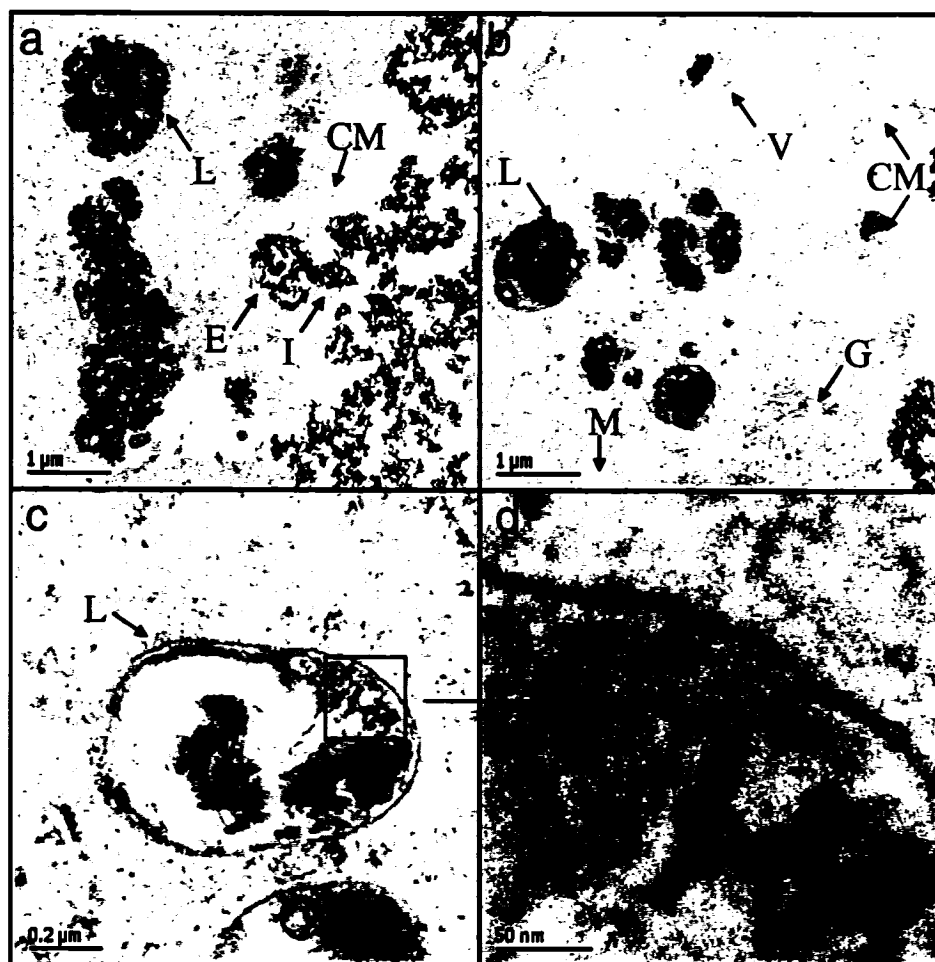


**Figure 5.6.** Composite TEM images of gold labeled micelles (0.73  $\mu\text{g}/\text{mL}$ ) internalized into different organelles of the lung A549 cells for 24 hours: (a) original magnification 21,000x, (b) original magnification 21,000x, (c) original magnification 100,000x, and (d) original magnification 500,000x. Symbols are represented as follows: cellular membrane (CM), endosome (E), golgi apparatus (G), entry point (I), lysosome (L), mitochondria (M) and invagination (V).

The sizes of the gold particles inside the lysosome, as seen in the close-up TEM image in Figure 5.6d, are measured to be ca.  $7.5 \pm 1.2$  nm, which compares with our results obtained for the individual gold particle incorporated into each micelle as seen previously in Figure 5.2. Some possible insight into the process of entry into the cell can

be obtained from Figure 5.6a, which shows an entry point (I) of the gold labeled micelles into the cell. It also appears that the micelles invaginate (V) the cell membrane as aggregates as seen in Figure 5.6b.

The internalization data presented so far have dealt previously with A549 cells. It is useful to compare our findings on cellular internalization with those reported in the literature for the same cell type. Stearns et al. showed that aggregated 50 nm TiO<sub>2</sub> particles were phagocytosed into A549 cells and localized in vacuoles.<sup>62</sup> The localization of the TiO<sub>2</sub> particles near the cellular membrane and also the closing off of the membrane filled with particles was similar to what is observed in this present study for the gold labeled micelles, as shown in Figure 5.6a. Stearns et al. also found TiO<sub>2</sub> particles enmeshed in both loosely and tightly packed lamellar bodies; however, in this respect, our findings differ. Most probably, the affinity of the gold labeled micelles for the lamellar bodies was not as favorable. Similarly, 100 nm diesel exhaust particles were seen to be internalized in phagosomes of the A549 cells.<sup>63</sup> In addition, metal oxide particles (TiO<sub>2</sub> and Fe<sub>2</sub>O<sub>3</sub>) and air particulates (< 100 nm) were seen to be incorporated into epithelial cells.<sup>64</sup> The different compositions and varying affinities of the particles for subcellular structures result in differences in their internalization. Hence, it is likely that micelles composed of different block copolymers could potentially deliver incorporated drugs to different subcellular sites.

#### 5.4.4. Internalization of Gold Labeled Micelles into HEK 293 cells

In the case of the HEK 293 cells, Figure 5.7a shows a TEM image of the gold labeled micelles internalized in the cell after 24 hours. The subcellular organelles can be seen in the HEK 293 cells, for example the endoplasmic reticulum (ER).



**Figure 5.7.** TEM images of gold labelled micelles (0.32  $\mu\text{g}/\text{mL}$ ) internalized into different organelles of the HEK 293 cells after 24 hours incubation with original magnification (a) 50,000x and (b) 100,000x.

As seen in Figure 5.7b, the compartmentalization of the gold labeled micelles occurs in the endosome. It is possible that we captured the early stages of entry into the

endosome, eventually leading to entry into the lysosome. The HEK 293 cells also seemed to have internalized less micelles than the A549 cells, because they are more sensitive to the micelles. There are a few similarities with the internalization into both cell lines. The gold labeled micelles are found in lysosomes (labeled with L) as seen in Figure 5.7a or endosomes (labeled with E) as seen in Figure 5.7b. Also the micellar aggregates were found mostly close to the cellular membrane at early time points (5-10 minutes) whereas at later times (24 hours), there were mostly present in the endosomal compartments (results not shown).

Energy dispersive spectrometry was used to determine the chemical composition of the micellar aggregates within the endosomal compartments of both the A549 cells and the HEK 293 cells (previously seen in Figures 5.6 and 5.7 respectively). The insert of Figure 5.8 shows a TEM image of large interconnected aggregates internalized into endosomes of a HEK 293 cell, which was used for the analysis. An electron beam was focused on the indicated cell compartment. The energy dispersive spectrum is shown in Figure 5.8, and confirms the presence of the gold labeled micelles by the appearance of the gold bands (at 2.06 and 9.56 keV). The spectrum also shows the presence of lead (Reynolds lead citrate stain), uranium (uranyl acetate stain), osmium (osmium tetroxide stain) and copper (TEM grid).

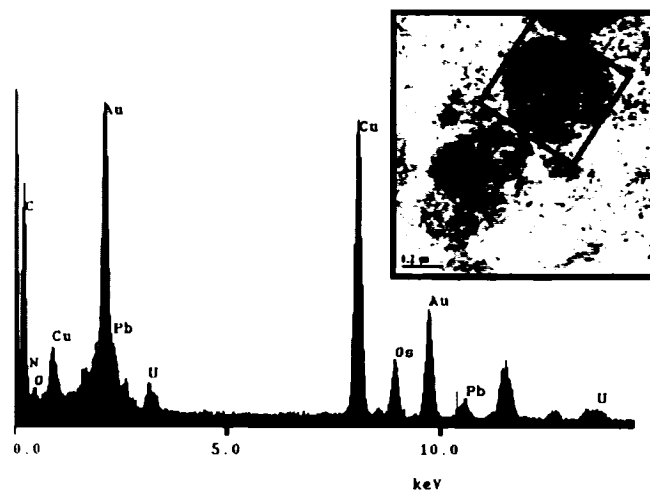


**Figure 5.8.** Energy dispersive spectrometry of gold labeled micelles (0.32  $\mu\text{g/mL}$ ) (inset) located inside of the HEK 293 cell after 24 hours incubation (original magnification 100,000x) showing an Au band.

#### 5.4.5. Aggregation of Gold Labeled Micelles

In all the TEM images, the gold labeled micelles were seen to be aggregated together within the cells in contrast to those TEM images of the gold labeled micelles in the absence of cells. We need to explore why this aggregation occurs. We showed that the interaction of the gold labeled micelles with cell medium containing fetal calf serum alone resulted in aggregation of the micelles as we observed in all of the TEM images involving cells as seen in Figures 3.6, 3.7 and 3.8. In terms of the internalization, even though the micelles were added to the growth medium as isolated colloidal particles, in the presence of the serum, aggregates formed. These aggregates tend to be located both inside and outside of the cells. In most cases, these aggregates are located near the sites of internalization. Our studies show that despite aggregation, these micelles can be internalized to a greater extent into lung cells. The serum components (specifically

albumin) may be important to the internalization process.<sup>34</sup> Gold particles coated with poly(ethylene oxide)-*block*-poly(propylene oxide) were endocytosed by liver endothelial cells in serum free medium, but not after preincubation with serum. The serum contains dysopsonins, which can help some particles minimize the interaction with phagocytes.<sup>34</sup> Also PEO and albumin actually form a weak complex, resulting in a camouflage effect in which the interface appears to look like native albumin.<sup>65</sup>

The role of the PEO corona also plays an important part in the cellular internalization of the P4VP-*b*-PEO micelles. Despite the fact that PEO has a large excluded volume and should prevent the P4VP<sub>21</sub>-*b*-PEO<sub>45</sub> micelles from aggregating, it is the density of the coverage of the PEO surface on the micelle that is important in preventing aggregation.<sup>15</sup> In our case, we do see aggregation in the cells or cell medium, which probably is a result of the insufficient coverage of the PEO corona on the surface of the hydrophobic poly(4-vinylpyridine) core. La et al. discussed the implications of hydrophobic-hydrophobic interactions or the van der Waals interactions between the exposed micellar cores as possibly contributing to the aggregation of the micelles.<sup>66</sup>

## 5.5. Conclusions

Poly(4-vinylpyridine)-*block*-poly(ethylene oxide) micelles containing an individual gold particle per micelle, ranging in size from 4 to 8 nm were used to assess the subcellular fate of the micelles in two different cell lines, human embryonic cells (HEK 293) and human lung carcinoma cells (A549). We have shown that they predominantly localize into either endosomes or lysosomes. The gold labeled micelles were not toxic to the cells for periods up to 24 hours and at concentrations less than 0.73 µg/mL. The micelles were visualized in high quality TEM images and a better than ten

fold improvement in terms of the resolution was obtained in comparison with the confocal microscopy. The micelles represent a proof of concept that gold labeled micelles can be used to determine the micellar distribution within the subcellular compartments of the cells.

The next chapter returns to the topic of block copolymer vesicles, which was reviewed in Chapter 2. Block copolymer vesicles are spherical, bilayer structures with a hydrophobic wall and an aqueous center in the middle. In the following chapter, a description is given of the incorporation of an anticancer drug, doxorubicin hydrochloride (DXR), using an active pH loading method, into polystyrene-block-poly(acrylic acid) (PS-*b*-PAA) vesicles. This system does not represent a drug delivery system, because it is not biodegradable or biocompatible. However, it is a good model system for the incorporation and release of a hydrophilic drug. The polystyrene walls of the vesicles are stable and robust, but since they are below the glass transition temperature, a plasticizer, dioxane, is used to soften the walls during the active loading period. Dioxane is also used for the release studies of the PS-*b*-PAA vesicles under dioxane/water sink conditions. Diffusion coefficients are determined from the release of DXR from the vesicles at different dioxane/water contents.

## 5.6. Acknowledgement

We sincerely thank Dr. Yu. A. Kabachii for synthesizing the copolymer, for the preparation of samples in connection with another project.<sup>49</sup> This work was supported by the Natural Sciences and Engineering Research Council of Canada and in part by the NATO Science for Peace Programme (grant SfP-974173).

## 5.7. References

- (1) Hadjichristidis, N.; Pispas, S.; Floudas, G. A. *Block Copolymers Synthetic Strategies, Physical Properties, and Applications*; John Wiley & Sons, Inc.: Hoboken, NJ, USA, 2003.
- (2) Forster, S.; Plantenberg, T. *Angewandte Chemie, International Edition* **2002**, *41*, 688-714.
- (3) Zhang, L.; Eisenberg, A. *Science* **1995**, *268*, 1728-1731.
- (4) Antonietti, M.; Wenz, E.; Bronstein, L.; Seregina, M. *Advanced Materials* **1995**, *7*, 1000-1005.
- (5) Shen, H.; Zhang, L.; Eisenberg, A. *Journal of the American Chemical Society* **1999**, *121*, 2728-2740.
- (6) Zhang, Q.; Remsen, E. E.; Wooley, K. L. *Journal of the American Chemical Society* **2000**, *122*, 3642-3651.
- (7) Alexandridis, P.; Lindman, B., Editors. *Amphiphilic Block Copolymers: Self-Assembly and Applications*; Elsevier Science B.V.: Amsterdam, 2000.
- (8) Discher, D. E.; Eisenberg, A. *Science* **2002**, *297*, 967-973.
- (9) Jain, S.; Bates, F. S. *Science* **2003**, *300*, 460-464.
- (10) Wang, X.-S.; Arsenault, A.; Ozin, G. A.; Winnik, M. A.; Manners, I. *Journal of the American Chemical Society* **2003**, *125*, 12686-12687.
- (11) Liu, G.; Yan, X.; Li, Z.; Zhou, J.; Duncan, S. *Journal of the American Chemical Society* **2003**, *125*, 14039-14045.
- (12) Lim Soo, P.; Eisenberg, A. *Journal of Polymer Science: Part B: Polymer Physics* **2004**, *42*, 923-938.
- (13) Gref, R.; Minamitake, Y.; Peracchia, M. T.; Trubetskoy, V.; Torchilin, V.; Langer, R. *Science* **1994**, *263*, 1600-1603.
- (14) Kwon, G. S.; Naito, M.; Kataoka, K.; Yokoyama, M.; Sakurai, Y.; Okano, T. *Colloids and Surfaces B: Biointerfaces* **1994**, *2*, 429-434.
- (15) Allen, C.; Maysinger, D.; Eisenberg, A. *Colloids and Surfaces B: Biointerfaces* **1999**, *16*, 3-27.

- (16) Kataoka, K.; Matsumoto, T.; Yokoyama, M.; Okano, T.; Sakurai, Y.; Fukushima, S.; Okamoto, K.; Kwon, G. S. *Journal of Controlled Release* **2000**, *64*, 143-153.
- (17) Torchilin, V. P. *Journal of Controlled Release* **2001**, *73*, 137-172.
- (18) Lavasanifar, A.; Samuel, J.; Kwon, G. S. *Advanced Drug Delivery Reviews* **2002**, *54*, 169-190.
- (19) Rapoport, N.; Pitt, W. G.; Sun, H.; Nelson, J. L. *Journal of Controlled Release* **2003**, *91*, 85-95.
- (20) Jones, M.-C.; Ranger, M.; Leroux, J.-C. *Bioconjugate Chemistry* **2003**, *14*, 774-781.
- (21) Riley, T.; Heald, C. R.; Stolnik, S.; Garnett, M. C.; Illum, L.; Davis, S. S.; King, S. M.; Heenan, R. K.; Purkiss, S. C.; Barlow, R. J.; Gellert, P. R.; Washington, C. *Langmuir* **2003**, *19*, 8428-8435.
- (22) Francis, M. F.; Piredda, M.; Winnik, F. M. *Journal of Controlled Release* **2003**, *93*, 59-68.
- (23) Tang, Y.; Liu, S. Y.; Armes, S. P.; Billingham, N. C. *Biomacromolecules* **2003**, *4*, 1636-1645.
- (24) Liu, J.; Xiao, Y.; Allen, C. *Journal of Pharmaceutical Sciences* **2004**, *93*, 132-143.
- (25) Kabanov, A. V.; Slepnev, V. I.; Kuznetsova, L. E.; Batrakova, E. V.; Alakhov, V. Y.; Melik-Nubarov, N. S.; Sveshnikov, P. G.; Kabanov, V. A. *Biochemistry International* **1992**, *26*, 1035-1042.
- (26) Batrakova, E. V.; Han, H.-Y.; Miller, D. W.; Kabanov, A. V. *Pharmaceutical Research* **1998**, *15*, 1525-1532.
- (27) Liaw, J.; Aoyagi, T.; Kataoka, K.; Sakurai, Y.; Okano, T. *Pharmaceutical Research* **1999**, *16*, 213-220.
- (28) Rapoport, N.; Marin, A. P.; Timoshin, A. A. *Archives of Biochemistry and Biophysics* **2000**, *384*, 100-108.
- (29) Liu, J.; Zhang, Q.; Remsen, E. E.; Wooley, K. L. *Biomacromolecules* **2001**, *2*, 362-368.
- (30) Zastre, J.; Jackson, J.; Bajwa, M.; Liggins, R.; Iqbal, F.; Burt, H. *European Journal of Pharmaceutics and Biopharmaceutics* **2002**, *54*, 299-309.
- (31) Allen, C.; Yu, Y.; Eisenberg, A.; Maysinger, D. *Biochimica Biophysica Acta* **1999**, *1421*, 32-38.

- (32) Savic, R.; Luo, L.; Eisenberg, A.; Maysinger, D. *Science* **2003**, *300*, 615-618.
- (33) Stephens, D. J.; Allan, V. J. *Science* **2003**, *300*, 82-86.
- (34) Moghimi, S. M.; Muir, I. S.; Illum, L.; Davis, S. S.; Kolb-Bachofen, V. *Biochimica et Biophysica Acta* **1993**, *1179*, 157-165.
- (35) Marinakos, S. M.; Novak, J. P.; Brousseau, L. C., III; House, A. B.; Edeki, E. M.; Feldhaus, J. C.; Feldheim, D. L. *Journal of the American Chemical Society* **1999**, *121*, 8518-8522.
- (36) Otsuka, H.; Akiyama, Y.; Nagasaki, Y.; Kataoka, K. *Journal of the American Chemical Society* **2001**, *123*, 8226-8230.
- (37) Ohno, K.; Koh, K.-m.; Tsujii, Y.; Fukuda, T. *Macromolecules* **2002**, *35*, 8989-8993.
- (38) Sun, Y.; Xia, Y. *Science* **2002**, *298*, 2176-2179.
- (39) Kamata, K.; Lu, Y.; Xia, Y. *Journal of the American Chemical Society* **2003**, *125*, 2384-2385.
- (40) Mayer, A. B. R.; Mark, J. E. *Colloid and Polymer Science* **1997**, *275*, 333-340.
- (41) Forster, S.; Antonietti, M. *Advanced Materials* **1998**, *10*, 195-217.
- (42) Spatz, J. P.; Roescher, A.; Moeller, M. *Advanced Materials* **1996**, *8*, 337-340.
- (43) Moffitt, M.; Eisenberg, A. *Chemistry of Materials* **1995**, *7*, 1178-1184.
- (44) Moffitt, M.; Vali, H.; Eisenberg, A. *Chemistry of Materials* **1998**, *10*, 1021-1028.
- (45) Corbierre, M. K.; Cameron, N. S.; Sutton, M.; Mochrie, S. G. J.; Lurio, L. B.; Ruehm, A.; Lennox, R. B. *Journal of the American Chemical Society* **2001**, *123*, 10411-10412.
- (46) Liu, S.; Weaver, J. V. M.; Save, M.; Armes, S. P. *Langmuir* **2002**, *18*, 8350-8357.
- (47) Jungmann, N.; Schmidt, M.; Maskos, M. *Macromolecules* **2003**, *36*, 3974-3979.
- (48) Bronstein, L. M.; Sidorov, S. N.; Valetsky, P. M.; Hartmann, J.; Coelfen, H.; Antonietti, M. *Langmuir* **1999**, *15*, 6256-6262.
- (49) Sidorov, S. N.; Bronstein, L. M.; Kabachii, Y. A.; Valetsky, P. M.; Lim Soo, P.; Maysinger, D.; Eisenberg, A. *Langmuir* **2004**, *20*, 3543-3550.
- (50) Lee, J. H.; Lee, H. B.; Andrade, J. D. *Progress in Polymer Science* **1995**, *20*, 1043-1079.

- (51) Mayer, A. B. R.; Mark, J. E. *European Polymer Journal* **1998**, *34*, 103-108.
- (52) Xia, J.; Zhang, X.; Matyjaszewski, K. *Macromolecules* **1999**, *32*, 3531-3533.
- (53) Wilkinson, G. *Comprehensive coordination chemistry : the synthesis, reactions, properties, & applications of coordination compounds*; Pergamon Press: New York, 1987.
- (54) Giard, D. J.; Aaronson, S. A.; Todaro, G. J.; Arnstein, P.; Kersey, J. H.; Dosik, H.; Parks, W. P. *Journal of the National Cancer Institute* **1973**, *51*, 1417-1423.
- (55) Lieber, M.; Smith, B.; Szakal, A.; Nelson-Rees, W.; Todaro, G. *International Journal of Cancer* **1976**, *17*, 62-70.
- (56) Smith, B. T. *American Review of Respiratory Disease* **1977**, *115*, 285-293.
- (57) Simmons, N. L. *Experimental Physiology* **1990**, *75*, 309-319.
- (58) Graham, F. L.; Smiley, J.; Russell, W. C.; Nairn, R. *Journal of General Virology* **1977**, *36*, Pt. 1, 59-72.
- (59) Mosmann, T. *Journal of Immunological Methods* **1983**, *65*, 55-63.
- (60) Denizot, F.; Lang, R. *Journal of Immunological Methods* **1986**, *89*, 271-277.
- (61) Bronstein, L. M.; Chernyshov, D. M.; Volkov, I. O.; Ezernitskaya, M. G.; Valetsky, P. M.; Matveeva, V. G.; Sulman, E. M. *Journal of Catalysis* **2000**, *196*, 302-314.
- (62) Stearns, R. C.; Paulauskis, J. D.; Godleski, J. J. *American Journal of Respiratory Cell and Molecular Biology* **2001**, *24*, 108-115.
- (63) Juvin, P.; Fournier, T.; Boland, S.; Soler, P.; Marano, F.; Desmonts, J.-M.; Aubier, M. *Archives of Environmental Health* **2002**, *57*, 53-60.
- (64) Stringer, B.; Imrich, A.; Kobzik, L. *Experimental Lung Research* **1996**, *22*, 495-508.
- (65) Vert, M.; Domurado, D. *Journal of Biomaterials Science, Polymer Edition* **2000**, *11*, 1307-1317.
- (66) La, S. B.; Okano, T.; Kataoka, K. *Journal of Pharmaceutical Sciences* **1996**, *85*, 85-90.

---

---

## Appendix

---

---

### **1. Details of the cell culture.**

HEK 293 cells were maintained in an incubator at 37°C and in an environment of 95% air and 5% CO<sub>2</sub> in RPMI 1640 medium with 10% fetal calf serum added. Similarly, the A549 cells were maintained in the same environment using DMEM medium with 10% fetal calf serum added. Cells were grown in six well plates (Sarstedt, Canada) until a proper density (i.e., 80% confluency) was reached. The cells formed a monolayer at the bottom of the wells. An aliquot of the cell medium was removed from each cell well and replaced with the same volume of solution containing gold labeled micelles reconstituted in the appropriate biological medium. The cells were thus treated with different concentrations (0.2-0.73 µg/mL) of the gold labeled micelles; they were then placed in an incubator at 37°C for times up to 24 hours.

### **2. Cell culture treatment for transmission electron microscopy studies.**

The cell culture medium was removed from the wells by aspiration and replaced with 2.5% glutaraldehyde in 0.1 M sodium cacodylate buffer to fix the cells. The cells were kept in the fixative at 4°C for 24 hours. The fixative solution was then carefully removed and the cells were washed with 0.1 M cacodylate washing buffer. The washing was repeated three times, waiting 10 minutes in between each washing. For post-fixation, 1% osmium tetroxide (OsO<sub>4</sub>) in a 1.5% potassium ferrocyanide (K<sub>4</sub>Fe(CN)<sub>6</sub>) solution was added. The cells were then kept at 4°C for 30 minutes to allow the cells to be immersed

in the reduced OsO<sub>4</sub> solution. OsO<sub>4</sub> was then removed and the cells were again washed with 0.1 M cacodylate washing buffer. After 10 minutes, the cells were dehydrated with ethanol in increments of 10% from 30% up to 90% allowing five minute intervals in between each step. The cells were then further dehydrated twice with 100% ethanol allowing for 10 minute intervals between each change. The cells were then infiltrated by adding increasing amounts of epon to ethanol (in increasing increments from 1:1 to 3:1) to each of the cell wells allowing 30 minutes intervals between each subsequent addition. Finally pure epon that has been de-aerated under vacuum (at constant pressure, not exceeding 25 psi), was added to the cell wells. The cells were then allowed to sit for 1 hour under vacuum to remove the ethanol residue and the air bubbles in the epon. Then the wells were refilled with new epon and placed into an oven at 60°C for 48 hours to polymerize the epon.

### **3. Details of the MTT assay.**

Briefly, the cell medium was aspirated from the well plates and washed with phosphate buffered saline (PBS) followed by two additional washings. The washings were required to remove any non-incorporated gold labeled micelles. An aliquot of the cell medium was added to each of the well plates. The cells were incubated with 0.45 mg/mL of MTT in PBS (5 mg/mL) in a humidified atmosphere (e.g. 37°C, 95% air and 5% CO<sub>2</sub>) for three hours. The medium was then removed and dimethyl sulfoxide (DMSO) was added to each of the well plates to lyse the cells. The yellow tetrazolium salt was reduced in metabolically active cells to form insoluble purple formazan crystals, which are solubilized in DMSO. A Bio-Rad Benchmark microplate reader was used to measure the absorbance at 595 nm.

#### 4. Calculation of the number of gold atoms in a P4VP<sub>21</sub>-*b*-PEO<sub>45</sub> micelle

Given

Mean micelle diameter of micelle: 18.4 nm (as calculated from DLS)

Radius of a micelle: 9.2 nm

Approximate block copolymer density: 1 g/cm<sup>3</sup>

$$1 \text{ cm}^3 = 1 \times 10^{21} \text{ nm}^3$$

#### Volume of a micelle (assuming a spherical shape)

Volume of a sphere:

$$V = 4/3 \pi r^3$$

$$V = 4/3 \pi (9.2 \text{ nm})^3$$

$$V = 3.26 \times 10^3 \text{ nm}^3$$

#### Weight of 1 micelle

Density:

$$D = g/v$$

$$g = D \times v$$

$$g = 1 \text{ g/cm}^3 \times 3.26 \times 10^3 \text{ nm}^3 \times 1 \times 10^{21} \text{ nm}^3$$

$$g = 3.26 \times 10^{-18} \text{ grams}$$

#### Weight of the block copolymer solution

Given

Molecular weight of AuCl<sub>3</sub>: 303.33 g/mol

Weight of AuCl<sub>3</sub>:  $8.1 \times 10^{-3}$  g

Avogadro's number:  $6.023 \times 10^{23}$  atoms/ molecule

Concentration of copolymer solution: 4 g/L

Volume of solution: 4 mL

Weight of copolymer solution:

$$= \text{Concentration} \times \text{volume}$$

$$= 4 \text{ g/L} \times 4 \text{ mL} \times 1 \times 10^{-3} \text{ L/mL}$$

$$= 1.6 \times 10^{-2} \text{ g}$$

**Calculate the total number of micelles**

Number of micelles

$$= \text{Weight of block copolymer} / \text{Weight of micelle}$$

$$= 0.016 \text{ g} / 3.26 \times 10^{-18} \text{ g}$$

$$= 4.91 \times 10^{15} \text{ micelles}$$

Moles of  $\text{AuCl}_3$

$$= \text{Weight of AuCl}_3 / \text{MW of AuCl}_3$$

$$= 8.1 \times 10^{-3} \text{ g} / 303.33 \text{ g/mol}$$

$$= 2.67 \times 10^{-5} \text{ moles}$$

Number of gold atoms = moles of  $\text{AuCl}_3 \times \text{Avogadro's \#}$

$$= 2.67 \times 10^{-5} \times 6.023 \times 10^{23}$$

$$= 1.61 \times 10^{19} \text{ gold atoms}$$

If we assume that the number of gold atoms is evenly distributed in the micelles.

= Number of gold atoms / Number of micelles

$$= 1.61 \times 10^{19} \text{ atoms/micelle} / 4.91 \times 10^{15} \text{ micelles}$$

$$= 3.28 \times 10^3 \text{ gold atoms}$$

**5. Calculation of the size of the gold particle**

Assume that all of gold atoms combine to form the diameter of a gold particle.

Given

Density of gold:  $19.2 \text{ g/cm}^3$

Molecular weight of gold:  $196.97 \text{ g/mol}$

$$1 \text{ cm}^3 = 1 \times 10^{21} \text{ nm}^3$$

Volume of the gold particles:

$$V = 1/\text{Density} \times \text{MW} \times 1/N_A \times \# \text{ of gold atoms}$$

$$V = (1/19.2) \times 196.97 \times (1/6.023 \times 10^{23}) \times 3.3 \times 10^3 \times 1 \times 10^{21}$$

Units:  $\text{cm}^3/\text{g} \times \text{g}/\text{mol} \times \text{mol}/\text{atoms} \times \text{nm}^3$

$$V = 5.6 \times 10^1 \text{ nm}^3$$

Volume of a gold particle

$$V = \frac{4}{3} \pi r^3$$

$$5.6 \times 10^1 \text{ nm}^3 = \frac{4}{3} \pi r^3$$

$$1.3 \times 10^1 = r^3$$

$$2.4 \text{ nm} = r$$

Therefore the diameter of the gold particles is approximately 4.8 nm.

## 6. Gold labeled micelles

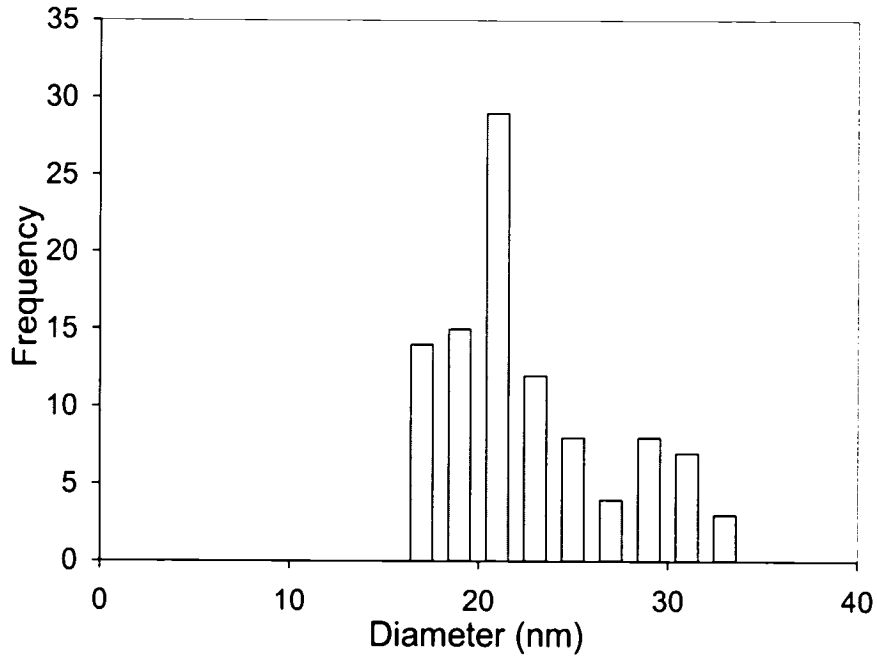


**Figure A3.** Histogram of gold labeled P4VP<sub>21</sub>-b-PEO<sub>45</sub> micelles from TEM.

## Chapter 6

---

---

### Active Loading and Tunable Release of Doxorubicin from Block Copolymer Vesicles

---

---

#### 6.1. Abstract

Polystyrene-*b*-poly(acrylic acid) copolymers (PS-*b*-PAA) can self-assemble in solution to form aggregates of different morphologies, including thermodynamically stable vesicles. Block copolymer vesicles can be used as nano-containers in areas such as cosmetics, pollution control and drug delivery. The wall of a polymeric vesicle is thicker and tougher than that of a liposome, but the permeability of the wall is tunable for loading and release. In this study, PS<sub>310</sub>-*b*-PAA<sub>36</sub> vesicles (wall thickness  $\cong$  30 nm) are loaded with an anticancer drug, doxorubicin hydrochloride (DXR), using an active loading method in the presence of dioxane, a plasticizer for the polystyrene wall. The vesicle walls are plasticized just prior to loading to increase the permeability. A pH gradient is established across the membrane of the vesicles (pH inside = 2.5 and pH outside = 6.3) to concentrate doxorubicin inside the internal aqueous cavity. Because of this gradient, the DXR is found to be incorporated mainly in the vesicle interior cavity as opposed to the external solution, with only traces interacting with the polystyrene wall and poly(acrylic acid) surfaces. By removing the plasticizer after loading, the vesicle walls are hardened again and the vesicle structure is stable indefinitely. The release of DXR is studied under dioxane/water sink conditions. The plasticizer is added to the system just prior to the release study, to make the polystyrene wall more permeable, and the permeability can be fine tuned by the quantity of the plasticizer. Diffusional coefficients of DXR release from the PS<sub>310</sub>-*b*-PAA<sub>36</sub> vesicles range from  $10^{-15}$  to  $10^{-13}$  cm<sup>2</sup>/sec, show the fine control exerted by the quantity of the plasticizer on the vesicle wall. The release profile of DXR from the vesicles is fitted to the Higuchi model and shown to be diffusional.

## 6.2. Introduction

Block copolymer vesicles have been of great interest to workers in both the academic and industrial fields. Their versatility has made them attractive for potential applications in areas such as pollution control, cosmetics and drug delivery. Vesicles can be prepared under different conditions from a variety of diblock<sup>1-13</sup> and triblock copolymers<sup>14-16</sup> which have become available due to the development of a range of synthetic techniques.<sup>17,18</sup> Block copolymer vesicles resemble biological membranes due to their spherical bilayer structure,<sup>19</sup> but are more stable and robust compared to lipid based analogs (i.e., liposomes). A most useful feature of vesicles is their ability to incorporate hydrophilic materials (such as proteins and peptides) into the aqueous center and, at the same time, hydrophobic materials into the vesicle wall. The wall plays an important role in imparting stability to the vesicles and controls the extent of release of incorporated molecules.

Doxorubicin (DXR) or adriamycin is a potent anticancer drug that has been used for the treatment of a variety of leukemias, lymphomas and solid tumours.<sup>20,21</sup> However, in addition to having general toxic effects, DXR is limited in its maximal single dose and also cumulative dosage because it can lead to irreversible cardiotoxicity. In an effort to improve the therapeutic index (ratio of maximum nontoxic dose over the minimum effective dose) of DXR and to reduce the accumulation of the drug in the heart, drug delivery carriers, such as micelles<sup>22-26</sup> and liposomes,<sup>21,27,28</sup> have been used to deliver DXR. Studies have shown that delivery of DXR incorporated into liposomes maintains or improves its therapeutic activity in tumours and decreases the cardiotoxicity.<sup>21,27</sup> Developing a suitable liposomal-DXR formulation requires studies involving the composition, size, charge, and drug to composition ratio in order to achieve high potency

and low toxicity.<sup>29</sup> In addition, the stability of the carrier and its drug retention (i.e. minimum leakage) are also important factors.

Obtaining high loading levels of DXR in liposomes is also an important consideration for developing a delivery system. Nichols and Deamer were the first to apply a pH gradient to load weak amines into liposomes.<sup>30</sup> In their study, they reported a 10-20 fold increase, when a pH gradient (pH inside = 5, pH outside = 8) was applied across an egg phosphatidylcholine (PC) membrane, compared to the absence of a pH gradient (pH inside = pH outside). This concept of “active loading” was also used by Mayer et al. to obtain high loading efficiencies and loading levels of 100 mM doxorubicin in egg PC and egg PC-cholesterol liposomes.<sup>31</sup> Additional work from this group resulted in the use of the transmembrane gradient to concentrate doxorubicin and other types of drugs (all of which were weak bases) to obtain high loading levels into egg PC liposomes.<sup>32</sup> High loading levels of DXR (200-300 mM) were also achieved by Perkins’ group by employing a transmembrane pH gradient for egg PC and cholesterol liposomes.<sup>33</sup> Despite achieving high loading levels, the permeability of the liposome membrane to protons can make the pH gradient difficult to maintain, and in some instances, the resulting leakage of the incorporated molecules was significant. For example, approximately 50% of quinidine is released from egg PC vesicles within 30 minutes due to the loss of the pH gradient.<sup>32</sup> Also 10-18% of DXR leakage was observed for some egg PC/cholesterol liposomes stabilized in lactobionic acid (used to buffer the vesicle interior) after only 10 minutes.<sup>33</sup> For block copolymers, DXR has been loaded passively, i.e., loading the drug while preparing the vesicles.<sup>34</sup> Recently, a transmembrane ammonium sulfate gradient was used to load DXR into polymer vesicles.<sup>35</sup>

In addition to achieving high loading efficiencies, controlling the rate of release of DXR is also important for developing a suitable delivery system. Tunable release allows for controllable delivery of the molecule of interest, which is important for achieving optimal drug concentrations at the designated area. Most controlled release devices tend to be governed by a diffusion type drug release.<sup>36</sup> Polymeric vesicles offer a more robust and thicker hydrophobic wall and are more inherently stable than liposomes. The tunable and permeable wall would be used to control the release of DXR from the vesicles. Discher's group has shown controlled release by blending degradable copolymers into polybutadiene-*block*-poly(ethylene glycol).<sup>35</sup>

The present chapter deals with polystyrene-*block*-poly(acrylic acid) vesicles (PS<sub>310</sub>-*b*-PAA<sub>36</sub>). An active loading method is applied by creating a pH gradient across the vesicle membrane (pH inside = 2.5, and pH outside = 6.3). In order to increase the permeability of the polystyrene (PS) wall, different contents of dioxane, a plasticizer for the PS wall, are added to each solution (both samples and controls) prior to loading. The dioxane partitions between the PS wall and the aqueous solution. For comparison, DXR is added to another series of vesicle solutions, in which no pH gradient is established. The extent of DXR incorporation, using both methods, is determined as a function of the permeability of the polystyrene wall of the vesicle, which is tuned via the dioxane content of the solution. Possible interactions of doxorubicin with the polystyrene wall of the vesicles and with the poly(acrylic acid) (PAA) surfaces are estimated using model systems. The release of DXR from the vesicles is investigated also in the presence of a plasticizer, specifically under different dioxane/water sink conditions. The dioxane content is shown to have a strong effect on the rate of release of DXR from the PS<sub>310</sub>-*b*-PAA<sub>36</sub> vesicles. The release is fitted to the Higuchi model and diffusion coefficients at

different dioxane/water ratios are calculated showing that the release from the system is finely tunable.

### 6.3. Experimental Section

#### 6.3.1. Materials

Polystyrene<sub>310</sub>-*b*-poly(acrylic acid)<sub>36</sub> copolymer (PS<sub>310</sub>-*b*-PAA<sub>36</sub>) (where the subscripts denote the number of units of each copolymer) was synthesized by anionic polymerization. A detailed description of the synthesis and characterization procedures has been published elsewhere.<sup>37,38</sup> The whole copolymer has a polydispersity of 1.03, as determined by size exclusion chromatography using polystyrene standards. HPLC grade dioxane was purchased from ACP Chemicals (St. Leonard QC, Canada) and doxorubicin hydrochloride (DXR) was purchased from Sigma-Aldrich (Oakville ON, Canada); both were used as received. DXR has a molecular weight of 580 g/mol and a pKa of 8.25. The structure of doxorubicin hydrochloride is shown in Table A4 in the Appendix. Dialysis chambers (Slide-A-Lyzer® Mini Dialysis Unit) used for the loading and release experiments were purchased from MJS BioLynx Inc. (Brockville ON, Canada) and had a molecular weight cutoff of 3500 g/mol.

#### 6.3.2. Preparation of PS<sub>310</sub>-*b*-PAA<sub>36</sub> Vesicles

Vesicle solutions were prepared by first dissolving the copolymer in dioxane, a good solvent for both blocks. The initial polymer concentration was 0.5 % (w/w). To induce self-assembly, water of a pH of 2.5 was added dropwise at a rate of 0.2 % (w/w) per minute. Water was added until a final concentration of 15 % (w/w) was reached. At this water content, block copolymer vesicles are present in solution. Polystyrene constitutes the wall of the vesicle, and poly(acrylic acid) chains cover the internal and

external surfaces. The vesicle solution was allowed to stir overnight, then quenched in a large amount of water, which extracts much of the dioxane from the PS wall and raises the glass transition temperature ( $T_g$ ) well above room temperature. This preserves the vesicle morphology before it is dialyzed against water (pH = 2.5) to remove the residual dioxane. The presence of vesicles was confirmed using transmission electron microscopy (TEM).

### 6.3.3. Active Loading of Doxorubicin Hydrochloride into Vesicles

The aqueous solution obtained after dialysis has a pH of ca. 2.5, and contains vesicles with an internal aqueous cavity of the same pH. This solution was divided into a series of vials, to each of which a given amount of dioxane and doxorubicin (as an aqueous solution) was added. The dioxane content ranged between 0 and 60 % (w/w), while the doxorubicin concentration was kept constant in all solutions at ca.  $5.6 \times 10^{-4}$  M. The solutions were allowed to stir for about 4 hours, and then the pH of each solution was measured and adjusted to a value of approximately 6.3 pH units (AR10 pH meter; Fisher Scientific, Ottawa ON, Canada), using small volumes of NaOH aqueous solution (Sigma Aldrich, Oakville ON, Canada). A pH difference between the interior of the vesicles (pH inside = 2.5) and the outside aqueous solution (pH outside = 6.3) was created. The vesicle solutions in which a pH gradient is created will be referred to as “samples”. For comparison, DXR was added to another set of solutions in which no pH gradient was established (i.e., no NaOH was added, and pH inside = pH outside = 2.5). These solutions will be referred to as “controls”.

After allowing the solutions to stir for three days, during which the loading of the drug took place, an aliquot of each solution (both samples and controls) was quenched in

excess water (ca. 7 fold dilution), and dialyzed against water for three days in order to remove unloaded drug molecules. Quenching in water prior to dialysis decreases the percentage of dioxane in the solution and, therefore, the dioxane content in the polystyrene wall of the vesicles. This, in turn, reduces greatly the permeability of the wall, and minimizes the diffusion and loss of the incorporated molecules during dialysis. It should be recalled that the dialysis process also removes residual dioxane from the wall. The concentration of doxorubicin present in each vesicle solution after dialysis was determined by dissolving the vesicles in an aliquot of dioxane to release the DXR. The fluorescence was measured using a SPEX FluoroMax 2 at an excitation wavelength of 488 nm.

#### 6.3.4. Determining the Ethylbenzene-Water Partition Coefficient

A partition coefficient of DXR was calculated using model systems in order to determine the relative affinity of the drug for either the aqueous interior or the PS wall. A known concentration of DXR was added to two solutions: the first is a mixture of 1.5 mL of ethylbenzene and 2.0 mL of pH = 2.5 water, and the second is a mixture of 1.5 mL of ethylbenzene and 2.0 mL of pH = 6.3 water. Each solution, which consists of two immiscible phases, was allowed to mix for two weeks. The aqueous phase was then separated from the ethylbenzene phase, and the concentration of DXR in each phase was determined using fluorescence spectroscopy. The ethylbenzene-water partition coefficient,  $K_{EB/H_2O}$  was then calculated as the ratio between the concentration of DXR in the ethylbenzene phase to the concentration of DXR in the water phase (i.e.,  $K_{EB/H_2O} = [DXR]_{EB}/[DXR]_{H_2O}$ ).

#### 6.3.5. Determining the Interaction of DXR with Poly(acrylic acid)

The interaction of DXR with PAA was investigated to see how much the drug interacts with the poly(acrylic acid) surfaces of the vesicles. Two aqueous solutions of homo poly(acrylic acid) (average molecular weight = 450,000 g/mol) containing the same concentration of DXR were prepared. The pH of the solutions was adjusted to approximately 2.5 and approximately 6.3 respectively, and the solutions were allowed to stir for three days. A 400  $\mu$ L aliquot of each solution was then placed in a dialysis chamber, and dialyzed against water for three days, which corresponds to the period of time over which DXR loaded vesicles were dialyzed, to remove free, unincorporated drug molecules. The concentration of doxorubicin present in each solution after dialysis was determined using fluorescence spectroscopy. The obtained fluorescence signal is assumed to be due to doxorubicin molecules interacting with poly(acrylic acid).

#### 6.3.6. Transmission Electron Microscopy

The vesicle solutions were examined using a JEOL JEM-2000FX electron microscope instrument operating at an accelerating voltage of 80 keV. A drop (approximately 10  $\mu$ L) of a dilute vesicle solution in water was deposited on 400 mesh copper grids (EMS Sciences, USA) that were precoated with a thin film of carbon. The grids were then left overnight to air dry. Digital images were taken with a Gatan 792 Bioscan 1k x 1k Wide Angle Multiscan CCD camera (JEM-2000 FX).

#### 6.3.7. Release of DXR from the Vesicles under Sink Conditions

The DXR loaded PS-*b*-PAA vesicle samples used for the release experiment were exhaustively dialyzed for three days to remove any traces of unincorporated DXR. The

DXR loaded vesicle samples used for the release experiment had a polymer concentration of 0.08 % (w/w) and the total initial DXR concentration was 240  $\mu\text{M}$ . A 200  $\mu\text{L}$  solution of DXR loaded vesicles was placed into a dialysis chamber (MWCO: 3500 g/mol). The composition of the solution was adjusted to give a ratio of 50% water/50% dioxane, 75% water/25% dioxane or 100% water. A number of dialysis chambers were prepared and placed into a dialysis float device. The device was then placed into a large reservoir, which contained twenty liters of solution. The solvent composition in the reservoir was also adjusted to match the same content inside of the dialysis chambers (i.e., 50% to 75% to 100% water). The release of DXR is assumed to be under sink conditions, since the volume of the solution in the reservoir is 50,000 times larger than the volume of the solution of the DXR loaded vesicles in the dialysis chamber. The beginning of the drug release was assumed to start as soon as the dialysis float device containing the dialysis chambers was placed into the reservoir. The large reservoir was kept under constant stirring, and at various time points, one of the dialysis chambers was removed. The concentration of DXR in the dialysis chamber was quantified using fluorescence spectroscopy.

## 6.4. Results and Discussion

### 6.4.1. Loading of DXR as a Function of Dioxane Content

The loading of doxorubicin hydrochloride (DXR) into polystyrene<sub>310</sub>-*b*-poly(acrylic acid)<sub>36</sub> vesicles was carried out for a series of samples and controls. In the samples, a transmembrane pH gradient was created for the vesicles (pH inside = 2.5 and pH outside = 6.3). In the control solutions, no pH gradient was established (pH inside = pH outside = 2.5). Incorporation into the vesicle cavity must involve diffusion through

the polystyrene wall, because in both cases (samples and controls), the drug was added to solutions of preformed vesicles. Therefore, the permeability of the wall is important in determining the extent of loading. In order to increase the permeability, different amounts of dioxane, the plasticizer, were added to both samples and controls. In dioxane/water mixtures, the polystyrene wall swells with dioxane, which is a better solvent for polystyrene than water. This can be understood by examining the solubility parameters of polystyrene, dioxane and water, which are  $\delta_{\text{PS}} = 8.1-9.9$ ,  $\delta_{\text{dioxane}} = 10.0$ , and  $\delta_{\text{water}} = 23.4 \text{ [cal/cm}^3\text{]}^{1/2}$ , respectively. The dioxane partitions between the PS wall and the water, hence the higher the dioxane content in solution, the higher is its content in the polystyrene wall.<sup>39</sup> Yu et al. showed that the solvent content of dioxane in the PS rich phase increases from approximately 0.4 (v/v) to approximately 0.65 (v/v) when the dioxane content is increased from 83 wt% to 91 wt%.<sup>39</sup>

The results of DXR uptake in the samples and controls as a function of dioxane content are shown in Figure 6.1.

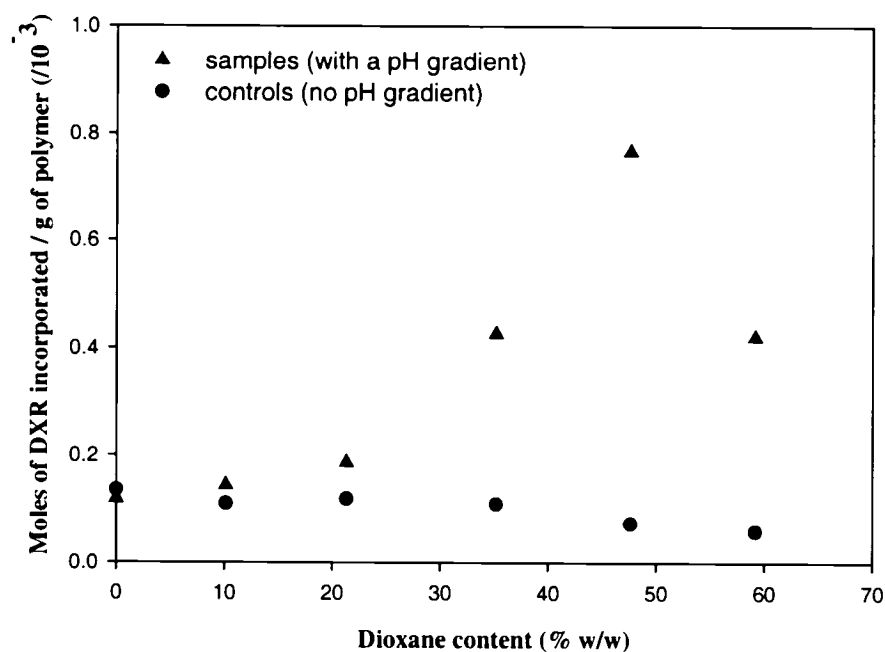


**Figure 6.1.** Extent of incorporation of doxorubicin hydrochloride in PS<sub>310</sub>-*b*-PAA<sub>36</sub> vesicles as a function of the dioxane content in solution.

In the presence of the dioxane, the loading level of DXR loaded into the samples is higher than that in the controls, reflecting the ability of the pH gradient to enhance loading. At 0% (w/w) dioxane content, however, there is not a great difference in the loading between the samples and the controls. This indicates that in the absence of a plasticizer, the period of three days that the solutions were allowed to stir are not sufficient for a significant amount of the drug molecules to diffuse, and therefore, for a concentration difference between the samples and the controls to develop. This is not surprising in view of the rigidity of the wall.

A transmembrane pH gradient (in which the inside of the vesicle is acidic) has been used by many groups to enhance the loading of doxorubicin in liposomes.<sup>29-33,40,41</sup> The proposed loading mechanism assumes that the concentration of the neutral (non-

protonated) form of the drug is equal on both sides of the liposome membrane. The distribution of the protonated molecules, on the other hand, is governed by the pH difference on the opposite sides of the membrane and can be expressed using the following equation:

$$\frac{[\text{XNH}_3^+]_{\text{In}}}{[\text{XNH}_3^+]_{\text{Out}}} = \frac{[\text{H}_3\text{O}^+]_{\text{In}}}{[\text{H}_3\text{O}^+]_{\text{Out}}} \quad (6.1)$$

where  $[\text{XNH}_3^+]$  is the concentration of the protonated form of the drug,  $[\text{H}_3\text{O}^+]$  is the proton concentration and the subscripts “in” and “out” are the inside and the outside of the vesicle membrane, respectively. The derivation for equation 6.1 and an explanation of the equilibria involved in the loading process are given in the Appendix.

The degree of loading of DXR is strongly dependent on the dioxane content for the samples in the present isochronal experiments. The dependence is principally a kinetic effect. As the dioxane content increases, the permeability of the polystyrene wall is increased and the diffusion of the drug molecules becomes faster. After a given period of time (i.e., before equilibrium is reached) and for a given external concentration of DXR, the amount loaded is proportional to the speed of the diffusion, and hence to the dioxane content. However, when the system is given sufficient time (i.e., when equilibrium is reached), the degree of DXR loading should be independent of the dioxane content. With higher dioxane content, one would expect the system to get closer to equilibrium during the period of the experiment. The loading of DXR into liposomes was also found to be time dependent although, in general, shorter times were required to reach equilibrium.<sup>30,31</sup> Mayer et al. showed that loading of DXR into egg PC and egg PC-cholesterol liposomes increases over time, but levels off after approximately 60

minutes.<sup>31</sup> The liposome wall is much thinner (3-5 nm) than that of polymeric vesicles (e.g., 30 nm in the present system) and is generally more fluid. This leads to a faster diffusion through the membrane and shorter loading times compared to polymeric vesicles.

As seen in Figure 1, the amount of DXR loaded into the samples increases with increasing amount of dioxane content (from 0% to 48% (w/w)) added. However, the extent of loading in the samples drops when the dioxane content increases from 48 to 58 % (w/w). It is likely that the high permeability of the polystyrene wall at such high dioxane contents permits a significant diffusion of protons. The resulting decrease in the pH gradient (i.e., in the difference in pH on the opposite sides of the membrane) would lead to a decrease in the extent of incorporation.

In the absence of a pH gradient (i.e. for the control solutions), one would expect the amount of DXR accumulated into the vesicles vs the external aqueous solution to be proportional to the volume ratio between the vesicle interior and the solution in which the vesicles are suspended. For the present system, the ratio between the total cavity volume of vesicles and the external solution does not exceed  $1.7 \times 10^{-3}$  (details of the calculation are given in the Appendix). It is therefore surprising that the amount of drug loaded into control vesicles ranges between 4 and 28%. This is somewhat puzzling and requires further investigation in order to understand what is occurring.

#### 6.4.2. Determining the Internal Concentration of Doxorubicin

The transmembrane pH gradient in the vesicles (inside acidic) was shown to enhance successfully the loading of DXR into the samples compared to the controls. The internal concentration of DXR in the vesicles can be estimated from the amount of DXR

incorporated and the total internal volume of the vesicles. Details of the calculation of the internal concentration of DXR in the vesicles are given in the Appendix. The internal concentrations were calculated to range between 0.12 and 0.80 M in the presence of a pH gradient (e.g., samples) as shown in Table 6.1.

**Table 6.1.** Concentrations of DXR in the vesicle samples and controls

<b>Dioxane content % (w/w)</b>	<b>Concentration of DXR in Samples (pH gradient) (M)</b>	<b>Concentration of DXR in Controls (no pH gradient) (M)</b>	<b>Enhancement</b>
0	0.12	0.14	0.9
10	0.15	0.11	1.3
22	0.19	0.12	1.6
35	0.44	0.11	3.9
48	0.80	0.08	10.4
58	0.44	0.06	7.1

For the controls, the internal concentrations ranged from 0.06 and 0.14 M. The enhancement due to the presence of the pH gradient ranges from 1 to 10 times. TEM was used to image the DXR loaded vesicles, which are shown in Figure 6.2.

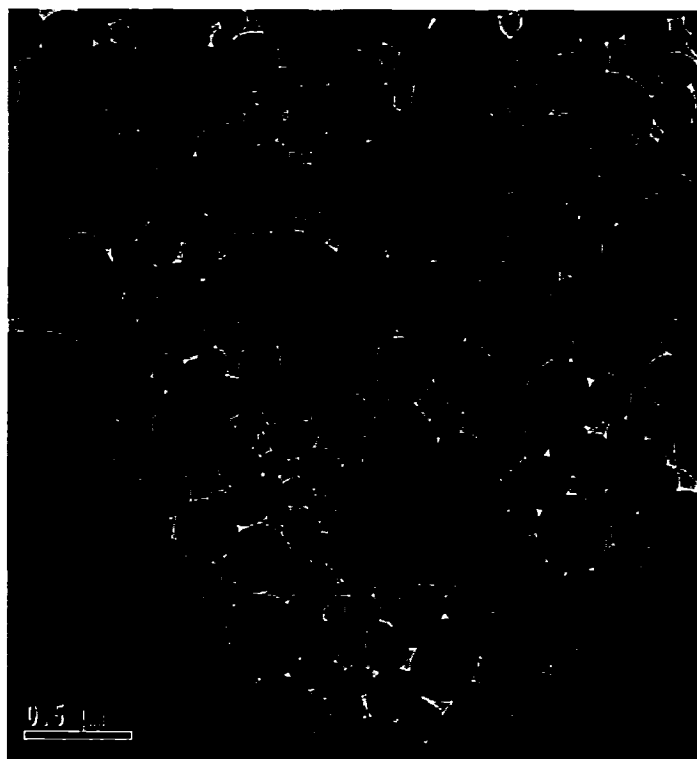


**Figure 6.2.** TEM image of PS<sub>310</sub>-*b*-PAA<sub>36</sub> vesicles loaded with DXR using a pH gradient at 22% dioxane/78% water content. Initial polymer concentration is 0.5 % (w/w). Internal concentration of the drug is approximately 0.19 M.

The average vesicle diameter as determined by TEM is approximately 210 nm and the average wall thickness is approximately 30 nm.

The use of a pH gradient for loading DXR into liposomes resulted in similar internal concentrations (e.g., up to 0.1 M<sup>31</sup>, 0.12 M<sup>41</sup>, 0.2-0.3 M<sup>33</sup>). The physical state of DXR inside the liposomes has been examined, and a possible explanation suggests that the high internal concentration of drug might be due to precipitation<sup>32,33,42</sup> or aggregation.<sup>41,43</sup> Li et al. showed that at internal concentrations between 0.2 and 0.3 M, DXR forms fiber bundles of stacked drug molecules.<sup>33</sup> Abraham et al. showed that DXR forms a precipitate when the drug to lipid ratio is greater than 0.05:1 (w/w).<sup>42</sup> In the

present study, no independent experiments were conducted to examine the physical state of DXR.

#### 6.4.3. Estimating the Interactions of DXR with PS and with PAA

The most likely location of the DXR is in the aqueous cavity of the vesicle, since DXR is water soluble and positively charged under acidic conditions ( $\text{pH}_{\text{inside}} = 2.5$ ). However, interactions of DXR with the polystyrene wall or with the poly(acrylic acid) surfaces are also possible and might contribute to the extent of loading. The extent of such interactions was estimated by using model systems. The solubility of doxorubicin in polystyrene was estimated using ethylbenzene as a model solvent. The partition coefficient of DXR between ethylbenzene and water at two different pH's (2.5 and 6.3) was determined to be  $K_{\text{EB}/\text{H}_2\text{O}} = 0.19$ . This value is independent of the pH. Leo et al. calculated the octanol-water partition coefficient of DXR to be 0.08.<sup>44</sup>

The interaction of DXR with the PS wall was calculated (refer to Appendix for details) and the number of moles possibly solubilized by PS ranges between  $7.0 \times 10^{-3}$  and  $2.1 \times 10^{-2}$  % of the total moles of DXR present in solution. The interaction of DXR with PAA chains covering the internal surface of the vesicle was estimated by determining the amount of DXR solubilized by a solution of homo poly(acrylic acid) in water at  $\text{pH} = 2.5$ . A similar determination was carried out at  $\text{pH} = 6.3$  in order to evaluate the possible interactions between DXR and the acrylic acid chains on the external surface of the vesicle. At  $\text{pH} = 2.5$  and  $\text{pH} = 6.3$ , the number of moles of DXR that are possibly solubilized by PAA range between  $1.8 \times 10^{-3}$  to  $5.4 \times 10^{-3}$  % (mol/mol) and  $2.0 \times 10^{-1}$  and  $4.0 \times 10^{-1}$  % (mol/mol) of the total moles of DXR present in solution,

respectively. Details of the calculation of the interaction of DXR with the PAA chains on the inside and outside are given in the Appendix. The calculations, based on model systems, of the interaction of DXR with the PS wall and the PAA chains may not reflect the exact content of DXR in these different parts of the vesicle, but still provide a useful estimate. Based on these estimates, we conclude that the contribution of the DXR loading from the interaction of the DXR with the PS wall and the PAA surfaces (inside and outside) are minor, and that the aqueous cavity of the vesicle is the main incorporation site.

#### 6.4.4. Release of DXR from the Vesicles

The release of DXR from PS-*b*-PAA vesicles was studied for vesicles present in dioxane/water mixtures of different ratios (dioxane content = 0%, 25% and 50% (w/w)). The results of the release study, summarized in Figure 6.3, show that as the amount of dioxane in the solvent mixture increases from 0%, to 25% and then to 50%, a greater percentage of DXR is released from the vesicles within the same time period.



and egg PC/cholesterol (1:1) liposomes after 16 and 30 hours, respectively.<sup>40</sup> Recently, Discher's group has shown that the addition of chloroform to vesicles formed from polybutadiene-*block*-poly(ethylene glycol) blended with poly(lactic acid)-*block*-poly(ethylene glycol) completely disintegrates the vesicle and releases all of the encapsulant (i.e., sucrose or tritc-dextran) in very rapid time periods from 15 minutes to 2 hours.<sup>46</sup>

The release profile of DXR from the PS-*b*-PAA vesicles does not show a burst release, (i.e., a large amount of drug released initially over a very short time period). Typically this occurs when DXR is surface absorbed<sup>45</sup> or loosely bound<sup>47</sup> to the delivery vehicle. For the present system, the absence of burst release is most probably due to the fact that the PS-*b*-PAA vesicles were exhaustively dialyzed to remove any non-incorporated DXR. The absence of a burst release is very desirable for drug delivery as it prevents a large amount of drug from being delivered initially, but instead leads to a long and sustained release.

To determine the diffusion coefficients of DXR through the PS wall of the vesicle, the release data were fitted to the Higuchi model. This model was designed to describe the release through a planar system having a homogeneous matrix.<sup>48</sup> The equation that was used is expressed as follows:

$$Q = \sqrt{2DtC_0C_s} \quad (6.2)$$

where Q is the amount of DXR released per unit area of PS wall (expressed in units of M/cm<sup>2</sup>) after a time t, D is the diffusion coefficient of DXR through the PS wall (expressed in units of cm<sup>2</sup>/sec), C<sub>0</sub> is the total amount of DXR inside the vesicles per unit volume of PS (expressed in units of M/cm<sup>3</sup>) and C<sub>s</sub> is the solubility of DXR in the PS

wall per unit volume of PS (expressed in units of  $M/cm^3$ ). More details of the derivation of the equation can be found in the Appendix. Higuchi's model describes the release as a diffusion process based on Fick's 1<sup>st</sup> law with a square root time dependence.<sup>48</sup>

Figure 4 shows the fit of the Higuchi model using equation 6.2 for PS-*b*-PAA vesicles present in different dioxane/water mixtures.

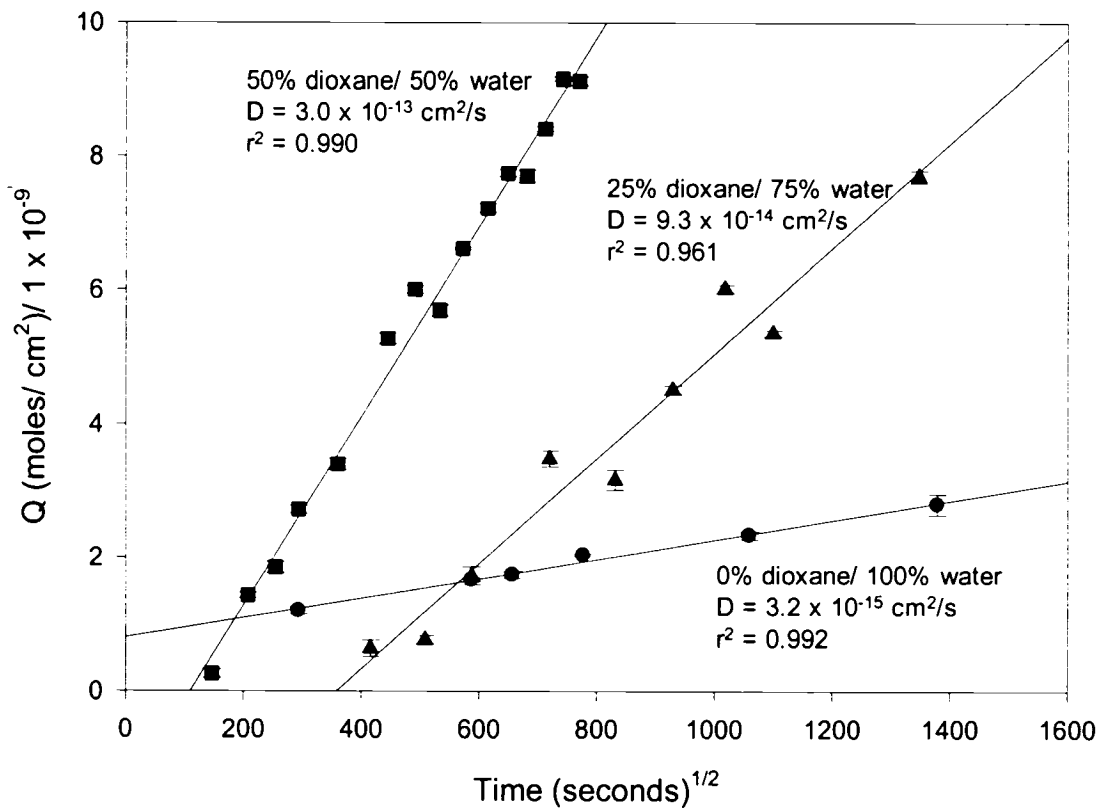


**Figure 6.4.** The fit of the release data to the Higuchi model in different dioxane/water mixtures. The linearity of the line of best fit is indicative of a diffusional release mechanism.

The linear behavior for each of the different dioxane contents, as shown by the very good correlation coefficients (0.992 for 0% dioxane, 0.961 for 25% dioxane and 0.990 for 50%

dioxane), indicate that the release mechanism can be described as diffusional. The diffusion coefficients, determined from the slope of the equation, are approximately  $3.2 \times 10^{-15}$  cm<sup>2</sup>/sec in 0% dioxane,  $9.3 \times 10^{-14}$  cm<sup>2</sup>/sec in 25% dioxane and  $3.0 \times 10^{-13}$  cm<sup>2</sup>/sec in 50% dioxane. Details of the calculations of the diffusion coefficients are given in the Appendix. There is a large change in the diffusion coefficient (i.e., a factor of approximately 30) from 0 to 25% dioxane. Recall that at room temperature, polystyrene is in a glassy state ( $T_g = 100$  °C). By adding dioxane, which is a plasticizer for polystyrene, the viscosity of the vesicle wall is reduced and diffusion is enhanced. This is reflected in an increase in the value of the diffusion coefficient (and the extent of release) with the dioxane content in the vesicle solution.

To the best of our knowledge, these are the first reported diffusion constants for DXR through polystyrene vesicle walls specifically or through polystyrene in general. To compare our values with other similar systems in the literature, we looked at the following: the diffusion coefficient of DXR, released from albumin-heparin conjugate microspheres into phosphate buffer solution, was calculated to be approximately  $2.5 \times 10^{-10}$  cm<sup>2</sup>/sec.<sup>49</sup> The release from such microspheres should occur more quickly than through PS-*b*-PAA vesicles, because highly, water swollen albumin has a much lower local viscosity than polystyrene. Also there is a lag time that is seen in Figure 4, in the release profiles of DXR from the vesicles at 25 and 50% dioxane. The release did not start immediately (i.e., at time zero); instead, there is a delay for both systems. Interestingly enough, at 0% dioxane, the release seems to have started immediately. Likely there was some residual DXR still present in the system, not completely dialyzed that resulted in an initial release.

We are able to control the rate of release of DXR from the PS-*b*-PAA vesicles by varying the amount of added plasticizer. Without any dioxane (i.e., 100% water), the release is much slower as shown by the release profiles in Figures 6.3 and 6.4, and also by the lower values of the diffusion coefficient. Other groups have also observed the use of external additives to aid in the enhancement of the release of doxorubicin. Sawaya showed that release of DXR was less than 5% in 24 hours from cross-linked albumin microspheres ranging in size from 200-315  $\mu\text{m}$  in water.<sup>50</sup> However, the presence of 0.9% NaCl allowed more than 70% of DXR to be released in the same time period. In addition, Sawaya et al also showed that divalent cations (i.e.  $\text{Ca}^{2+}$ ) had a more pronounced effect on the release than univalent cations (i.e.  $\text{Na}^+$ ).<sup>50</sup> The release rate of DXR from sulfopropyl dextran microspheres was also found to be dependent on the type and concentration of the electrolytes present.<sup>51</sup> Decout et al. showed that release of DXR from polyisohexylcyanoacrylate nanospheres is enhanced by the presence of proteins (i.e., bovine serum albumin or rabbit liver esterase).<sup>52</sup> They explain that the protein forms a layer on the nanosphere and modifies its surface making it more susceptible for penetration by the drug.

## 6.5. Conclusions

In the absence of a plasticizer, the wall permeability of the PS<sub>310</sub>-*b*-PAA<sub>36</sub> vesicles is very small ( $D$  is approximately  $10^{-15}$ ). A plasticizer, i.e., dioxane, can be added just prior to loading, the vesicles are loaded (i.e., active loading with pH inside = 2.5 and pH outside = 6.3) in the presence of the plasticizer. After loading, the plasticizer can be removed which stabilized the vesicle with the active ingredient inside (i.e., doxorubicin hydrochloride). Up to a tenfold fold increase in the amount of DXR incorporated using

the active method was achieved in comparison when no pH gradient was used. The plasticizer is added again just prior to release, in quantities depending on the desired rate of release. Control over the diffusion coefficient can be exerted over a range of greater than two orders of magnitude. The release results were fitted to the Higuchi model and shown to be diffusional. The vesicles could serve as a good functional model for potential drug delivery applications using biocompatible and biodegradable polymeric vesicles.

### 6.7. Acknowledgments

The authors would like to thank NSERC for funding this research and Professor Christine Allen for useful discussions and use of her laboratory for preliminary experiments.

### 6.8. References

- (1) van Hest, J. C. M.; Delnoye, D. A. P.; Baars, M. W. P. L.; van Genderen, M. H. P.; Meijer, E. W. *Science* **1995**, *268*, 1592-1595.
- (2) Zhang, L.; Eisenberg, A. *Science* **1995**, *268*, 1728-1731.
- (3) Jenekhe, S. A.; Chen, X. L. *Science* **1998**, *279*, 1903-1907.
- (4) Cornelissen, J. J. L. M.; Fischer, M.; Sommerdijk, N. A. J. M.; Nolte, R. J. M. *Science* **1998**, *280*, 1427-1430.
- (5) Kabanov, A. V.; Bronich, T. K.; Kabanov, V. A.; Yu, K.; Eisenberg, A. *Journal of the American Chemical Society* **1998**, *120*, 9941-9942.
- (6) Ding, J.; Liu, G. *Journal of Physical Chemistry B* **1998**, *102*, 6107-6113.
- (7) Huang, H.; Remsen, E. E.; Kowalewski, T.; Wooley, K. L. *Journal of the American Chemical Society* **1999**, *121*, 3805-3806.
- (8) Discher, B. M.; Won, Y.-Y.; Ege, D. S.; Lee, J. C. M.; Bates, F. S.; Discher, D. E.; Hammer, D. A. *Science* **1999**, *284*, 1143-1146.

- (9) Kukula, H.; Schlaad, H.; Antonietti, M.; Foerster, S. *Journal of the American Chemical Society* **2002**, *124*, 1658-1663.
- (10) Checot, F.; Lecommandoux, S.; Klok, H. A.; Gnanou, Y. *European Physical Journal E: Soft Matter* **2003**, *10*, 25-35.
- (11) Vriezema, D. M.; Hoogboom, J.; Velonia, K.; Takazawa, K.; Christianen, P. C. M.; Maan, J. C.; Rowan, A. E.; Nolte, R. J. M. *Angewandte Chemie, International Edition* **2003**, *42*, 772-776.
- (12) Du, J.; Chen, Y.; Zhang, Y.; Han, C. C.; Fischer, K.; Schmidt, M. *Journal of the American Chemical Society* **2003**, *125*, 14710-14711.
- (13) Bellomo, E. G.; Wyrsta, M. D.; Pakstis, L.; Pochan, D. J.; Deming, T. J. *Nature Materials* **2004**, *3*, 244-248.
- (14) Nardin, C.; Hirt, T.; Leukel, J.; Meier, W. *Langmuir* **2000**, *16*, 1035-1041.
- (15) Liu, F.; Eisenberg, A. *Journal of the American Chemical Society* **2003**, *125*, 15059-15064.
- (16) Napoli, A.; Valentini, M.; Tirelli, N.; Mueller, M.; Hubbell, J. A. *Nature Materials* **2004**, *3*, 183-189.
- (17) Discher, D. E.; Eisenberg, A. *Science* **2002**, *297*, 967-973.
- (18) Lim Soo, P.; Eisenberg, A. *Journal of Polymer Science: Part B: Polymer Physics* **2004**, *42*, 923-938.
- (19) Nardin, C.; Widmer, J.; Winterhalter, M.; Meier, W. *European Physical Journal E: Soft Matter* **2001**, *4*, 403-410.
- (20) Rang, H. P.; Dale, M. M. *Pharmacology*, 2nd ed.; Churchill Livingstone: New York, 1991.
- (21) Barenholz, Y.; Amselem, S.; Goren, D.; Cohen, R.; Gelvan, D.; Samuni, A.; Golden, E. B.; Gabizon, A. *Medicinal Research Reviews* **1993**, *13*, 449-491.
- (22) Kwon, G.; Naito, M.; Yokoyama, M.; Okano, T.; Sakurai, Y.; Kataoka, K. *Journal of Controlled Release* **1997**, *48*, 195-201.
- (23) Rapoport, N. *Colloids and Surfaces, B: Biointerfaces* **1999**, *16*, 93-111.
- (24) Alakhov, V.; Klinski, E.; Li, S.; Pietrzynski, G.; Venne, A.; Batrakova, E.; Bronitch, T.; Kabanov, A. *Colloids and Surfaces, B: Biointerfaces* **1999**, *16*, 113-134.

- (25) Kataoka, K.; Matsumoto, T.; Yokoyama, M.; Okano, T.; Sakurai, Y.; Fukushima, S.; Okamoto, K.; Kwon, G. S. *Journal of Controlled Release* **2000**, *64*, 143-153.
- (26) Pruitt, J. D.; Pitt, W. G. *Drug Delivery* **2002**, *9*, 253-258.
- (27) Gabizon, A.; Dagan, A.; Goren, D.; Barenholz, Y.; Fuks, Z. *Cancer Research* **1982**, *42*, 4734-4739.
- (28) Rosoff, M.; Editor. *Vesicles*; Marcel Dekker, Inc.: New York, 1996; Vol. 62.
- (29) Mayer, L. D.; Reamer, J.; Bally, M. B. *Journal of Pharmaceutical Sciences* **1999**, *88*, 96-102.
- (30) Nichols, J. W.; Deamer, D. W. *Biochimica et Biophysica Acta* **1976**, *455*, 269-271.
- (31) Mayer, L. D.; Bally, M. B.; Cullis, P. R. *Biochimica et Biophysica Acta* **1986**, *857*, 123-126.
- (32) Madden, T. D.; Harrigan, P. R.; Tai, L. C. L.; Bally, M. B.; Mayer, L. D.; Redelmeier, T. E.; Loughrey, H. C.; Tilcock, C. P. S.; Reinish, L. W.; Cullis, P. R. *Chemistry and Physics of Lipids* **1990**, *53*, 37-46.
- (33) Li, X.; Hirsh, D. J.; Cabral-Lilly, D.; Zirkel, A.; Gruner, S. M.; Janoff, A. S.; Perkins, W. R. *Biochimica et Biophysica Acta* **1998**, *1415*, 23-40.
- (34) Brown, M. D.; Schaetzlein, A.; Brownlie, A.; Jack, V.; Wang, W.; Tetley, L.; Gray, A. I.; Uchegbu, I. F. *Bioconjugate Chemistry* **2000**, *11*, 880-891.
- (35) Ahmed, F.; Discher, D. E. *Journal of Controlled Release* **2004**, *96*, 37-53.
- (36) Siepmann, J.; Ainaoui, A.; Vergnaud, J. M.; Bodmeier, R. *Journal of Pharmaceutical Sciences* **1998**, *87*, 827-832.
- (37) Zhong, X. F.; Varshney, S. K.; Eisenberg, A. *Macromolecules* **1992**, *25*, 7160-7167.
- (38) Luo, L.; Eisenberg, A. *Langmuir* **2001**, *17*, 6804-6811.
- (39) Yu, Y.; Zhang, L.; Eisenberg, A. *Macromolecules* **1998**, *31*, 1144-1154.
- (40) Mayer, L. D.; Bally, M. B.; Hope, M. J.; Cullis, P. R. *Biochimica et Biophysica Acta* **1985**, *816*, 294-302.
- (41) Haran, G.; Cohen, R.; Bar, L. K.; Barenholz, Y. *Biochimica et Biophysica Acta* **1993**, *1151*, 201-215.

- (42) Abraham, S. A.; Edwards, K.; Karlsson, G.; MacIntosh, S.; Mayer Lawrence, D.; McKenzie, C.; Bally Marcel, B. *Biochimica et Biophysica Acta* **2002**, *1565*, 41-54.
- (43) Lasic, D. D.; Ceh, B.; Stuart, M. C. A.; Guo, L.; Frederik, P. M.; Barenholz, Y. *Biochimica et Biophysica Acta* **1995**, *1239*, 145-156.
- (44) Leo, A.; Hansch, C.; Elkins, D. *Chemical Reviews* **1971**, *71*, 525-616.
- (45) Khopade, A. J.; Caruso, F. *Biomacromolecules* **2002**, *3*, 1154-1162.
- (46) Ahmed, F.; Hategan, A.; Discher, D. E.; Discher, B. M. *Langmuir* **2003**, *19*, 6505-6511.
- (47) Jones, C.; Burton, M. A.; Gray, B. N. *Journal of Pharmacy and Pharmacology* **1989**, *41*, 813-816.
- (48) Higuchi, T. *Journal of Pharmaceutical Sciences* **1963**, *52*, 1145-1149.
- (49) Cremers, H. F. M.; Verrijck, R.; Noteborn, H. P. J. M.; Kwon, G.; Bae, Y. H.; Kim, S. W.; Feijen, J. *Journal of Controlled Release* **1994**, *29*, 143-155.
- (50) Sawaya, A.; Fickat, R.; Benoit, J. P.; Puisieux, F.; Benita, S. *Journal of Microencapsulation* **1988**, *5*, 255-267.
- (51) Liu, Z.; Cheung, R.; Wu, X. Y.; Ballinger, J. R.; Bendayan, R.; Rauth, A. M. *Journal of Controlled Release* **2001**, *77*, 213-224.
- (52) Decout, A.; Dubernet, C.; Henry-Toulme, N. *Journal of Colloid and Interface Science* **1996**, *181*, 99-107.

---



---

## Appendix

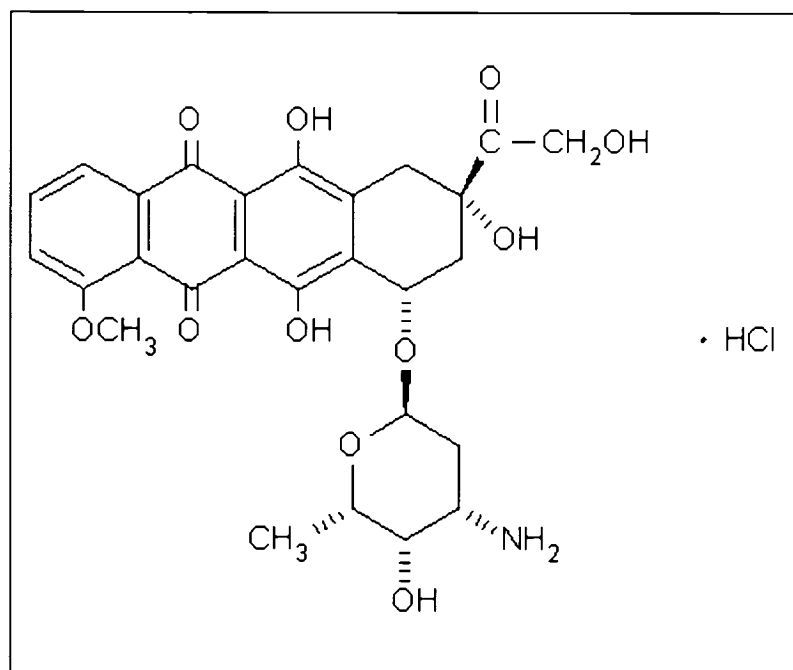
---



---

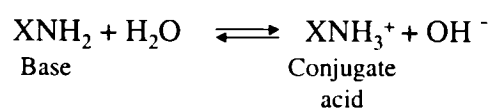
### 1. Hydrophilic fluorescent drug

**Table A4.** Structure of Doxorubicin Hydrochloride (DXR)



### 2. Derivation of equation 1 in the chapter and describing the equilibria involved in doxorubicin (DXR) loading via a pH gradient.

Doxorubicin (XNH<sub>2</sub>) is a weak base and in an aqueous solution, it exists in equilibrium with its conjugate acid (XNH<sub>3</sub><sup>+</sup>) (pK<sub>a</sub>=8.25):



The equilibrium constant for this reaction, K<sub>b</sub>, can be expressed as:

$$K_b = \frac{[\text{XNH}_3^+][\text{OH}^-]}{[\text{XNH}_2]} \quad (\text{A6.1})$$

Given that  $K_w = K_a K_b$  and  $K_w = [\text{H}_3\text{O}^+][\text{OH}^-]$

Recalling that  $K_b = \frac{K_w}{K_a}$ , and that  $[\text{OH}^-] = \frac{K_w}{[\text{H}_3\text{O}^+]}$ , equation (A6.1) can be written as:

$$[\text{H}_3\text{O}^+] = K_a \frac{[\text{XNH}_3^+]}{[\text{XNH}_2]} \quad (\text{A6.2})$$

Taking the negative logarithm of both sides of equation A6.2 yields the Henderson-Hasselbach equation:

$$\text{pH} = \text{p}K_a - \log \frac{[\text{XNH}_3^+]}{[\text{XNH}_2]} \quad (\text{A6.3})$$

Equation (A6.3) shows that the relative concentration of the protonated to the neutral form of doxorubicin is determined by the pH of the solution.

For example, inside the vesicle cavity, at  $\text{pH} = 2.5$ , equation A6.3 gives:

$$\frac{[\text{XNH}_3^+]}{[\text{XNH}_2]} = 10^{(\text{p}K_a - \text{pH})} = 10^{(8.25 - 2.5)} = 10^{5.75}$$

In the external aqueous solution (i.e., outside the vesicle membrane), the  $\text{pH} = 6.3$ , and the relative concentration of the charged to the neutral form of the drug is:

$$\frac{[\text{XNH}_3^+]}{[\text{XNH}_2]} = 10^{(\text{p}K_a - \text{pH})} = 10^{(8.25 - 6.3)} = 10^{1.95}$$

The equilibrium between doxorubicin ( $\text{XNH}_2$ ) and its conjugate acid ( $\text{XNH}_3^+$ ) exists inside the aqueous cavity of the vesicle, as well as in the aqueous solution in which the vesicles are suspended. Therefore, using equation A6.2, one can write:

$$[\text{XNH}_2]_{\text{in}} = K_a \frac{[\text{XNH}_3^+]_{\text{in}}}{[\text{H}_3\text{O}^+]_{\text{in}}} \quad (\text{A6.4})$$

$$[\text{XNH}_2]_{\text{out}} = K_a \frac{[\text{XNH}_3^+]_{\text{out}}}{[\text{H}_3\text{O}^+]_{\text{out}}} \quad (\text{A6.5})$$

where  $[\text{XNH}_3^+]$  is the concentration of the protonated form of the drug,  $[\text{XNH}_2]$  is the concentration of the neutral form,  $[\text{H}_3\text{O}^+]$  is the proton concentration, and the subscripts “in” and “out” refer to the inside and outside of the vesicle membrane, respectively. Assuming that the equilibrium constant,  $K_a$ , is the same on both sides of the membrane, and that at equilibrium, the concentration of the neutral form of doxorubicin, which is membrane permeable, is equal on both sides of the membrane, equations A6.4 and A6.5 can be equated to give:

$$\frac{[\text{XNH}_3^+]_{\text{in}}}{[\text{XNH}_3^+]_{\text{out}}} = \frac{[\text{H}_3\text{O}^+]_{\text{in}}}{[\text{H}_3\text{O}^+]_{\text{out}}}$$

The above equation (which corresponds to equation 6.1 in the text) shows that the relative concentration of DXR molecules (in their protonated form) inside and outside the vesicle membrane is dictated by the pH on the opposite sides of the membrane.

### 3. Internal concentration of doxorubicin

The internal concentration of DXR in the vesicles can be estimated using the amount incorporated (moles of DXR per gram of polymer), and the total internal volume of the vesicles, Total  $V_{\text{int}}$ , expressed in litre per gram of polymer and defined according to the following equation:

$$\text{Total } V_{\text{int}} = \text{Avg. internal vol. per vesicle} \times \# \text{ of vesicles per gram of polymer} \quad (\text{A6.6})$$

**a) Determination of the number of vesicles per gram of polymer**

The number of vesicles per gram of polymer can be expressed as:

$$\# \text{ of vesicles per gram of polymer} = \frac{\text{Weight of PS per gram of polymer}}{\text{Average weight of PS per vesicle}} \quad (\text{A6.7})$$

For the copolymer used in this study, PS<sub>310</sub>-*b*-PAA<sub>36</sub>, the polystyrene (PS) content by weight is 92.5 %. The weight of PS per gram of polymer is, therefore, equal to approximately 0.925 g/g.

The volume of PS per one vesicle is calculated using equation A6.8 below, and the results are summarized in the last column of Table A5.

$$V_i^{\text{PS}} = \frac{4}{3}\pi[(D_i/2)^3 - ((D_i/2) - W)^3] \quad (\text{A6.8})$$

The average volume of polystyrene per vesicle,  $\bar{V}_{\text{PS}}$ , calculated using equation A6.9 below, is approximately  $4.6 \times 10^6 \text{ nm}^3$ .

$$\bar{V}_{\text{PS}} = \frac{\sum N_i V_i^{\text{PS}}}{\sum N_i} \quad (\text{A6.9})$$

Assuming that the density of PS equals 1.04 g/mL, the number of vesicles present per gram of polymer, calculated using equation A6.7, is approximately  $2.0 \times 10^{14}$  vesicle/g.

**b) Determination of the average internal volume per vesicle**

The average internal volume per vesicle,  $\bar{V}_{\text{int}}$  is calculated using the volume and the volume distribution of the vesicles, rather than their average diameter.  $\bar{V}_{\text{int}}$  is defined according to the following equation:

$$\bar{V}_{\text{int}} = \frac{\sum N_i V_i}{\sum N_i} \quad (\text{A6.10})$$

where  $N_i$  is the number of vesicles having an internal volume  $V_i$ .  $V_i$  is calculated using the vesicle diameter,  $D_i$ , and wall thickness,  $W$ , as seen in Figure A4 and expressed in the following equation:

$$V_i = \frac{4}{3}\pi[(D_i/2) - W]^3 \quad (\text{A6.11})$$

The wall thickness,  $W = 30$  nm, and the size distribution of the vesicles (given in the first two columns of Table A5 below), were determined from transmission electron microscopy (TEM).

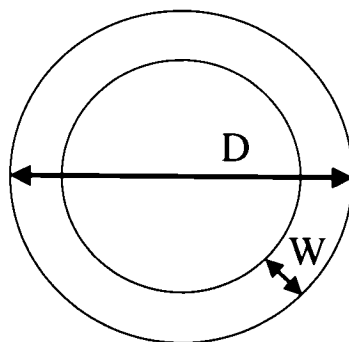


**Figure A4.** Schematic representation of a block copolymer vesicle having a diameter,  $D_i$  and a wall thickness,  $W$ .

**Table A5.** Vesicle size distribution as determined from TEM, the internal volume  $V_i$ , calculated using equation (A6.11), and the volume of polystyrene per vesicle,  $V_i^{PS}$ , calculated using equation (A6.8)

Diameter, $D_i$ , (nm)	Number of Vesicles, $N_i$	Internal Volume, $V_i$ , (nm <sup>3</sup> )	Volume of PS per vesicle, $V_i^{PS}$ (nm <sup>3</sup> )
100	1	$3.4 \times 10^4$	$4.9 \times 10^5$
150	31	$3.8 \times 10^5$	$1.4 \times 10^6$
200	70	$1.4 \times 10^6$	$2.8 \times 10^6$
250	35	$3.6 \times 10^6$	$4.6 \times 10^6$
300	23	$7.2 \times 10^6$	$6.9 \times 10^6$
350	14	$1.3 \times 10^7$	$9.7 \times 10^6$
400	5	$2.1 \times 10^7$	$1.3 \times 10^7$
450	2	$3.1 \times 10^7$	$1.7 \times 10^7$
500	0	$4.5 \times 10^7$	$2.1 \times 10^7$
550	2	$6.2 \times 10^7$	$2.6 \times 10^7$

The average internal volume per vesicle calculated using equation A6.10 and the data given in Table A5 is:  $\bar{V}_{int} = 4.8 \times 10^6 \text{ nm}^3$ .

**c) Determination of the total internal volume of the vesicles**

The total internal volume per one gram of polymer is then calculated using equation A6.6 as follows:

$$\begin{aligned}
 \text{Total } V_{int} &= \bar{V}_{int} * \# \text{ of vesicles per gram of polymer} \\
 &= 4.8 \times 10^6 \text{ nm}^3/\text{vesicle} \times 2.0 \times 10^{14} \text{ vesicle/g} \\
 &= 9.6 \times 10^{20} \text{ nm}^3 / \text{g of polymer.} \\
 &= 9.6 \times 10^{-4} \text{ L / g of polymer}
 \end{aligned}$$

The calculated average internal volume per vesicle,  $\bar{V}_{int}$ , is ca.  $4.8 \times 10^6 \text{ nm}^3 / \text{vesicle}$ , and the total internal volume of vesicles is ca.  $9.6 \times 10^{-4} \text{ L / g of polymer}$ .

#### 4. Determination of the ratio of the vesicle internal volume to solution volume

For the different samples and controls used in this study, the volume of solution per gram of polymer ranges between 0.58 and 1.66 L/g of polymer. Recalling that the total internal volume of vesicles is ca.  $9.6 \times 10^{-4}$  L/g of polymer, the ratio between the internal volume of the vesicles and the volume of the solution in which these vesicles are suspended ranges between  $1.7 \times 10^{-3}$  and  $5.8 \times 10^{-4}$ .

#### 5. Interaction of DXR with PS wall

In a given vesicle solution (volume = 100  $\mu$ L), the volume of polystyrene is known (between  $3.7 \times 10^{-8}$  and  $1.1 \times 10^{-7}$  L, depending on the polymer concentration), and so is the concentration of doxorubicin in the aqueous phase (approximately  $5.6 \times 10^{-4}$  M). The total number of moles of DXR present in the solution can be calculated as follows:

Molarity = moles/volume

$$5.6 \times 10^{-4} \text{ M} = \text{moles} / 1 \times 10^{-4} \text{ litre}$$

$$\text{moles} = 5.6 \times 10^{-8}$$

Using  $K_{\text{EB}/\text{H}_2\text{O}} = 0.19$ , the number of moles of DXR present in the above volume of polystyrene can be calculated as follows:

$$K_{\text{EB}/\text{H}_2\text{O}} = [\text{DXR}]_{\text{EB}} / [\text{DXR}]_{\text{H}_2\text{O}}$$

$$0.19 = [\text{DXR}]_{\text{EB}} / 5.6 \times 10^{-4} \text{ M}$$

$$[\text{DXR}]_{\text{EB}} = 1.06 \times 10^{-4} \text{ M}$$

Molarity = moles/volume of PS

$$1.06 \times 10^{-4} \text{ M} = \text{moles} / 3.7 \times 10^{-8} \text{ litre}$$

$$\text{Moles of PS} = 3.9 \times 10^{-12} \text{ moles}$$

Similarly for a volume of PS of  $1.1 \times 10^{-7}$  L, the number of moles of DXR present would be  $1.2 \times 10^{-11}$  moles. The number of moles possibly solubilized by polystyrene ranges between  $7.0 \times 10^{-3}$  and  $2.1 \times 10^{-2}$  %.

#### 6. Interaction of DXR with PAA chains (inside and outside)

The number of moles of doxorubicin solubilized by one gram of poly(acrylic acid) is approximately  $3.5 \times 10^{-7}$  mol/g at pH = 2.5, and  $2.8 \times 10^{-5}$  mol/g at pH = 6.3. Based on the weight of poly(acrylic acid) present in 100  $\mu$ L of the vesicle solution (between  $3.0 \times 10^{-6}$  and  $8.6 \times 10^{-6}$  g, depending on the polymer concentration), the number of moles of DXR present in the above solution can be calculated as follows:

At pH = 2.5

$$\text{Moles of DXR in PAA solution} = 3.5 \times 10^{-7} \text{ mol/g} \times 3.0 \times 10^{-6} \text{ g} = 1.0 \times 10^{-12}$$

$$\text{Moles of DXR in PAA solution} = 3.5 \times 10^{-7} \text{ mol/g} \times 8.6 \times 10^{-6} \text{ g} = 3.0 \times 10^{-12}$$

Similarly, at pH = 6.3, the range of moles of DXR interacting with acrylic acid ranges from  $8.4 \times 10^{-11}$  and  $2.4 \times 10^{-10}$  mol. Recall that total number of moles of DXR in solution, as calculated in the previous section is  $5.6 \times 10^{-8}$  moles. Therefore, the number of moles possibly solubilized by poly(acrylic acid) range between  $1.8 \times 10^{-3}$  and  $5.4 \times 10^{-3}$  % at pH = 2.5, and  $2.0 \times 10^{-1}$  and  $4.0 \times 10^{-1}$  % at pH = 6.3.

## 7. Derivation of equation for release from a planar system having a homogeneous matrix<sup>1</sup>

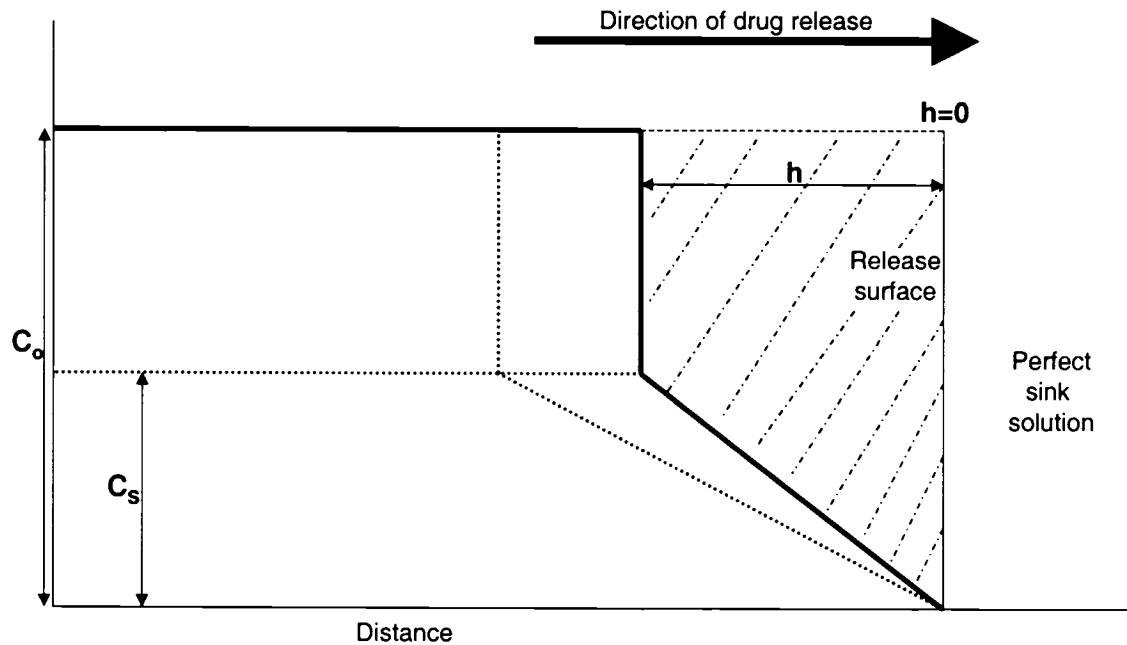


**Figure A5.** Theoretical drug concentration profile of a matrix system in contact with a perfect sink solution.

The solid line represents the concentration gradient existing after a time,  $t$ , in the matrix system normal to the release surface, under perfect sink conditions (i.e., all the drug is rapidly diffused). The total drug concentration shows a sharp discontinuity at a distance  $h$  from the release surface and no drug dissolution could occur until the concentration drops below the matrix drug solubility ( $C_s$ ). For distances greater than  $h$ , the concentration gradient will be constant, provided  $C_0 \gg C_s$ . The linearity of the gradient in this region follows Fick's 1<sup>st</sup> law. At a time  $t$ , the amount of drug released corresponds to the shaded region in Figure A5.

Appendix for Chapter 6

The amount of drug released,  $dQ$ , is related to  $dh$  and the movement of the release front can be expressed as:

$$dQ = C_o dh - \frac{1}{2}(C_s dh) \quad (\text{A6.12})$$

From Fick's first law:  $\frac{dQ}{dt} = \frac{DC_s}{h}$  (A6.13)

Substitute equation A6.12 into equation A6.13 gives the following:

$$\frac{C_o dh - \frac{1}{2}(C_s dh)}{dt} = \frac{DC_s}{h} \quad (\text{A6.14})$$

or

$$\frac{C_o dh}{dt} - \frac{1}{2}C_s \frac{dh}{dt} = \frac{DC_s}{h} \quad (\text{A6.15})$$

$$\frac{h(2C_o - C_s)dh}{2DC_s} = dt \quad (\text{A6.16})$$

Integrating equation 6.16 gives the following:

$$t = \frac{h^2}{4DC_s}(2C_o - C_s) + K \quad (\text{A6.17})$$

where  $K$  is the integration constant and will be equal to zero if time was measured from zero, so:

$$t = \frac{h^2}{4DC_s}(2C_o - C_s) \quad (\text{A6.18})$$

Rearranged to solve for  $h$ :

$$h = 2\sqrt{\frac{DtC_s}{(2C_o - C_s)}} \quad (\text{A6.19})$$

From Figure A5, the amount of drug released,  $Q$  after a time  $t$  can be expressed as:

$$Q = hC_o - \frac{hC_s}{2} \quad (\text{A6.20})$$

or

$$Q = 2h(C_o - C_s) \quad (\text{A6.21})$$

Substituting equation 6.19 into equation 6.21 gives the following:

$$Q = 2\sqrt{\frac{DtC_s}{(2C_o - C_s)}}(C_o - C_s) \quad (\text{A6.22})$$

or

$$Q = \sqrt{DtC_s(2C_o - C_s)} \quad (\text{A6.23})$$

For the common case when  $C_s \lll C_o$

$$Q = \sqrt{2DtC_oC_s} \quad (\text{A6.24})$$

where  $Q$  is the amount of DXR released per unit area of PS wall (expressed in units of  $M/cm^2$ ) after a time  $t$ ,  $D$  is the diffusion coefficient of DXR through the PS wall (expressed in units of  $cm^2/sec$ ),  $C_o$  is the total amount of DXR inside the vesicles per unit volume of PS (expressed in units of  $M/cm^3$ ) and  $C_s$  is the solubility of DXR in the PS wall per unit volume of PS (expressed in units of  $M/cm^3$ ).

Higuchi originally proposed the equation A6.24 for the release of drugs suspended in ointment bases into a perfect sink<sup>2</sup>, but showed that it could also be used for the release of drugs from a planar system having a homogenous matrix into a perfect sink.<sup>1</sup>

## 8. Determination of the diffusion coefficient

From equation A6.24,  $Q = \sqrt{2DtC_oC_s}$ , the diffusion coefficient of the release of doxorubicin from the vesicles can be calculated.

### a) Determination of total amount of DXR inside vesicle ( $C_o$ ) per unit volume of PS

At 0% dioxane

Given that the weight of the polymer in the solution is  $1.67 \times 10^{-5}$  g and recall from section 2a that the PS content by weight is 92.5%, then the amount of PS present in the solution is  $1.55 \times 10^{-5}$  cm<sup>3</sup>. The average number of moles of DXR is  $9.63 \times 10^{-8}$  moles (measured by fluorescence), however the actual amount of moles of DXR used in the release experiment at time =0 is  $4.82 \times 10^{-8}$  moles, so that the total amount of DXR inside the vesicles can be calculated as follows:

$$\begin{aligned}C_o &= \text{Total amount of DXR inside vesicle/ Volume of PS in solution} \\ &= 4.82 \times 10^{-8} \text{ moles/ } 1.55 \times 10^{-5} \text{ cm}^3 \\ &= 3.11 \times 10^{-3} \text{ moles/cm}^3\end{aligned}$$

### b) Determination of maximum solubility of DXR inside PS wall ( $C_s$ ) per unit volume of PS

Recall from section 4 that the calculated concentration of doxorubicin in PS ( $[DXR]_{EB}$ ) is  $1.06 \times 10^{-4}$  M, the number of moles of DXR inside PS wall per unit volume of PS is calculated as follows:

$$\begin{aligned}\text{Moles of DXR inside PS wall per unit volume of PS} &= (\text{Molarity of DXR in PS} \times \text{Volume of PS in solution}) / \text{Volume of PS in solution} \\ &= (1.06 \times 10^{-4} \text{ M} \times 1.55 \times 10^{-5} \text{ ml} \times 1/1 \times 10^{-3} \text{ l}) / 1.55 \times 10^{-5} \text{ cm}^3 \\ &= 1.06 \times 10^{-7} \text{ mol/cm}^3\end{aligned}$$

**c) Determination of the amount of DXR released after time t, per unit area of PS wall, Q.**

The average vesicle size was approximately 210 nm, hence the average volume of PS per vesicle was calculated from Table A5 to be approximately  $4.6 \times 10^{-15} \text{ cm}^3$ . Knowing that the volume of PS in the solution is  $1.55 \times 10^{-5} \text{ cm}^3$ , the average number of vesicles in the solution is  $3.36 \times 10^9$ . The area of one vesicle can be calculated from:

$$\begin{aligned} \text{Area of vesicle} &= 4 \pi r^2 \\ &= 4 \pi (105 \text{ nm} \times 1/1 \times 10^{-7} \text{ cm/nm})^2 \\ &= 1.38 \times 10^{-9} \text{ cm}^2 \end{aligned}$$

So the area of the vesicle solution is  $4.65 \text{ cm}^2$ .

Hence the value for Q can be calculated as follows:

At time = 86400 seconds

$$\begin{aligned} Q &= \text{Amount released (determined by fluorescence)} / \text{Total area of vesicles} \\ &= 5.54 \times 10^{-9} \text{ moles} / 4.65 \text{ cm}^2 \\ &= 1.2 \times 10^{-9} \text{ moles/cm}^2 \end{aligned}$$

This is repeated for all of the various time points.

**d) Calculation of the diffusion coefficient, D**

By plotting Q vs. the square root of time ( $t^{1/2}$ ), we obtain a linear relation and the slope obtained is  $1.46 \times 10^{-12}$ , which is equal to  $\sqrt{2DC_oC_s}$ . By solving for D, we obtain the diffusion constant as shown in the following calculation:

$$\begin{aligned} \text{Slope} &= \sqrt{2DC_oC_s} \\ D &= (1.46 \times 10^{-12})^2 / (2C_oC_s) \\ &= (1.46 \times 10^{-12} \text{ mol/cm}^2 \text{ sec}^{1/2})^2 / (2 \times 3.11 \times 10^{-3} \text{ mol/cm}^3 \times 1.06 \times 10^{-7} \text{ mol/cm}^3) \\ &= 3.2 \times 10^{-15} \text{ cm}^2 / \text{sec} \end{aligned}$$

The procedure (7a to 7d) is repeated at 25% dioxane and at 50% dioxane to obtain a diffusion constant of  $9.3 \times 10^{-14} \text{ cm}^2 / \text{sec}$  and  $3.0 \times 10^{-13} \text{ cm}^2 / \text{sec}$  respectively.

**References**

- (1) Higuchi, T. *Journal of Pharmaceutical Sciences* **1963**, *52*, 1145-1149.
- (2) Higuchi, T. *Journal of Pharmaceutical Sciences* **1961**, *50*, 874-875.

# Chapter 7

---

---

## Conclusions, Contributions to Original Knowledge and Suggestions for Future Work

---

---

### 7.1. Conclusions and Contributions to Original Knowledge

This section reports on the principal findings that are discussed in the thesis, focusing mainly on the original aspects of the dissertation. The physico-chemical characterization of micelles for drug delivery applications was described in Chapters 3, 4 and 5. Experiments involving biological studies were reported in Chapters 4 and 5. The physico-chemical properties of vesicles as drug carriers were discussed in Chapter 6.

Chapter 3 reports on the investigation of the loading properties, the partition coefficients and the release behavior of two model compounds with different hydrophobicities (DiI and benzo[a]pyrene) from block copolymer micelles of PCL-*b*-PEO. The maximum loading efficiency of DiI and benzo[a]pyrene were 87% and 32%, respectively. The loading of the model compounds was a strong function of their compatibility with the PCL core. To determine the affinity of the probe molecules for the micelles, partition coefficient values were examined between the micelles and the external solution. A partition coefficient value of 5800 was obtained for DiI compared to 690 for benzo[a]pyrene. DiI was found to be more compatible with the PCL core than benzo[a]pyrene due to the higher partition coefficient value which indicates it has a greater affinity for the micelles than benzo[a]pyrene. The partition coefficient values were related to the loading and release properties of the probes from the micelles. The release of the probes was studied under “perfect sink” conditions, which ensured that all

of the probe molecules released from the micelles would be washed away. We are not aware of any reports in the literature of release studies from micellar systems being performed under true sink conditions. The release of both probes was fitted to the Higuchi model and shown to follow a diffusional mechanism. The diffusion coefficients were determined to be of the order of  $10^{-15}$  cm<sup>2</sup>/s. The type and concentration of the probe influenced the loading and release from the micelles. Also the compatibility between the agent of interest and the block copolymer micelle was shown to be an important factor in developing a suitable drug delivery system.

In Chapter 4, the incorporation and release of a model hydrophobic drug (E2) from PCL-*b*-PEO micelles is reported. In order to assess the micelles as a potential delivery vehicle for estradiol, a number of properties pertaining to the loading and release parameters were evaluated. The micelles were spherical aggregates of 20-40 nm in diameter. E2 can be loaded into the micelles at a maximum loading efficiency of 96%, which represents a drug content of 190% (w/w) and a drug capacity of up to 4000 molecules of E2. The loading was also studied as a function of the PCL block length and shown to be linear. The release of E2 from the micelles was studied using “perfect sink” conditions. The “perfect sink” apparatus was improved by using individual dialysis chambers as opposed to dialysis tubing as reported in Chapter 3; this allowed for a simpler removal of the micelles containing E2 for sampling and subsequent analysis. The release of E2 was shown to be diffusional, as shown by the linearity of the release as a function of the square root of time. Diffusion coefficients were determined to be of the order of  $10^{-17}$  cm<sup>2</sup>/s. The release of E2 from different PCL block lengths was also studied and shown that a smaller core diameter results in a quicker release than for a larger core diameter. The initial concentration of E2 and the PCL block length were shown to

influence both the loading and release. *In vivo* experiments using C57BL female mice showed that the E2 retained its biological activity after the preparation of the micelles.

Gold labeled P4VP-*b*-PEO micelles were prepared and characterized for cellular internalization studies as discussed in Chapter 5. The subcellular fate of the micelles was the key motivation for these studies. Despite a number of papers stating that micelles are internalized by endocytosis, there is a lack of visual proof of the actual micelles inside of the subcellular structures. Gold labeled micelles were internalized for up to 24 hours in two different cell lines (human embryonic kidney (HEK 293) cells and human lung carcinoma (A549) cells). We estimated that the micelles contain 3200 atoms and since the TEM cannot distinguish between gold atoms readily, we assumed that the atoms would form a gold particle. We estimated the size of the gold particle to be approximately 5 nm and this was confirmed by transmission electron microscopy (4-8 nm). TEM also revealed that the entry of the micelle into the cell was time and concentration dependent. The cells survived greater than 24 hours in the presence of the gold labeled micelles and up to a micellar concentration of 0.73  $\mu\text{g}/\text{mL}$ . The micelles could clearly be seen inside of the endosomes and lysosomes of both cell lines using TEM. In comparison to fluorescently labeled micelles, there is a greater than a ten fold improvement in the resolution. Thus, gold labeled micelles can serve as a valuable and useful tool for exploring the interactions between micelles and subcellular compartments of cells for drug delivery applications.

The active loading of an anticancer drug, doxorubicin hydrochloride, and its release from PS<sub>310</sub>-*b*-PAA<sub>36</sub> copolymer vesicles are reported in Chapter 6. An active loading method, in the presence of dioxane, a plasticizer for the polystyrene wall, is used

to load DXR into the vesicles. The vesicle walls are plasticized just prior to loading to increase the permeability. A pH gradient is created across the membrane of the vesicles (pH inside = 2.5 and pH outside = 6.3) to concentrate DXR inside the internal aqueous cavity. DXR was found to interact very minimally with the PS wall and the PAA chains of the vesicle. Hence, DXR was found to be incorporated mainly in the vesicle interior cavity due to the pH gradient. The plasticizer is removed after loading, and the vesicle walls are hardened again, and the vesicle structure stays stable indefinitely with the active ingredient still intact. Up to a tenfold fold increase in the amount of DXR incorporated using the active method was achieved in comparison when no pH gradient was used. The permeability of the polystyrene wall is tunable for loading and release. The release of DXR is studied under dioxane/water sink conditions. The release profile of DXR from the vesicles is fitted to the Higuchi model and shown to be diffusional. The plasticizer is added to the system just prior to release, to make the polystyrene wall more permeable. The permeability can be fine tuned by the quantity of the plasticizer; diffusional coefficients of DXR release from the vesicles ranged from  $10^{-15}$  to  $10^{-13}$  cm<sup>2</sup>/s.

## **7.2. Suggestions for Future Work**

The contents of the thesis cover many different topics. Much of the work described here represents a preliminary examination of the use of block copolymer aggregates for drug delivery applications. There remain a number of studies that could be performed as a result of the work reported in this thesis; these proposed studies will be discussed in the following section.

Two model hydrophobic probes (CM-DiI and benzo[a]pyrene) and a female hormone drug (17 $\beta$ -estradiol) were incorporated into the PCL-*b*-PEO micelles. Also,

previous work by Allen et al. dealt with the incorporation of a number of lipophilic compounds into PCL-*b*-PEO micelles.<sup>1-3</sup> However, a more systematic and extensive study of the incorporation into these micelles of families of molecules with different physical properties could be initiated. Their loading properties, partition coefficients and release properties from the micelles would provide useful information in a library or classification system for the purposes of matching an appropriate drug for the micellar system. The compatibility between the drug of interest and the polymer is important in evaluating the effectiveness of the micellar delivery vehicle.

More specifically concerning to estradiol, studies could be performed on the incorporation of testosterone, the principal male steroid, into PCL-*b*-PEO micelles. Testosterone cannot be analyzed by fluorescence, but high performance liquid chromatography (HPLC) or enzyme linked immunosorbent assays (ELISA), which don't require fluorescence properties could be used. It is important to be able to compare the results using the same techniques, so HPLC or ELISA studies would have to be conducted for estradiol. Also, many of these drugs are available in a radiolabeled form, so a scintillation counter would be used to quantitate the amount of drug loaded and released from the micelles. In addition, a combination of hormones could be studied for loading and release experiments. The study of hormones remains a topic of increasing and continuing interest due to the extensive use of hormone replacement therapies for different ailments.

Partition coefficients of estradiol or other hydrophobic drugs of interest could also be determined for future studies. However, it is important to know that the method that we used to determine the partition coefficients requires a large amount of copolymer and the method requires a lot of time to prepare all of the samples needed.<sup>4</sup> It is advisable that

if there is a wealth of information on the drug of interest, as was the case with estradiol, then the literature values should be used. Computer software programs may provide another way of determining partition coefficients.

Differential scanning calorimetry (DSC) studies would be used to conduct studies of the crystallinity of the estradiol in the PCL core. It is important that a high enough concentration is present in the micelles in order to be able to detect any crystallinity. The crystallinity is important to the drug release since a drug in the crystalline form inside a micellar delivery system would first have to dissolve before diffusing through the core of the micelle.

Studies of the long-term storage of a drug in the PCL-*b*-PEO micelles would also be of interest for potential pharmaceutical applications. The determination of how long the drug remains stable, i.e., without precipitating from solution, within the micellar formulation over long periods of time (i.e., greater than 1 year) would be useful. Also the micelles could be lyophilized and sterilized and stored as a powder. However, long-term stability studies would need to be conducted to ensure that the drug remains stable. The stability of the drug would depend on factors such as the properties of the micellar system and the polymer-drug compatibility.<sup>5</sup>

The polymer-drug compatibility can be assessed using solubility parameters of the polymer and the drug. Computer modeling programs such as Molecular Modeling Pro have been used to determine the solubility parameters of different polymers and the selected drug.<sup>6</sup> Similar studies could be used to compare a range of biodegradable and biocompatible polymers for the drug of interest. These preliminary theoretical studies would be complementary to the actual experimental physiochemical studies to be

conducted. Hence a micellar delivery vehicle could be designed and tailored for the drug of choice.

Drug release was studied using “perfect sink” conditions with tap water, because it would have been difficult to have a continuous flow of biological relevant media (e.g., phosphate-buffered saline (PBS)). Many release studies have been conducted using PBS at a physiological temperature, i.e. 37 °C and at a pH = 7.4; however, we are not aware of any of these studies being performed using “perfect sink” conditions. For future studies, the release from the PCL-*b*-PEO micelles should be performed under physiological conditions (i.e., 37 °C, pH = 7.4) and using PBS while maintaining true sink conditions.

Fourier transform infrared (FTIR) spectroscopic imaging has been used to study polymer/drug formulations in contact with aqueous solution.<sup>7</sup> This technique provides specific chemical information on the materials of interest obtained from their IR spectra. FTIR has the advantage of having faster acquisition times than NMR imaging, and is noninvasive and nondestructive.<sup>7</sup> FTIR can be coupled with attenuated total reflectance infrared [(ATR)-IR] microscopic imaging which is useful for the study of aqueous solutions.<sup>7</sup> The combination of the two techniques could be used to study the release of a drug and potentially reveal the mechanism of release for the micellar and vesicular formulations.

Various liposomes and micellar systems have been used in order to incorporate various contrast agents (i.e., Gd or Tc) for magnetic resonance imaging (MRI).<sup>8</sup> Metals were attached to poly(4-vinylpyridine)-*block*-poly(ethylene oxide) micelles such as gold for cellular internalization. Conceivably, Gd or Tc could be attached to these micelles for MRI studies. In addition, PCL-*b*-PEO micelles could incorporate either of these contrast agents inside the PCL core.

Finally, radiolabeled micelles would also provide another quantitative means of determining how many micelles are located in the different subcellular compartments (i.e., endosomes and lysosomes). This information coupled, with the results previously obtained by our group for fluorescently labeled micelles and gold labeled micelles would provide a more complete picture in terms of the cellular internalization of block copolymer micelles.

### 7.3. References

- (1) Zhao, J.; Allen, C.; Eisenberg, A. *Macromolecules* **1997**, *30*, 7143-7150.
- (2) Allen, C.; Yu, Y.; Maysinger, D.; Eisenberg, A. *Bioconjugate Chemistry* **1998**, *9*, 564-572.
- (3) Allen, C.; Han, J.; Yu, Y.; Maysinger, D.; Eisenberg, A. *Journal of Controlled Release* **2000**, *63*, 275-286.
- (4) Kabanov, A. V.; Nazarova, I. R.; Astafieva, I. V.; Batrakova, E. V.; Alakhov, V. Y.; Yaroslavov, A. A.; Kabanov, V. A. *Macromolecules* **1995**, *28*, 2303-2314.
- (5) Yang, L.; Alexandridis, P. *Current Opinion in Colloid and Interface Science* **2000**, *5*, 132-143.
- (6) Liu, J.; Xiao, Y.; Allen, C. *Journal of Pharmaceutical Sciences* **2004**, *93*, 132-143.
- (7) Kazarian, S. G.; Chan, K. L. A. *Macromolecules* **2003**, *36*, 9866-9872.
- (8) Torchilin, V.; Babich, J.; Weissig, V. *Journal of Liposome Research* **2000**, *10*, 483-499.

## **Appendix**

short core-forming block (one which is able to interact with metal compounds); thus, the presence of metal ions can lead to different morphologies. When fully protonated PEO-*b*-P2VP was allowed to interact with metal compounds, micelle formation was also induced, resulting in formation of spherical micelles.<sup>22</sup>

In this paper, we report on the micellization of a PEO<sub>45</sub>-*b*-P4VP<sub>28</sub> block copolymer in water. We follow the micelle transformations after metalation with three types of gold compounds followed by reduction, resulting in gold particle formation in the micelle cores. Unlike P2VP, P4VP units are subject to stronger interactions between each other and with the metal compounds, which results in a significant difference in the micellization behavior of this block copolymer in water.

### Experimental Section

**Materials.** CH<sub>2</sub>Cl<sub>2</sub> (99.6%, Aldrich) was purified by shaking with a small amount of H<sub>2</sub>SO<sub>4</sub> twice until the acid remained nearly colorless. Then CH<sub>2</sub>Cl<sub>2</sub> was washed with water (twice), then with a 5% solution of NaHCO<sub>3</sub>, again with water (twice), and then left under anhydrous CaCl<sub>2</sub> overnight. The CH<sub>2</sub>Cl<sub>2</sub> was then mixed with CaH<sub>2</sub> for 1 h, boiled for 2 h, and distilled over CaH<sub>2</sub>. Toluene (99.5%, Aldrich) was kept under CaCl<sub>2</sub> overnight and then distilled. AuCl<sub>3</sub> (99.99%), HAuCl<sub>4</sub>·3H<sub>2</sub>O (99.9+%), NaAuCl<sub>4</sub>·H<sub>2</sub>O (99.999%), and hydrazine hydrate (N<sub>2</sub>H<sub>4</sub>·H<sub>2</sub>O, 98+%) were purchased from Aldrich and used as received.

Poly(ethylene glycol) monomethyl ether (PEO,  $M_n$ (calculated) = 2000 g/mol, Aldrich), was dried by distillation of water as the azeotrope with toluene. PEO was mixed with toluene (7 mL of toluene per 1 g of PEO) and distilled at 125–130 °C. After evaporation of the toluene, PEO was dried under vacuum at 65 °C for 1 h. The product was stored under argon.

4-Vinylpyridine (4VP, Aldrich) was stirred with a small amount of CaH<sub>2</sub> at 40–50 °C for 2 h. Then 4VP was decanted, degassed via three freeze–thaw cycles, and distilled under vacuum into a Schlenk tube. The Schlenk tube containing 4VP filled with argon was stored in a refrigerator at –15 °C. 2-Propanol (2-PrOH) was purified in a manner similar to that used for 4VP and stored under argon at room temperature. 2-Chloropropionyl chloride (2CPC, 97%, Aldrich), triethylamine (TEA, >99.5%, Fluka), and CuCl (98+, Aldrich) were used as received. Tris-(2-dimethylaminoethyl)amine (Me<sub>6</sub>TREN) was obtained as described elsewhere.<sup>23</sup>

**Synthesis. Modification of PEO with 2-Chloropropionyl Chloride.** PEO with a 2-chloropropionyl terminated group (PEO-2CPC) was prepared using a modified version of the technique described by Jankova et al.<sup>24</sup> The modification consisted of the use of only TEA as the HCl absorber. No polymer chain destruction was observed.

**Synthesis of PEO-*b*-P4VP.** The PEO-*b*-P4VP block copolymer was synthesized by atom transfer radical polymerization (ATRP) of 4VP with a PEO-2CPC macroinitiator using an approach described by Matyjaszewski et al.<sup>25</sup> A Schlenk tube equipped with a magnetic stir bar was loaded with 0.107 g (1.08 mmol) of CuCl, 9.6 mL of 2-PrOH, 4.54 g (43.2 mmol) of 4VP, and 0.249 g (1.08 mmol) of Me<sub>6</sub>TREN, degassed via three freeze–thaw cycles and stirred until the complete dissolution of CuCl. Then degassed PEO-2CPC (2.88 g, 44 mmol) was added into the Schlenk tube in argon counterflow at 40 °C under vigorous stirring. The homogeneous mixture in the Schlenk tube was placed in a bath at 50 °C, stirred for 8 h, and kept overnight at room temperature. The Schlenk tube content was then dissolved in 50 mL of THF, and the 4VP conversion was evaluated by gas chromatography (95%). The solution was filtered through Al<sub>2</sub>O<sub>3</sub> powder to remove

Cu complex, and the THF was distilled off until a residual volume of 20 mL was obtained. The polymer was precipitated in diethyl ether and dried under vacuum at 40 °C for 5 h. The yield was 5.6 g (76%). The number-average degree of polymerization of the P4VP blocks was determined from the degree of polymerization of the PEO (45) using <sup>1</sup>H NMR (CDCl<sub>3</sub>). In the resulting PEO-*b*-P4VP copolymer, the molecular weight of P4VP block was 2940; i.e., the degree of polymerization was 28. The polydispersity ( $M_w/M_n$ ) of the copolymer was 1.23 using size exclusion chromatography, performed under the conditions described elsewhere.<sup>26</sup>

**Metalation of PEO<sub>45</sub>-*b*-P4VP<sub>28</sub> Micelles.** PEO<sub>45</sub>-*b*-P4VP<sub>28</sub> block copolymers were dissolved in water to provide a 4 g/L concentration. To 4 mL of PEO<sub>45</sub>-*b*-P4VP<sub>28</sub> solution 8.1 × 10<sup>-3</sup> g (2.64 × 10<sup>-5</sup> mol) of AuCl<sub>3</sub> (or 10.5 × 10<sup>-3</sup> g of HAuCl<sub>4</sub>·3H<sub>2</sub>O, or 9.6 × 10<sup>-3</sup> g of NaAuCl<sub>4</sub>·H<sub>2</sub>O) was added to provide a molar ratio 4VP: Au = 4:1, while for the molar ratio 4VP:Au = 8:1 half the amount of gold compound was used. After the solution containing the gold complex was stirred for 2 days, it was reduced with 5-fold molar excess of hydrazine hydrate (6.5 × 10<sup>-3</sup> mL for a molar ratio 4VP:Au = 4:1).

**Characterization.** Dynamic light scattering (DLS) measurements were performed on a Brookhaven Instruments photon correlation spectrophotometer with a BI9000 AT digital correlator. The instrument is equipped with a compass 315M-150 laser (Coherent Technologies), which was used at a wavelength of 532 nm. Dust-free vials were used for the aqueous solutions, and measurements were made at 20 °C at an angle of 90°. The CONTIN algorithm was used to analyze the data.

Transmission electron microscopy (TEM) studies were conducted using a JEOL 2000FX instrument operating at an acceleration voltage of 80 kV. Dilute solutions of the gold-labeled micelles were deposited on copper grids (400 mesh) that had been precoated with a thin film of Formvar (poly(vinylformal)) and then coated with carbon. The samples were applied to the grids and allowed to air-dry overnight.

UV–vis spectra were recorded on a Cary 50 Bio UV–Visible Spectrophotometer (Varian, USA), equipped with two silicon diode detectors and a xenon flash lamp.

### Results and Discussion

**PEO<sub>45</sub>-*b*-P4VP<sub>28</sub> Micelles before Metalation.** The synthesis of the PEO<sub>45</sub>-*b*-P4VP<sub>28</sub> block copolymer was carried out using ATRP of 4VP with modified monomethylated PEO as a macroinitiator (see Experimental Section). Similar to PEO-*b*-P2VP, water is a selective solvent for this block copolymer; however, while PEO-*b*-P2VP becomes molecularly soluble at a pH of 5.0,<sup>12</sup> PEO<sub>45</sub>-*b*-P4VP<sub>28</sub> requires a slightly lower pH (4.5–4.7) for its dissolution.

Direct dissolution of PEO<sub>45</sub>-*b*-P4VP<sub>28</sub> in water at room temperature for 24 h results in a turbid solution denoted as “as-prepared” PEO<sub>45</sub>-*b*-P4VP<sub>28</sub>. A mean micelle diameter obtained from DLS is 57 nm, and the micelle size distribution is broad (Figure 1a). The value of the mean micelle diameter greatly exceeds the value for a hypothetical micelle with fully extended block copolymer chains (about 38 nm). This can be due to two possible reasons: either the micelles are not spherical or, along with the spherical micelles, micellar aggregates are formed. The TEM image of this sample, presented in Figure 1b, shows a mixture of spherical micelles with a mean diameter of about 24 nm and rodlike micelles with the same cross-sectional diameter (about 24 nm) and lengths ranging from 75 to 180 nm. Evidently, due to the presence of rodlike micelles, the DLS data do not reflect the actual micelle size. A close look at the TEM image shows that, in some cases, the rodlike micelles are actually necklace-like; i.e., they consist of spherical micelles attached to each other, suggesting that rods form by collision of the spherical micelles followed by fusion. These phenomena have been

(21) Chernyshov, D. M.; Bronstein, L. M.; Boerner, H.; Berton, B.; Antonietti, M. *Chem. Mater.* **2000**, *12*, 114.

(22) Bronstein, L. M.; Sidorov, S. N.; Valetsky, P. M.; Hartmann, J.; Coelfen, H.; Antonietti, M. *Langmuir* **1999**, *15*, 6256.

(23) Ciampolini, M.; Nardi, N. *Inorg. Chem.* **1966**, *5*, 41.

(24) Jankova, K.; Chen, X.; Kops, J.; Batsberg, W. *Macromolecules* **1998**, *31*, 538.

(25) Xia, J.; Zhang, K.; Matyjaszewski, K. *Macromolecules* **1999**, *32*, 3531.

(26) Fragouli, P. C.; Iatrou, H.; Hadjichristidis, N. *Polymer* **2002**, *43*, 7141.

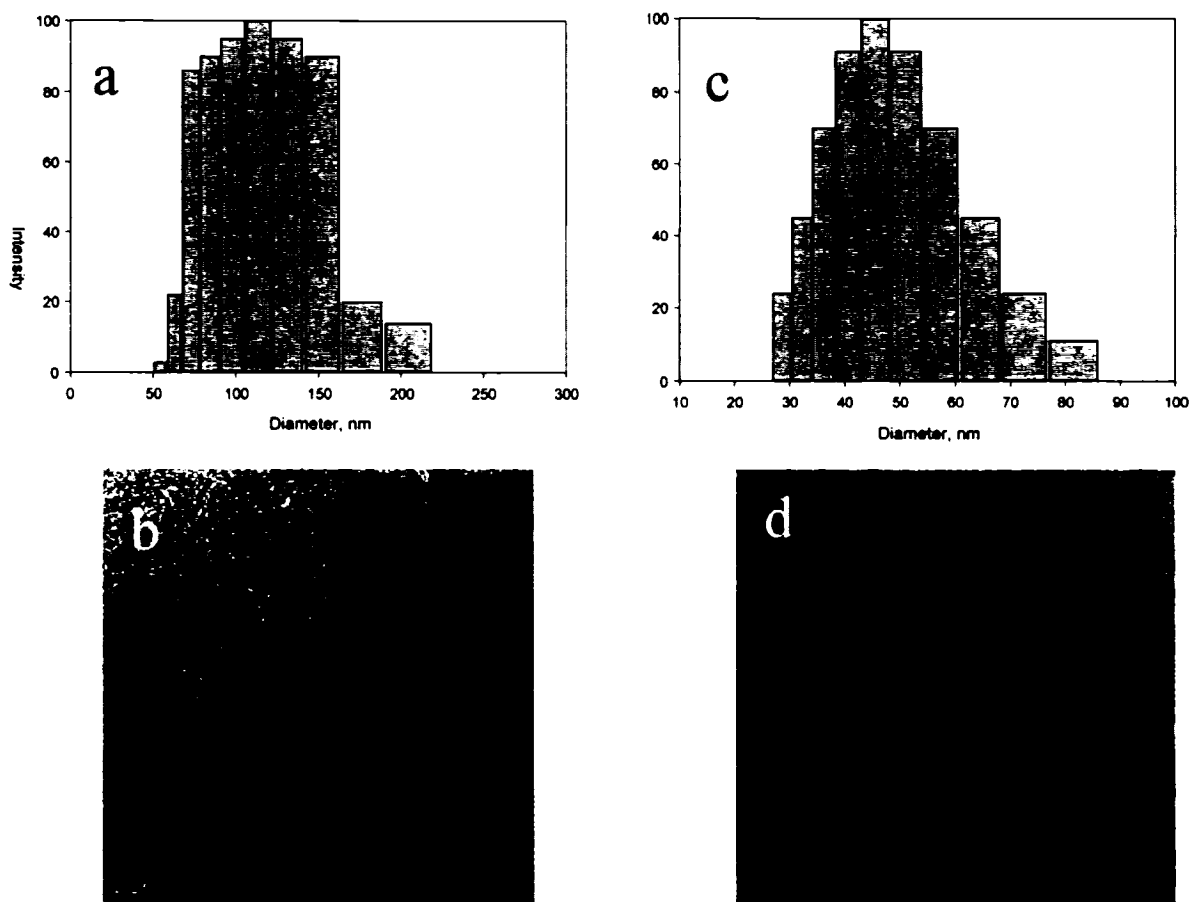


**Figure 1.** Light scattering data (a, c) and TEM images (b, d) of as-prepared PEO<sub>45</sub>-*b*-P4VP<sub>28</sub> (a, b) and PEO<sub>45</sub>-*b*-P4VP<sub>28</sub> after thermal treatment at 70 °C for 3 days (c, d). Scale bar is 200 nm.

**Table 1. Characteristics of Metalated PEO<sub>45</sub>-*b*-P4VP<sub>28</sub> Micelles**

block copolymer notation <sup>a,b</sup>	gold compound	4VP: Au (mol)	pH		micelle diameter (nm)				$d_{TEM}^c$ (nm)
			before reduction	after reduction	before reduction		after reduction		
					DLS	TEM	DLS	TEM	
as prepared					57.0	23.7 ± 2.5			
thermally treated					47.5	28.5 ± 4.3			
P-19	NaAuCl <sub>4</sub> ·H <sub>2</sub> O	4:1	4.22	7.39	73.0	28.5 ± 3.6	57.0	20.0 ± 2.3	7.3 ± 1.10
T-26		4:1	3.49	7.40	74.0	27.0 ± 3.0	112	28.0 ± 6.7	8.6 ± 1.36
P-9	HAuCl <sub>4</sub> ·3H <sub>2</sub> O	4:1	2.45	5.18	99.0	21.0 ± 3.2	102	23.0 ± 2.6	9.1 ± 1.24
P-10		8:1	3.34	5.01	105	22.0 ± 2.7	67.0	22.0 ± 4.7	3.6 ± 0.73
T-24		4:1	2.83	6.06	62.0	29.5 ± 5.7	43.0	25.0 ± 5.8	4.5 ± 0.69
T-25		8:1	3.39	4.57	69.0	23.0 ± 3.7	48.0	27.0 ± 5.7	4.6 ± 0.63
P-7	AuCl <sub>3</sub>	4:1	2.71	5.56	97.1	24.0 ± 2.7	65.2	17.5 ± 2.5	3.6 ± 0.84
P-8		8:1	3.47	5.26	96.0	21.5 ± 2.9	58.0	26.0 ± 5.3	3.9 ± 0.73

<sup>a</sup> P, as prepared. <sup>b</sup> T, thermally treated. <sup>c</sup> Au particle diameter.

explored in some detail recently.<sup>27</sup> It is noteworthy that formation of irregular aggregates is negligible while necklace-type aggregation prevails.

On the other hand, one might suggest that these rods are nonequilibrium structures because thermal treatment of the as-prepared block copolymer at 70 °C for 3 days transforms the rods into spherical micelles (see Figure 1d) of a larger diameter (28.5 nm). The mean micelle diameter found from DLS data is again much higher: 47.5 nm (Figure 1c). This can be explained by formation of some fused micelles (out of two or more individual micelles) and larger micellar aggregates (Figure 1d) which strongly influence the light scattering and the average micelle size.

In the following sections we describe the micelle transformations during metalation in both as-prepared micellar solutions (notation "P" in Table 1) and in thermally treated ones (notation "T" in Table 1).

**Metalation with a Neutral NaAuCl<sub>4</sub>.** Incorporation of a neutral salt (NaAuCl<sub>4</sub>) into the as-prepared micellar solution at molar ratio 4VP: Au = 4:1 (P-19) leads to an increase of the micelle size to 28.5 nm, while the amount of rodlike micelles remains unchanged (Figure 2a). It is worth mentioning that incorporation of NaAuCl<sub>4</sub> into the PEO-*b*-P2VP micelles at the same molar ratio induced no changes in the micelle sizes.<sup>22</sup> Apparently, the complexation of the nitrogen atoms (complexation occurs by replacement of Cl in AuCl<sub>4</sub><sup>-</sup> ions) located in the *p*-position relative to the polymer chain disturbs the micelle core,

(27) Burke, S. E.; Eisenberg, A. *Langmuir* 2001, 17, 6705.

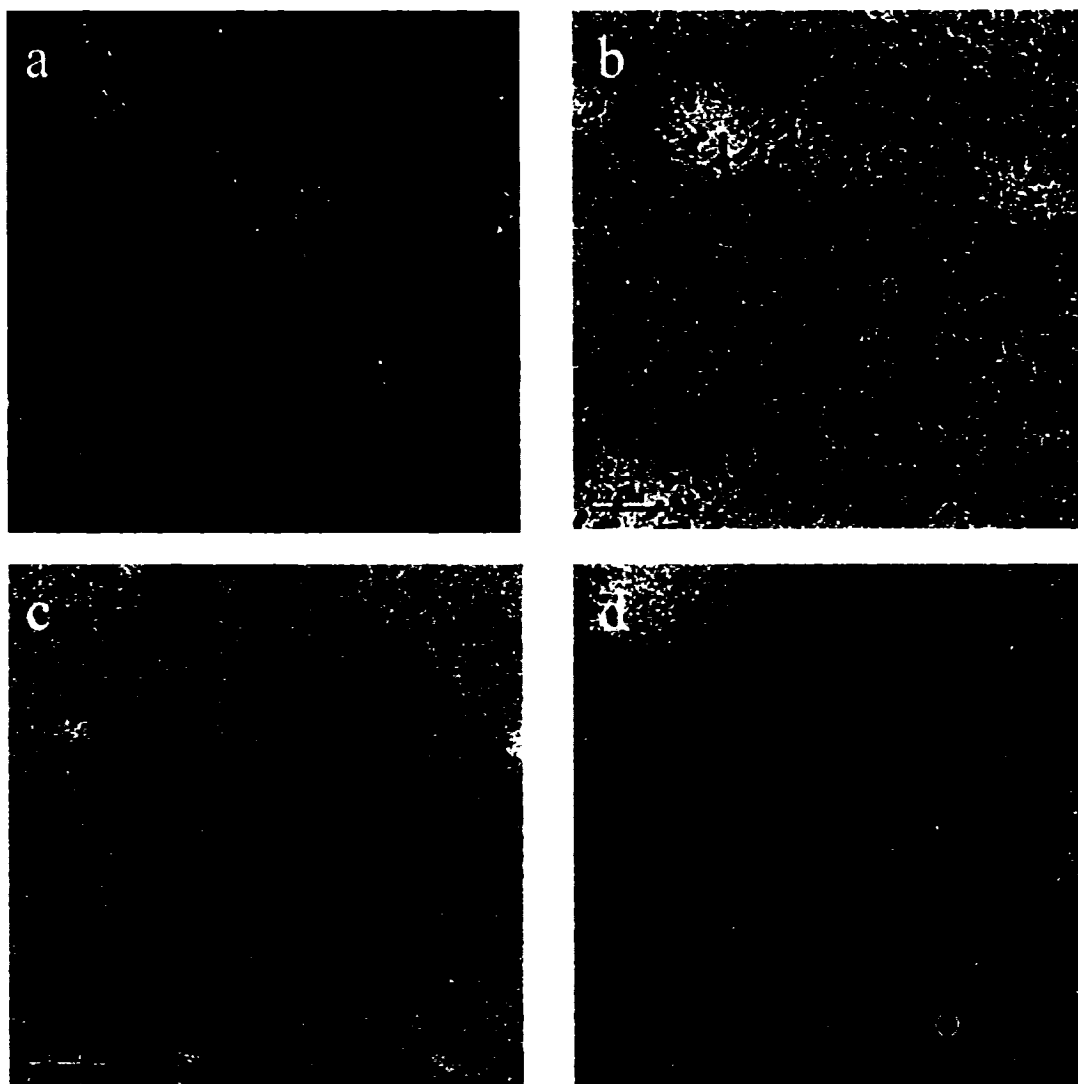


**Figure 2.** TEM images of as-prepared (a, b) and thermally treated (c, d) PEO<sub>45</sub>-*b*-P4VP<sub>28</sub> loaded with NaAuCl<sub>4</sub> at molar ratio 4VP: Au = 4:1 before (a, c) and after (b, d) reduction.

resulting in a change in the micelle size. The higher value of the mean diameter obtained from DLS data is caused by an increase of the spherical micelle size as well as some extramolecular aggregation. Reduction of the metal complexes with hydrazine hydrate leads to the formation of gold particles with a mean diameter of 7.3 nm both for the spherical micelles and the rods (Figure 2b). After reduction, both the spherical micelles and the rods shrink (to a mean diameter of 20.0 nm) despite the fact that the micelles have to accommodate the nanoparticles. Since the reduction results in no visible increase or decrease of the rodlike micelle fraction, we can speculate that the decrease in the micelle size occurs solely due to an increase of the micelle density and not due to the change in the aggregation number.

When metalation with NaAuCl<sub>4</sub> is carried out with the thermally treated block copolymer solution (T), incorporation of the metal salt induces micelle fusion (Figure 2c). Instead of mainly individual micelles in T, in the T-26 sample (Table 1) one can see small rods and rod bundles. This sample looks very similar to the P-19 sample and is characterized by similar micellar parameters (see Table 1). This shows that the sphere-to-rod transition is favored for larger micelles. Clearly, in the larger T micelles, metal complexes are easily accommodated without a change of

the micelle size. When these metalated micelles are reduced with hydrazine hydrate (Figure 2d), the individual micelle size does not change. It should be mentioned that, along with small spherical and rodlike micelles, this sample also contains large spherical aggregates. The size histograms of the micelles shown in Figure 2a–d, are presented in Figure 3.

**Metalation with HAuCl<sub>4</sub>.** Incorporation of HAuCl<sub>4</sub> results in local protonation of the 4VP units (protonation only of those units which participate in complexation) followed by electrostatic interaction of the quaternary ammonium species with AuCl<sub>4</sub><sup>-</sup> anions. Protonation might result in swelling of the micelle cores (fully protonated P4VP is soluble in water) due to increase in osmotic pressure.<sup>28,29</sup> However, as can be seen from Table 1 and Figure 4a,c, incorporation of HAuCl<sub>4</sub> at molar ratios of 4VP: Au = 8:1 and 4:1 in the as-prepared polymer does not result in an increase in the micelle size. On the contrary, micelles are even slightly smaller and the rods are very short. The necklace-type micelles and the majority of the

(28) Kostarelou, K.; Luckham, P. F.; Tadros, T. F. *J. Chem. Soc., Faraday Trans.* **1998**, *94*, 2159.

(29) Groenewegen, W.; Egelhaaf, S. U.; Lapp, A.; van der Maarel, J. R. C. *Macromolecules* **2000**, *33*, 3283.

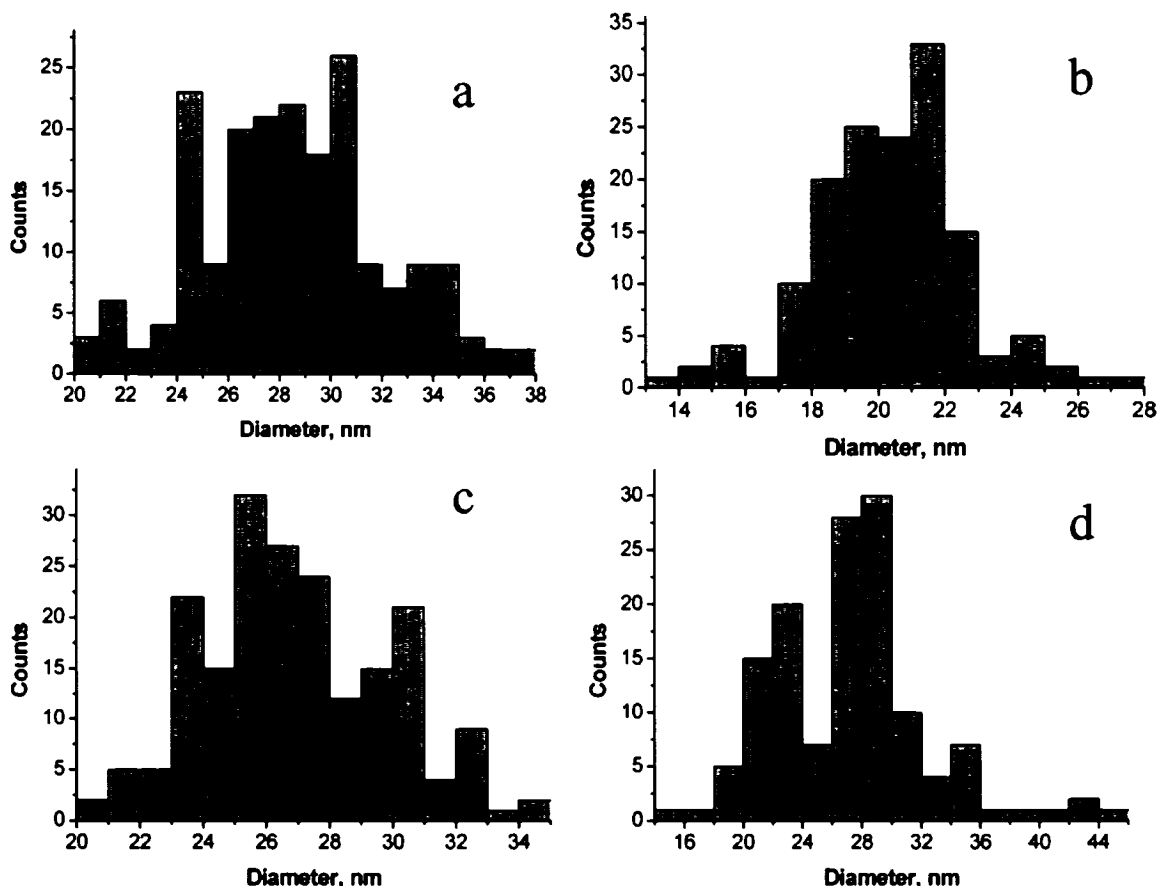


**Figure 3.** Particle size histograms derived from TEM images such as those presented in Figure 2. On average, the mean diameters were calculated for 150 micelles.

rods disintegrate; thus, not surprisingly, protonation suppresses regular aggregation of the PEO<sub>45</sub>-*b*-P4VP<sub>28</sub> micelles. The higher values of the mean diameters obtained from DLS measurements can be explained by the presence of a few large aggregates, which influence the scattering, but which do not appear on the TEM images (on average, the mean diameters were calculated from 150 micelles).

When HAuCl<sub>4</sub>-filled micelles are reduced with hydrazine hydrate, two events take place: (i) gold nanoparticle formation (Figure 4b,d) and (ii) an increase of the pH of the micellar solution and deprotonation of pyridine units (Table 1). These changes result in the formation of a larger fraction of rodlike micelles, while the micelle diameters practically do not change. Increase of pH in the absence of a reducing agent does not induce a similar morphological change. An increase in the HAuCl<sub>4</sub> loading (4VP: Au = 4:1) results in an even more prominent increase of the rodlike micelle fraction. Here, the change of micelle morphology occurs during gold compound reduction. However, the thermally treated PEO<sub>45</sub>-*b*-P4VP<sub>28</sub> block copolymer micelles filled with HAuCl<sub>4</sub> and reduced with hydrazine hydrate (Figure 5) do not show a similar trend: the TEM images of these samples look practically identical to those of block copolymer derived from NaAuCl<sub>4</sub> after reduction (Figure 2d). This surprising difference is likely due to different packing in the as-prepared and thermally treated PEO<sub>45</sub>-*b*-P4VP<sub>28</sub> micelles filled with HAuCl<sub>4</sub>. One can assume that, in the former case, the P4VP chains are very densely packed within the smaller micelle cores, so a sharp change of pH during reduction might cause strong morphological change. In the case of a thermally treated

sample, micelles are less dense so a pH change clearly does not change morphology.

**Metalation with AuCl<sub>3</sub>.** Dissolution of AuCl<sub>3</sub> in aqueous solution results in the hydrolysis of AuCl<sub>3</sub> followed by the formation of the corresponding acid, HAuCl<sub>3</sub>(OH).<sup>30</sup> Indeed, incorporation of AuCl<sub>3</sub> and HAuCl<sub>4</sub> results in solutions with similar pH values (Table 1), while incorporation of a neutral salt gives solutions with higher pH values. Based on the acidic nature of HAuCl<sub>3</sub>(OH) and its ability to protonate P4VP, one might expect that micelle characteristics of AuCl<sub>3</sub>-filled and HAuCl<sub>4</sub>-filled PEO<sub>45</sub>-*b*-P4VP<sub>28</sub> micelles should be similar. Indeed, comparison of Figures 4a and 6a and Table 1 shows that micellar diameters are similar and that the fraction of rodlike micelles is low. However, samples P-10 and P-8 obtained after reduction of the gold compounds with hydrazine hydrate are quite different. The AuCl<sub>3</sub>-based sample, after reduction, contains an amount of rods and spheres similar to that of the nonreduced sample (Figure 6), while the HAuCl<sub>4</sub>-based sample contains a higher fraction of rods (compare Figure 4a,b). The major difference between AuCl<sub>3</sub>(OH)<sup>-</sup> and AuCl<sub>4</sub><sup>-</sup> is the presence of the OH ligand, which is able to form hydrogen bonds with nonprotonated pyridine units.<sup>31,32</sup> This factor can impede diffusion of gold ions within the micelle core, thus decreasing the attractive forces between micelles during reduction (which results

(30) Wilkinson, G. *Comprehensive coordination chemistry: the synthesis, reactions, properties, & applications of coordination compounds*; Pergamon Press: New York, 1987.

(31) Jeffrey, G. A. *An introduction to hydrogen bonding*; Oxford University Press: New York, 1997.

(32) Wojtulewski, S.; Grabowski, S. J. *Chem. Phys. Lett.* **2003**, *378*, 388.

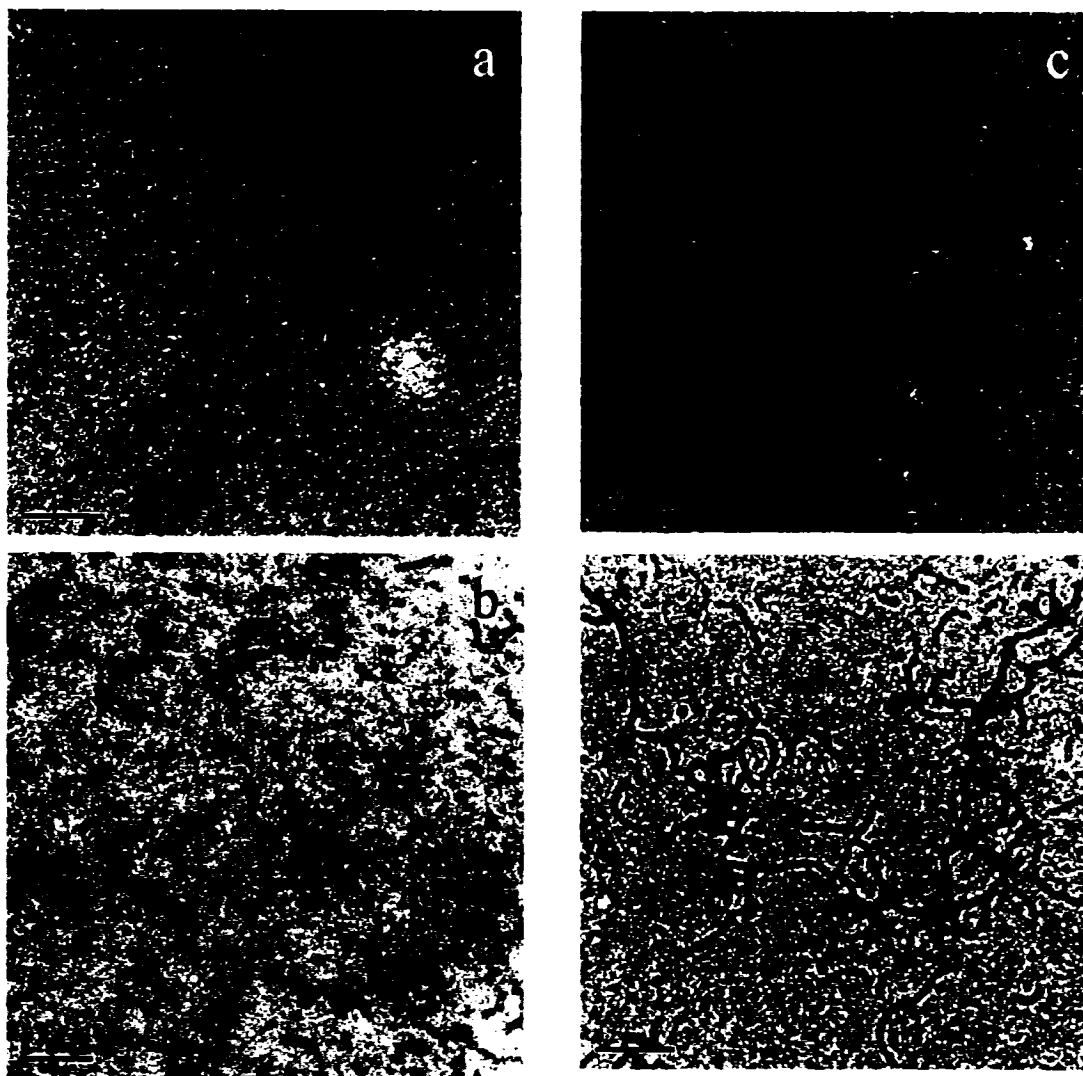


**Figure 4.** TEM images of metalated block copolymer micelles based on as-prepared PEO<sub>45</sub>-*b*-P4VP<sub>28</sub> after incorporation of H<sub>2</sub>O (a, c) and after Au nanoparticle formation (b, d). In images a and b, molar ratio 4VP: Au = 8:1, while in images c and d 4VP: Au = 4:1. Scale bar is 200 nm.

in the absence of rod formation) and limiting the gold particle size (see the next section).

**Gold Nanoparticles.** The size of the nanoparticles prepared by the reduction of the gold species in block copolymer micelles normally depends on a number of parameters, such as the type of reducing agent and the loading of the metal precursor.<sup>33</sup> The former parameter determines the rate of nucleation and particle growth: slow reduction produces large particles, while fast reduction gives small particles. The metal compound loading factor determines the local concentration of metal species: the higher the concentration, the larger the particles. Although in this work we used only hydrazine hydrate (a sluggish reducing agent), the rate of nucleation might vary, since in the aqueous system it can depend on the pH of the reacting solution.<sup>34</sup> Another important factor is the micelle density. At the same level of metal compound loading, a higher micelle density will provide a higher local concentration of the metal species, but also higher diffusion limitations. In turn, the micellar density of the

Brønsted basic block copolymers depends on the pH. All these factors influence the nanoparticle size. As a result, in block copolymer micelles filled with NaAuCl<sub>4</sub>, where no local protonation or pH change take place, the nanoparticles are comparatively large in both the P and the T samples, suggesting that the micelles are dense and nucleation is slow. At the same time, in the AuCl<sub>3</sub>-filled and HAuCl<sub>4</sub>-filled micelles with similar pH values, nanoparticle formation is different. Despite the local protonation of the pyridine units, the strong interaction of AuCl<sub>3</sub>(OH)<sup>-</sup> ions with the nonprotonated P4VP core results in smaller particles than in HAuCl<sub>4</sub>-filled micelles. On the contrary, easy diffusion of metal species in HAuCl<sub>4</sub>-filled micelles and attractive forces between micelles during reduction result in the facilitated exchange between micelles, leading to uneven distribution of large nanoparticles. This is especially clearly seen for P-9 after reduction (Figure 4d) where some rods contain a few nanoparticles, while others contain many nanoparticles.

Based on the mean micellar diameter of ca. 24 nm ( $23.7 \pm 2.5$  nm, root-mean-square error =  $\pm 0.7$  nm) and the approximate block copolymer density of  $1 \text{ g/cm}^3$ , one can calculate the weight of one micelle ( $7.24 \times 10^{-18}$  g) and the number of micelles for a block copolymer loading

(33) Antonietti, M.; Wenz, E.; Bronstein, L.; Seregina, M. *Adv. Mater.* **1995**, *7*, 1000.

(34) Antonietti, M.; Gröhn, F.; Hartmann, J.; Bronstein, L. *Angew. Chem., Int. Ed. Engl.* **1997**, *36*, 2080.

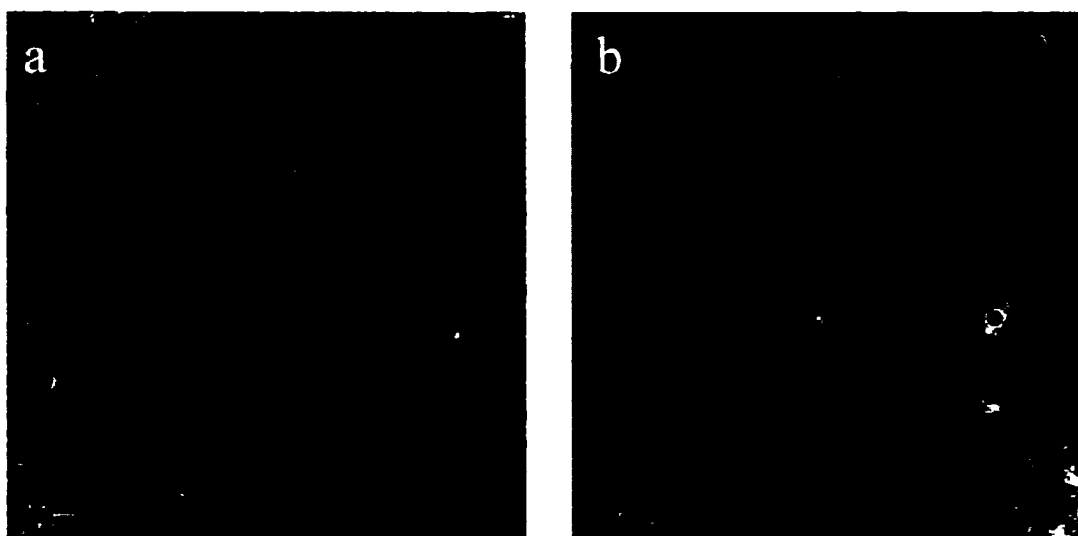


**Figure 5.** TEM images of metalated block copolymer micelles based on thermally treated PEO<sub>45</sub>-*b*-P4VP<sub>28</sub> and HAuCl<sub>4</sub>·H<sub>2</sub>O after Au nanoparticle formation. Molar ratios are 4VP: Au = 8:1 for T-25 (a) and 4VP: Au = 4:1 for T-24 (b). Scale bar is 200 nm.

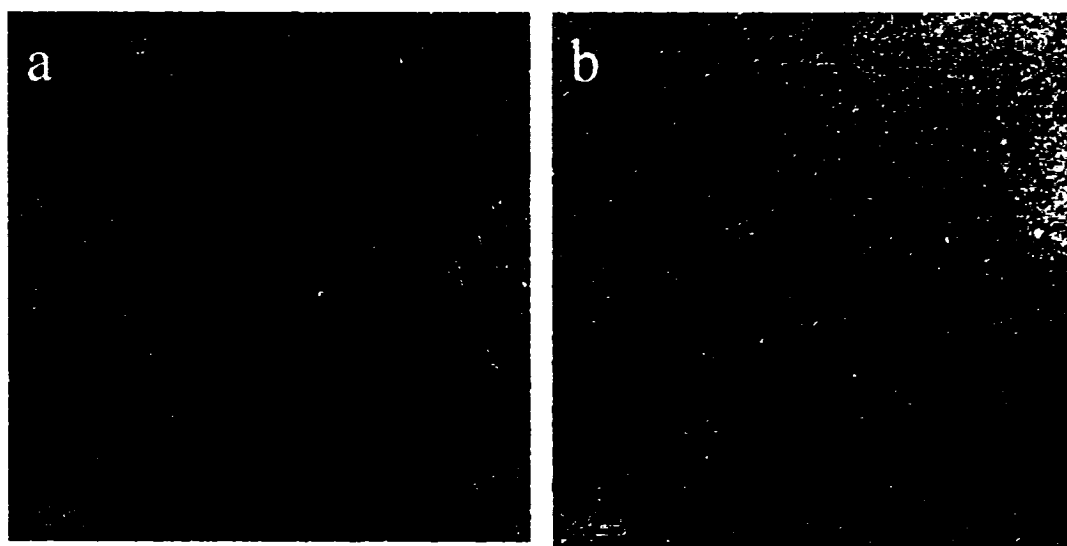


**Figure 6.** TEM images of metalated block copolymer micelles based on as-prepared PEO<sub>45</sub>-*b*-P4VP<sub>28</sub> after incorporation of AuCl<sub>3</sub> at molar ratio 4VP: Au = 8:1 (a) and after Au nanoparticle formation (b). Scale bar is 200 nm.

of 0.016 g, yielding the value of  $2.21 \times 10^{15}$ . Based on the HAuCl<sub>4</sub>·3H<sub>2</sub>O loading ( $2.64 \times 10^{-5}$  mol) and Avogadro's number ( $6.02 \times 10^{23}$ ), the micellar solution contains  $1.59 \times 10^{19}$  gold atoms. In the case of even distribution of HAuCl<sub>4</sub>·3H<sub>2</sub>O molecules in micelles, each micelle should contain  $7.19 \times 10^3$  gold atoms. Using van der Waals Au radius of ca. 0.17 nm, one can calculate the particle size, assuming that each gold particle is formed from the all the gold atoms contained in each micelle. This calculation yields a particle diameter of 6.4 nm. Thus, formation of gold nanoparticles with a mean diameter of 9.1 nm suggests active exchange between micelles leading to uneven distribution of gold nanoparticles.

Figure 7 presents UV-vis spectra of the micellar solutions P-7, P-8, P-9, and P-10 (Table 1) after gold nanoparticle formation. The absorbance spectra have been normalized at a common wavelength, 520 nm, to allow an easy comparison of the peak widths. One can see that the positions of the absorption peaks and their widths are very close for all four samples, independent of the particle size. This is in good agreement with the prediction of a classical Mie theory for spherical particles with diameters

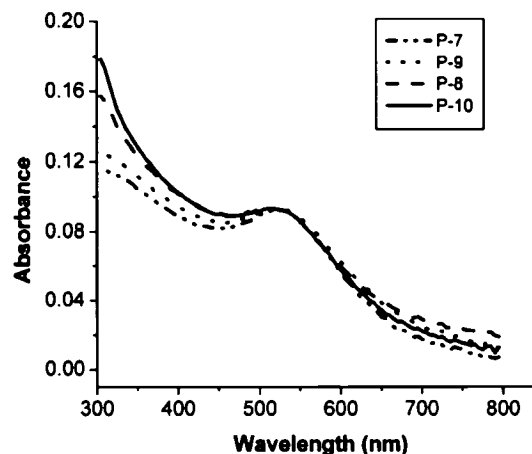


**Figure 7.** UV-vis spectra of P-7, P-8, P-9, and P-10 samples (see Table 1 for details) with absorption maxima at 520.1, 517.6, 520.1, and 515.1 nm. The absorbance spectra have been normalized at a common wavelength, 520 nm, to allow an easy comparison of the peak widths.

of about 10 nm and smaller,<sup>35</sup> where the plasmon band position becomes independent of the particle size.

### Conclusions

We have investigated the influence of metalation (incorporation of gold compounds and gold nanoparticle formation) on the morphologies of the PEO<sub>45</sub>-*b*-P4VP<sub>28</sub> block copolymer micelles, and the sphere-to-rod micellar transition. Direct dissolution of PEO<sub>45</sub>-*b*-P4VP<sub>28</sub> in water at room temperature results in solutions containing both spherical and rodlike micelles, while thermal treatment of this solution leads to rod disassembly. At the same time, incorporation of a neutral gold salt (NaAuCl<sub>4</sub>) into the thermally treated block copolymer solution again induces sphere-to-rod transition so that the NaAuCl<sub>4</sub>-filled samples derived from as-prepared and thermally treated block copolymer solutions are similar. This indicates that the mixture of spheres and rods is favorable for these metalated micelles.

By contrast, the incorporation of HAuCl<sub>4</sub>, which causes

the protonation of the pyridine units, does not promote a sphere-to-rod transition, while reduction with hydrazine hydrate does. We ascribe this effect to a high density of as-prepared micelles filled with HAuCl<sub>4</sub>, slow nucleation, and easy transport of gold ions; thus, an increase of pH yields a morphological change and also the largest gold particle size (9.1 nm) in this system.

However, this is not the case for AuCl<sub>3</sub>, which transforms into HAuCl<sub>3</sub>(OH) under dissolution in water. The major difference between AuCl<sub>3</sub>(OH)<sup>-</sup> and AuCl<sub>4</sub><sup>-</sup> is the presence of the OH ligand, which is able to form hydrogen bonds with nonprotonated pyridine units, impeding the diffusion of gold ions within the micelle core, thus decreasing the attractive forces between micelles during reduction (which results in the absence of rod formation), and limiting the gold particle size.

**Acknowledgment.** We sincerely thank the NATO Science for Peace Programme (Grant SfP-974173), Russian Foundation for Basic Research (Grant RFBR-01-03-32937), and NSERC for financial support of this research.

LA0360658

---

(35) Wilcoxon, J. P.; Martin, J. E.; Provencio, P. *J. Chem. Phys.* **2001**, *115*, 998.

*b*-polyethylene oxide (PCL<sub>21</sub>-*b*-PEO<sub>44</sub>) micelles containing the fluorescent probe DiI, one of a large group of dialkylindocarbocyanine derivatives [11]. Several non-micelle-incorporated members of this class of compounds have been recently utilized for studies of their trafficking in CHO cells by quantitative fluorescent microscopy [12]. Findings from these studies show that all investigated dyes enter sorting endosomes and suggest that endocytic organelles can sort DiI analogs based on their preference for association with the alkyl tail length or degree of unsaturation.

The aim of the present studies was to investigate the influence of block copolymer PCL<sub>21</sub>-*b*-PEO<sub>44</sub> in modulating or re-directing uptake of micelle-incorporated DiI. We employed primary neural cultures at different stages of development *in vitro* (from days 2 (2DIV) to 14 (14DIV)). Results from these studies suggest that both the block copolymer and age of neural cultures *in vitro* profoundly alter the rate and degree of DiI internalization.

## 2. Materials and methods

### 2.1. Materials

Cell Tracker<sup>®</sup> DiI was purchased from Molecular Probes. [<sup>3</sup>H]Benzo[*a*]pyrene ([<sup>3</sup>H]B(a)P) was obtained from Amersham Pharmacia. Some relevant physical

parameters of these agents are summarized in Table 1. Scintillation cocktail OptiPhase HiSafe 2 (Wallac) was purchased from Perkin Elmer Life Sciences. All tissue culture supplies were obtained from Gibco BRL. Tissue culture chambers were from Nunclon.

### 2.2. Methods

#### 2.2.1. Preparation of micelles containing DiI

The poly(caprolactone)<sub>21</sub>-*b*-poly(ethylene oxide)<sub>44</sub>, PCL<sub>21</sub>-*b*-PEO<sub>44</sub>, block copolymer ( $M_r = 4330$  g/mol) was synthesized by anionic polymerization [14]. Ten  $\mu$ l of 10  $\mu$ M DiI (dissolved in dimethylformamide (DMF)) were placed in an empty glass vial and solvent was evaporated. Five mg of PCL<sub>21</sub>-*b*-PEO<sub>44</sub> were dissolved in 0.15 g of DMF and added to the vial containing DiI. The solution was stirred for 4 h. Micellization was induced by drop wise addition ( $\sim 1$  drop/10 s) of MilliQ distilled water and the solution was stirred overnight. The solution was dialyzed in a dialysis bag (protected from light) against MilliQ distilled water. The water was changed every hour for the first 4 h and then every 3 h for the following 12 h.

#### 2.2.2. Incorporation of [<sup>3</sup>H]B(a)P into micelles

An aliquot (8.3  $\mu$ l, 0.64 nM) of a [<sup>3</sup>H]B(a)P solution in toluene was added to an empty glass vial, and the toluene was allowed to evaporate. Five mg of PCL<sub>21</sub>-*b*-PEO<sub>44</sub> copolymer were then added to the

Table 1  
Some physical, chemical and biological properties of probes incorporated in poly(caprolactone)<sub>21</sub>-*b*-poly(ethylene oxide)<sub>44</sub> micelles

Probes	CellTracker <sup>®</sup> CM-DiI [11,12]	Benzo[ <i>a</i> ]pyrene [13]
Chemical formula	C <sub>68</sub> H <sub>105</sub> Cl <sub>2</sub> N <sub>3</sub> O	C <sub>20</sub> H <sub>12</sub>
Molecular mass	1051	257
Solubility in water	Low	3.8 × 10 <sup>-6</sup> g/l
Extinction coefficient	134 000 cm <sup>-1</sup> M <sup>-1</sup>	Not available
Fluorescence	$\lambda_{exc.} = 530$ nm $\lambda_{em.} = 570$ nm	$\lambda_{exc.} = 365$ nm $\lambda_{em.} = 407$ nm
Specific activity	0	5.0 mCi/ml
Cytotoxicity	Low	High
Cellular localization	Cytoplasmic/perinuclear	Membrane/non-nuclear
Micelle-incorporated probes		
Total no. of micelles formed/ml	1.1 × 10 <sup>16</sup>	1.1 × 10 <sup>16</sup>
No. of probe molecules per micelle	1.05	0.04
Stability of the micelles in the culture medium	At least 4 weeks	At least 4 weeks
Stability of the micelles in the PBS	At least 3 months	At least 3 months

vial followed by 0.15 g of DMF. The solution was stirred for 4 h at which point 0.33 g of water was added slowly to the vial to make a 0.5% (w/w) copolymer solution. The micelle solution was then stirred overnight and dialyzed against distilled water.

### 2.2.3. Spectrofluorometry and liquid scintillation counting

Determination of DiI concentration in micelles or the amounts of DiI released from micelles was determined from 60- $\mu$ l aliquots of micelles or 3.5 ml of dialysate, respectively. Micelles containing DiI were disintegrated in 3.94 ml of DMF and fluorescence intensities measured using Spex Fluorolog spectrometer at  $\lambda_{\text{exc}} = 570$  nm. Concentrations were determined from the linear portion of the standard curve from 10  $\mu$ M to 1.88 mM using the Sigma Plot 4.0 program. Liquid Scintillation Counter Wallac 1410 was used for detection of [ $^3\text{H}$ ]B(a)P incorporated or non-incorporated into micelles (5  $\mu$ l). Four ml of the scintillation cocktail were added to the samples, which were then left to equilibrate for a minimum of 1 h. Samples were counted using an Easy Count program (Liquid Scintillation Counter Wallac 1410).

### 2.2.4. Cell cultures

Primary neuronal cultures were prepared from neocortex and hippocampi (combined preparation) of mice (Swiss Webster, Taconic, embryonic day 16–18) and placed in Neurobasal medium with 10% fetal bovine serum [15]. The tissue was mechanically dissociated by pipetting. Neurons were plated at 100 000 cells/cm<sup>2</sup> on 0.025% poly-D-lysine coated four-chamber glass slides. After neurons had attached to the substrate (1 h), media were replaced with serum free Neurobasal medium containing 2% B27 supplement. The cultures were maintained at 37°C with 5% CO<sub>2</sub> in a tissue culture incubator. The medium was changed every 5–7 days, and the cells were used for experiments within 2–14 days in vitro (2DIV–14DIV).

### 2.2.5. Cellular internalization of micelle-incorporated probes

Neural cells grown in serum free medium (2DIV–14DIV) were incubated with micelle-incorporated (1  $\mu$ M, final concentration) or non-micelle-incorporated DiI (1  $\mu$ M, final concentration) for 15, 30, 60 min

and 4 h. Micelle-incorporated [ $^3\text{H}$ ]B(a)P, 0.04  $\mu$ M final concentration, and non-micelle-incorporated [ $^3\text{H}$ ]B(a)P, 0.04  $\mu$ M final concentration, were incubated for the same amount of time as with DiI. Following the incubation, an aliquot of supernatant was transferred to the scintillation vials and 4 ml of the scintillation cocktail were added. The cells were then washed once with acidified wash (0.5 M NaCl, 0.2 M CH<sub>3</sub>COOH; pH 2.5) and twice with PBS (phosphate-buffered saline). Following the washes, 200  $\mu$ l of lysis buffer were added to each chamber and the cells were lysed for 20 min on ice. Cell lysates were transferred to scintillation vials and 4 ml of scintillation cocktail were added to each vial. Samples were equilibrated for a minimum of 1 h and counted using Easy Count. Polymer concentrations in all experiments were 0.02%. To rule out the toxicity of the PCL<sub>21</sub>-b-PEO<sub>44</sub> cells were incubated with different concentrations of the polymer (0.01–0.1%) for 24 h and viability was assessed. Briefly, at the end of the experiment *N*-(1-naphthyl)ethylenediamine dihydrochloride, 3-(4,5-dimethylthiazol-2-yl)-2,5-diphenyltetrazolium bromide (MTT) (Sigma) was added (final concentration 250  $\mu$ g/ml) and cells were incubated for 2 h, then washed twice with PBS. DMSO (200  $\mu$ l/chamber) was used to dissolve the reduced MTT and the absorbance was measured at 595 nm using a microplate reader.

To study the subcellular distribution of DiI in neural cultures, cells (14DIV) were treated with Lyso Tracker Bodipy (0.2  $\mu$ g/ml, Molecular Probes) and Brefeldin A Bodipy (0.2  $\mu$ g/ml, Molecular Probes) together with DiI. Colocalization of organelle markers with DiI was assessed by confocal microscopy (BioRad 1024) at different times (< 15 min to 1 h). Minimum of 30 cells were analyzed per condition.

### 2.2.6. Immunocytochemistry

For the immunocytochemical analysis the cultures were rinsed in TBS (Triton-X buffered saline) and fixed in 2% paraformaldehyde for 15 min. Nonspecific immunostaining was blocked by incubating cells in 3% non-fat dry milk in TBS. The cells were then permeabilized with 0.5% Triton X-100 and incubated in primary antibody overnight at 4°C. To reveal neuronal cells and astrocytes MAP2 (microtubule associated protein 2, Sigma, dilution 1:500) or GFAP (antibody against glial fibrillar acidic protein, Sigma,

dilution 1:200) antibodies were used, respectively. Hudy 1 (Upstate Biotechnology, Lake Placid, NY, dilution 1:200) antibodies were used to detect dynamin 1. Control cells were incubated with 3% non-fat dry milk in TBS without primary antibody. CY3 or Bodipy conjugated antibodies (Jackson Labs) were used as a secondary antibody. After washing with TBS the slides were coverslipped with GVA-Mount (Zymed, San Francisco, CA). The images of immunostained cells were analyzed with a confocal microscope (BioRad 1024) equipped with an argon/krypton laser with 488, 568 and 647 nm lines, mounted on a Nikon TE-300 microscope, and a computer system coupled to an optical disk for image storage. All images were generated and processed using Adobe Photoshop software. For the quantitative analysis the images of all DiI-positive cells within a visual field (eight fields/condition) were collected using constant settings on a confocal microscope (BioRad 1024). The intensity of fluorescence (photon counts) in the cell was analyzed using Adobe Photoshop software. The data were collected from three independent experiments. To gain more quantitative data for dynamin-1, 500  $\mu$ l of cell lysates from 2DIV and 14DIV were immunoprecipitated with Hudy-1 (4  $\mu$ l/500  $\mu$ l cell lysate), separated using Protein A Agarose beads. Western blotting was done using the same antibody (0.2  $\mu$ g/ml) according to the supplier's protocol. The intensity of 100 kDa band was assessed by densitometry.

#### 2.2.7. Statistical analysis

Data were analyzed by Systat software version 9.0. The tests performed include Student's *t*-test or two-way analysis of variance (ANOVA) followed by multiparametric post hoc Tukey's test.  $P < 0.05$  was considered significant.

### 3. Results

#### 3.1. Properties of the PCL<sub>21</sub>-b-PEO<sub>44</sub> micelles and of the incorporated probes

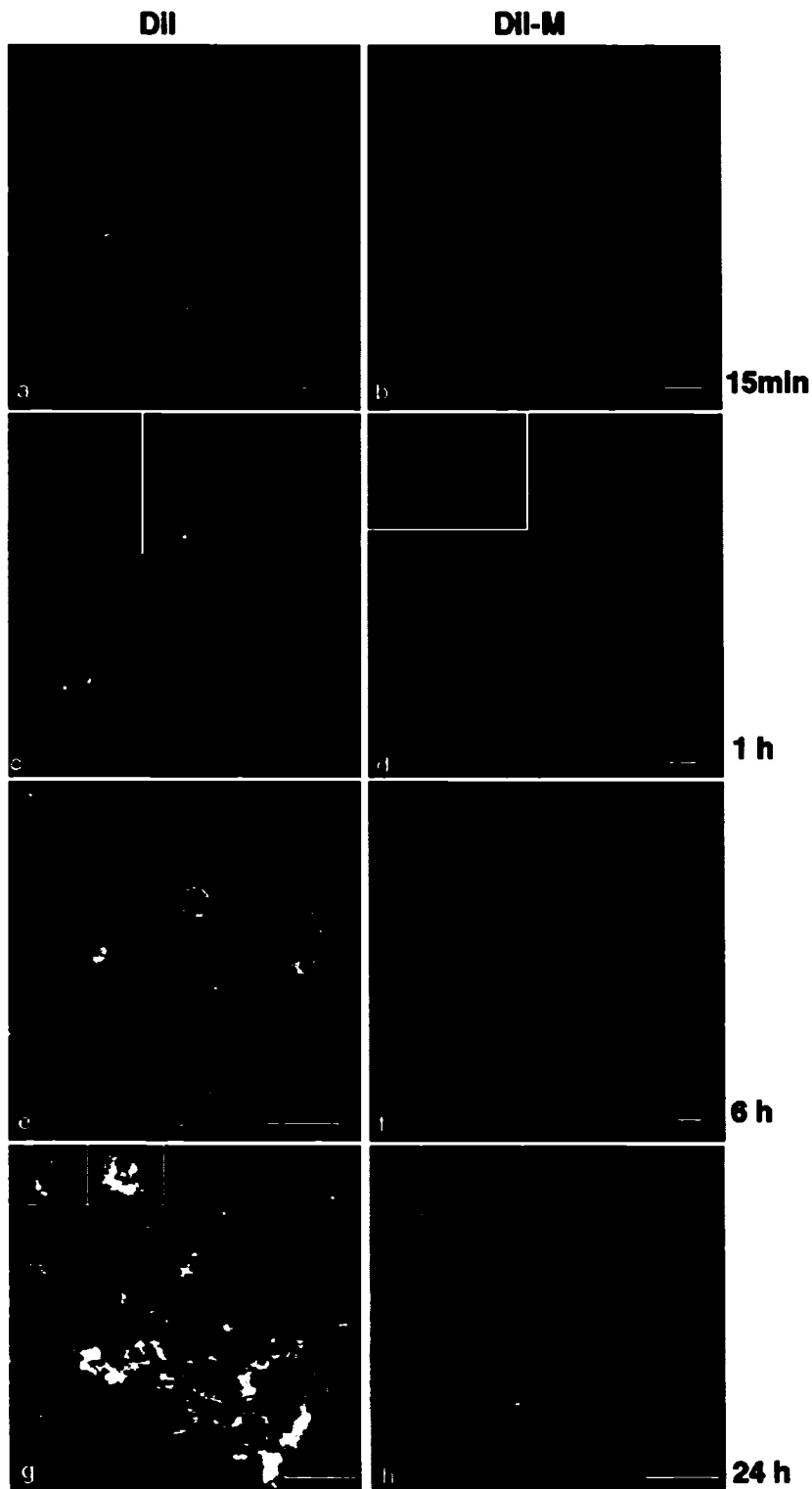
PCL<sub>21</sub>-b-PEO<sub>44</sub> micelles were prepared from copolymer solution in DMF and the micellization was induced by drop-wise addition of water. The micelles formed, studied by dynamic light scattering, reveal the effective diameter of 25–50 nm [10]. The total number of micelles formed in 1 ml of 0.5% (w/w) micellar solution is  $1.1 \times 10^{16}$  micelles/ml (Table 1). The critical micellar concentration and aggregation number were previously determined to be  $2.8 \times 10^{-7}$  M and 125, respectively [16]. Two lipophilic probes, DiI and [<sup>3</sup>H]B(a)P, were incorporated into PCL<sub>21</sub>-b-PEO<sub>44</sub> micelles. The physical and chemical properties of these probes are summarized in Table 1. The number of molecules incorporated per micelle was 26 times greater for DiI than for [<sup>3</sup>H]B(a)P (Table 1). The total number of DiI molecules in  $1.1 \times 10^{16}$  micelles is  $1.2 \times 10^{16}$ , and that of [<sup>3</sup>H]B(a)P is  $4.4 \times 10^{14}$ . Prior to internalization studies, biocompatibility of the PCL<sub>21</sub>-b-PEO<sub>44</sub> polymer was tested. No significant differences in the number of viable cells were detected in cultures treated with the polymer and in its absence, within 24 h. The stability of the micelles was assessed in the cell culture medium and in the PBS. The micelles were stable in both solutions for at least one month (Table 1), as assessed by dynamic light scattering and electron microscopy [10,16].

#### 3.2. Internalization of micelle-incorporated DiI into neural cells

A comparative analysis of internalized DiI upon

---

Fig. 1. Time-dependent DiI and DiI-M internalization into 6DIV neural cultures. DiI could be seen in the primary neurons following 15 min incubation, whereas DiI-M requires at least 1 h incubation to be taken up by neurons. Inserts in d,g,h show astrocytes. The bar represents 50  $\mu$ m. The images were acquired by confocal microscope (BioRad 1024) equipped with an argon/krypton laser with 488, 568 and 647 nm lines, mounted on a Nikon TE-300 microscope, and a computer system coupled to an optical disk for image storage. All images were generated and processed using Adobe Photoshop software. The intensity of fluorescence (photon counts) in the cell was analyzed using Adobe Photoshop software and expressed as relative fluorescence intensity (RFI). The data were collected from three independent experiments. The concentration of both micelle-incorporated and non-micelle-incorporated DiI was 1  $\mu$ M. Cells were grown in chemically defined serum-free medium and incubated 15 min and up to 24 h with DiI or micelle-incorporated DiI (DiI-M). The values in i represent the mean  $\pm$  S.E.M. (minimum 30 cells/condition were analyzed). RFI, relative fluorescence intensity.



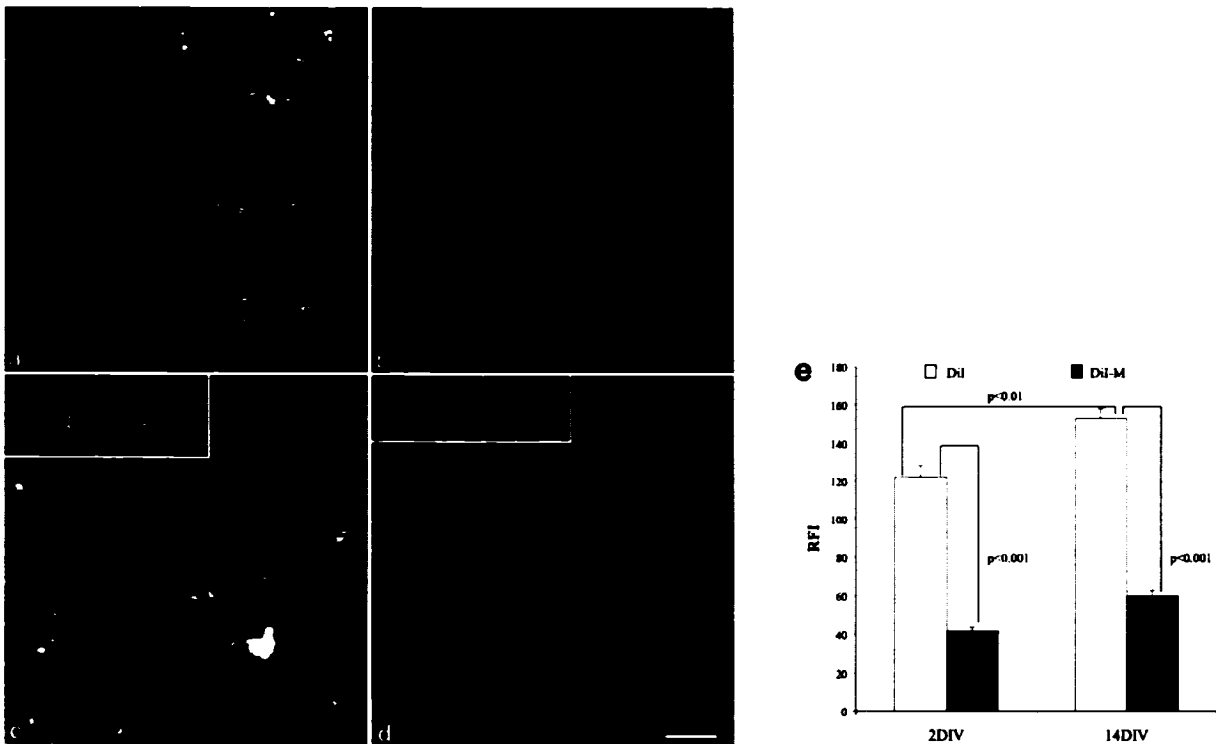
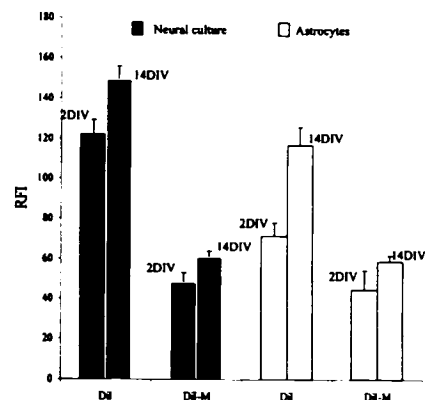


Fig. 2. Internalization of DiI and DiI-M into 2DIV (a,b) and 14DIV (c,d) primary neural cultures. The cells were incubated with DiI or DiI-M for 1 h at 37°C. There is an extensive uptake of DiI alone in both 2DIV and 14DIV neurons, whereas DiI-M internalization is only detectable in 14DIV old neurons (very faint signals in 2DIV cultures). The bar represents 50 μm. The concentration of both micelle incorporated and non micelle incorporated DiI is 1 μM. The values in e represent the mean ± S.E.M. ( $n = 30$ ). Student *t*-test was performed and  $P < 0.05$  was considered significant.

treatment of the cultures with either non-micellar DiI, (DiI), or the equivalent concentrations of micelle-incorporated DiI, (DiI-M) was performed for different periods of time (15 min, 1, 6, and 24 h). Fig. 1 shows accumulation of the fluorescence with

time in 6DIV neuronal cultures. Using direct confocal microscopy we were able to detect DiI incorporation into neurons after 15 min of the incubation with DiI (Fig. 1a), while in DiI-M-treated cells there was no uptake observed at this time (Fig. 1b). Mi-

Fig. 3. Internalization of micelle-incorporated and non-micelle-incorporated DiI into neural cultures and astrocytes. Neural cultures and astrocytes (2DIV and 14DIV) were treated with micelle-incorporated DiI (1 μM) and free DiI (1 μM). Images were acquired by confocal microscopy as described in Fig. 1. The bars represent the mean ± S.E.M. from three independent experiments. The data were analyzed by two-way ANOVA followed by Tukey's multiparametric post-hoc test.  $P < 0.05$  was considered significant. Relative fluorescent intensities (RFI) correspond to average fluorescent intensity per cell, from more than 30 neuronal cells and astrocytes. RFIs for non-micelle-incorporated DiI in neural cultures and astrocytes at 2DIV and 14DIV are significantly different ( $P < 0.001$ ). RFIs for micelle-incorporated DiI were not significantly different at 2DIV and 14DIV, either in neural cultures or astrocytes.



celle-incorporated DiI could hardly be seen after 1 h (Fig. 1d), whereas this is sufficient time to detect the signal of non-micellar DiI (Fig. 1c). The incorporation of DiI-M into cells was increased with time (Fig. 1b,d,f,h), but the intensity and number of labeled cells was significantly greater in cultures exposed to non-micellar DiI (Fig. 1a,c,e,g) at any time point tested. Relative fluorescence intensities (RFIs) from 30 randomly selected cells (three independent experi-

ments) are shown in Fig. 1i. These data support the finding that PCL<sub>21</sub>-b-PEO<sub>44</sub> block copolymer significantly alters the rate and extent of internalized DiI fluorescence in neural cultures within 24 h.

Next we analyzed the DiI staining of neural cultures after two days in vitro (2DIV) (Fig. 2a,b) and much later, when neurons are fully differentiated and have formed the synaptic contacts (14DIV) (Fig. 2c,d). Both 2DIV and 14DIV cell cultures exposed

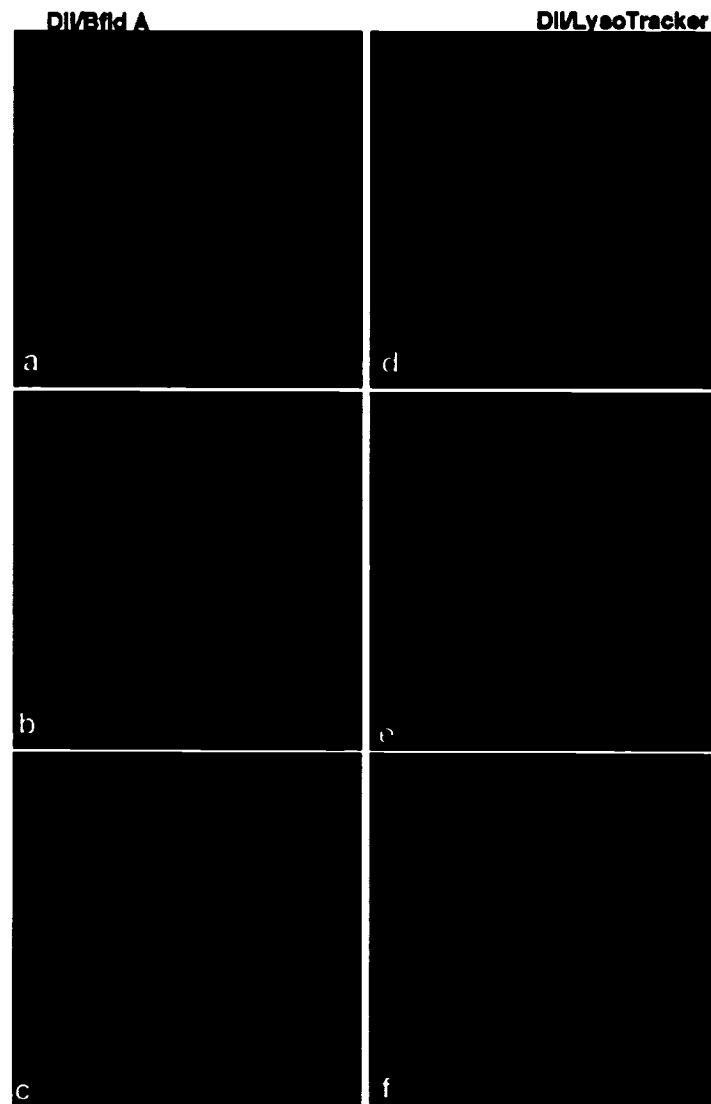


Fig. 4. Subcellular distribution of DiI colocalization with Lyso Tracker Bodipy. Neural cells were incubated with Lyso Tracker Bodipy (0.2  $\mu\text{g}/\text{ml}$ ) or Brefeldin A-Bodipy (0.2  $\mu\text{g}/\text{ml}$ ) for 15 min. The cells were then incubated for 60 min with DiI (1  $\mu\text{M}$ ) and images were acquired by confocal microscope BioRad 1024 (for details see Section 2). (a,d) DiI alone; (b) Brefeldin A-Bodipy alone; (e) Lyso Tracker Bodipy alone; (c) DiI and Brefeldin A-Bodipy; (f) DiI and Lyso Tracker Bodipy. Note: colocalization of DiI with the Lyso Tracker Bodipy (f).

to DiI showed a significant incorporation of the dye into neurons as well as astrocytes after 1 h of the incubation with DiI (Fig. 2a,c). At later times in vitro (14DIV) DiI-M could be detected, but again, the intensity and number of labeled cells was significantly greater in cultures exposed to non-micellar DiI. There is a highly significant difference ( $P < 0.001$ ) in the RFIs between micelle-incorporated and non-micelle-incorporated DiI at both 2DIV and 14DIV (Fig. 2e). DiI is internalized both by neurons and astrocytes (see inserts in Fig. 1c,d,g,h). RFIs for DiI in neural cultures and astrocytes at 2DIV and 14DIV are significantly different ( $P < 0.001$ ) (Fig. 3, DiI), whereas they are not significantly different for micelle-incorporated DiI (Fig. 3, M-DiI). Intense fluorescence of non-micelle-incorporated DiI is detected in 14DIV in neural cultures (RFI =  $149.2 \pm 6.7$ ) and astrocytes (RFI =  $116.8 \pm 9.0$ ) and it is significantly reduced (57.9% and 49.7%) for micelle-incorporated DiI in neural cultures and astrocytes, respectively (Fig. 3). Next we studied the subcellular distribution of DiI by using three specific markers for organelle labeling: Hoechst 33342 (nuclear staining), Brefeldin A-Bodipy (Golgi, Fig. 4a–c) and Lyso Tracker Bodipy (lysosomes, Fig. 4d–f). The signal of DiI in the Golgi was very faint and could hardly be detected in double staining experiments using Brefeldin A-Bodipy (Fig. 4c). Initially, (< 15 min) DiI is seen in the cell membrane and later on (30 min) in endosomes and lysosomes (colocalization with Lyso Tracker Bodipy) (unpublished observation). There was no retention of DiI in the nucleus at any time point (15 min–24 h). The fluorescence from micelle-incorporated DiI was too weak to provide convincing evidence for colocalization with Brefeldin A-Bodipy and Lyso Tracker Bodipy (not shown).

Due to the limited detection of the internalized micelle-incorporated fluorescent probe by confocal microscopy, we carried out a series of experiments using a micelle-incorporated radiolabeled probe. Since DiI was not available in tritiated or  $^{14}\text{C}$ -labeled form, we used  $[^3\text{H}]\text{B(a)P}$  as an alternative.

### 3.3. Uptake of the radiolabeled $[^3\text{H}]\text{B(a)P}$ by glia and neurons in the mixed cultures

The internalization of  $[^3\text{H}]\text{B(a)P}$  into mixed cultures between 2DIV and 14DIV and glial cultures

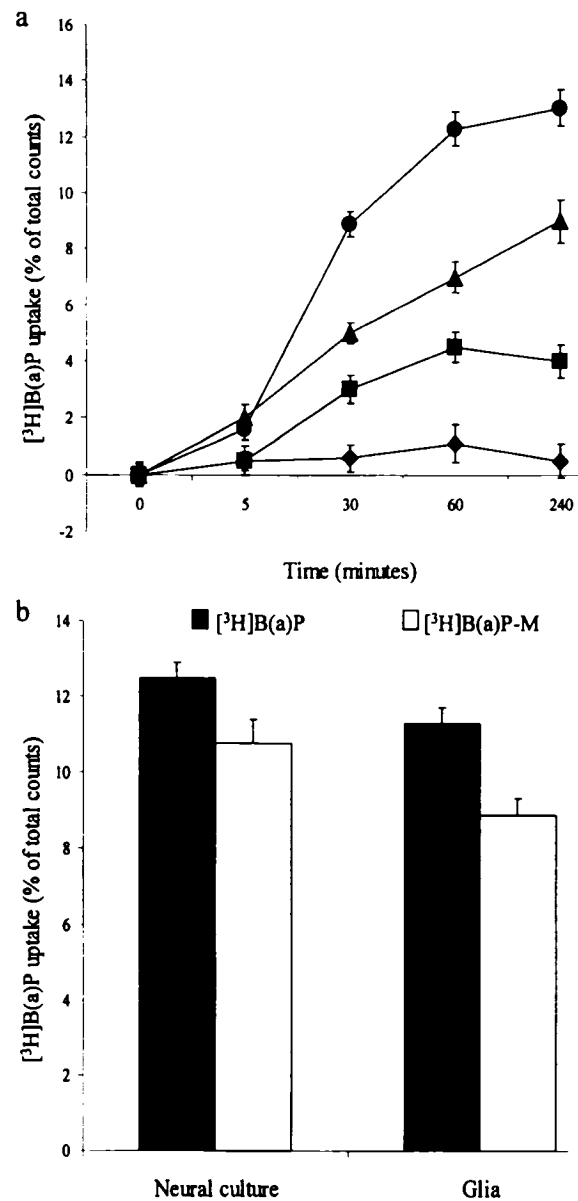


Fig. 5. Time-dependent  $[^3\text{H}]\text{B(a)P}$  uptake by mixed neuron–glia cultures and pure glia. (a) The extent of micelle-incorporated  $[^3\text{H}]\text{B(a)P}$  uptake in the mixed neural cultures (2DIV (◆), 5–6DIV (■), 9DIV (▲), 14DIV (●)). (b) The internalization of  $[^3\text{H}]\text{B(a)P}$  and micelle incorporated  $[^3\text{H}]\text{B(a)P}$  in glial cultures following 30 min incubation. The bars represent the mean  $\pm$  S.E.M. ( $n = 3$ ).

is shown in Fig. 5a. As in the experiment with DiI, cells were incubated for different time periods and the rate and extent of internalization was assessed. Lysed cells and supernatants were collected and

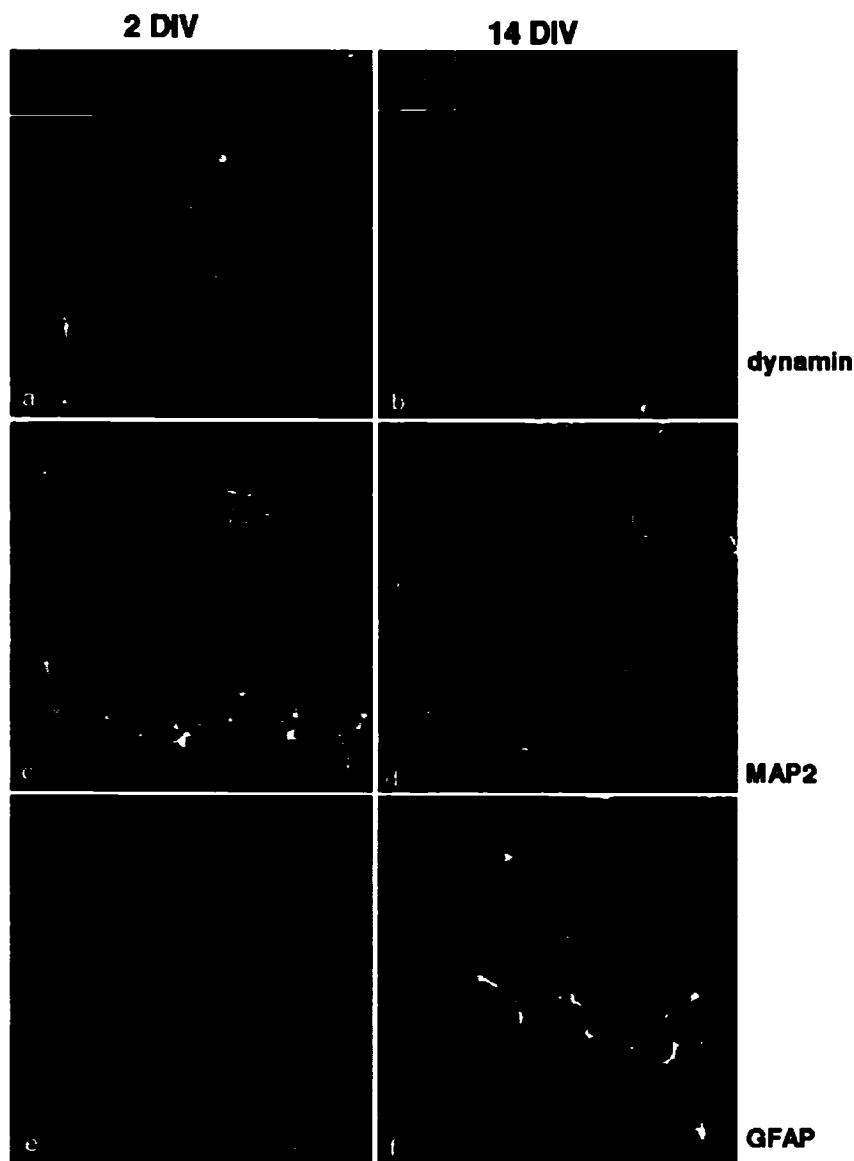


Fig. 6. Confocal images of 2DIV and 14DIV primary neural cultures immunostained with dynamin (a,b), neuron-specific MAP-2 (c,d) and astrocyte-specific (GFAP) antibodies (e,f). The immunostaining was performed as described in Section 2.2.6. Antibody concentrations used: anti-MAP-2 (1:500); anti-GFAP (1:200); Hudy 1 (1:200). Control cells were incubated with 3% non-fat dry milk in TBS without primary antibody. The intensity of dynamin immunoreactivity appears to be similar in 2DIV and 14DIV neurons (while the intensity of DiI-M internalization is significantly higher in 14DIV neurons compared with 2DIV neurons). There are fewer astrocytes in 2DIV cultures than in 14DIV cultures. The bar represents 50  $\mu\text{m}$ .

quantified by liquid scintillation counting. Both temporal and developmental dependence of micelle-incorporated [ $^3\text{H}$ ]B(a)P internalization is presented (Fig. 5a). There is a small and steady increase in the uptake with time up to 4 h. Similar result was obtained using micellar DiI (Fig. 1b,d,f,h). The extent of micelle-incorporated probe is significantly

larger at 14DIV than at 2DIV, 5–6DIV or 9DIV, at any times between 30 and 240 min. We then compared [ $^3\text{H}$ ]B(a)P internalization in neural cultures and glia. The free probe is internalized to a greater extent, and the difference between micelle-incorporated and non-incorporated probe is smaller than that with DiI (Fig. 1b,d,f,h,i). This may be in part

due to the different partition coefficients of the two probes. Results from pure glial cultures (14DIV) strongly suggest that a great amount of the probe was taken up by glia (88%) (Fig. 5b). We then assessed the cellular composition of neural cultures (2DIV and 14DIV) by immunohistochemical analyses employing the antibodies against MAP-2, GFAP and dynamin.

#### 3.4. Immunoreactivity of MAP-2, GFAP, and dynamin in 2DIV and 14DIV neuronal cultures

The cell composition of the 2DIV and 14DIV cultures was determined by immunostaining with neuron specific MAP-2 and astrocyte specific GFAP antibodies (Fig. 6). At 2DIV about 95–98% of the cells were neurons (MAP-2-positive, Fig. 6c), and less than 1% were GFAP-positive (Fig. 6e), showing that the vast majority of the cells in 2DIV cultures are neurons. By 14DIV, the number of GFAP-positive cells significantly increased due to a proliferation of the glial cells, and became about 20–30% of the total cell population.

To study whether the increase of the uptake was due to increased dynamin-mediated endocytosis in 14DIV neural cultures, we immunostained 2DIV and 14DIV cultures with anti-dynamin antibody. The intensity of dynamin staining and densitometric analysis of immunoreactive bands corresponding to immunoprecipitated dynamin reveal no significant difference in the protein expression in 14DIV (not shown), in agreement with the previous report showing low levels of dynamin 1 expression in embryonic tissues and a significant increase in the postnatal period [17].

## 4. Discussion

The present study demonstrates that the internalization of fluorescent- and radiolabeled probes into neural cells is significantly retarded when the probe is incorporated into PCL<sub>21</sub>-b-PEO<sub>44</sub> block copolymer micelles. The dramatic effect of the micelles was demonstrated by direct confocal microscopy of the living cultures. Immunocytochemical data showed that internalization increases as the neural composition changes during aging of the mixed cultures (2DIV–

14DIV) demonstrating the influence of the recipient cell type on the extent of internalization. The studies employing DiI and [<sup>3</sup>H]B(a)P showed that this effect is mainly due to an increase of uptake into non-neuronal cells.

#### 4.1. Micelles containing fluorescent probes as tools to study core-probe-cell relationship

Block-copolymer micelles can be considered as nano-containers from which agents are released in a sustained manner [18]. This is of particular interest for *in vivo* studies where the success of micelles for the delivery of neuroactive agents depends on the stability of the micelle, the degree of partitioning of the drug between the polymer and the biological environment, the stability of the drug within the micelle core and the drug release kinetics (reviewed in [18]). The nature of the corona has a known influence on internalization [1,18]. Our studies show that the nature of the cells themselves (in the present study revealed by the changes associated with aging of the mixed cell cultures), the core of the copolymer accommodating the probe, and the physical properties of the probe itself influence the probe internalization into cells. Interestingly, the polyethylene oxide corona attached to the charge-charge complex-forming cores has an effect of promoting rather than retarding internalization of the incorporated agent. This effect, attributable in part to the nature of the core, is opposite to that seen in the present study – highly lipophilic compounds incorporated into micelles with PEO corona but with a neutral core are slowly internalized by cells. Previous studies by Astafieva et al. [19] describe the synthesis and some characteristics of fluorescent-labeled polymer, but their subcellular distribution in the primary cultures of the nervous system was not examined. In the present study fluorescent and radiolabeled probes were incorporated into the non-fluorescent block copolymer with the similar corona (polyethylene oxide *i.e.* PEO) as in the Astafieva's studies [19]. By employing nuclear, lysosomal and Golgi fluorescent markers we found that DiI does not enter the nucleus and very little colocalizes with Lyso Tracker and even less with Golgi fluorescent marker. The exact subcellular distribution (with high resolution) of micelles and micelle-incorporated probes would require gold-labeled

polymer and electron microscopy. Such polymers are not presently available.

Due to the increasing number of biomacromolecules such as peptides, proteins, oligonucleotides and poorly soluble but highly neuroactive agents as potential therapeutics in neurodegenerative and other disorders, suitable delivery vehicles must be developed and characterized. Potential application of polymers in the delivery of drugs to the central and peripheral nervous system has been investigated by several groups [20,21]. We have been investigating a number of biocompatible and biodegradable block-copolymers [22], including a group of polycaprolactone-*b*-polyethylene oxides [10,17,18,23]. DiI is internalized by neural cells and shows granular cytoplasmic distribution, resembling that reported for DiI 18 [12]. The slow internalization rate of DiI-M seen in the present study concurs with the notion that the detectable signal after 6 and 24 h derives from both diffused DiI (with similar distribution as non-micellar DiI) and micelle-incorporated DiI (<5% total fluorescence). The differences of the internalization of [<sup>3</sup>H]B(a)P and DiI, micelle-incorporated vs. non-micelle-incorporated, into neural cultures (Fig. 1i and Fig. 5b), are significantly greater in the case of DiI. It is conceivable that the smaller difference in the internalization of micellar vs. non-micellar [<sup>3</sup>H]B(a)P into neural cultures can be attributed at least in part to different partition coefficient (micelles/aqueous medium) for [<sup>3</sup>H]B(a)P ( $K_v = 693$ ) and DiI ( $K_v = 6122$ ) (unpublished observations). This study is the first in the series of studies on cellular localization of fluorescent labels incorporated into micelle cores employing confocal microscopy. However, use of the fluorescent probe cannot answer the question whether or not the micelles themselves are internalized. To this end we have investigated the internalization of fluorescent-labeled polymer, obtaining results which suggest that a small proportion of micelles get into cells and that the kinetics of entry is slow (the signal is detectable after 4 h and reaches the maximum after 12 h; unpublished observation).

The DiI probe incorporated in PCL<sub>21</sub>-*b*-PEO<sub>44</sub> micelles diffuses out slowly and steadily. Thus, PCL<sub>21</sub>-*b*-PEO<sub>44</sub> block copolymer could be useful as a delivery vehicle for therapeutic agents with short plasma and CSF half-lives. Major limitation of PCL<sub>21</sub>-*b*-PEO<sub>44</sub> nano-containers is that they cannot deliver

drugs in a site-specific manner, and the slow release of the micelle-incorporated probe may limit their use. However, it does not preclude the use of the individual polymer units (unimers of PCL<sub>21</sub>-*b*-PEO<sub>44</sub>) carrying the drug molecule. Indeed, recent studies by Kabanov's group clearly show a polymer-enhanced accumulation of the fluorescent probe Rhodamine 123 into a bovine brain microvessel endothelial cell monolayer [24] at monomer concentrations below the CMC (0.01%). The enhancement was interpreted as being a consequence of the P-gp efflux transport system [25]. Such polymeric vehicles also have limitations, e.g., low loading capacity, lack of selectivity and possibly undesirable inhibition of transport systems away from the target tissue in which the drug is supposed to exert its biological effect by attaining an effective concentration. Tissue specific delivery and subcellular compartment delivery can be achieved in a number of ways, including the synthesis of functionalized polymers, thereby converting the non-specific to a receptor-mediated endocytosis. Our group is particularly interested in development of micelles able to deliver drugs to subcellular compartments.

#### 4.2. *Micelles and changes in neural composition alter the degree of the probe's internalization*

The current study provides data showing that internalization of the micelle-incorporated probe is strongly influenced by properties of the receiving cells themselves. In this instance these properties were determined by the 'age' of the mixed neuron-glia and pure glia cultures (2DIV vs. 14DIV) the data deriving from the neuronal and glial markers expressed during the course of 2 to 14 days *in vitro*.

In mixed cells at 2DIV, some cells are still vimentin positive, suggesting the presence of some progenitor cells (not shown). At 6DIV, MAP-2 staining is strong, but a number of GFAP positive cells (astrocytes) have increased as compared to 2DIV. In these cultures, DiI is effectively internalized within 30 min and micelle-containing DiI within 4 h. GFAP immunostaining is very strong at 14DIV, suggesting that at that stage mixed cultures have more astrocytes than neurons. A number of reports provide evidence for the role of dynamin in different cell types. Recent studies of growing astrocytes in primary cultures show that astrocytes have a developed endocytotic

system mainly composed of caveolae, clathrin coated pits and vesicles, tubulo-vesicular and spheric endosomes and multivesicular bodies [26]. The same studies also show that ethanol impairs protein trafficking and causes reduction of caveolin, clathrin, rab 5 and beta-COP levels. In contrast, data from the present study show that dynamin staining does not change significantly between 2DIV to 14DIV, suggesting that the expression of this protein does not correlate with the extent of internalization of probe contained in the nanosized delivery vehicle within this time period of neural cultures *in vitro*. Indeed, dynamin expression enhances mainly during the postnatal period [17]. Whether dynamin [27], amphiphysin [28], intersectin [29] and caveolin [30] play a role in internalization of micelles is currently under investigation.

In conclusion, the rate and the extent of uptake of the DiI probe incorporated into PCL<sub>21</sub>-*b*-PEO<sub>44</sub> micelles are significantly altered by the block copolymer and by the characteristics of the cells, which change from 2DIV to 14DIV; the former retards internalization of the fluorescent probe used, while the age-related changes in cellular composition of the culture enhance it.

### Acknowledgements

The authors thank the Natural Sciences and Engineering Research Council of Canada (NSERC) for funding this research.

### References

- [1] K. Kataoka, A.V. Kabanov (Eds.), *Colloids and Surfaces B: Biointerfaces*, Special issue: Polymeric Micelles in Biology and Pharmaceuticals, *Colloids Surf. B Biointerfaces* 16 (1999) 1–329.
- [2] S. Cammas, K. Kataoka, Site specific drug-carriers: polymeric micelles as high potential vehicles for biologically active molecules, in: S.E. Webber et al. (Eds.), *Solvents and Self-Organization of Polymers*, 1996, pp. 83–113.
- [3] A. Zhang, A. Eisenberg, Multiple morphologies and characteristics of 'crew-cut' micelle like aggregates of polystyrene-*b*-poly(acrylic acid) diblock copolymers in aqueous solution, *J. Am. Chem. Soc.* 118 (1996) 3168–3181.
- [4] K. Yu, L. Zhang, A. Eisenberg, Novel morphologies of 'crew-cut' aggregates of amphiphilic diblock copolymers in dilute solution, *Langmuir* 12 (1996) 5980–5984.
- [5] H.M. Burt, X. Zhang, P. Toleikis, L. Embree, A.V. Kabanov, Development of copolymers of poly(D,L-lactide) and methoxypropylene glycol as micellar carriers of paclitaxel, *Colloids Surf. B Biointerfaces* 16 (1999) 161–171.
- [6] K. Kataoka, H. Togawa, A. Harada, K. Yasugi, T. Matsumoto, S. Katayose, Spontaneous formation of polyion complex micelles with narrow distribution from antisense oligonucleotide and cationic block copolymer in physiological saline, *Macromolecules* 29 (1996) 8556–8557.
- [7] A.V. Kabanov, S.V. Vinogradov, Y.G. Suzdaltseva, V.Y. Alakhov, Water-soluble block polycations as carriers for oligonucleotide delivery, *Bioconjug. Chem.* 6 (1995) 639–643.
- [8] S. Katayose, K. Kataoka, Water-soluble polyion complex associates of DNA and poly(ethylene glycol)-poly(L-lysine) block copolymer, *Bioconjug. Chem.* 8 (1997) 702–707.
- [9] V.A. Kabanov, A.V. Kabanov, Interpolyelectrolyte and block ionomer complexes for gene delivery: physico-chemical aspects, *Adv. Drug Deliv. Rev.* 30 (1998) 49–60.
- [10] C. Allen, Y. Yu, D. Maysinger, A. Eisenberg, Polycaprolactone-*b*-poly(ethylene oxide) block copolymer micelles as a novel drug delivery vehicle for neurotrophic agents FK506 and L-685,818, *Bioconjug. Chem.* 9 (1998) 564–572.
- [11] R.P. Haughland, *Handbook of Fluorescent Probes and Research Chemicals*, Molecular Probes Inc., 1996, p. 310.
- [12] S. Mukherjee, T.T. Soe, F.R. Maxfield, Endocytic sorting of lipid analogues differing solely in the chemistry of their hydrophobic tails, *J. Cell Biol.* 144 (1999) 1271–1284.
- [13] International Agency for Research on Cancer (IARC), *IARC Monographs on the Evaluation of the Carcinogenic Risk of Chemicals to Humans*, 1983.
- [14] C. Allen, Y. Yu, S. Chijiwa, D. Maysinger, A. Eisenberg, Synthesis and characterization of a biodegradable and biocompatible amphiphilic diblock copolymer of poly(*ε*-caprolactone)-*b*-poly(ethylene oxide), *Macromolecules* (2001) in press.
- [15] O. Berezovska, P. McLean, R. Knowles, M. Frosh, F.M. Lu, S.E. Lux, B.T. Hyman, Notch1 inhibits neurite outgrowth in postmitotic primary neurons, *Neuroscience* 93 (1999) 433–439.
- [16] C. Allen, J. Han, Y. Yu, D. Maysinger, A. Eisenberg, Polycaprolactone-*b*-poly(ethylene oxide) copolymer micelles as a delivery vehicle for dihydrotestosterone, *J. Controlled Release* 63 (2000) 275–286T.
- [17] T. Cook, K. Mesa, R. Urrutia, Three dynamin-encoding genes are differentially expressed in developing rat brain, *J. Neurochem.* 67 (1996) 927–931.
- [18] C. Allen, D. Maysinger, A. Eisenberg, Nano-engineering block copolymer aggregates for drug delivery, *Colloids Surf. B Biointerfaces* 16 (1999) 3–27.
- [19] I. Astafieva, I. Maksimova, E. Lukanidin, V. Alakhov, A. Kabanov, Enhancement of the polycation-mediated DNA uptake and cell transfection with Pluronic P85 block copolymer, *FEBS Lett.* 389 (1996) 278–280.
- [20] R. Langer, Drug delivery and targeting, *Nature* 392 (1998) 5–10.
- [21] D.W. Miller, A.V. Kabanov, Potential applications of poly-

- mers in the delivery of drugs to the central nervous system, *Colloids Surf. B Biointerfaces* 16 (1999) 321–330.
- [22] G.S. Kwon, Diblock copolymer nanoparticles for drug delivery, *Crit Rev. Ther. Drug Carrier Syst.* 15 (1998) 481–512.
- [23] J. Zhao, C. Allen, A. Eisenberg, Partitioning of pyrene between 'crew-cut' block copolymer micelles and H<sub>2</sub>O/DMF solvent mixtures, *Macromolecules* 30 (1997) 7143–7150.
- [24] D.W. Miller, E.V. Batrakova, T.O. Waltner, V.Y. Alakhov, A.V. Kabanov, Interactions of pluronic block copolymers with brain microvessel endothelial cells: evidence of two potential pathways for drug absorption, *Bioconjug. Chem.* 8 (1997) 649–657.
- [25] M.M. Nerurkar, P.S. Burton, R.T. Borchardt, The use of surfactants to enhance the permeability of peptides through Caco-2 cells by inhibition of an apically polarized efflux system, *Pharm. Res.* 13 (1996) 528–534.
- [26] L. Megias, C. Guerri, E. Fornas, I. Azorin, E. Bendala, M. Sancho-Tello, J.M. Duran, M. Tomas, M.J. Gomez-Lechon, J. Renau-Piqueras, Endocytosis and transcytosis in growing astrocytes in primary culture. Possible implications in neural development, *Int. J. Dev. Biol.* 44 (2000) 209–221.
- [27] H. Damke, Dynamin and receptor-mediated endocytosis, *FEBS Lett.* 389 (1996) 48–51.
- [28] C. David, P.S. McPherson, O. Mundigl, P. de Camilli, A role of amphiphysin in synaptic vesicle endocytosis suggested by its binding to dynamin in nerve terminals, *Proc. Natl. Acad. Sci. USA* 93 (1996) 331–335.
- [29] N.K. Hussain, M. Yamabhai, A.R. Ramjaun, A.M. Guy, D. Baranes, J.P. O'Bryan, C.J. Der, B.K. Kay, P.S. McPherson, Splice variants of intersectin are components of the endocytic machinery in neurons and nonneuronal cells, *J. Biol. Chem.* 274 (1999) 15671–15677.
- [30] E.J. Smart, G.A. Graf, M.A. McNiven, W.C. Sessa, J.A. Engelman, P.E. Scherer, T. Okamoto, M.P. Lisanti, Caveolins, liquid-ordered domains, and signal transduction, *Mol. Cell. Biol.* 19 (1999) 7289–7304.